Potential of hydrochars obtained by hydrothermal carbonization under saline conditions

Von der Fakultät für Mathematik und Naturwissenschaften der Carl von Ossietzky
Universität Oldenburg zur Erlangung des Grades und Titels eines

Doktor der Naturwissenschaften (Dr. rer. nat.)

angenommene Dissertation

von Herrn Hendrik Multhaupt

geboren am 28.10.1988 in Wilhelmshaven

Gutachter: Prof. Dr. Michael Wark
Weitere Gutachter:
Prof. Dr. Adrian Schumpe
Apl. Prof. Dr. Axel Brehm

Tag der Disputation: 14.02.2018

Department of Mathematics and Science
Institut of Chemistry
Work group for Chemical Technology 1 -
Photocatalysis & sustainable feedstock utilization
Carl von Ossietzky University Oldenburg

Potential of hydrochars obtained by hydrothermal carbonization under saline conditions

Dissertation for obtaining the academic degree
Doctor rerum naturalium (Dr. rer. nat.)
in the Department of Mathematics and Natural Sciences
(Work group for Chemical Technology)
at the Carl von Ossietzky University of Oldenburg

Submitted by
Hendrik Multhaupt

born 28th of October, 1988 in Wilhelmshaven

Oldenburg, in February 2018

This work was conducted at the Carl von Ossietzky University of Oldenburg in the time starting July of 2014 to the end of December 2017 supervised by Prof. Dr. Michael Wark in the work group Chemical technology 1 - Photocatalysis & sustainable feedstock utilization belonging to the Institute of Chemistry. The practical studies were conducted in the laboratories of the Department of Mathematics and Science of the Carl von Ossietzky University of Oldenburg.

Reviewers:	Prof. Dr. Michael Wark, Carl von Ossietzky University Oldenburg
	Prof. Dr. Adrian Schumpe, Technical University Braunschweig
	Apl. Prof. Dr. Axel Brehm, Carl von Ossietzky University Oldenburg
Day of disputation:	14th February, 2018

Acknowledgments

At this point I would like to thank everyone who contributed to the success of the present work in any way.

Special thanks go to my advisor Prof. Dr. Michael Wark for the chance to conduct my doctoral studies in his workgroup of Chemical technology. Especially for granting me the necessary freedom to develop my own research ideas and for the suggestions provided throughout the development of this work. Whenever the research seemed to end up in a blind alley he provided inspirational ideas in our discussions and motivated me to evoke new ways of rethinking the situation to further develop my ideas.

Further thanks are given to Prof. Dr. Adrian Schumpe for agreeing to examine this work as a second supervisor.

I would also like to thank most of the former and current colleagues at the workgroup Chemical technology in Oldenburg for the pleasant working atmosphere. Great appreciation goes to Bernd Werner and Rainer Bölts for their help in any questions about technical constructions or craftsmanship. Special thanks go to my officemates Markus Becker and Florian Meyer but also to Dr. Martin Pilarski, Dr. Dereje Hailu Taffa and Dr. Jaybalan Tamahrajah for the scientific as well as not so scientific discussions that helped to go through every day. Thanks go also to Nicole Lenkering for her kind help in everything regarding organization.

I thank Dr. Thomas Greve and Dr. Jan Ohlert for their introduction and insight into the challenging world of the hydrothermal carbonization.

Additional thanks to everyone that helped in the successful measurements of my samples, mostly Sandra Susanne Zahl, Eleonore Gründken, Edith Kieselhorst, Janine Leppin and Nadine Pilinksi as well as Tim Woriescheck. Special thanks here go to Dr. Christopher Seidler for giving me much insight in physical sorption techniques and Dr. Patrick Bottke for his NMR measurements.

Very special thanks go to Prof. Dr. Jürgen Gmehling, Apl. Prof. Dr. Axel Brehm, assoc. Prof. Hiroyuki Matsuda, Prof. h.c. Jürgen Rarey and Dr. Benjamin Burfeind who I see as inspirational influences to my personal development in the world of science.

Lastly, I would like to give endless thanks to my mother Sabine, my brother Helge and my wife Erino. Your never-ending support and understanding helped me through the hardest of times. This work is dedicated to you.

Abstract

This work reports on the synthesis of carbon materials (hydrochars) via the hydrothermal carbonization (HTC) method. The main focus of the study laid on how different process parameters, especially the presence of additives such as salts, alter the hydrochar properties such as elemental composition, morphology, functionality and surface area. For this, different starting materials like various biomass substrates and their building units were used and carbonized in the presence of different salts and their mixtures (salt-hydrochars) or in pure water for comparison (normal-hydrochars). Additionally, the effect of the process parameters temperature, time and water content was also studied. Here, the presence of zinc chloride as well as an increased reaction temperature were found as the main driving forces for obtaining hydrochars with optimized characteristics such as a more aromatic structure and increased microscopic visible roughness. The latter point resulted in higher specific surface areas up to 100-200 $m^2 \cdot g^{-1}$ for the hydrochars synthesized with an additive present, with a meso- to macroporous pore system. Especially the Lewis acid $ZnCl_2$ catalyzed degradation reactions of the biomass parts such as those from cellulose and at high temperatures also those from lignin. The salt could easily be washed out of the resulting carbon material and reused in following cycles.

Moreover, to further increase the specific surface areas by introduction of microporosity, steam activation at increased temperatures (e.g. 500 °C) was conducted on several samples. Since the initial pore system of the salt-hydrochars maintained in their activated forms besides the then introduced microporosity, chars based on renewable materials that have a pore system with a variety of pore sizes could be obtained. However, due to the high activation temperatures a lot of surface functionality was lost in the activated hydrochars.

For a possible application, the obtained hydrochars were tested as sorption agents for the removal of two dyes, methylene blue and methyl orange, from aqueous solution. Here, the salt-hydrochars showed the fastest and highest dye uptake and capacity when compared to normal-hydrochars and the activated forms. A combination of available surface functionality, hydrophilicity and accessible pores are discussed as the reason for the observed results. The maximum monolayer adsorption capacity of the methylene blue (q_m) for a hydrochar from coconut shell powder obtained in the presence of zinc chloride was found from the Langmuir isotherm with 277.01 $mg \cdot g^{-1}$. The mechanism of dye sorption was studied and it could be shown that possible intraparticle diffusion is not the only rate-limiting step. Therefore, an external diffusion is probably also important for the whole adsorption process. However, the results indicated a strong potential for an industrial relevance as sorption materials.

Abriss

Die vorliegende Arbeit berichtet über die Synthese von Kohlenstoffmaterialien (Hydrokohlen) mittels hydrothermaler Karbonisierung (HTC). Im Mittelpunkt der Studie stand wie unterschiedliche Prozessparameter, insbesondere das Vorhandensein von Additiven wie Salzen, die Eigenschaften der Hydrokohlen wie z.B. elementare Zusammensetzung, Morphologie, Funktionalität und spezifische Oberfläche verändern. Hierzu wurden verschiedene Ausgangsstoffe wie Biomassesubstrate und deren Baueinheiten Glucose, Cellulose und Lignin in Gegenwart verschiedener Salze und deren Mischungen (Salz-Hydrokohlen) oder in reinem Wasser zum Vergleich (normale Hydrokohlen) karbonisiert. Zusätzlich wurde der Einfluss der Prozessparameter Temperatur, Zeit und Wassergehalt untersucht. Hier wurden das Vorhandensein von Zinkchlorid sowie eine erhöhte Reaktionstemperatur als die Hauptantriebskräfte zum Erhalten optimierter Eigenschaften wie einer aromatischeren Struktur und einer erhöhten mikroskopischen sichtbaren Rauigkeit gefunden. Letzterer Punkt führte zu höheren spezifischen Oberflächen von bis zu 100-200 $m^2 \cdot g^{-1}$ für die Hydrokohlen, welche in Anwesenheit eines Additivs synthetisiert wurden, mit einem Porensystem, welches Meso- und Makroporen enthält. Insbesondere die Lewis-Säure $ZnCl_2$ katalysiert Abbaureaktionen der Biomasseteile wie z.B. solchen aus Cellulose und bei hohen Temperaturen auch solchen aus Lignin. Das Salz kann leicht aus dem resultierenden Kohlenstoffmaterial ausgewaschen und in den folgenden Zyklen wiederverwendet werden.

Um die spezifischen Oberflächen durch Einführung von Mikroporosität weiter zu erhöhen, wurde darüber hinaus eine Dampfaktivierung bei erhöhten Temperaturen (beispielsweise 500 °C) an mehreren Proben durchgeführt. Da das anfängliche Porensystem der Salz-Hydrokohlen auch in deren aktivierten Form außer der dann eingeführten Mikroporosität beibehalten wurde, konnten auf erneuerbaren Materialien basierende Hydrokohlen mit einem Porensystem mit einer Vielzahl von Porengrößen erhalten werden. Aufgrund der hohen Aktivierungstemperaturen ging jedoch ein großer Teil der Oberflächenfunktionalität in den aktivierten Hydrokohlen verloren.

Für eine mögliche Anwendung wurden die erhaltenen Hydrokohlen als Sorptionsmittel für die Entfernung von zwei Farbstoffen (Methylenblau und Methylorange) aus wässriger Lösung getestet. Hier zeigten die Salz-Hydrokohlen die schnellsten und höchsten Farbstoffaufnahmen und -kapazitäten im Vergleich zu den normalen und aktivierten Formen. Eine Kombination aus verfügbarer Oberflächenfunktionalität, Hydrophilie und zugänglichen Poren wird als Grund für die beobachteten Ergebnisse diskutiert. Die maximale Monoschicht-Adsorptionskapazität des Methylenblau (q_m) für eine Hydrokohle aus Kokosnussschalenpulver, welche in Gegenwart von Zinkchlorid erhalten wurde, wurde aus der Langmuir-Isotherme mit 277,01 $mg \cdot g^{-1}$ gefunden.

Der Mechanismus der Farbstoffsorption wurde untersucht und es konnte gezeigt werden, dass eine mögliche intrapartikuläre Diffusion nicht der einzige geschwindigkeitsbestimmende Schritt ist. Daher ist wahrscheinlich auch eine externe Diffusion für den gesamten Adsorptionsprozess wichtig. Die Ergebnisse zeigten jedoch ein starkes Potenzial für eine industrielle Relevanz der Hydrokohlen als Sorptionsmaterialien.

Table of contents

Potential of hydrochars obtained by hydrothermal carbonization under saline conditions

Hendrik Multhaupt, Dissertation 2017

Chapter 1

Introduction

The ever increasing world population (7.2 billion in 2014 estimated to become 9.6 billion until 2050[1]) together with the resulting higher consumption and need of energy (cf. figure 1a) is one of the biggest issues for the present day mankind. While the rising carbon dioxide emissions play a major role in the ever imminent climate change[2, 3], whose main symptom is seen as the global surface temperature increase (figure 1b), the feedstocks of the still widely as energy sources used fossil raw materials are finite and said to last just a few more decades (crude oil and natural gas) to a few hundred years (coal and lignite)[4].

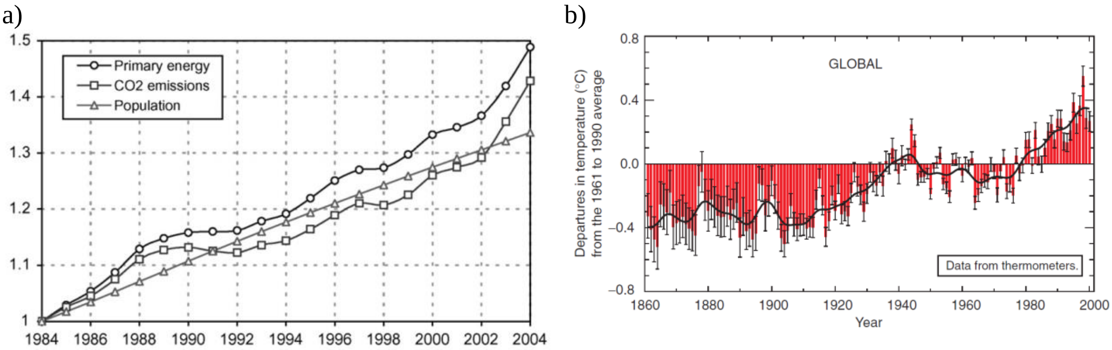

Figure 1 a) Primary energy consumption, CO_2 emissions and world population with reference to the year 1984 (image taken from Perez-Lombard *et al.*[5]); b) Variation of the earth's surface temperature in the last centuries (image taken from Houghton *et al.*[3]).

Currently, renewable raw materials make up only 13 % of the world's energy supply, with approximately 80 % still provided from using fossil fuels.[4] It is estimated that the amount used will increase to 18 % by 2035.[6] Continuous research in new fields of sustainable energies and materials as well as the optimization of existing techniques and strategies based on these are therefore important and required to be prepared for future needs, such as decreasing the greenhouse gas emissions and limit the increase of the global average temperature as stated in the Paris agreement, which was supported by all of the 195 countries in the world when it was signed in 2015[7].

1.1 Motivation

Biomass is estimated to grow roughly 118 billion tons per year (dry matter)[8] and therefore represents an abundant material to use for energy production. More interestingly, biomass is discussed as a potential carbon sink due to its binding of CO_2 in the plant material.[9] However, since the carbon dioxide is released in the same amount when the biomass is microbiological decomposed the need of a method in fixing the carbon has to be established. What was done over millions of years as natural coal formation is now desired to be possible by preferably low-cost operations on a timescale of a few hours.

In recent years, the approach of hydrothermal carbonization (HTC) was brought to light as a possible solution to the problem of carbon fixation that could help to limit CO_2 emissions. With this method, the biomass is simply heated in water at elevated temperatures of around 200 °C under self assembled pressure for times as short as a few minutes to several days. The result is a peat like coal - the so called hydrochar - together with a liquid waste phase.

Some of the major strengths of the HTC include the simplicity of the process, the possibility to use nearly any kind of wet or dry biomass feedstock together with the generation of further usable products from the hydrochar or different interesting compounds like e.g. the platform chemical hydroxymethylfurfural (HMF) found in the liquid phase towards a full cycle biorefinery process (compare figure 2). These lead to increased interest by scientists as well as engineers all over the world with hundreds of research papers released since the mid 2000's and several HTC plants build in different countries.

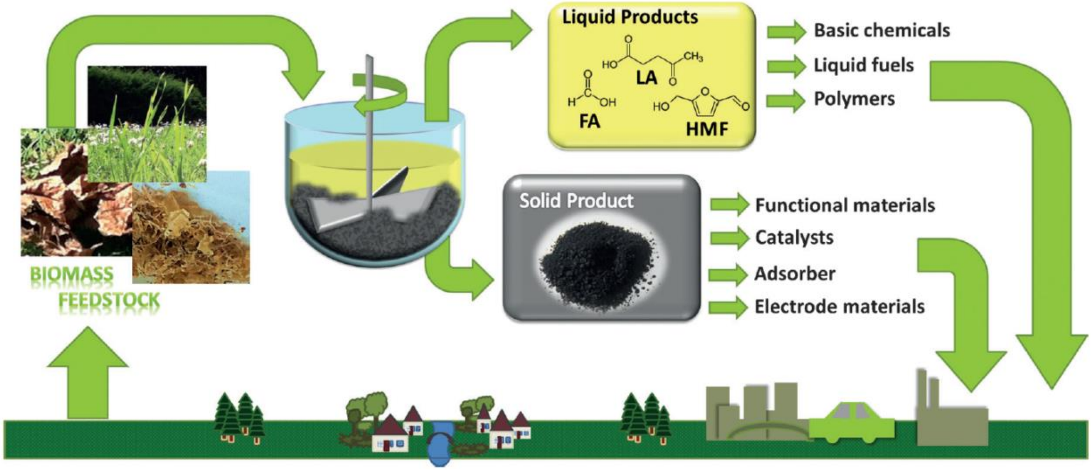

Figure 2 Hydrothermal carbonization in a biorefinery concept as described by Reiche *et al.*[10]

However, the structural complexity of the nature based biomass feedstocks and the variety of reactions and consecutive side reactions taking place in the HTC make the process overall difficult to generalize and every new feedstock might bring new issues to overcome by process optimization. A lot of research has been done to try to understand the reactions taking place from biomass building units from simple sugars like glucose to more complex parts like cellulose, hemicellulose or the very stable lignin, together with enhancing operation conditions, pushing the hydrothermal carbonization forward as an economical and green process for potential use in industrial applications.

While the liquid phase with its huge amount of possibly naturally harmful compounds can be another issue for the industrial implementation, the use of the solid product is at the moment unfortunately mostly limited to combustion for energy generation. The problem is that many applications like the use as functional materials or catalyst support require a material with a certain high enough surface area or porosity. While some groups showed in their research that it's possible to receive porous carbonaceous materials, these are often either synthesized from simple molecules like sugars to avoid problems cause by the structural complexity of a real biomass, or treated subsequent in terms of a post-activation, leading to increased production costs. Nonetheless, some promising approaches included the simple use of mixtures of commonly available salts as additives to the HTC of different starting materials[11-14] that gave the foundation for the ideas developed within this thesis.

1.2 Thesis focus

The present work focuses onto the hydrothermal carbonization of different starting materials like various biomass substrates and their building units such as glucose, cellulose and lignin with special regards onto the effect of using different salts and their mixtures as additives. Clues about the reactions taking places as well as the effect of the different additives or the variation of the parameters temperature and time onto the obtained hydrochars are drawn from various characteristics. The reaction yields as well as the elemental analysis (EA) give first information about the extent of the carbonization. Detailed images on a scale of micro- to nanometers of the hydrochars are obtained by electron microscopy (SEM/TEM), while X-ray powder diffraction (XRD) and solid state ^{13}C magnetic resonance spectroscopy (SS-^{13}C-NMR) allow the characterization on a molecular level. These are supported by Fourier transform infrared spectroscopy (FTIR) and X-ray photoelectron spectroscopy (XPS) that show which functional groups are present on the hydrochar surfaces and how the elements like carbon and oxygen are distributed within them. Gas sorption experiments are carried out with different gases (N_2, CO_2 and H_2O) to characterize a possible porosity and the surface areas. With thermogravimetric analysis (TGA) the thermal stability of the hydrochars is studied, from which a fitting activation temperature can be chosen for an optional post-treatment.

On top of the prior mentioned methods, characterization of the liquid phase is broached by collected data of the total organic carbon content (TOC) as well as peak spectra from high-performance liquid chromatography (HPLC).

As an additional and optional step, effects of a post-HTC treatment in terms of activation by steam onto the then activated hydrochar characteristics like development of porosity and change in surface functionality are studied.

Since the removal of water pollutants such as dyes from aqueous solutions is often discussed as a possible application of the hydrochars, such studies are also conducted for this thesis. Here, especially the comparison of the hydrochars to their activated forms gives insight about the adsorption mechanism, pointing out strengths of the product hydrochar.

Chapter 2

Fundamentals

The following chapters will give an overview about current literature knowledge on the process of hydrothermal carbonization and its resulting hydrochars with special focus on how their properties alter with changing conditions. Therefore, after an overall introduction (2.1) and brief description of the history of HTC research (2.2), the reaction networks of different biomass compounds (2.3.1 and 2.3.2) and the resulting main hydrochar characteristics (2.3.3), as well as the importance of the present water (2.3.4), will be discussed before the influence of various process parameters like temperature, time and additives is in the focus (2.4). Additionally, current knowledge found in literature for the post-activation of hydrochars (2.5) and the use of the different materials as low-cost adsorbents for different waste water contaminants like dyes (2.6) is discussed.

2.1 Introduction to the hydrothermal carbonization

The hydrothermal carbonization (HTC) of various biomass substrates technically enables in a few hours what took nature several hundreds to millions of years to achieve: the formation of peat or coal by carbonization. The natural coalification in means of decomposition of carbohydrates found in the dead biomass was triggered simply from the pressure induced by layers and layers of rocks and stones together with the absence of oxygen. Since HTC in a laboratory is usually carried out in a sealed autoclave, elevated temperatures, typically between 180 and 220 °C, with self-generated pressures around 10 bars are applied to imitate the effect of geological time intervals and enable faster reaction rates (compare figure 3). Reaction times can vary from as short as one minute to several days.[15] By using cheap and natural precursors, industrially interesting materials in form of the so called hydrochars can be obtained with diverse imaginable fields of applications such as for energy production up to synthesis of nanostructured carbons.[16] Ideally, the properties of the final product can be tailored for different applications by changing process parameters or by the use of versatile additives, further widening their potential and scientific importance for utilization in various applications such as for adsorption, catalysis or activated carbon synthesis.[17]

Since the initial carbon content remains mostly in the non-volatile products, the process gives also possibilities for a synthetic carbon sink in terms of sequestration, counteracting CO_2 emissions and therefore global warming. This is especially advantageous compared to a typically composting of biowaste in terms of a microbiological degradation, where mainly carbon dioxide is produced.[18]

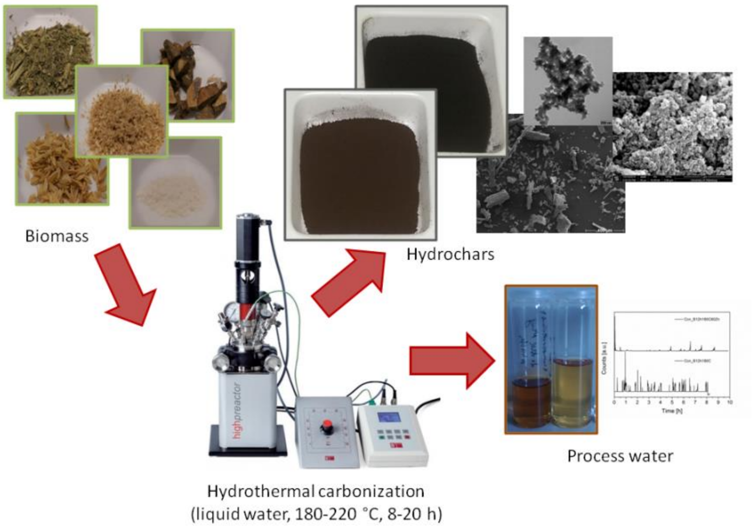

Figure 3 Scheme for the HTC of different biomass to hydrochars (the image of the autoclave was taken from a Berghof product brochure[19]).

A major advantage of the HTC process shines through when comparing its product to commercial available chars currently mostly used in the industry, such as activated carbons (AC), particularly in regards for sustainable development. Traditionally, activated carbons are synthesized from fossil fuels resulting in a dependency of finite supplies. Via the more environmentally friendly and green HTC however, recyclable and regrowing biomass, abundantly available across earth, can be used, reducing the cost of raw materials. With elevated temperatures (180-220 °C) the process is also a lot cheaper to maintain since the AC synthesis usually takes place around > 500 °C. While these comparatively mild conditions are used, the HTC is an overall exothermic process from a thermodynamic point of view, inducing potential for not only a product but also a technological usage.[20]

Another strength of the HTC lies in the fact that it does not require intensive drying of the raw material prior to reaction as compared to industrial biomass conversion processes like pyrolysis or torrefaction, where this energy-intensive step is mostly included. Often, additional water is added up to even 70 wt% or more, up to water to biomass (w/w) ratios of 5:1-20:1.[15, 21] The HTC therefore allows the direct use of wet raw materials such as highly available sewage sludge. Since the latter are currently a global and challenging issue for the ever increasing world population in terms of waste production, first studies showed huge potential in this field with improved mechanical dewatering of the obtained hydrochars, leading to better fuel properties, reduced transporting cost and possibilities for nutrient recovery.[22-26] The HTC therefore not only offers an interesting product but also a variety of possible solutions for waste management.

Besides the previously outlined advantages of the overall process and substrate possibilities, the most interesting point of the HTC from a pure material side lays in the surface properties of the resulting product. Usually, the surface of the hydrochars is covered with a variety of oxygenated functional groups (OFG) originating from the raw materials.[17] These play a major role in the possibility to use the HTC-chars as adsorbents for e.g. gas washing or waste water cleaning. Additionally, by using them as precursors for the production of chemically or physically activated carbon, a lot of their positive characteristics can also be partly transferred onto the activated carbons. This additional step is of main interest in scientific research since the low specific surface areas of the hydrothermal carbons can be increased by introducing inner porosity.

2.2 Brief history of the hydrothermal carbonization

Important scientific research on the hydrothermal carbonization started already in 1911 when Friedrich Bergius did some of the first experiments on the area of synthetic carbon synthesis.[27, 28] While other researchers previously attempted to convert biomass into coal but encountered an issue with the decomposition of cellulose, he prevented superheating and therefore the decomposition into gases by carbonizing the biomass in the presence of water in a high-pressure vessel.[28] He received coal like chars by heating up cellulose, peat or lignin with water under pressure at elevated temperatures. Even though originating from different starting materials, he assigned identical properties to them, concluding that all three substrates play an important role in natural coal formation. In the works of Berl and Schmidt from 1932, more interesting insights on thoughts by scientist of that time about the influence of the different compounds in biomass can be found.[29] Their results showed that over a range of different carbonization temperatures, lignin always had higher yields when compared to cellulose. From this they concluded more stability of the former. Beside physical parameters (temperature and pressure), initial biological effects like digestion by bacteria were also contemplated to affect the natural coal formation. As a main factor an increased temperature was seen. They could also observe that the outcome of the carbonization of cellulose could be altered by adding sodium chloride into the reaction. Doing the same with lignin as substrate showed no significant change. Until a tested temperature of 400 °C the exterior main structure of lignin remained intact. When applying mineral acids, no particular insights of lignin degradation were seen as well. Therefore, nearly a century ago scientists were already interested in understanding the influence of different factors like e.g. substrate, reaction conditions as well as additives, on the hydrochar obtained by HTC which are also topic of this work.

Luckily, nowadays a lot more techniques and measurement devices like e.g. solid state nuclear magnetic resonance spectroscopy or Fourier transform infrared spectroscopy together with knowledge from many publications over the century are available, allowing detailed study and characterization of the HTC process and the obtained hydrochars. The works of the mentioned workgroups thus put an important cornerstone in the research of the HTC process which was resumed just a few decades ago around the 1980s, with renewed increasing interest and attention in recent history, with the first industrial companies starting large-scale HTC production.[15-17, 30]

2.3 Principles of the hydrothermal carbonization

In principle, the hydrothermal carbonization (HTC) is a process in which a biomass is carbonized in water to a carbonaceous product, the so called hydrochar. Other names found in literature for the process include hydrothermal carbonification, coalification, hydrothermal coalification, hydrothermal treatment, hot-compressed-water hydrolysis, liquid hot water pretreatment, aqueous pyrolysis, aqueous phase carbonization, hydrothermolysis or wet torrefaction, while the product is also called char, HTC char, biochar, bio-coal and biocarbon.[15] These different names can lead to issues when comparing the HTC and its product with other processes or carbons based on biomass. The hydrochar is formed mostly out of degradation products of the compounds present in the biomass. While structures resistant to the HTC reactions can maintain in the hydrochar, usually particles of the biomass break under the hydrothermal conditions as shown in figure 4.

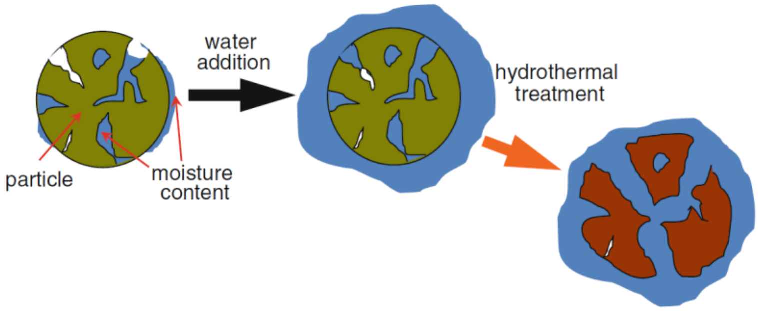

Figure 4 Particle breakage due to hydrothermal treatment.[31]

Derivates or intermediates that do not contribute to the solid are either found in the liquid phase as sugar monomers and their decomposition products as well as organic acids, or in the gas phase as mainly CO_2, depending on the reaction temperature applied (compare figure 5).[15, 32]

Depending on the starting material, the product distribution between solid residue, water soluble compounds, oil and gas varies. While cellulose shows a higher conversion and therefore more water soluble compounds than biomass or lignin, the latter shows more solid residue.[33] The HTC is usually carried out at elevated temperatures between 150-250 °C with regards to the decomposition temperature of the different parts inside the starting material and the desired char properties.[17] Closely related to the HTC are hydrothermal liquefaction and gasification which aim at producing a liquid and gaseous fuel, respectively. These are usually carried out at higher temperatures above 400 °C (compare figure 5b).[34-38]

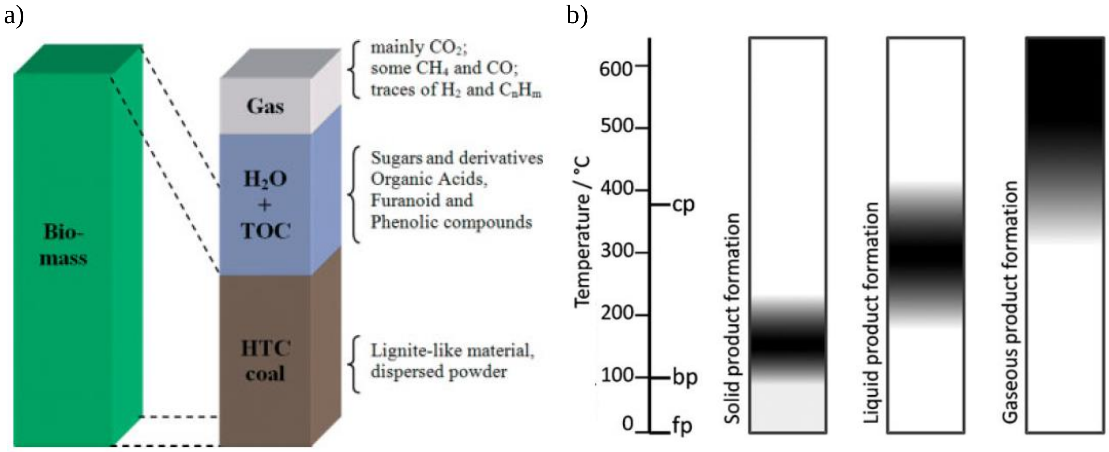

Figure 5 a) Examples of products formed in the hydrothermal carbonization.[32] b) Temperature dependence of hydrothermal biomass transformation processes (altered from Möller *et al.*[39]).

The reactions taking place in the HTC of biomass materials are indicated mostly as hydrolysis and dehydration of the compounds found in the substrate, since the resulting hydrochars have a decreased oxygen and hydrogen content with a higher percentage in carbon content. This is often illustrated by plotting the atomic ratios of oxygen to carbon against the atomic ratios of hydrogen to carbon in a van Krevelen diagram that allows the classification of biomass and hydrochars in comparison to other coals in terms of effectiveness of the HTC for fuel enhancement, with points closer to the graph origin representing a higher fuel value (cf. figure 6).[15] Since for industrial usage of the hydrochar as an energy source, the mass yield and the ratio of heat value or energy density are most important, optimizations of the process are often described for these in literature.[15] Collecting data over a range of parameters (e.g. different temperatures and times), the course of change can be visualized. The three responsible main reactions (decarboxylation, dehydration and demethylation) can then be followed with arrows as shown in figure 6.

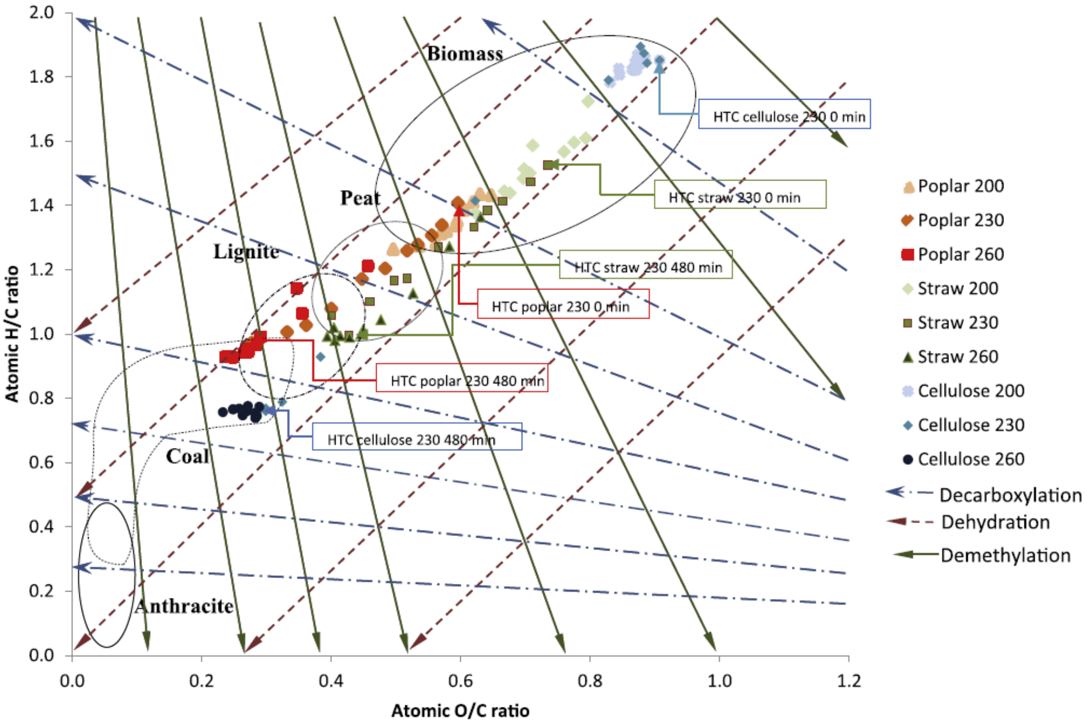

Figure 6 Van Krevelen diagram for various hydrochars from different starting materials at changed temperatures together with regions for various solid fuels and major reaction lines.[40]

Extensive research is done in literature to understand the exact mechanism of the various reactions that lead from the biomass to the final carbon product, with the complexity and amount of variations from each biomass with dozens of side reactions always providing an issue to solve. Therefore, the biomass is usually divided into smaller building units (sugars or carbohydrates, cellulose and lignin), whose reactions are in focus. The following subchapters will thus summarize the current knowledge about the various reaction mechanisms inside the HTC as divided into those for the building units and the resulting characteristics of typical hydrochars.

2.3.1 Biomass composition

In principle, any kind of biomass can be carbonized hydrothermally ranging from agricultural residues, energy crops, wood, algae to manure or sewage sludge, mostly depending on the price or availability from an industrial point of view, or the characteristics of the resulting hydrochar from a more scientific viewpoint.[41, 42]

In this work, different dry lignocellulosic biomass and its building units were used. As seen in figure 7, the cell walls of plant cells found in lignocellulosic biomass usually consist of cellulose, hemicellulose and lignin. These three form microfibril and macrofibril structures, which are responsible for the structural stability in the plant cell walls.

Further breaking down the chemical structure of the three building units shows that the cellulose, which is the main structural fiber in the plant kingdom, consists of thousands to hundreds of thousands chain linked glucose monomers, linked by β-1→4 glycosidic bonds, whose layers are stabilized by hydrogen bonds (see figure 7).[43, 44]

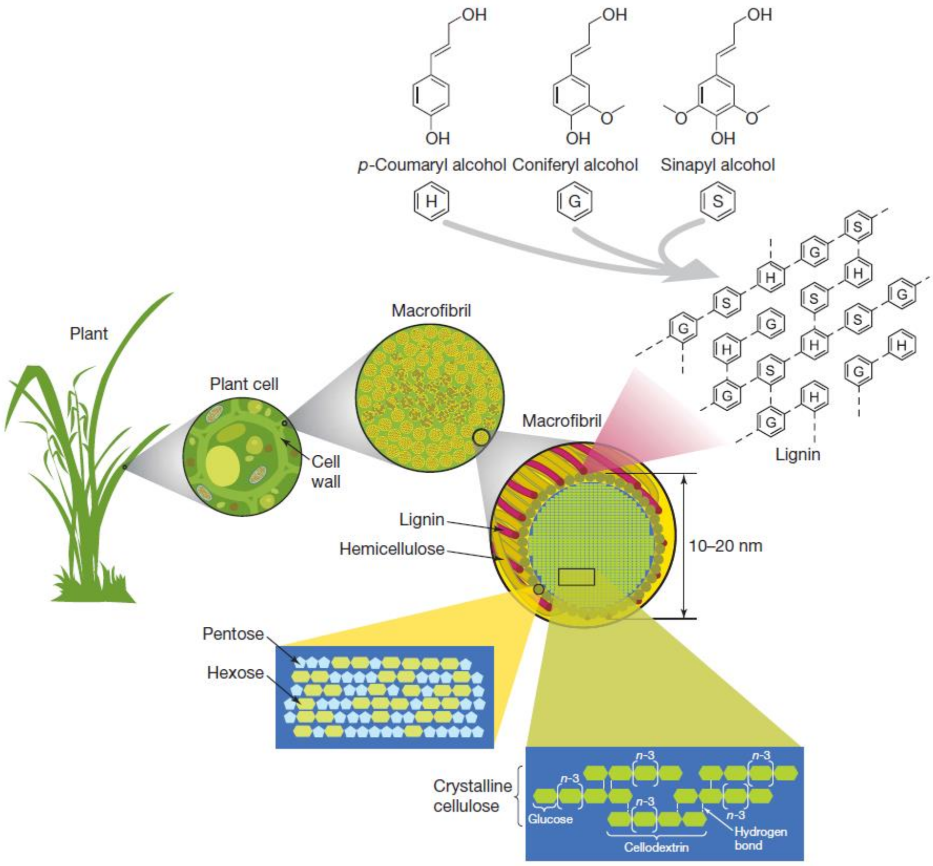

Figure 7 Structure of a lignocellulosic biomass.[43]

The cellulose molecules align into microfibrils with a diameter of around 3-4 nm and crystalline as well as noncrystalline regions. These microfibrils are aligned into macrofibrils, bound by a matrix of hemicellulose and lignin.[44] Importantly for biomass conversion processes like HTC, cellulose is insoluble in conventional solvents such as water.[45] The short chain Hemicellulose (500-3000 monomer units) is composed of various 5- and 6-carbon sugars such as arabinose, galactose, glucose, mannose and xylose.[43, 44] The phenolic compounds *p*-coumaryl alcohol, coniferyl alcohol and sinapyl alcohol are the three major components building up the lignin (see figure 7), with their ratio varying from different biomass.[43] The cellulose and hemicellulose are bound via hydrogen bonds while the latter forms covalent bonds with the lignin.[46] Figure 8 shows some of the physical and chemical properties of the three building units of lignocellulosic biomass, as summarized by Kambo *et al.*[47]

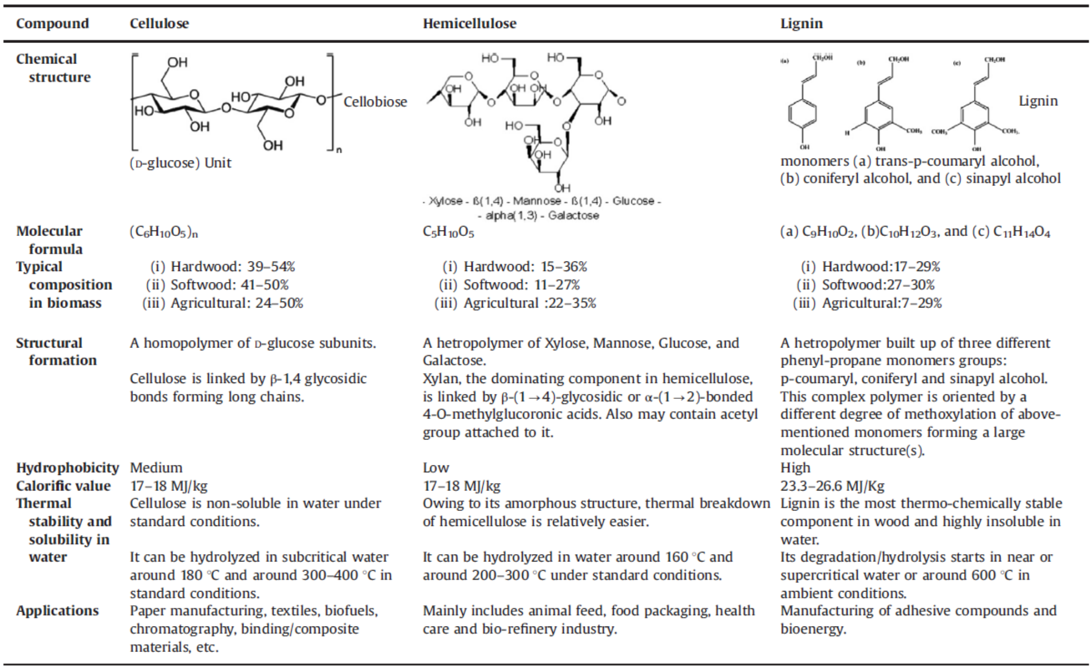

Compound	Cellulose	Hemicellulose	Lignin
Chemical structure	Cellobiose (D-glucose) Unit	- Xylose - ß(1,4) - Mannose - ß(1,4) - Glucose - - alpha(1,3) - Galactose	Lignin monomers (a) trans-p-coumaryl alcohol, (b) coniferyl alcohol, and (c) sinapyl alcohol
Molecular formula	$(C_6H_{10}O_5)_n$	$C_5H_{10}O_5$	(a) $C_9H_{10}O_2$, (b)$C_{10}H_{12}O_3$, and (c) $C_{11}H_{14}O_4$
Typical composition in biomass	(i) Hardwood: 39–54% (ii) Softwood: 41–50% (iii) Agricultural: 24–50%	(i) Hardwood: 15–36% (ii) Softwood: 11–27% (iii) Agricultural :22–35%	(i) Hardwood:17–29% (ii) Softwood:27–30% (iii) Agricultural:7–29%
Structural formation	A homopolymer of D-glucose subunits. Cellulose is linked by β-1,4 glycosidic bonds forming long chains.	A hetropolymer of Xylose, Mannose, Glucose, and Galactose. Xylan, the dominating component in hemicellulose, is linked by β-(1→4)-glycosidic or α-(1→2)-bonded 4-O-methylglucoronic acids. Also may contain acetyl group attached to it.	A hetropolymer built up of three different phenyl-propane monomers groups: p-coumaryl, coniferyl and sinapyl alcohol. This complex polymer is oriented by a different degree of methoxylation of above-mentioned monomers forming a large molecular structure(s).
Hydrophobicity	Medium	Low	High
Calorific value	17–18 MJ/kg	17–18 MJ/kg	23.3–26.6 MJ/Kg
Thermal stability and solubility in water	Cellulose is non-soluble in water under standard conditions. It can be hydrolyzed in subcritical water around 180 °C and around 300–400 °C in standard conditions.	Owing to its amorphous structure, thermal breakdown of hemicellulose is relatively easier. It can be hydrolyzed in water around 160 °C and around 200–300 °C under standard conditions.	Lignin is the most thermo-chemically stable component in wood and highly insoluble in water. Its degradation/hydrolysis starts in near or supercritical water or around 600 °C in ambient conditions.
Applications	Paper manufacturing, textiles, biofuels, chromatography, binding/composite materials, etc.	Mainly includes animal feed, food packaging, health care and bio-refinery industry.	Manufacturing of adhesive compounds and bioenergy.

Figure 8 Physical and chemical properties of the main units in lignocellulosic biomass.[47]

The ratios of the different parts present in the biomass vary depending on its type (cf. figure 8), but cellulose usually contributes the highest percentage, ranging from 33-51 %, and lignin the lowest with around 21-32 % (figure 9).[48] Other parts of the biomass can be inorganic compounds, usually described as ash, or extractives. Figure 9 shows an average composition of lignocellulosic biomass, together with some of the main derived hydrolysis products.

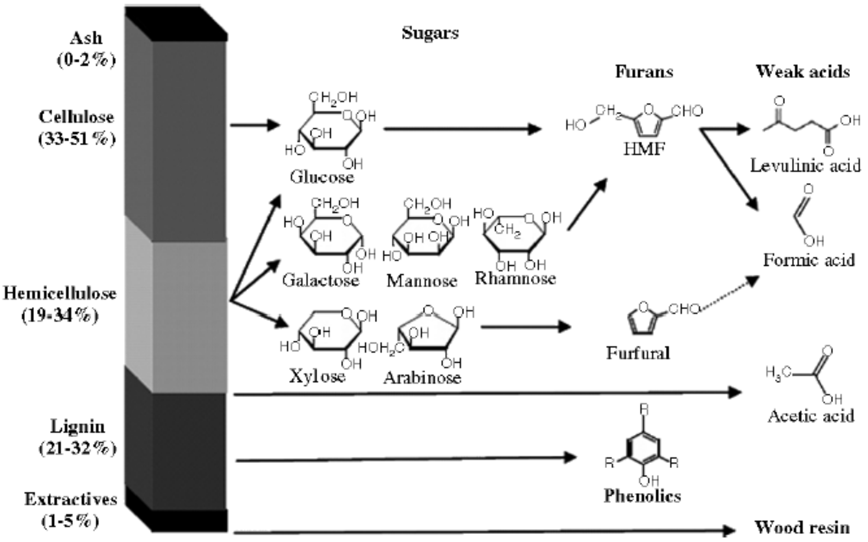

Figure 9 Average composition of lignocellulosic biomass with the main derived hydrolysis products (taken from Almeida *et al.*[48]).

The different reactions behind the formation of these will be the focus of the next subchapter.

Each building unit has not only a different solubility but also another stability as shown in figure 10 for the pyrolysis of the different components. Hemicellulose is considered the least stable while lignin seems to be stable over a wide temperature range (cf. also figure 8).[49] Additionally, when comparing the yields of the carbonization of the different biomass units as a factor for their stability as well as their actual thermal stability from thermogravimetric analysis, the trend can be described as lignin > cellulose > hemicellulose, with lignin as the most resistant.[50]

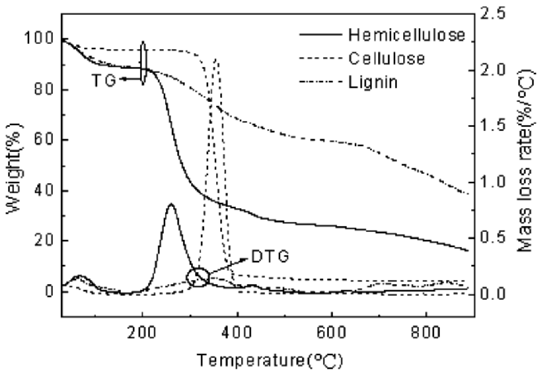

Figure 10 Pyrolysis curves of three biomass components.[49]

As mentioned earlier, the HTC process breaks up the structures of the biomass, resulting in solved and unsolved biomass fragments, their degradation products as well as resistant structures. Figure 11 underlines how the different parts of the biomass are found as a mixture making up the solid phase with water (from the reaction medium and from the bound water in the biomass) together with degradation products make up the liquid phase. Usually the solid hydrochar precipitates to the bottom of the vessel and can be collected by e.g. filtration methods.

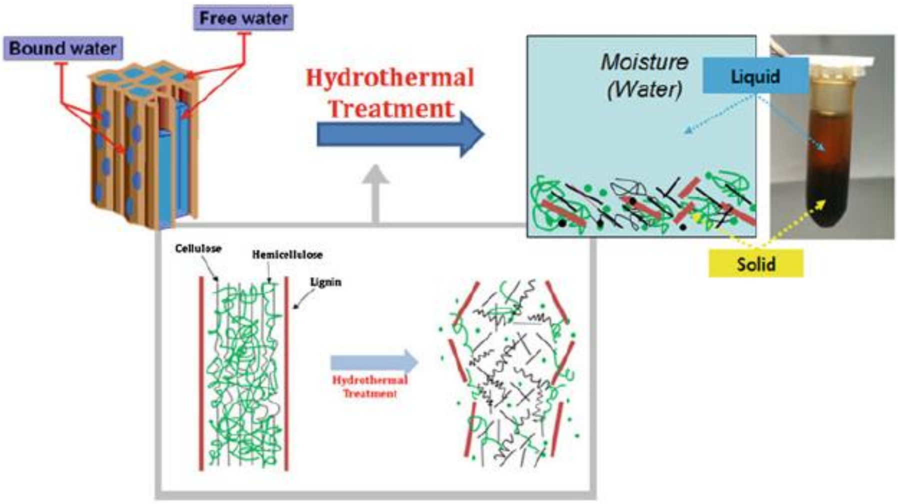

Figure 11 Change of physical structure of biomass by the hydrothermal treatment.[31]

Depending on the type and composition of the biomass used, or in other words the ratio of the building units and amount of ash present, different structural disintegration pathways take place.[16, 51, 52] For an easier classification, biomass can be grouped into hard or soft biomass. If an increased amount of lignin or crystalline cellulose scaffolds are present in the biomass, it can be classified as hard. The lignin is usually resistant under hydrothermal conditions and the crystalline cellulose provides additional stability.[52, 53] The macro and microstructure of the biological tissues in the biomass is therefore often mainly preserved in the resulting hydrochar as visible in images obtained by electron microscopy (compare figure 12a and 12c).[52] Soft biomass has an increased amount of easily carbonizable compounds present that form liquid intermediates which polymerize towards spherical particles (see figure 12d), as also seen for the HTC of most sugars, intermediates and derivates like e.g. hydroxymethylfurfural (HMF) or pure starch.[54]

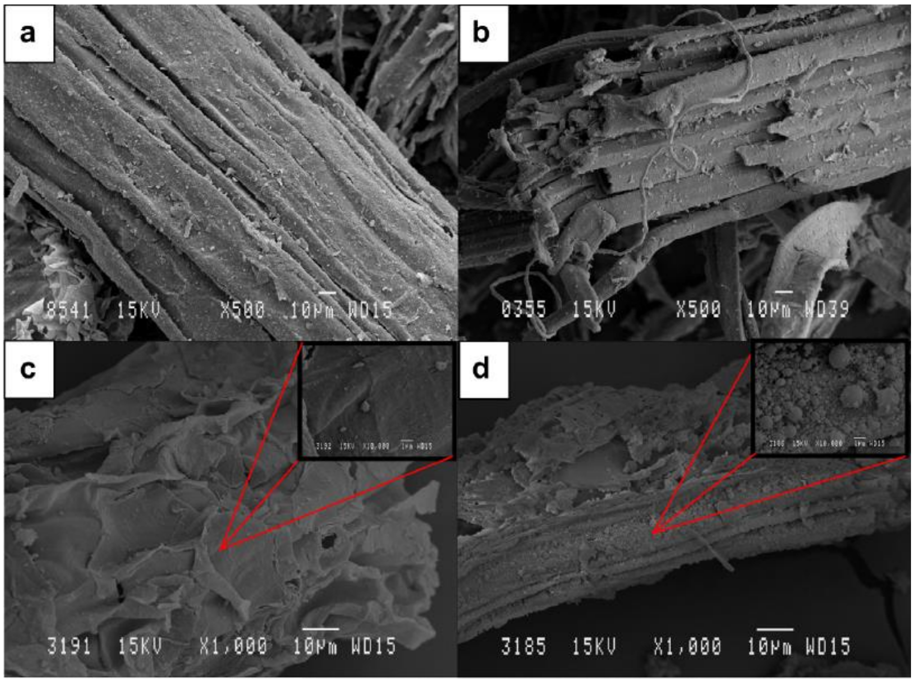

Figure 12 SEM images of a hard (a - coconut fiber matting (CFM)) and soft biomass (b - banana tree pseudostem (BPS)) and their resulting hydrochars (c - CFM; d- BPS). Taken and altered from Romero-Anaya *et al.*[52]

Therefore, depending on the type and composition of a chosen raw material, the resulting hydrochars can have a great diversity in morphology and thus characteristics, opening the possibilities for various fields of applications.

2.3.2 Reaction pathways

A scheme for principle reaction pathways in the hydrothermal carbonization from the three biomass building units hemicellulose, cellulose and lignin is shown in figure 13, as described by Kruse, Funke and Titirici.[55, 56] The main reactions include hydrolysis, dehydration, aromatization, decarboxylation and polymerization, which can all run simultaneously. The first hydrolysis reactions decompose parts of the biomass, resulting in a disrupting of its structure, with the soluble fragments undergoing further decomposition reactions to organic acids and ultimately carbon dioxide while reactive intermediates undergo polymerization towards different solid products (fractions in figure 13) that form the resulting hydrochar.[55] Depending on the reaction conditions, parts of the biomass structure can stay intact due to the compound stability, e.g. crystalline structures or HTC resistant lignin parts as described in the prior subchapter. For lignin, solid-solid interactions are also found in the scheme, implying reactions similar to a pyrolysis (see also chapter 2.3.2.3).

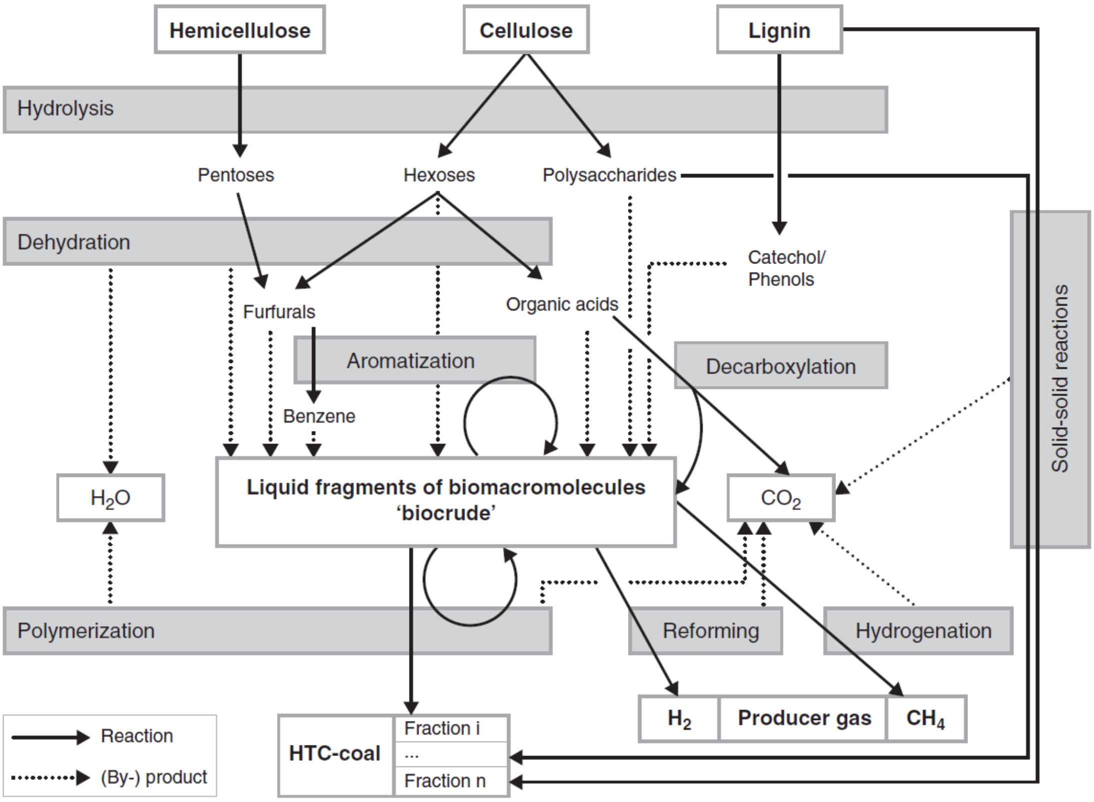

Figure 13 Principle reaction pathways within a hydrothermal carbonization.[56]

In this subchapter, the different decomposition pathways towards the hydrochar will be discussed subsequent for the three biomass building units together with their first intermediates (carbohydrates) and also complex mixtures of them.

2.3.2.1 Cellulose to hydrochar

Hydrochars from the hydrothermal carbonization of cellulose usually result in a hydrochar made up of micrometer sized spheres in the range of 2-10 µm.[57] Several studies on the mechanism of the reactions that take place when cellulose is treated hydrothermally can be found in literature and were summarized by Sevilla and Fuertes as shown in figure 14.[15, 57-62] Depending on the temperature, different changes in the cellulose structure are dominant. The first step is the breaking of the cellulose to cellulose oligomers or its glucose monomers by hydrolysis, catalyzed by hydronium ions generated through water autoionization.[57] The oligomers of the cellulose, which are already formed at around temperatures as low as 100 °C, can crosslink towards a solid product. This process increases with temperature and becomes significant towards temperatures of around 270 °C.[61] While formation of glucose monomers out of the amorphous cellulose parts by breaking of the glycosidic bonds can take place at temperatures of around 150 °C, above 180 °C are necessary to break crystalline cellulose portions for the formation of glucose due to its strong intra- and intermolecular hydrogen bond network.[63] Since only relatively small concentrations of monomeric sugars are usually detected in the reaction solutions a rapid degradation of cellulose to furfurals can be suspected (center of figure 14).[64]

The formed glucose and its isomerization product fructose can on one hand decompose to form different organic acids that can be found in the liquid phase and which result in the creation of further hydronium ions that catalyze degradation in subsequent reaction stages. On the other hand, they can change by dehydration and fragmentation reactions (i.e. ring opening and C-C bond breaking) to different compounds, most interestingly furfural-like compounds (e.g. hydroxymethylfurfural (HMF) (cf. figure 15)). While the degradation of those can further result in the formation of more acids and also aldehydes, polymerization or condensation reactions like intramolecular dehydration and keto-enol tautomerism, respectively, lead to the formation of soluble polymers. These can form aromatic molecules that can cluster together to bigger aromatic structures by dehydration. Here, a lot of C=O groups due to the dehydration of water from the hydroxylgroups of the monomers and also C=C bounds from the keto-enol tautomerism or from intramolecular dehydration, are formed, which are some of the main groups found when characterizing hydrochars by e.g. infrared spectroscopy.

Most importantly, at the critical saturation point of the aromatic clusters, solid particles start to form by nucleation. Their growth is supported by other chemical species present in the solution that bind to their surface through oxygen functionalities, resulting in the formation of stable oxygen groups such as ether or quinone groups. The oxygen present in the final hydrochars therefore forms less reactive groups in the core (i.e. ether, quinone, pyrone, etc.), while the outer surface contains a high concentration of reactive oxygen groups (i.e. hydroxyl, carbonyl, carboxylic, ester, etc.) as shown in the bottom part of figure 14.[57]

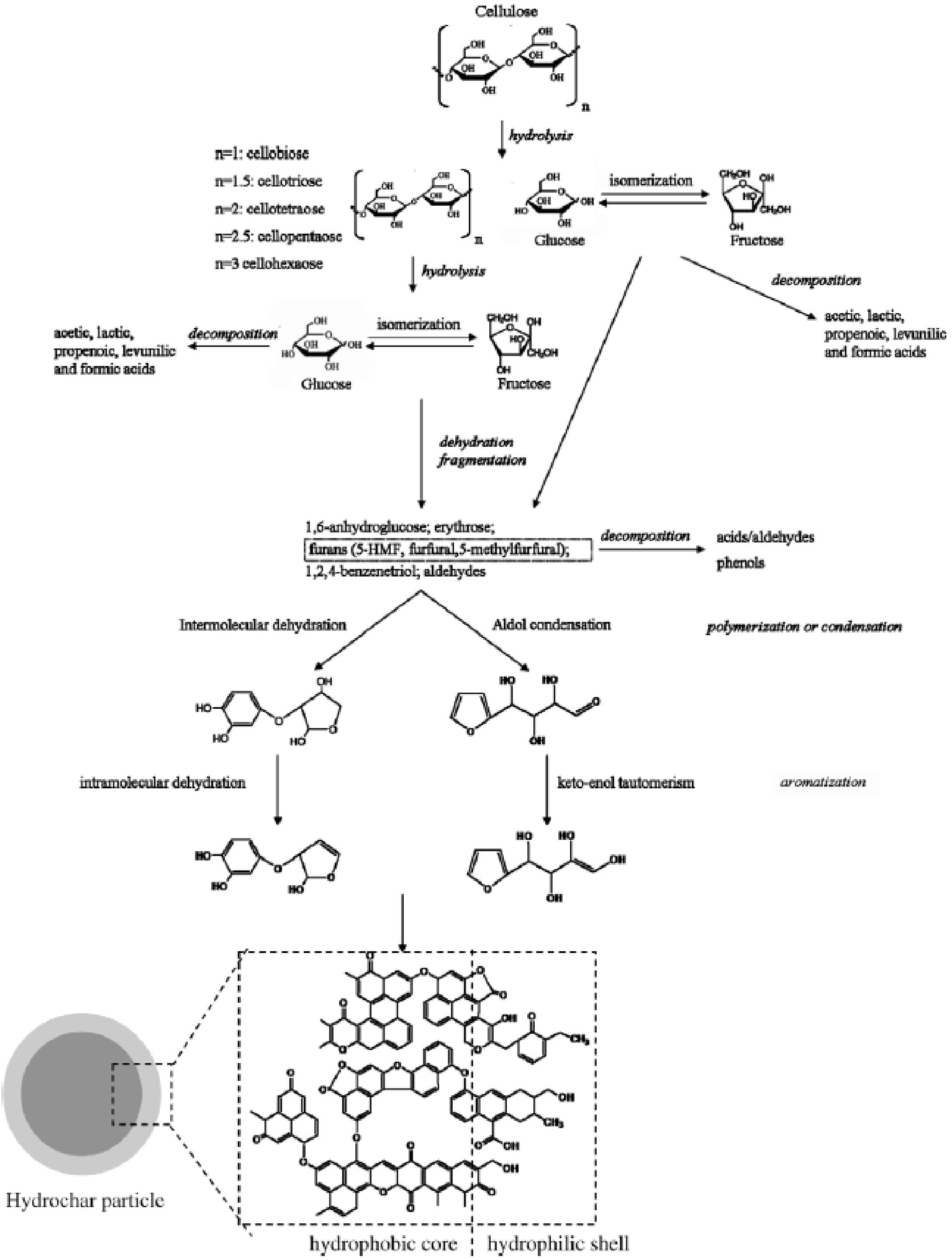

Figure 14 Mechanism of formation of hydrochar particles from cellulose as summarized by Sevilla and Fuertes.[57]

Besides the route over the polyfuranic intermediates as shown in figure 14 after hydrolysis into individual monosaccharides, Falco *et al.*[53] described a direct transformation of the cellulosic substrate towards the hydrochars as the major mechanism route above 200 °C in the absence of a strong acid catalyst or harsher processing conditions (T < 280 °C) similar to a pyrolysis (figure 15). In this, only a minor part of the cellulose in direct contact with the water undergoes hydrolysis towards glucose. Mostly intramolecular condensation, dehydration and decarboxylation reactions lead to an aromatic network composed hydrothermal carbon.

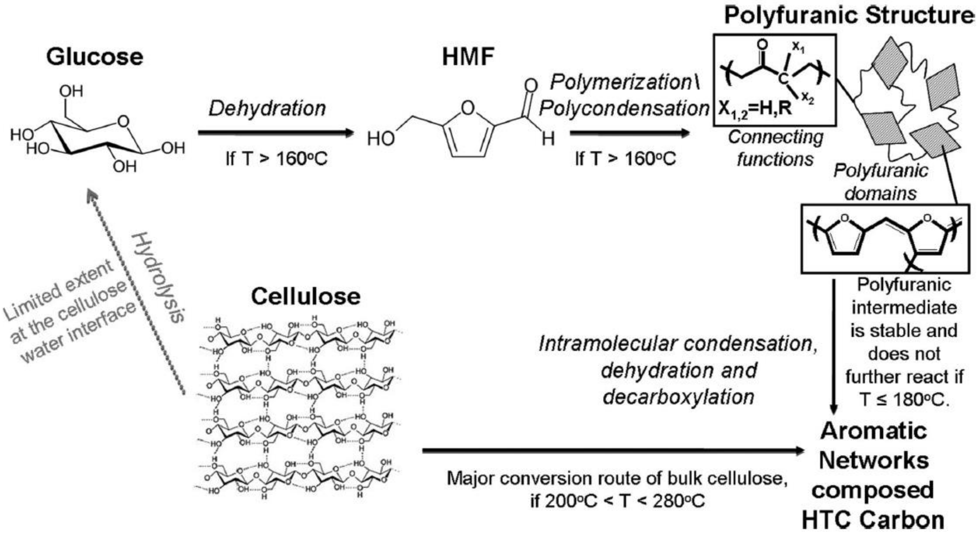

Figure 15 Reaction pathways for the HTC of cellulose as proposed by Falco *et al.*[53]

2.3.2.2 Hemicellulose to hydrochar

Due to its amorphous nature and better water solubility[65], hemicellulose is more reactive under hydrothermal conditions than cellulose.[15] Its heterocyclic ether bonds that chain different monosaccharide units (compare figure 7) such as hexoses (galactose, glucose and mannose) and pentoses (arabinose and xylose), are available for hydrolysis reactions, catalyzed by the hydronium ions formed in the HTC process. For the understanding of the reactions included in hemicellulose carbonization, Pikowska *et al.* described the decomposition of xylan as a model compound, as shown in figure 16a. Following their scheme, xylose (2), arabinose (3) and acetic acid (4) are the first intermediates after depolymerization and cleavage of acetyl groups of the xylan (1). Different furfurals form from the dehydration of the pentoses (4-5). Pinkowska *et al.* discussed mostly the degradation of the furfurals towards acids (9, 12), aldehydes (7-8, 11) and acetones (10) found in the liquid phase, but an aromatization and polymerization similar to that discussed for cellulose (compare figure 14), is likely to appear accordingly, resulting in the formation of a solid HTC-coal.

Such similar pathway was proposed for D-xylose by Kang *et al.* (figure 16b).[50] They received microspheres with diameters of 1-5 µm from the carbonization of D-xylose.

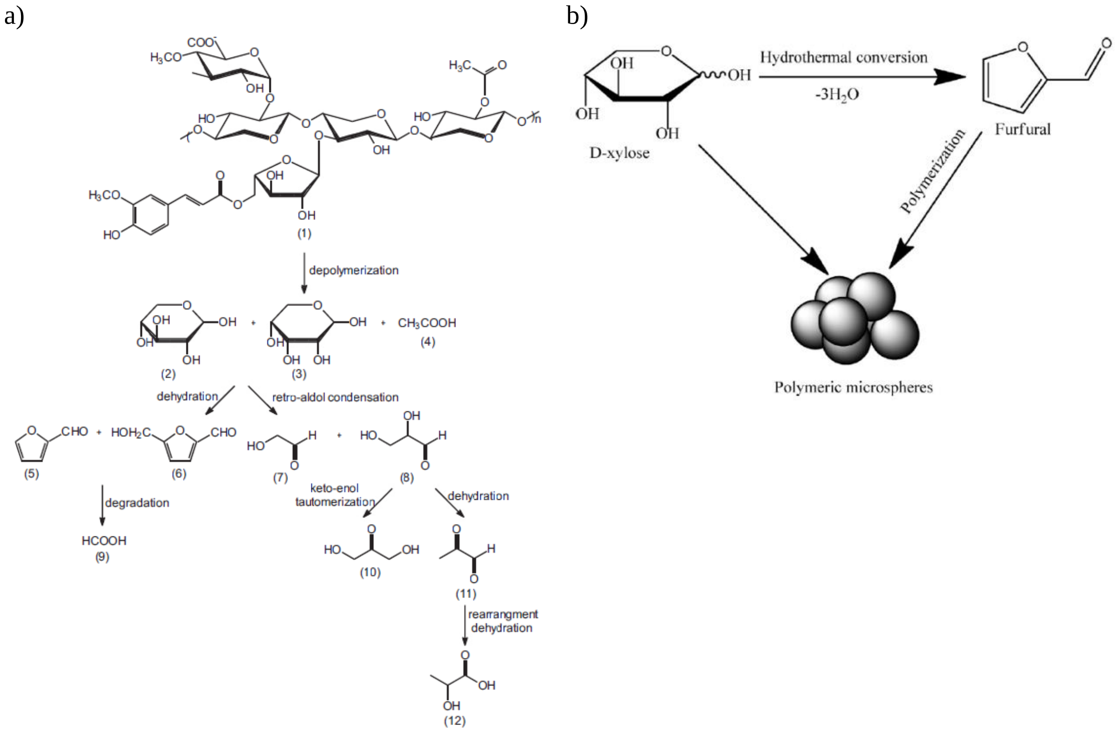

Figure 16 Reactions involved in the hydrothermal carbonization of xylan.[50, 66]

2.3.2.3 Lignin to hydrochar

Usually, lignin is reported as mostly resistant under usual HTC conditions[67], with e.g. no degradation of the phenolic compounds taking place until 260 °C.[40, 68] While some parts are reported to be soluble at already 200 °C[69], the structure is reported to change slightly around 240 °C due to demethylation and dealkylation reactions.[70] However, some lignin fragments and intermediate structures remain even at 375 °C.[71] Above 377 °C lignin dissolves and undergoes hydrolysis and pyrolysis to phenolics.[72] Dissolved lignin fragments decompose to phenols even at lower temperatures through hydrolysis that can locate on the surface of the polyaromatic hydrochar formed from the nondissolved lignin, as shown in figure 17.[50] At temperatures below 300 °C, solid-solid conversions seem to be the preferential reaction with the hydrochar resulting from a heterogeneous pyrolysis like reaction of the non-dissolved lignin. The resulting hydrochars shows a perforated structure with carbonized fragments located on its surface.[50, 67]

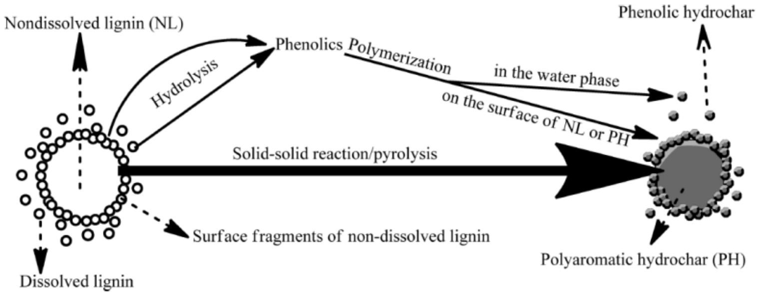

Figure 17 Mechanism of hydrochar formation from lignin as proposed by Kang *et al.*[50]

While the exact reaction pathway for the HTC of lignin is still unknown, vanillin and its precursor guaiacol were determined as the first degradation products found in the liquid fraction after HTC of lignin at around 280 °C.[73]

2.3.2.4 Carbohydrates to hydrochar

The reaction of the pure carbohydrates like D-glucose or D-fructose can be expected to follow the same reaction pathways as those shown in figure 14 for the HTC of cellulose. With special regards to these substrates, Peterson *et al.* summarized different reaction pathways of the two sugars as shown in figure 18.[74] Degradation of them leads to the formation of organic acids due to dehydration and fragmentation (ring opening), while intermolecular dehydration and aldol condensation lead to polymers that undergo aromatization followed by nucleation towards the solid hydrochars.

While it can be suspected that the formation of carbon spheres from different carbohydrates all go over the furfurals in the end, it was reported for that e.g. different cyclodextrins (cyclic connected glucose molecules) that differ in their glucose monomer number, hydrochar particles with slightly different characteristics are obtained (e.g. some result in higher aromatic carbon content than others).[75] When comparing carbons from HTC of pentoses and hexoses, Titirici *et al.* found that they both react over a different intermediate, HMF and furfural, respectively (figure 19).[54] While all carbons produced from the same type of sugar (e.g. all hexoses) showed similar characteristics in their studies, those received from another type of sugar (e.g. hexoses) were relatively different as seen by results of solid state ^{13}C NMR. Further insight into the reactions of the furfural intermediates can be found in the works of Baccile *et al.*[76]

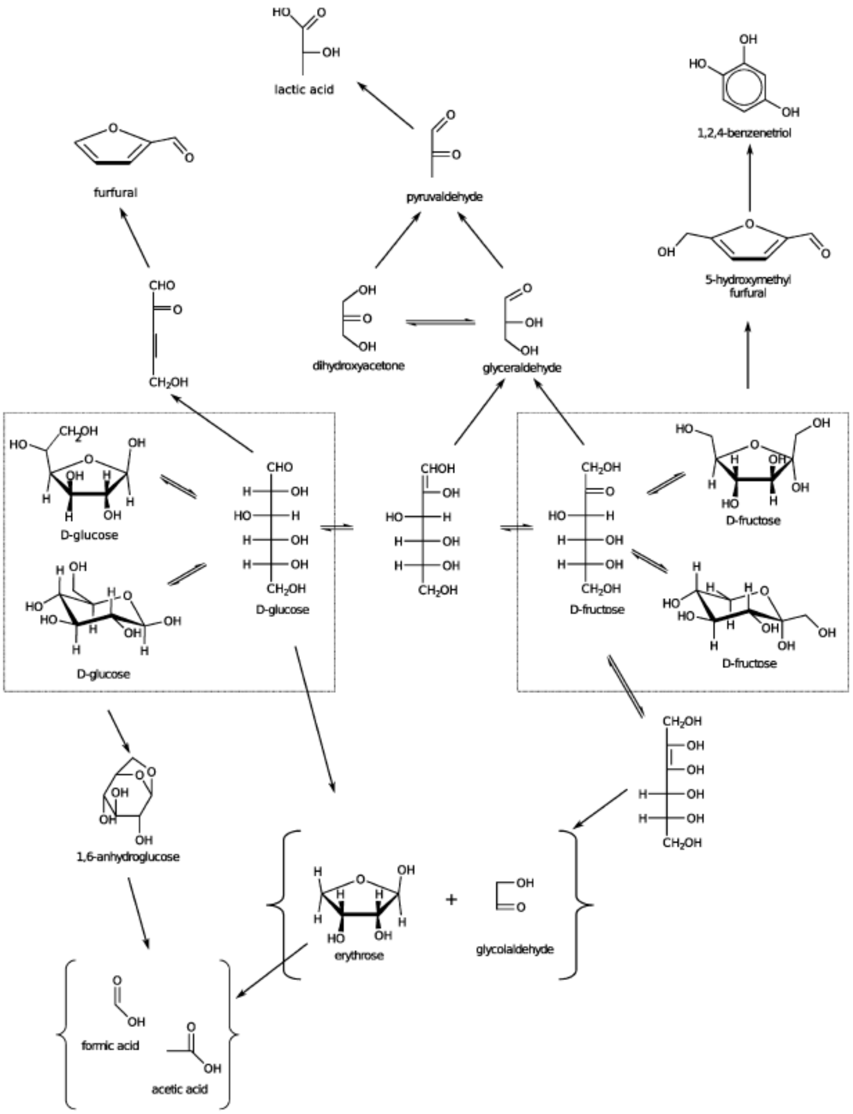

Figure 18 Pathways for the degradation of D-glucose and D-fructose.[74]

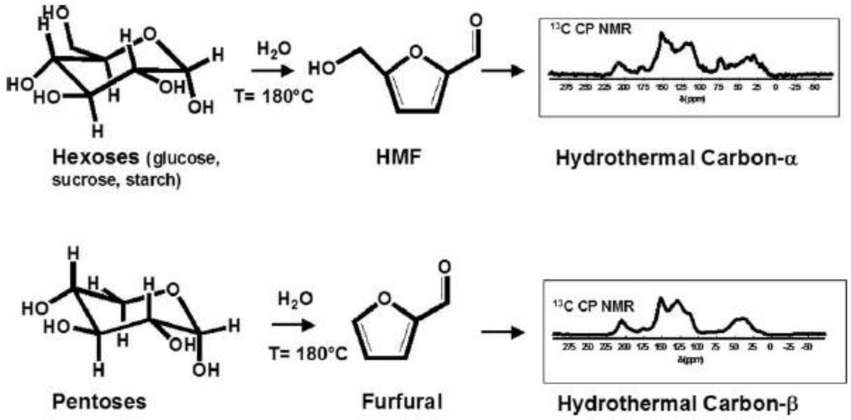

Figure 19 Reaction pathways for the formation of hydrochars from hexose and pentose sources.[54]

Contrary to the prior discussed possible reaction schemes, Yao *et al.* reported that carbon spheres form from glucose without the intermediate HMF. While for glucose temperatures of at least 170-180 °C are needed, fructose results in carbon spheres at already 120-140 °C.[77] Additionally, fructose reacts over the intermediate HMF. The presence of a more reactive furanose unit of the fructose compared to the stable pyranose group of the glucose was discussed as the main reason for the difference in needed temperature. On top of that, while glucose results in spherical carbon particles, those obtained from fructose have a rougher surface (raspberry structure) as seen in figure 20.

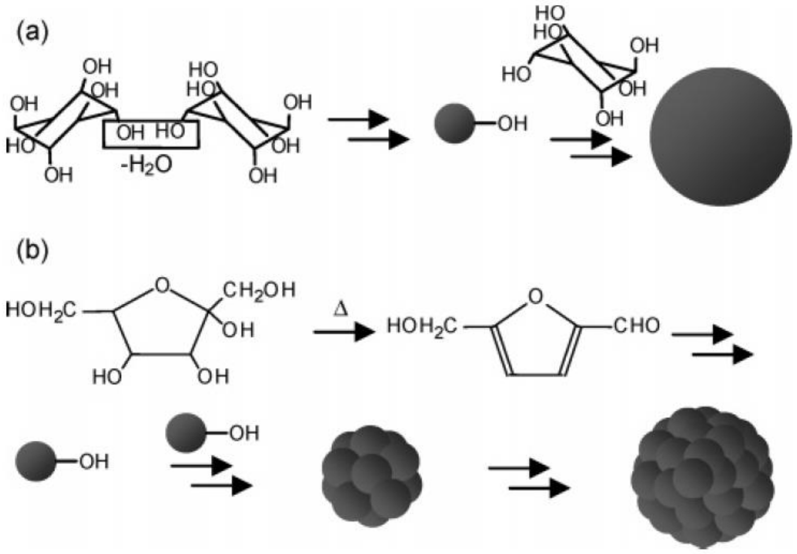

Figure 20 Dehydration and carbonization process of glucose (a) and fructose (b).[77]

The growth of carbon spheres however is agreed to result from a short single burst of nucleation when the critical supersaturation is reached, following the LaMer model[78] as shown in figure 21.[79] The final size of the spherical particles can be influenced by reaction temperature, time and initial concentration.

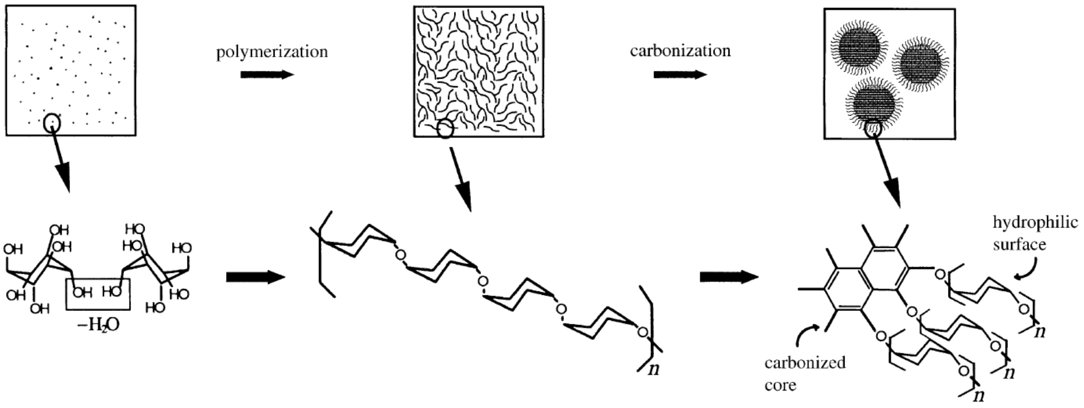

Figure 21 Schematic growth of carbon spheres.[79]

Overall, for the initial dissolved sugars (as compared to cellulose or lignin that are initially just mixed with the water), the temperature seems more crucial for a solid product to form. Sun *et al.* found out that a HTC temperature of at least 140°C is necessary to receive carbon spheres from polysaccharides (glucose).[79] An orange to red color of the solution together with an increased viscosity indicated the formation of aromatic compounds and oligosaccharides. However, the temperature is not sufficient enough for a nucleation to spherical particles and higher temperatures (e.g. 180 °C) are necessary for a hydrochar to form.

2.3.2.5 Biomass to hydrochar

While the reaction pathways of the different building units of the biomass are relatively good explained in literature, no exact mechanisms of how they might influence each other in a real natural substrate like e.g. wood could be found so far. Many workgroups use a simplified representation of reaction pathways taking place in the formation of hydrochar from complex biomass as shown in figure 22. Carbohydrate parts of the biomass preferably follow path A, degrading to solved intermediates which polymerize towards carbon particles, while stable lignin parts mainly follow solid-solid conversion processes, as described in the prior sections.[67, 80]

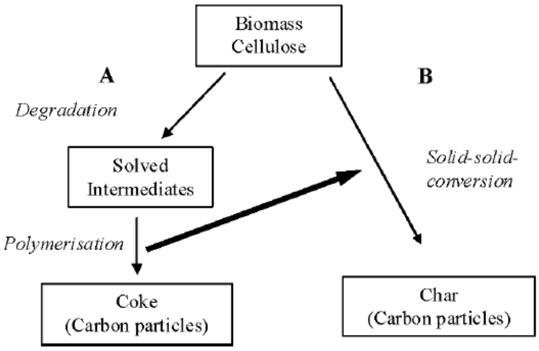

Figure 22 Simplified reaction pathways for the formation of hydrochars.[80]

Unlike for the pure building units, those present in the biomass however are expected to interact with each other, influencing the reaction pathways.[50, 67] For example, lignin was reported to enclose carbohydrates present in the biomass, inhibiting the release of soluble intermediate products.[67] Furthermore, interactions between cellulose or hemicellulose and lignin result in structure stabilization, slowing down condensation reactions.[32, 53] Due to the resistance of the lignin to hydrothermal conditions, it also maintains part of the initial macrostructure of the biomass.[53]

2.3.3 Hydrochar properties

While the properties of a hydrochar obtained by hydrothermal carbonization strongly depend and varies with the substrate, precursor or biomass used and process conditions like temperature, pressure or time and even additives, some of its features are characteristic for HTC derived carbonaceous materials, which will be discussed in the following. The direct influence of the process parameters onto these will be discussed in a later subchapter (see 2.4).

It was reported that some major characteristics of hydrochars from complex biomass substrates do not differ strongly spectroscopically and by elemental analysis from those obtained by cellulose, starch or glucose.[51] This can be explained that these follow similar degradation pathways as discussed in the previous chapter. A main difference might rise from the use of complex lignocellulosic biomass. Usually, hydrochars contain spherical carbon particles formed from HTC reactions of parts of the initial substrate, and persisting macrostructures due to temperature stable lignin parts if a complex lignocellulosic biomass was used. Hydrochars received from polysaccharides like e.g. glucose, xylose, sucrose or starch result in interconnected particles and spheres with different sizes and size distributions.[54] If the carbonization temperature is high enough, these are also found in hydrochars obtained from cellulose or lignocellulosic biomass, resulting from the degradation reactions as described under 2.3.2.[53] Contrary, due to the low carbonization temperatures, parts of the natural macrostructure often maintains in the HTC of complex biomass substrates. Therefore, the received hydrochar consists of structures found in the initial material, with the formed spherical particles on top of them (compare figure 23).[53]

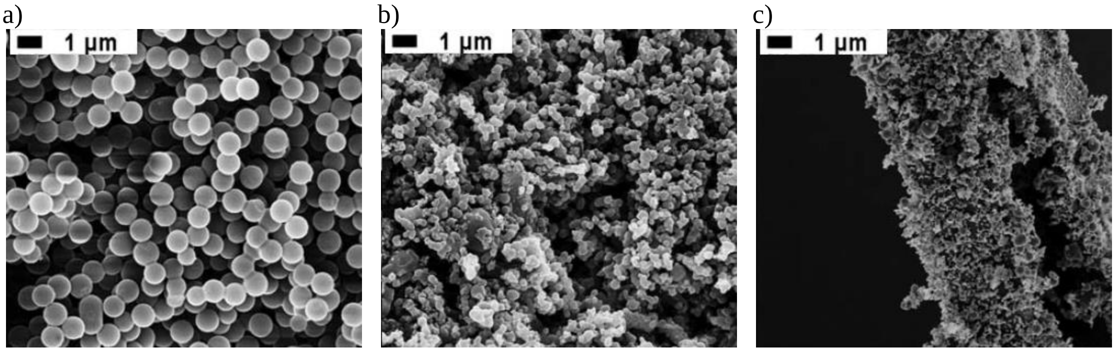

Figure 23 SEM images of hydrochars obtained from glucose (a), cellulose (b) and a lignocellulosic biomass (c; rye straw). Adapted from Falco *et al.*[53]

Together with the resulting structures, the yield and carbon content strongly depend on the used temperature. At e.g. 200 °C usually a brown to black powder is obtained with a yield between 20-50 %[81] or 40-50 %[53] for carbohydrates, cellulose or biomass (yield of pure lignin carbonization: 80-90 %) and a carbon content of around 54-55 %[81] or 60-70 %[53, 82]. Hydrogen and oxygen composition is usually in the range of around 6 % and around 40 %, respectively.[81] Thus, respective to their parent material, the hydrochars have a higher content of carbon and lower hydrogen and oxygen present.[83] Elementally and spectroscopically all hydrochars are similar to peat.[51]

Prominent strengths of hydrochars can be seen when comparing them to conventional chars (bio- or pyrochars) obtained by high temperature pyrolysis in terms of their surface functionality (figure 24a). While they have a less stable structure (dominated by alkyl moieties) than the pyrochars (dominated by aromatics) and a lower degree of carbonization (figure 24b), their surface is rich in functional groups, resulting in a promising application possibilities like higher cation exchange capacity.[84]

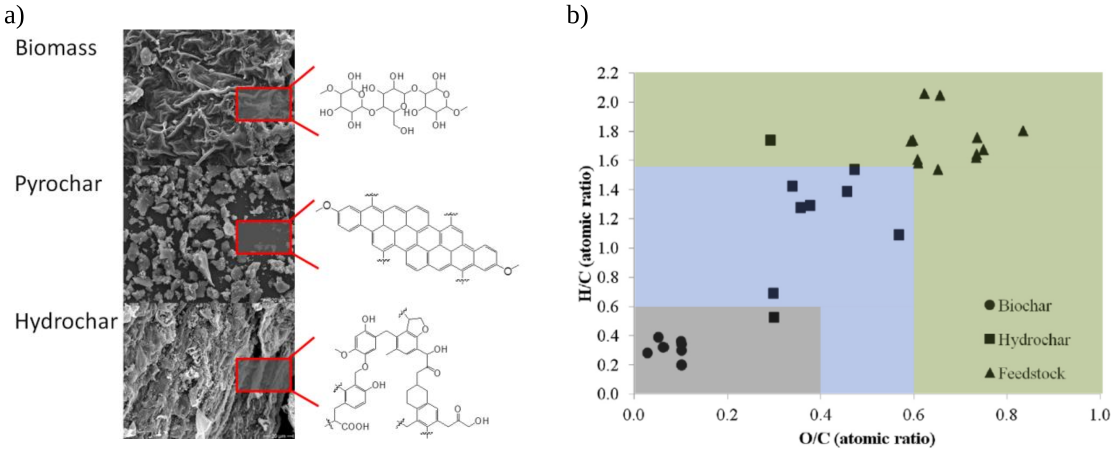

Figure 24 Comparison of biomass, bio/pyrochar and hydrochar in terms of surface functionality (a; adapted from Wiedner[85]) and their placement in a van Krevelen diagram (b; taken from Wiedner *et al.*[84]).

While pyrolysis leads to a decrease of oxygen-containing groups (OFG) up to 50 % of initial OFG, hydrothermal carbonization can increase the relative amount of OFG on the hydrochar (e.g. increasing up to 95 % when compared to the substrate), making it an effective material for ion removal from aqueous solutions.[83, 86, 87] Due to the OFG, the pH value of the hydrochars is usually in the acidic region below pH 6 whereas biochars are alkaline.[81, 82, 84, 88] Additionally, metal contents from initial biomass are less in hydrochars than pyrolytic biochars due to loss into the liquid phase, resulting in higher energy contents.[68, 89]

Typical functional groups present in hydrochars include phenolic residues, carbonyl and hydroxyl functions together with aliphatic double bonds, indicating a very polar surface structure (compare figure 25).[51] When compared to typical FTIR spectra obtained from biomass, the absorbance peak around 1700 cm^{-1} (C=O) becomes stronger.[90]

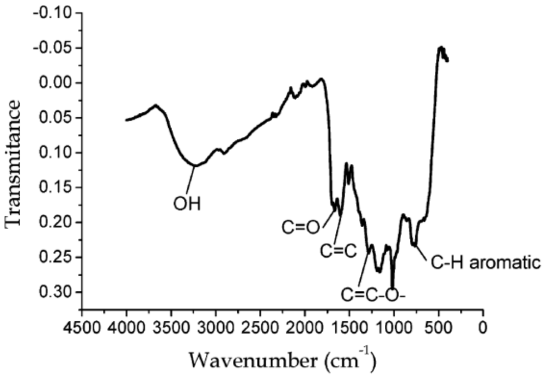

Figure 25 Typical IR spectrum of a hydrochar.[51]

An issue with hydrochars for many possible industrial applications is their poor porosity (compare table 1). Those obtained without presence of any additives, further treatment or subsequent activation process have a low or near to none porosity with low surface areas.[17]

Table 1 Specific surface areas (SSA) of hydrochars from different biomass as found in literature.

Biomass	**T [°C]**	**t [min]**	**SSA [m^2·g^{-1}]**	**Reference**
Hickory wood	200	300	3	Sun *et al.*[81]
Bagasse	200	300	4	Sun *et al.*[81]
Bamboo	200	300	1	Sun *et al.*[81]
Orange peels	200	960	< 1	Titirici *et al.*[51]
Oak leafs	200	960	16	Titirici *et al.*[51]
Pine cone	200	960	34	Titirici *et al.*[51]
Pine needles	200	960	12	Titirici *et al.*[51]
Pinewood	300	20	21	Liu *et al.*[86]
Sunflower stem	220	1200	27	Roman *et al.*[91]
Walnut shells	220	1200	31	Roman *et al.*[91]
Olive stones	220	1200	22	Roman *et al.*[91]
Palm oil fruit bunch	150-350	20	2-8	Parshetti *et al.*[92]
Glucose	180	240	< 1	Aydincak *et al.*[93]
Lactose	180	240	< 1	Aydincak *et al.*[93]
Olive oil waste	180	240	22	Aydincak *et al.*[93]
Hazelnut shell	180	240	45	Aydincak *et al.*[93]
Peanut hull	300	300	1	Xue *et al.*[94]
Corn stover	250	240	4	Fuertes *et al.*[82]
Eucalyptus sawdust	250	120	4	Sevilla *et al.*[95]
Barley straw	250	120	8	Sevilla *et al.*[95]
Cellulose	190-270	360-600	3-28	Mumme *et al.*[96]
Maize silage digestate	190-270	360-600	1-12	Mumme *et al.*[96]
Bagasse	200-300	360	4-11	Fang *et al.*[97]
Hickory	200-300	360	2-9	Fang *et al.*[97]
Peanut hull	200-300	360	< 1 - 7	Fang *et al.*[97]
Cellulose	250	240	30	Sevilla and Fuertes[57]
Holocellulose	230	540	12	Liu and Guo[98]
Wood powder	230	540	17	Liu and Guo[98]

2.3.4 Importance of subcritical water

Already Bergius described the importance of water for the hydrothermal carbonization (compare 2.2) at the beginning of the 20th century, as biomass above the liquid surface would not carbonize.[32] While he found out that it was also possible to use oil as reaction medium, other researchers clarified later that the water not only accelerates but also initiates or catalyses most reactions taking place within the carbonization.[99-101] Albeit primarily acting as the solvent but also as a catalyst (both acidic and basic), the water also participates as a reactant in the HTC. Due to changes in its chemical and physical properties over a range in temperature it can carry out cleavage, condensation or hydrolysis reactions and even effect selective ionic chemistry.[102] Because of its crucial role in the hydrothermal carbonization, the quality of the used water has a great influence on the carbonization product.[103]

Surprisingly, the amount of water needed to maintain the prior mentioned influences has been determined as very small.[32] The fact that it plays an important role in the reversion equilibrium and hydrolysis of hydroxymethylfurfural (HMF), one of the first and most important degradation intermediates of the biomass, can be used to influence the resulting compound distribution. While interested in manufacturing the platform chemical HMF, Kuster *et al.* could showed that by mixing the water with organic solvents, the yield of HMF increased, resulting in a decreased amount of solid hydrochar obtained.[104]

For dry biomass, it is also imaginable to provide water as steam in terms of a vapothermal carbonization (VTC), reducing the used water to a minimum. It was shown that the chars from VTC show a lower carbon content than those obtained by HTC, underlining the importance of the amount of water present.[105] Water dissolves fragments formed in the HTC out of the matrix, allowing the formation of spherical particles on the surface of the as-formed chars.[106] The use of a closed autoclave allows maintaining water in its liquid form at temperatures used for HTC, which are well above its boiling point of 100 °C but below its critical temperature of 374 °C, resulting in subcritical water.

2.4 Influence of HTC process parameters

Parameters that govern the resulting hydrochar properties include i.a. type of starting material, temperature, time, pressure, pH, initial concentrations (substrate as well as water) and additives. All of these influence each other, creating a complex dependency of various hydrochar characteristics upon them.[17] Here, the two main parameters, temperature and time, as well as the influence of additives onto certain hydrochar properties will be discussed. Since these are always reported for different substrates in literature, it is important to distinguish between influence as observed by building units (i.a. glucose, cellulose, and lignin) and complex biomass substrates. However, it was also reported that for hydrochars from complex biomass, the influence of the feedstock was mainly found to be crucial for N content and recovery of the hydrochar, while the temperature was the main driving force to determine the chemical composition.[88]

Earlier chapters and figures like a typical van Krevelen diagram (see figure 6) already hinted that by increasing either temperature or time, the hydrochar properties change more and more from biomass over peat towards lignite or coal. Here, it is important to discuss both parameters separately, since chars received by reactions at high temperatures for short durations are not equivalent to those received after long durations at low temperatures.[107]

2.4.1 Temperature

A first important fact of an increase or decrease of the reaction temperature is that it changes decisive properties of the water like e.g. viscosity, influencing the carbonization process.[32] Besides that, the main differences are seen in the product distributions.

The hydrothermal carbonization is usually carried out at temperatures ranging from 180 °C to around 250 °C. Since the temperature is the main factor to trigger the carbonization and degradation reactions in the HTC process, its extent decides what kind of reactions can take place. While at lower temperatures mainly e.g. ionic reactions take place, higher temperatures can lead to e.g. homolytic bond cleavage.[39] For example, the carbonization of glucose at 180 °C results in a solid material mainly composed of highly cross-linked furan units while with increasing temperature more and more condensed polyaromatic carbon structures are formed.[108] Furthermore, at temperatures above 230 °C the degradation of glucose rapidly increases.[62] Therefore, the product distribution is strongly dependent on the chosen temperature.[41] Also, due to the harsher reaction conditions, the yield of obtained hydrochars usually decreases with increasing temperature.[50]

As already mentioned prior in the discussion of the reaction pathways of the different biomass building units, certain temperature thresholds are necessary to initiate carbonization reactions and therefore structural changes depending on the material. Falco *et al.* studied the temperature dependence of glucose, cellulose and a lignocellulosic biomass (rye straw).[53] They reported a loss of yield and increase of carbon content with increasing temperature (figure 26).

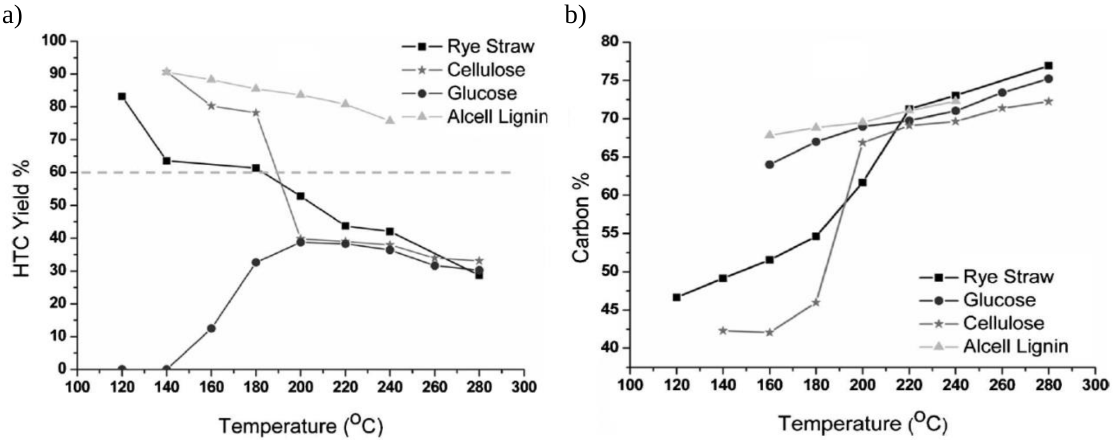

Figure 26 Yield (a) and carbon content (b) of hydrochars obtained from various materials.[53]

For glucose, a temperature of at least 160 °C was necessary to receive a carbonaceous material out of the solution (figure 26a). The initial low decrease of cellulose yield until a sudden drop between 180 °C and 200 °C indicated this region as the most crucial for the degradation of cellulose. The lignin was obtained at high yields, showing a resistance up to at least 240 °C. The rye straw as the mixture of cellulose, hemicellulose and lignin showed a mixed behavior, supporting the idea that the different building units influence each other (compare chapter 2.3.2.5). These findings are highlighted in their SEM images as shown in figure 27.

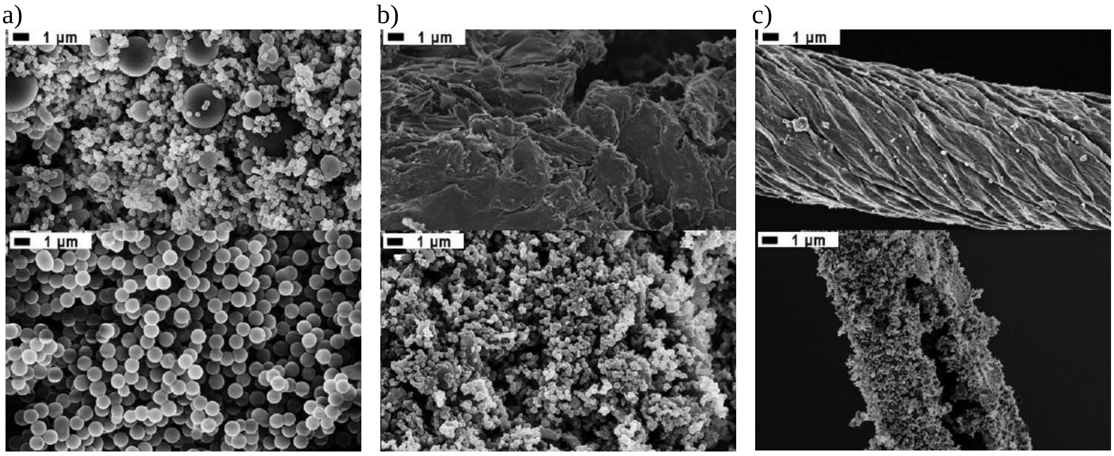

Figure 27 Structural changes of hydrochars with temperature. Hydrochars from a) glucose at 160 °C (top) and 260 °C (bottom), cellulose at 160 °C and 220 °C (b) and rye straw at 160 °C and 240 °C (c). Adapted from Falco *et al.*[53]

Glucose at 160 °C forms spherical particles, whose size distribution changes towards a more uniform size at higher temperatures (figure 27a). The cellulose and rye straw structure is maintained at a temperature of 160 °C, while carbonized particles are found on the initial structures at higher temperatures. But even at temperatures such as 240 °C, the natural macrostructure prevails due to the lignin present. They showed with solid state ^{13}C NMR spectra (figure 28), that a temperature of 280 °C is necessary to alter carbons bound in lignin methoxy groups. While in the rye straw the peaks in the area attributed to cellulose (δ = 50-110 ppm) are found until a temperature of 240 °C (contrary to raw cellulose reacting already at 200 °C), those signals also found in the lignin material are stable and weaken only at HTC unusual high temperatures of 280 °C.

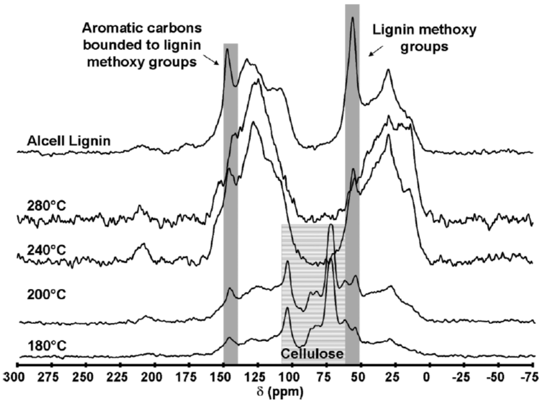

Figure 28 Changes in rye straw hydrochar with increasing temperature as seen in solid state ^{13}C NMR spectra.[53]

While Falco *et al.* reported a change in cellulose structure at 200 °C, as supported by Romero-Anaya *et al.*[109] or Liu and Guo[98], other work groups found higher temperature thresholds. In the works of Yu *et al.* cellulose would not start to decompose until a temperature of over 230 °C while degradation of hemicellulose took place at already 180 °C.[62] Sevilla and Fuertes showed that hydrochars from cellulose at a carbonization temperature of 210 °C lead to no significant chemical transformation and at least 220 °C are necessary as supported by XRD and FTIR data (figure 29) as well as SEM images.[57] They also showed that above 220 °C a drastic change in the surface functionality (figure 29b) takes place, with the changes of the FTIR bands indicating aromatization processes. These findings are supported from other works that observed a weaken of peaks in FTIR spectra, especially from -OH and -CH groups with increasing temperature.[110, 111]

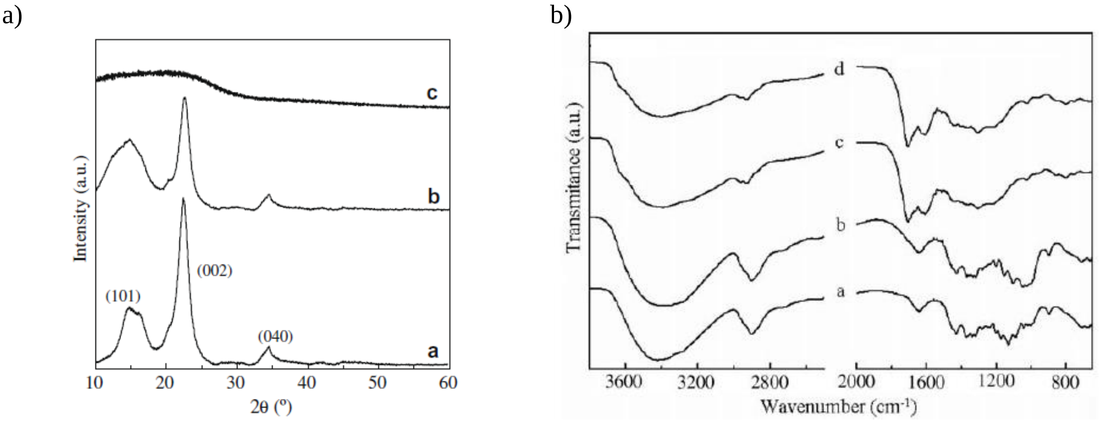

Figure 29 a) XRD patterns for pristine cellulose (a) and its chars from HTC at 210 °C (b) and 220 °C (c); b) FTIR spectra for pristine cellulose (a) and its chars from HTC at 210 °C (b), 220 °C (c) and 250 °C (d). Both images are adapted from Sevilla and Fuertes.[57]

Overall, hydrochars from various biomass become more aromatic with increasing temperature and depleted of carbohydrates.[71, 112]

2.4.2 Time

While the temperature is seen as the governing process parameter to influence hydrochar characteristics[112-117], different effects of the reaction time onto hydrochar properties like e.g. the oxygenated surface groups have been reported in literature.[17] Mainly, longer reaction times are reported to result in enrichment of nonprotonated aromatic carbons (e.g. for bark mulch or sugar beet pulp).[112]

Figure 30 shows the dependency of temperature and time exemplary for the HTC of cellulose. While at low temperatures the degradation does not significantly increase over time, at high temperatures a clear dependence is seen.[64]

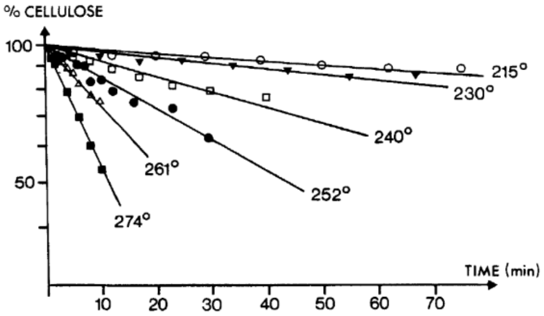

Figure 30 Percentage of original cellulose as a function of time and temperature at hydrothermal degradation.[64]

These effects may not be visible when comparing long residence times (e.g. 20 hours to 45 hours[118]) since complete hemicellulose and significant cellulose decomposition took place, but can be more obvious for shorter residence times (e.g. 3 hours to 6 hours).[119] While it was reported that most of the cellulose conversion takes place in the first 4 hours (above 225 °C)[120], the hydrolysis of carbohydrates like cyclodextrins into glucose requires 4-8 hours (at 160 °C)[75]. For sugar monomers, at high HTC temperatures (230-260 °C) nearly all solid phase reactions are finished after 30 minutes and only liquid-phase reactions take place.[121]

The spherical particles formed from carbohydrates or maybe decomposition of complex biomass building units can grow in size with increasing reaction time as seen in figure 31.[122, 123]

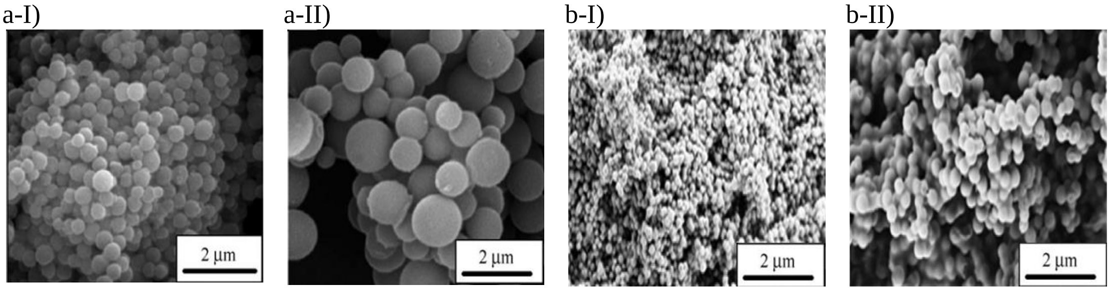

Figure 31 SEM images of hydrochars obtained by HTC of glucose for different times. a) 170 °C for 4.5 h (a-I) and 15 h (a-II); taken from Sevilla and Fuertes.[122] b) 190 °C for 5 h (b-I) and 8 h (b-II); adapted from Demir-Cakan *et al.*[123]

However, after a certain reaction time and particle size, the growth doesn't change further.[109] Kambo *et al.* reported that the effect of reaction time onto the extent of carbonization of the hydrochars is more prominent for high reaction temperatures (e.g. 260 °C).[113]

In regards of more complex biomass substrates, some works like those from Mumme *et al.* showed only a relatively little effect after varying the reaction time onto hydrochar properties like carbon content when maize silage digestate was carbonized at temperatures between 190 °C to 270 °C for 2 hours to 10 hours.[96] Heilmann *et al.* as well as Lynam *et al.* described the time as statistically insignificant when carbonizing microalgae or various lignocellulosic biomass between 30 minutes and 2 hours or 5 minutes and 20 minutes, showing positive implications for scaling from batch to continuous process methods.[117, 124] Contrary, groups like Benavente *et al.*[125], Guo *et al.*[90], Reza *et al.*[126] or Sermyagina *et al.*[119] described a decrease of mass yield with increasing reaction time and a resulting increased heating value for food wastes, lawn grass, loblolly pine or wood chips, respectively. Yet, after a certain time the yield can increase due to the formation of secondary char from increased polymerization of dissolved fragments in the liquid phase.[17] Gao *et al.* reported an increasing residence time (30 minutes to 24 hours) as favorable for the HTC of water hyacinth in terms of heating value and structural complexity as visible by SEM and TEM.[127] Increased time leads to more cellulose and hemicellulose dehydration and condensation polymerization processes, resulting in rich carbon microspheres. However, no distinct difference in the FTIR spectra of hydrochars obtained at 30 minutes, 6 hours or 24 hours was visible.

Lei *et al.* did also not observe a change in FTIR spectra when increasing the HTC time from 6 h to 44 h for corn stalk.[128] These observations were supported by the studies of the carbonization of sewage sludge by He *et al.*, who found that time did not have a significant effect on the surface functional groups formed as visible in FTIR.[23] However, detailed study of acid surface functional groups did reveal that carboxyl (-COOH) and phenolic hydroxyl (-OH) groups decreased with increasing time (4 hours to 12 hours), while the amount of lactonic groups (-C=O) increases. Guo *et al.* also observed a decrease of the bands associated with cellulose while those for C=O increased over time when lawn grass is carbonized at 240 °C.[90] Contrary, Zhang *et al.* reported an increase in carboxyl groups in the hydrochars from municipal sewage sludge when the time was increased from 1 hour to 24 hours.[129]

When looking more detailed into the hydrochar structure, Falco *et al.* showed that with increasing time polyfuranic chains composing the HTC react further by intramolecular condensation, dehydration and decarboxylation reactions towards a more condensed sp^2 hybridized aromatic chemical species, as indicated by their solid state ^{13}C NMR studies (figure 32).[53]

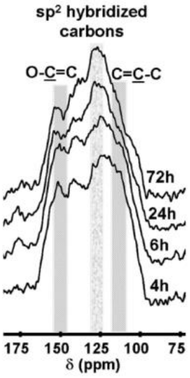

Figure 32 Structural changes in hydrochar from cellulose with increasing HTC time (T = 240 °C). Adapted from Falco *et al.*[53]

2.4.3 Additives

To change certain main characteristics of the hydrochars resulting from the HTC or to enhance the production of these, a wide range of different additives is conceivable. Often, the use of additives in terms of a catalyst for the main reactions taking place in the HTC is discussed in literature. This subchapter will therefore give an overview of additives used in the hydrothermal carbonization with regards to the initial scientific focus (obtain valuable chemicals like HMF) towards the effects on hydrochar properties.

2.4.3.1 Additives for reactions towards valuable chemicals

Early studies on the use of additives in aqueous low temperature reactions of biomass building units like hexose sugars such as glucose or fructose mostly had the production of their furan derivates (e.g. HMF) as important platform chemicals in focus. The hydrochar was usually just a solid byproduct. Aqueous mineral acids[130], organic acids[131], acidic ion exchange resins[132, 133], enzymatic catalysis[134], metal chlorides in ionic liquid solvents[135, 136], molecular sieves (MCM)[137] or zeolites[138] were found to have a catalytic effect onto many of the reactions taking place in the formation of the intermediates and byproducts. A drawback of many of these is the additional formation of unwanted levulinic acid and formic acid, resulting in increasing cost of product purification.[135] However, by using certain e.g. mineral acids, the yields of HMF and its rehydration product levulinic acid can be controlled.[139, 140] With increasing acidic conditions (pH 2.0 or 1.0) the yield of levulinic acid increases considerably while at less acidic conditions (pH 2.5) HMF and also its conversion product 1,2,4-benzenetriol are favored. While not explicitly mentioned in literature as crucial, the latter two in fact are major contribution intermediates to the formation of carbon particles by polymerization[141] and exact control of the acidic conditions would allow keeping the levulinic acid formation low towards higher hydrochar yields (compare figure 33).

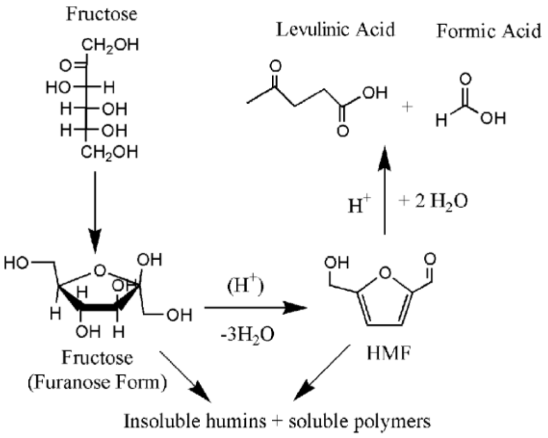

Figure 33 Reaction scheme for acid-catalyzed dehydration of carbohydrates. Adapted from Qi *et al.*[133]

Additionally, the nature of the acid has great influence on the decomposition pathway and therefore onto the yields and byproduct amounts. Phosphoric acid with a relatively weak acidity leads to less rehydration of HMF towards levulinic acid, resulting in higher HMF yields.[139, 140] Lanthanide(III) ions were also found to only catalyze the dehydration of hexoses towards HMF without further hydrolysis to levulinic acid.[142, 143] Different Lewis acids like boron trifluoride etherate ($BF_3O(C_2H_5)_2$) were also recommended for the HMF production from carbohydrates while other compounds like zinc chloride showed low HMF yields.[144]

When comparing homogeneous catalysts (H_2SO_4 and NaOH) with heterogeneous catalysts (TiO_2 and ZrO_2) for the HTC of glucose, Watanabe *et al.* found that acid catalyst promoted dehydration to HMF while alkali catalyst increased isomerization of glucose to fructose.[145] This was supported by Takagaki *et al.* who combined the HMF synthesis from monosaccharides and disaccharides by use of solid acid and base catalysts in a one-pot HTC reaction.[146] Cabiac *et al.* described that some heterogeneous catalysts like e.g. silicoaluminate zeolites, sulfonic resins or sulfated zirconia are not suitable for the use within the HTC since they are not stable under hydrothermal conditions.[45] They also pointed out that while an increasing temperature is favorable for cellulose hydrolysis, care has to be taken for the thermal stability of the catalyst. Chareonlimkun *et al.* concluded that heterogeneous acid catalyst like TiO_2, ZrO_2 or SO_4-ZrO_2 were beneficial for the production of furfural and HMF from sugars, cellulose and lignocellulose.[147] Interestingly, those prepared from chloride-based precursors (i.e $ZrOCl_2$) showed higher reactivity than those from nitrate-based precursors (i.e. $ZrO(NO_3)_2$) due to their greater acidity.

Similar research was done for cellulose, with focus on multifunctional catalysts for cellulose transformation towards valuable products such as sugars, alcohols, acids or polyols since simple solid acid catalysts showed poor activities as summarized by various work groups.[45, 148-151] Usually, homogenous catalyst are added to enhance cellulose hydrolysis (splitting of β-1,4-glycosidic bond). It was observed that acids like sulfuric acid or maleic acid can hydrolyze β(1-4) bonds of the cellulose parts towards glucose formation.[152] The sulfuric acid additionally catalyzes the degradation of the glucose, unlike the maleic acid. With increasing acidity a higher yield of glucose is obtained. For this, hydrochloric and sulfuric acid are mostly employed. Additionally, by swelling of cellulose in e.g. concentrated acid medium, the stable, crystalline cellulosic structure can be disrupted, easing the hydrolysis reactions. When looking at the HTC of cellobiose (disaccharide consisting of two linked β-glucose molecules) or cellulose, it was shown that different polyvalent transition metal salts of $PW_{12}O_{40}^{3-}$ can catalyze the hydrolysis into saccharides with the conversion rate increasing towards higher Lewis acidity of the cation.[153] The polyoxometalates can also act as stabilizer for primary carbon particles formed, preventing aggregation and allowing diameter control.[154] Qi *et al.* showed that HMF from cellulose can be obtained with optimized yield over a two step procedure, that included cellulose hydrolysis into glucose over a acidic cation exchange resins in an ionic liquid followed by a glucose to HMF reaction catalyzed by $CrCl_3$.[155] Additionally, alkaline solutions like sodium or potassium bicarbonate as well as reduced nickel catalyst were found to inhibit the formation of char from HTC of cellulose or biomass resulting in the formation of aqueous intermediate products and gases, respectively.[45, 156-158]

Due to their cheap and rather nontoxic nature when compared to other catalyst used for HMF production, the combination of Lewis acid metal chlorides (e.g. $AlCl_3$) and a Brønsted acid (HCl) proved beneficial.[159, 160] Molten salt hydrates were also reported as unconventional solvent systems for the dissolution of cellulose.[161, 162]

While zinc chloride showed lower HMF yields from glucose as written above, Cao *et al.* reported that it can be used as a solvent and catalyst for the hydrolysis of cellulose into smaller carbohydrates.[163, 164] On top of that, Deng *et al.* studied in detail how $ZnCl_2$ efficiently catalyzes the direct conversion of carbohydrates into HMF.[165] The strength of this additive is given by the fact that the Zn^{2+} ions in the aqueous $ZnCl_2$ solution could coordinate with two neighboring hydroxyl groups of carbohydrates or cellulose, effectively dissolving the water insoluble cellulose.[166, 167] Here, the concentration of the $ZnCl_2$ seems to be crucial, since the Zn-cellulose complex is unable to form at low concentrations. Abundant H_2O molecules lead to a complete coordination sphere of the Zn^{2+} ions as in a zinc chloride solution with e.g. 32 wt%. At high $ZnCl_2$ concentrations (> 60 wt%), not enough water molecules are present, leading to an incomplete coordinated Zn^{2+}. Therefore, higher concentrated solutions seemed beneficial for a high HMF yield.[165] Additionally, its strong acidity can enable the hydrolysis of cellulose and the dehydration of fructose to HMF. Deng *et al.* also proposed a mechanism based on the incomplete coordination sphere of the zinc ions as shown in figure 34.

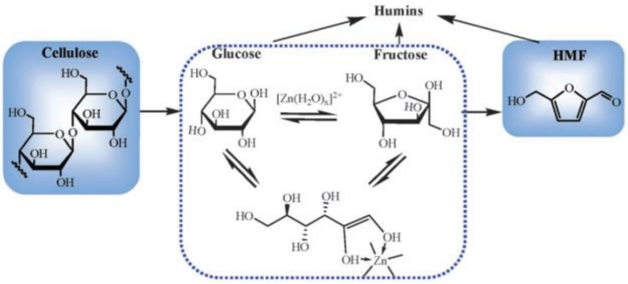

Figure 34 Transformation of cellulose into 5-hydroxymethylfurfural (HMF) catalyzed by $ZnCl_2$.[165]

They also mentioned the formation of humins (organic compounds insoluble in water) while no levulinic acid was detected. This points towards a beneficial use of the zinc chloride in the HTC towards not only HMF, but also humin formation since the degradation to the acid seems inhibited. The Zn^{2+} ions seemed to also catalyze degradation of HMF. Additionally, comparing an HCl aqueous solution with identical acidity to that of a 63 wt% $ZnCl_2$ solution, lower HMF yields were found, indicating the catalytic effect of the Zn^{2+} ions. On top of that, when comparing $ZnCl_2$ and $ZnBr_2$, they found out that although not showing a catalytic activity, the halogen ions could affect the catalytic performance of the active Zn^{2+} ions. Adding HCl or several other metal halides on top of $ZnCl_2$ resulted in an increase of HMF yield for some additives like HCl or $CrCl_3$ while others like $FeCl_2$, $MnCl_2$ or LiCl lead to a small decrease in HMF yield. Their workgroup expanded the research onto other starting materials like chitin and showed that concentrated $ZnCl_2$ aqueous solution can even catalyze HMF production from complex biomass. Here, a potential catalytic effect onto the HMF to humin degradation is considered since large amount of water-insoluble humins were formed.[168]

Other groups also reported that when using Zn^{2+} in terms of an metal sulfate (as well as other metal sulfates), an acceleration of degradation of xylose or glucose towards acids like lactic acid, levulinic acid or formic acid are observed.[141] Hence, the use of zinc ions like e.g. from zinc chloride would be most interesting when focused on the formed hydrochars.

2.4.3.2 Additives for altering hydrochar properties

While many literature studies focused on important chemical compounds mostly from the liquid phase like HMF, the use of catalysis in low-temperature carbon formation with main interest on the obtained hydrochars started just around 10 years ago by the workgroups around Sun and Li or involving Antonietti, Titirici, Yu, Demir-Cakan and Cui *et al.* in the years 2004-2006.[169-172] By using metal salts like silver nitrate[169], chlorides of platinum and ruthenium[173, 174] or iron nanoparticles[170, 175] in the HTC of different carbohydrates, metal/carbon nanoarchitectures with various shapes can be obtained. As-formed metal nanoparticles work as catalyst in the HTC reactions, greatly increasing the carbonization efficiency and speed. In these works however, the metals were encapsulated in the final carbonaceous product. Structure directing agents like anionic surfactants were also shown to have an influence on the obtained hydrochar morphology, resulting in structural complex nanomaterials.[171, 176] Furthermore, templates like silica particles can be used to alter the hydrochar morphology, its functional groups present on the surface as well as its surface area.[177, 178] Surface groups like amino groups could also be anchored onto the hydrochar surfaces as different methods showed.[179, 180] A drawback to these methods however is the necessary to remove the template by post-reaction treatment such as heat treatment or with glass-etchants like ammonium hydrogen difluoride. For example, Titirici *et al.* noted in their work, that when carbonizing glucose together with various metal salts such as magnesium chloride hexahydrate, the diameter of the obtained carbon spheres increases, indicating either catalysis of the HTC reactions or a positive influence onto the colloidal stability of primary particles formed.[181] However, no further examination of these mechanisms was done since the focus of the publication lay on obtaining metal oxide spheres with removal of the carbon via calcination. Since then, various hard templates were successfully used for the synthesis of carbon materials with different pore system.[182]

Away from really defined additives it was found that the morphology and chemical surface functionality of hydrochars can be controlled by the pH of the solution used in the HTC.[10] As an example, the HTC of wheat straw at different pH lead to an increase in the surface area towards lower pH with roughly 4 $m^2 \cdot g^{-1}$ at pH 12, over 6 $m^2 \cdot g^{-1}$ at pH 7 to 10 $m^2 \cdot g^{-1}$ at pH 2.[183] When using acids like sulfuric acids for catalyzing the HTC of rice husk, the diameter of resulting carbon spheres is also dependent on the acid concentration.[184] With increasing acid concentration, initially formed nuclei increase and grow at an accelerated rate, resulting in more irregular carbon clusters formed from aggregation of carbon nanoparticles. Many further works showed that a lot of different additives lead to carbon particles that show a rather rough surface when compared to those obtained by simply HTC. These seem to be formed from the aggregation of small particles whose size was stabilized, inhibiting their growth (compare figure 35).

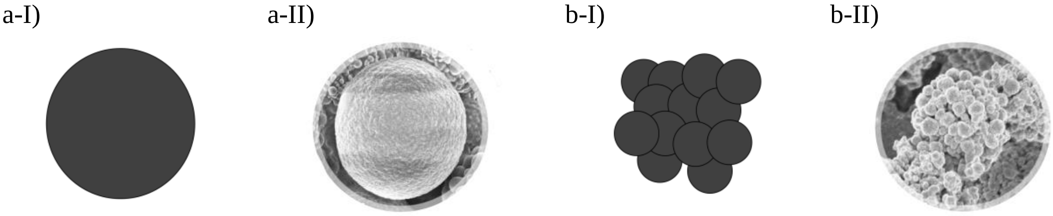

Figure 35 Idea of carbon particles formed by a) the growth of primary particles or by b) aggregation of stabilized smaller primary particles. Schematically drawn particles (I) and those seen in SEM (II, taken from Demir-Cakan *et al.*[123]).

While using e.g. *p*-toluenesulfonic acid in the HTC of furfural to introduce sulfonic acid groups, Xiao *et al.* reported that the resulting hydrochar particles showed a rougher surface than those obtained by HTC of the pure substrate.[185] The additive seemed to stabilize the as formed primary particles, preventing them from further growth before they aggregate to the carbon particles. Similar results were already reported by Demir-Cakan *et al.* who studied the HTC of glucose in the presence of acrylic acid (cf. figure 35).[123] They observed that particles with visible roughness were more present at high acid concentrations, underlining that enough acid needs to be present to stabilize all formed primary particles. They also reported that the samples obtained from pure glucose and those with acrylic acid showed no difference by Raman spectroscopy, indicating amorphous carbon materials. Except the structural change towards more visible roughness, a higher degree of carboxylic groups was present in the modified materials, resulting from incorporated carboxylic acid by cycloaddition mechanism of acrylic acid and HMF.

Further, Fechler *et al.* worked on the idea of stabilizing the primary particles and avoiding Ostwald ripening for an increased surface roughness by using salt-water mixtures with sufficient polarizability and Lewis acid character (such as especially mixtures of alkali metal chlorides with zinc chloride) for the HTC of glucose.[11] The size of the formed carbon particles are several orders of magnitude smaller than those observed from HTC of glucose without additives (figure 36). At sufficiently high concentrations of the primary particles, these can undergo cross-link towards porous materials. With increasing amount of salt, the size of the primary particles decreases, leading to high surface areas over 400 $m^2 \cdot g^{-1}$ up to 673 $m^2 \cdot g^{-1}$ (with a mixture of LiCl and $ZnCl_2$) of the resulting aggregated carbonaceous materials. However, from their results only mixtures with zinc chloride present seemed to result in increased surface area, indicating an importance role of the Lewis acid. Addition of LiCl, NaCl or KCl to the zinc chloride containing mixture is said to further lower the crystallization tendency, helping in stabilization of the primary particles.

They also pointed out that the dilution plays a crucial role, e.g. highly diluted experiments not resulting in any porous materials. Additionally, similar to as previously mentioned, different functionalities could be introduced like nitrogen by using 2-pyrrol-carboxaldehyde (PCA) as an additional additive next to the salts. Other ways to control the primary particle stability in hydrothermal carbonization of glucose while introducing nitrogen functions into the carbonaceous scaffolds was achieved by addition of proteins like ovalbumin as shown by Baccile *et al.*[186, 187] Furthermore, sulfur can be introduced next to nitrogen by adding sulfur incorporating co-monomers (e.g. 2-thienyl carboxaldehyde).[188] A wide range of other chemical modifications was summarized by Wohlgemuth *et al.*[189]

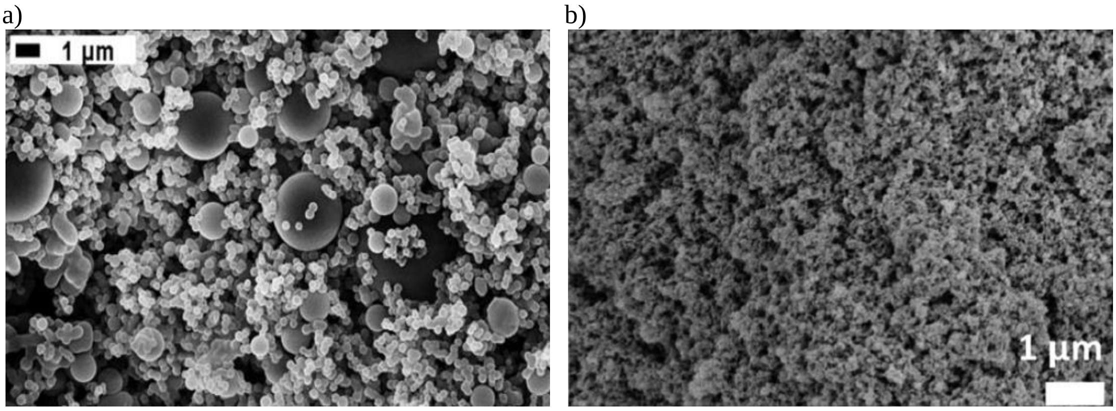

Figure 36 Hydrochars from glucose without any additive present (160 °C, 24 h) and with a salt-mixture ($NaCl/ZnCl_2$; 180 °C, overnight) as additive. Images taken from Falco *et al.*[53] (a) and Fechler *et al.*[11] (b).

Further research into the use of salt mixtures as additive like that by Alatalo *et al.* showed also high surface areas (400-500 $m^2 \cdot g^{-1}$) from well pronounced microporosity, which is unusual in hydrochars, measured by CO_2 sorption onto coals obtained from HTC of fructose in the presence of a $LiCl/ZnCl_2$ mixture, hinting an activation effect similar to those found for chemical activation.[13] Teh *et al.* showed that the use of a sodium chloride and zinc chloride mixture proved to be even more effective for catalyzing the HTC of biomass (oil palm shell fiber) due to an additional beneficial role of zinc chloride catalyzing reactions of nitrogen-containing structures present in the biomass.[14] The additives lead to increased carbon density, change in surface functionality (figure 37a), especially the disappearing of C-O signals, and increased stability (figure 37b) in the obtained hydrochars. Noticeably, lignocellulosic structures like crystalline cellulose that were present up to 220 °C in non-catalyzed HTC underwent complete degradation if the additive was present (figure 37c).

Similar results in terms of changes seen in FTIR and XRD were found by Ma *et al.* who studied the hydrothermal carbonization of corncob under saline conditions ($ZnCl_2$) for synthesizing a magnetic carbonaceous adsorbent. Interestingly, their obtained hydrochars showed increased surface areas when compared to usual hydrochars (compare table 1) to values of around 70 $m^2 \cdot g^{-1}$.[12]

However, these are only about 10 % of those obtained by Fechler *et al.*[11] or Alatalo *et al.*[13] from the more simple substrates glucose and fructose, probably reasoned by the structural complexity and stable parts of the biomass.

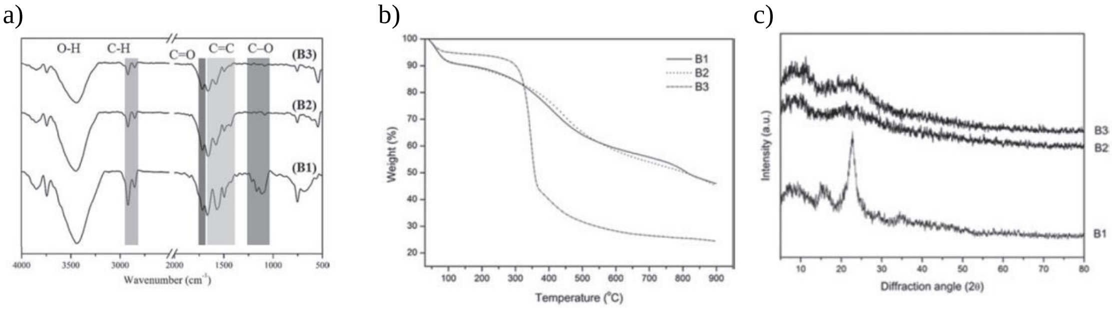

Figure 37 Characteristics (a) FTIR; b) TGA; c) XRD) of hydrochars obtained from oil palm shell fiber without additive at 220 °C (B1) or with NaCl/$ZnCl_2$ present (B2: 180 °C; B3: 220 °C). Altered from Teh *et al.*[14]

Other studies of the interactions of zinc chloride with biomass parts was done by Wang *et al.* in 2016.[190] While they focused on the formed degradation products found in the liquid phase by GC-MS chromatography with interest in converting these into chemicals and fuels, they could show that the Zn^{2+} ions in highly concentrated aqueous zinc chloride solutions can coordinate with C-O-C bonds present in lignin, leading to cleavage under hydrothermal conditions without disrupting the C-C network. Figure 38 shows their proposed mechanism for phenol formation from lignin catalyzed by Zn^{2+} ions. The zinc cations present in the highly concentrated aqueous solutions lack water molecules to form a complete coordination sphere and therefore form a coordination bond with the C-O-C bonds of the lignin (compare the role of zinc chloride discussed under 2.4.3.1 for the production of liquid products). The increased temperature in the hydrothermal carbonization triggers the disruption, resulting in the lignin degradation towards phenolic monomers and dimers.

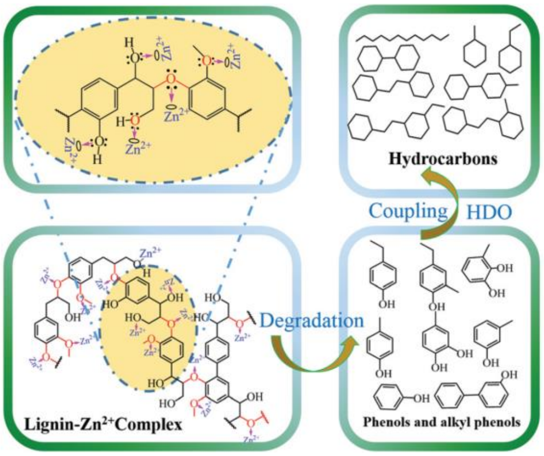

Figure 38 Interaction of lignin and Zn^{2+} ions in the hydrothermal carbonization (HDO - hydrodeoxygenation).[190]

While Zn^{2+} from zinc chloride seemed beneficial for the production of hydrochars with increased surface areas, Mai *et al.* stated that zinc ions from $ZnSO_4$ bond with acid functional groups of lignin, cellulose or xylose HTC degradation monomers, hindering a further dehydration and polymerization.[191] Similar as discussed for the catalytic effect for HMF production (2.4.3.1), the anion might play an important role onto the interaction of zinc ion with the organic compounds within the HTC reaction network.

The idea of using salts in the HTC as additives was also followed by Ming *et al.* who reported using sodium salts NaX ($X = SO_4^{2-}$, Cl^-, NO_3^-, CO_3^{2-}) in the HTC of glucose.[192] The salts such as Na_2SO_4 could accelerate the formation of visible carbon particles from glucose. Contrary to Fechler *et al.*[11], the diameter of the microparticles was several dimensions higher than those formed by HTC of pure glucose (157 nm (HTC) compared to 7.26 µm (with the salt)). Depending on the anion, different conversions of glucose degradation intermediates and carbonaceous materials took place. The resulting hydrochars had lower oxygen content when obtained with the salt present. Especially the sulfate could work as a template on one side and catalyze reactions like glucose to HMF and also intra/inter-dehydration, aromatization, cross-polymerization towards the carbon materials on the other side. Differences in the results of the both workgroups could be explained in the fact that no zinc chloride was used by Ming *et al.*, underlining the importance of the Zn^{2+}. However, both work groups showed that the salt is easily removed from the sample by washing with water and no noticeable amounts embedded or adsorbed onto the carbon particles.[11, 192]

Other salts that did not include zinc chloride like lithium chloride or calcium containing salts as well as acetic acid were also tested as additives to the HTC of loblolly pine. Lynam *et al.* observed a decrease of solid yield but an increased heating value of the hydrochar.[193, 194] From these observations, they assumed a catalytic effect of the acid as well as for the salt. No information about the surface areas was reported.

Ammonium chloride, ammonium dihydrogen phosphate, potassium chloride or sulfate and ferric chloride showed inefficient for surface area optimization in the HTC of glucose.[195, 196] Since these promote bigger particle sizes, the resulting hydrochars can have even lower surface areas ($1\text{-}2\ m^2\cdot g^{-1}$) than those from HTC of the pure substrate ($11\ m^2\cdot g^{-1}$).[196]

Other additives than salts that were also tested with the goal of increasing the surface area of the hydrochars within the process of the HTC included the use of borax (sodium borate) for the HTC of glucose as in the works by Fellinger *et al.*[197] They described the catalyzing effect of borax to be not limited only to the dehydration of glucose but also the formation of HMF by negatively charged complexes formed from sugar diols with the borax and promotion of interpolyfurance chain cross-linking reactions by a templating effect. The obtained carbon aerogels resulted from the aggregation of very small, spherical HTC nanoparticles (similar effect to that of the salts).

As with the hydrochars obtained by Fechler *et al.*, the method from Fellinger *et al.* was also extended to the introduction of nitrogen into the hydrochars by adding PCA.[198]

Additional to the structural change towards higher porosity by stabilizing effects, the yield of carbon microspheres in the HTC of sugars can also be enhanced by adding phenolic compounds since these react with the furfural and HMF formed out of the sugars.[199]

A summary of the history of the studies found in literature of hydrothermal carbonization with various additives in special regards to the surface area of the obtained hydrochars and the proposed effect of the additive can be found in table 2.

Table 2 Literature overview of HTC with additives.

Year	**Substrate**	**T, t**	**Additive**	**C%**	**SSA [$m^2 \cdot g^{-1}$]**	**Effect**	**Reference**
1998	Cellulose	200-350 °C, 1 h	$NaHCO_3$, Ni catalyst	-	-	Cat.[a]	Minowa *et al.*[156]
2004	Glucose, β-cyclodextrin, starch	160-200 °C, 12-96 h	Silver nitrate, Copper acetate, ammonium iron sulfate	-	-	Cat.[a]	Yu *et al.*[169]
2005	Glucose	180 °C, 3-8 h	Sodium dodecyl sulfate	-	-	Morph.[b]	Sun and Li[171]
2006	Furfuryl alcohol	180 °C, 24 h	Sodium dodecylbenzene sulfonate	-	-	Morph.[b]	Yan *et al.*[176]
2006	Fructose, sorbose, mannose, galactose, glucose, sucrose, cellobiose	200-320 °C, 15 min	HCl, H_2SO_4, H_3PO_4, citric acid, maleic acid, tosylic acid, oxalic acid	-	-	Cat.[a]	Asghari and Yoshida[140]
2006	Starch, rice grains	180-200 °C, 12-48 h	Ammonium iron sulfate, iron oxide nanoparticles, (ammonium bicarbonate)	-	114-402	Cat.[a], Morph.[b]	Cui *et al.*[170]
2007	Furfural	180 °C, 24 h	Silica particles	> 80	180-200	Temp[c]	Titirici *et al.*[177]
2007	Furfural	180 °C, 24 h	SBA-15	68-69	350-577	Temp[c]	Titirici *et al.*[179]
2007	Pine needles, pine cones, oak leaves, orange peels, sugar beet chips	200 °C, 16 h	Citric acid	68-73	0-34	pH < 7	Titirici *et al.*[51]
2008	Glucose	250 °C, 1-10 min	HCl, H_2SO_4, H_3PO_4	-	-	Cat.[a]	Takeuchi *et al.*[139]
2008	Glucose	-	Silicon nanoparticles	-	-	-	Demir-Cakan *et al.*[172]
2009	Glucose	190 °C, 16 h	Acrylic acid		< 50	Funct.[d]	Demir-Cakan *et al.*[123]
2010	Glucose	180 °C, 24 h	Ovalbumin	66-68	34-99	Morph.[b], Intr.[e]	Baccile *et al.*[186]
2010	Glucose	190 °C, 16 h	Vinyl imidazole with mesoporous silica template	70	170	Temp[c], Funct.[d]	Demir-Cakan *et al.*[180]
2010	Rice husk	95 °C, 6 h	H_2SO_4	62-64	-	Cat.[a]	Wang *et al.*[184]

Table 2 (continued).

Year	Substrate	T, t	Additive	C%	SSA [$m^2 \cdot g^{-1}$]	Effect	Reference
2010	Furfural	180 °C, 4 h	*p*-toluenesulfonic	-	-	Morph.[b], Funct.[d]	Xiao *et al.*[185]
2011	Loblolly pine	180-230 °C, < 1 h	Acetic acid, salts like LiCl or calcium salts	-	-	Cat.[a]	Lynam *et al.*[193, 194]
2012	Glucose	160 °C, 8 h	Polyoxometalates	-	-	Morph.[b]	Pan *et al.*[154]
2012	Glucose	180 °C, 8 h	Borax	64	84-209	Cat.[a], Temp[c]	Fellinger[18]
2012	Glucose	180 °C, 5.5 h	Lylophilized albumin powder, S-(2-Thienyl)-L-cysteine, 2-thienyl-carboxaldehyde	58-60	189-263	Intr.[e]	Wohlgemuth *et al.*[188]
2013	Glucose	180 °C	Borax, 2-pyrrol-carboxaldehyde	54-65	42-427	Cat.[a], Temp[c], Intr.[e]	Wohlgemuth *et al.*[198]
2013	Glucose	180 °C, overnight	$XCl/ZnCl_2$ (X = Li, Na, K), NaCl, $ZnCl_2$, 2-pyrrol-carboxaldehyde	65-70	0-673	Morph.[b], Intr.[e]	Fechler *et al.*[11]
2013	Glucose	180 °C, 5 h	NaX (X = SO_4^{2-}, Cl^-, NO_3^-, CO_3^{2-})	66	-	Cat.[a]	Ming *et al.*[192]
2014	Microalgae	170-210 °C, 6 h	Iron salt ($(NH_4)_2SO_4 \cdot FeSO_4 \cdot 6H_2O$)	-	38-128	Morph.[b], Intr.[e]	Peng *et al.*[175]
2015	Glucose, oil palm shell fiber	180-220 °C, 12 h	$NaCl/ZnCl_2$	56-64	598 (Act.[f])	Cat.[a]	Teh *et al.*[14]
2015	Wheat straw	200-260 °C, 6 h	Acetic acid, KOH	50-66	4-10	pH	Reza *et al.*[183]
2015	Corncob	180 °C, 6 h	$ZnCl_2$	-	70	Cat.[a]	Ma *et al.*[12]
2016	Fructose	180 °C, 16 h	$LiCl/ZnCl_2$, 2-Thiophenecarboxylaldehyde	66-70	431-554	Morph.[b], Intr.[e]	Alatalo *et al.*[13]
2016	Glucose	180-300 °C, 16 h	KCl, $NH_4H_2PO_4$, K_2SO_4, $FeCl_3 \cdot 6H_2O$	63-64	1-2	Seq.[g]	Reza *et al.*[195]
2016	Lignin	120-250 °C, 6 h	$ZnCl_2$, Ru/C catalyst	-	-	Cat.[a]	Wang *et al.*[190]
2017	Glucose	190 °C, 5 h	NH_4Cl	-	0-1	Intr.[e]	Zhang *et al.*[196]

[a] Catalyst
[b] Morphology control (e.g. stabilization of primary particles)
[c] Templating effect
[d] Change of functionality
[e] Heteroatom introduction (e.g. nitrogen or sulfur)
[f] After additional activation
[g] Sequestration of nutrients

2.5 Post-Activation of hydrochars

As shown in the previous subchapter, hydrochars usually have a rather low specific surface areas (SSA) that can't be compared to those usually found for activated carbons (e.g. SSA around 1000 $m^2 \cdot g^{-1}$), even if additives were used in the HTC process and especially not for those from complex biomass materials. Therefore, a subsequent activation step is often reported for hydrochars by either chemical activation (KOH, NaOH, $ZnCl_2$, H_3PO_4) or physical (CO_2) as reviewed and summarized by Jain *et al.*[17] While the values for the SSA vary depending on the method and starting material, a general trend shows that by chemical activation, higher surface areas (1000-3500 $m^2 \cdot g^{-1}$) are obtained than by CO_2 method (usually 400-600 $m^2 \cdot g^{-1}$). The reason for using hydrochars as precursors instead of just the raw biomass without an additional HTC step is justified by the enhanced properties of the activated carbons from hydrochars like a greater degree of micro- and/or mesoporosity, higher degree of structural order as well as increased surface functionality.[200-204] Additionally, pore size distribution of the activated carbon can be tuned by modification of the HTC temperature.[205]

For a physical activation, steam can also be used instead of carbon dioxide, potentially leading to overall better activated carbon properties like yield, surface area, ion uptake, etc.[206] When compared to chemical activation like KOH activation, a wider average pore diameter is observed for the activated carbons obtained by steam activation, pointing to a less specified product.[207] It was reported that the dense and low porous morphology of hydrochars (< 10 $m^2 \cdot g^{-1}$) can be enhanced by micropore formation after activation by steam to values of 500-600 $m^2 \cdot g^{-1}$.[208] During the activation process, decomposition of organic matter leads to the formation of the pores. The development of porosity changes with time, increasing to a certain point at which surface erosion results in decrease of surface area.

Generally, activation by steam contains the decomposition of unstructured parts of the carbonized precursor by reaction of carbon-free active sites with the water from the solution towards CO, CO_2 and H_2 which leads to the opening of pores enclosed in the carbon structure that are then enlarged by activation reactions.[209] Therefore, already existing pores in the carbonaceous precursors influence the pores present in the finished activated carbon. Removing materials closing or blocking the pores by high temperatures or use of oxidizing agents leads mainly to mesoporous hydrochars.[210]

Research was also done in the heat activation (1000 °C, nitrogen atmosphere) of hydrochars obtained in the presence of various additives such as H_3PO_4, $ZnCl_2$ or $CaCl_2$.[211] No notable differences were found in the surface properties after activation if zinc chloride was present in the HTC but washed out before the heat treatment while the other additives showed impact onto the pore sizes.

2.6 Hydrochars as low-cost adsorbents

The discovery and use of synthetic dyes for different applications such as e.g. coloring fabric has brought many advantages like cheaper production cost or higher color variety to various industries like the textile industry.[212] Annually, more than 700,000 t per year of dyes are produced (2013) and often industrial wastewaters contain various kinds of synthetic dyestuffs.[212, 213] Some of these are strongly toxic to humans, animals and plants and their nonbiodegradability increases the importance of wastewater cleaning. They are already visible at concentrations low as a thousandth of a ppm.[13] For this, the simple process of adsorption is often described as an easy and economic method that can remove pollutants too stable for other strategies like biological methods.[212] High production cost of active carbon restrict its widespread use, leading to the need of alternative and low-cost adsorbents.[214] Hydrochars have been found as low-cost, easily obtainable and recyclable adsorbents with high potential for an application in removal of dyes from wastewaters.[13, 215]

Various works studied the adsorption of dyes, especially the cationic dye methylene blue (figure 39a), onto different materials like e.g. activated carbons.[214, 216-218] Sometimes, methyl orange is used for testing an anionic dye (figure 39b).

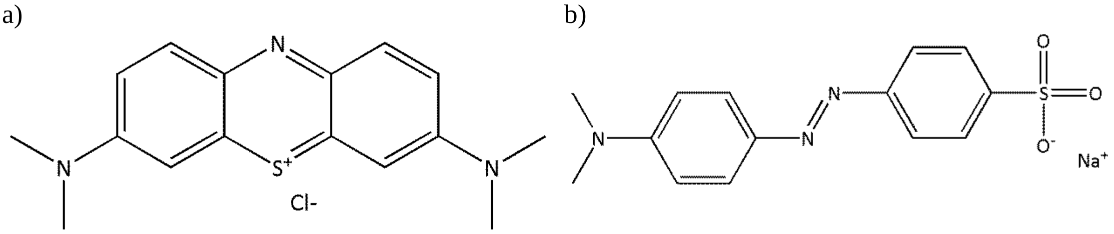

Figure 39 Molecular structure of methylene blue (a) and methyl orange (b).

Usually, the adsorption capacity at equilibrium q_e is reported for comparison of different materials. It is calculated in a way usually found in literature as described by e.g. Alatalo *et al.*[13] from the amounts of dye in solution before and after adsorption, the used volume of the solution and the mass of adsorbent (for an detailed explanation of the q_e value see chapter 3.2.3), allowing a comparison of various adsorbent materials. However, it is important to keep in mind that the comparison of adsorption values of bulky compounds like dyes can aggravate due to different states of adsorption as shown for the adsorption of methylene blue on HNO_3-etched silver surfaces, where either a lying-down or end-on state was observed, which was directly influenced by concentration of Cl^- ions in the bulk solution.[219] Here, it is imaginable that an end-on adsorption of the dye would allow more molecules to be adsorbed onto a specific area, therefore increasing the adsorption capacity.

The adsorption of the dye happens mainly due to electrostatic interactions and π-π dispersion interaction.[13] The amount adsorbed is influenced by many factors such as the surface area, particle size of the adsorbent, the solution pH and temperature, the contact time and the interaction of the dye and adsorbent.[212]

Hydrochars proved to have comparable adsorption capacities q_e to those found for activated carbons, indicating a potential application of low-cost chars obtained by HTC. Alatalo *et al.* described the use of hydrochars from fructose with a hypersaline salt mixture ($LiCl/ZnCl_2$) and found a fast adsorption process controlled by intraparticle diffusion.[13] By washing with ethanol, the dye could be desorbed and the char could be recycled for another methylene blue removal loop.

The adsorption of methylene blue onto activated carbons is considered to take place through different mechanisms (figure 40a) such as electrostatic interactions (I), hydrogen bonding formation (II), electron donor-acceptor (III) and π-π dispersion interaction (IV). Here, the most important is mechanism IV since the basal plane of an activated carbon is often constituted mainly of graphene layers with less functional groups present for the other mechanisms to take place.[220] In case of using hydrochars for the removal of cationic dyes, similar mechanisms are described in literature (figure 40b).

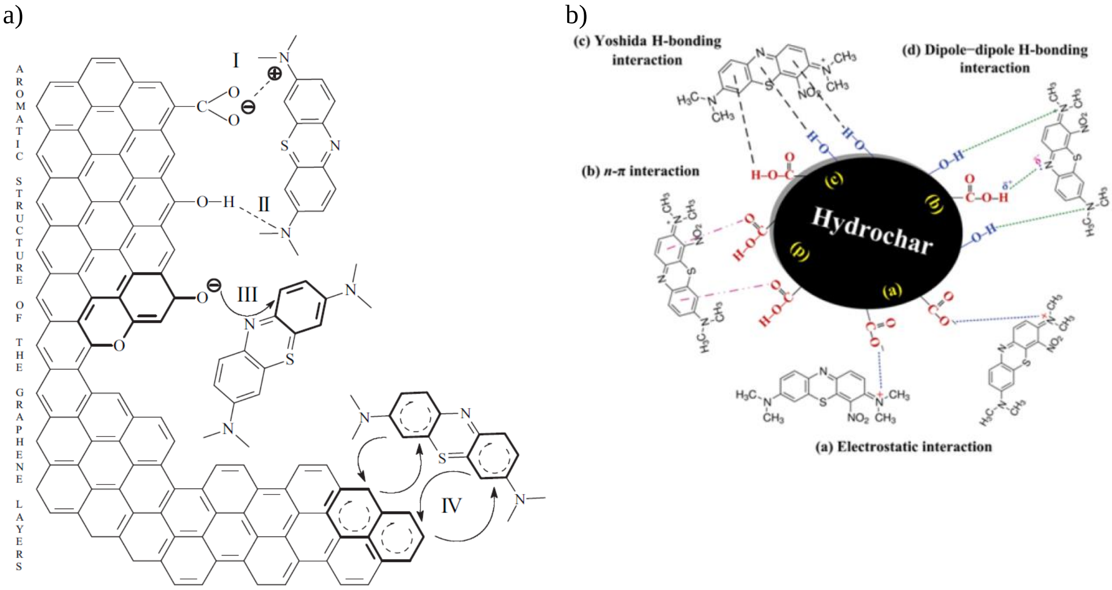

Figure 40 Proposed adsorption mechanism of cationic dyes onto different adsorbents. a) Methylene blue on activated carbon.[220] b) Methylene green on hydrochar.[221]

However, the π-π interactions seem to play a minor role in the adsorption of cationic dyes onto hydrochars since these have a weaker aromatic ring structure as supported by FTIR spectra before and after dye adsorption.[221] Figure 41 shows how the peaks corresponding to aromatic C=C bonds did not indicate a decrease, while those of -OH and C=O groups present on the hydrochar surface decrease in intensity and are shifted towards lower wavenumbers after adsorption of the cationic dye.

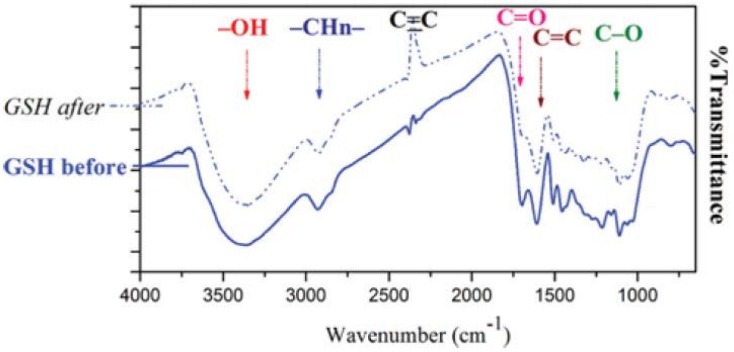

Figure 41 FTIR spectra of hydrochars before and after adsorption of methylene green (GSH - golden shower pod (biomass)). Taken and altered from Tran *et al.*[221]

It was reported for other compounds like copper, whose adsorption by carbonaceous materials follows a similar mechanisms, that hydrochars with a less well developed porous system can have higher adsorption capacities when compared to pyrolytic char obtained at higher temperatures due to the presence of more oxygen-containing groups on the surface.[86] It was shown that by increasing the surface functionality by oxygenation, the dye adsorption can be enhanced significantly.[221] Therefore, the concentration of total acidic groups (i.e. carboxylic and phenolic) present on the hydrochar surface plays a key role in its adsorption potential.

Another important factor beside the surface functionality is the available surface area. It was shown for the adsorption of dyes like e.g. methylene blue or malachite green onto activated carbons, that the type of pores available (preferably mesopores) has a big influence onto the adsorption kinetics.[222, 223] While microporous samples with surface areas of more than 2000 $m^2 \cdot g^{-1}$ took more than 25 hours to fully decolorize a methylene blue solution, similar samples that have lower surface areas (600 $m^2 \cdot g^{-1}$) but exhibit an increased amount of mesopores need less than 10 minutes.

Additionally, the size of the used dye is also crucial in the obtained adsorption capacity. While smaller dyes like the rather narrow and thin methyl orange can enter some of the pores on a micropore scale, bulkier ones like rhodamine B or fuchsin basic show limited uptake on activated carbons.[224] Since the hydrochars usually exhibit low surface areas without an extended porous structure, the contribution of pore filling in the adsorption mechanisms can be considered negligible. However, Tran *et al.* showed that after dye adsorption, the surface areas of hydrochars decrease due to pore filling which therefore seem to have in fact a certain contribution to the dye adsorption.[221]

The previous chapter introduced the idea of steam activating hydrochars to increase the surface area. Saetea and Tippayawong showed that such steam activated hydrochars are suitable for removal of methylene blue with an adsorption capacity of around 160 $mg \cdot g^{-1}$.[208] Other values of hydrochars or their activated forms found in literature for their adsorption capacities of methylene blue or methyl orange are summarized in table 3.

Table 3 Reported adsorption capacities of hydrochars or their activated forms for methylene blue (MB) or methyl orange (MO). Specific surface areas (SSA) are shown for comparison.

Substrate	**Synthesis**	**SSA [$m^2 \cdot g^{-1}$]**	**q_e (MB)**	**q_e (MO)**	**Reference**
Fructose	HTC with salts	431	83	-	Alatalo *et al.*[13]
Sewage sludge	HTC and steam activation (900 °C)	10[a], 500-600[b]	130-162	-	Saetea and Tippayawong[208]
Glucose	HTC with graphene oxide and activated	93[a], 567[b]	-	29[a], 82[b]	Martin-Jimeno *et al.*[224]
Corncob	HTC with $ZnCl_2$	70	99	-	Ma *et al.*[12]
Fructose	Ionothermal carbonization	600-1200	-	170	Lin *et al.*[225]
Finger citron	Activation	2887	935	581	Gong *et al.*[217]

[a] Hydrochar

[b] Activated hydrochar

Chapter 3

Materials and methods

Nearly all of the samples produced in this work were synthesized by the hydrothermal carbonization route with some of the most promising ones chosen for a subsequent physical activation with steam at increased temperatures as well as for tests of their potential in the removal of two different dyes from aqueous solutions. The samples were characterized by a number of methods including elemental analysis (EA), electron microscopy (SEM/TEM), X-ray powder diffraction (XRD), solid state ^{13}C magnetic resonance spectroscopy (SS-^{13}C-NMR), Fourier transform infrared spectroscopy (FTIR), X-ray photoelectron spectroscopy (XPS), gas sorption (N_2, CO_2, H_2O), thermogravimetric analysis (TGA), total organic carbon content (TOC) and high-performance liquid chromatography (HPLC).

Several substrates and additives in different cut sizes and amounts were used for the different reactions. The following chapter will give a summary of the used materials, the experimental procedure as well as an overview of the applied characterization methods.

3.1 Materials

For this work, eleven different materials in different cut sizes were used as substrates as shown in figure 42. No further treatment, purification or crushing was done and they were used as seen in each image. Each substrate is denoted by a three letter abbreviation, which is further used in the naming of the hydrochars. Some substrates were commercially available, such as glucose (Glu) by VWR (as *D(+)-Glucose anhydrous*), hydroxymethylfurfural (HMF) by Fluorochem (as *5-(Hydroxymethyl)-2-furaldehyde*), *α*-Cellulose (Cel) by Sigma (as *α-cellulose powder*) and lignin (Lig) by Aldrich (as *Lignin, alkali*). The mixture of different grasses and rushes (Gnr) was obtained from grassed areas in northeastern Oldenburg, Germany. It contained around 70 % common rush (*Juncus effusus*), 25-30 % grasses (*Poaceae*, *Cyperaceae*) and lower amounts of traces of herbs. The different grasses and rushes were already mixed and crushed to a particle size of about 0.2 mm when obtained. The coconut substrates were kindly provided from the Mahlwerk Neubauer-Friedrich Geffers GmbH as *Coconut shell granule < 1 Inch* (broken coconut shell pieces (Crw)) and *Coconut shell flour COCONIT 300* (coconut shell powder (Ccn)) and used as received.

Ricehusks (Rce) were ordered from the company Fa. kazulube and used as received. Dried dandelion leaves (Dnd) were obtained from kaninchenladen.de and shredded in a Kenwood CH580 chopper. Spirulina algae (Alg) were bought at Rakuten Deutschland GmbH as *Spirulina Platensis milled* and used as received. Sawdust (Saw) could be picked up from the mechanical workshop section of the Carl von Ossietzky University Oldenburg, Germany and was used as received.

Glucose (Glu) | Hydroxymethylfurfural (HMF) | α-Cellulose (Cel) | Lignin (Lig)

Mixture of different grasses and rushes (Gnr) | Broken coconut shell pieces (Crw) | Coconut shell powder (Ccn) | Rice husks (Rce)

Dried dandelion leaves (Dnd) | Spirulina algae (Alg) | Sawdust (Saw)

Figure 42 Images of the different substrates used in this work for the synthesis of hydrochars.

As additives to the hydrothermal carbonization, several salts were used including: zinc chloride (Acros Organics), lithium chloride (VWR), sodium chloride (Riedel-de Haën), potassium chloride (VWR), magnesium chloride hexahydrate (VWR), lithium perchlorate trihydrate (Sigma-Aldrich), sodium sulfate decahydrate (Carl Roth), sodium carbonate (Carl Roth) and zinc sulphate heptahydrate (VWR).

Two different dyes were used in the dye sorption studies which were received from ApllliChem (methylene blue) and Alfa Aesar (methyl orange). All chemicals were used without further purification.

3.2 Experimental procedure

The experimental procedure in this study contained between one to three steps, depending on the sample. First, the hydrochars were prepared by hydrothermal carbonization in a sealed autoclave (PTFE inlet) with the substrate mixed with either just water or a salt-water mixture (chapter 3.2.1). Some of these prepared hydrochars were then used for the physical activation with steam at elevated temperatures towards activated hydrochars (chapter 3.2.2). The most promising hydrochars and their activated forms were then used for the removal of two different dye molecules from an aqueous solution (chapter 3.2.3). The following chapter will describe these three steps in detail.

3.2.1 Preparation of hydrochars

For the preparation of the hydrochars starting from the substrates shown in figure 42, two different autoclave types were used (see figure 43). Small autoclaves allowed using sample solutions up to 200 mL (figure 43a). The mixtures were transferred in a PTFE inlet, which was put into the stainless steel autoclave and sealed using socket head screws. The autoclave was then put into a preheated oven and stored for the desired time. Neither use of a temperature ramp (heating phase) nor observation of the pressure inside the reactor was possible with this setup. Up to ten times more sample solution could be used in the setup shown in figure 43b, which included a 2 L stainless steel autoclave provided by the company Berghof.

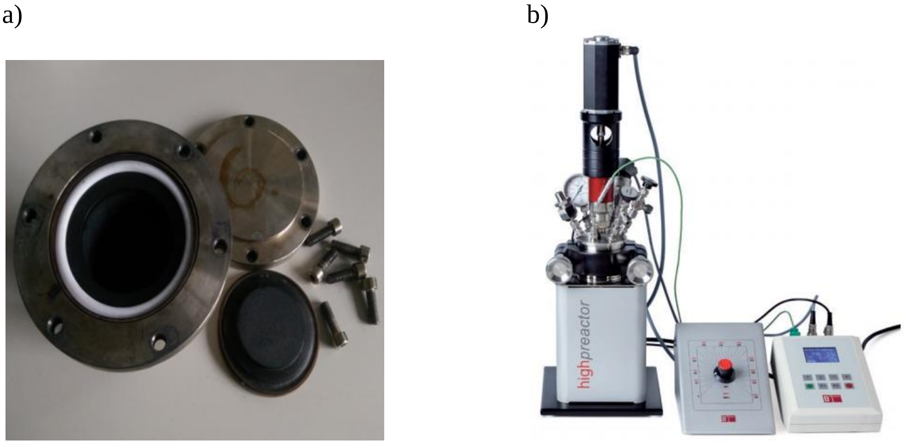

Figure 43 Autoclaves used in this work: 200 mL PTFE lined autoclaves (a) and a 2 L high pressure reactor BR-2000 by Berghof (b). Image b of the autoclave taken from a Berghof product brochure[19].

Here, also a PTFE lined inlet was used but it was also possible to heat the samples with a temperature ramp, monitor the pressure by a manual manometer (60 bar), stir the mixture with a magnet stirrer (not used) and cool the obtained sample mixture after reaction with an inbuilt temperature spiral (not used). The increased temperature was achieved through a heating mantle and controlled with an external temperature controller that was connected to a temperature sensor in the autoclave, reaching into the sample solution. Additionally, the data was visualized on a connected computer. The desired temperature was reached with a programmed ramp of 2 °C·min^{-1}. Usually, the actual temperature (T_{act}) followed the set temperature (T_{set}) quite nicely. Due to the communication of the temperature sensor, controller and mantle, T_{act} could shortly increase up to 10 °C beyond T_{set} until it settled to vary between +/- 2 °C, as exemplary shown in figure 44.

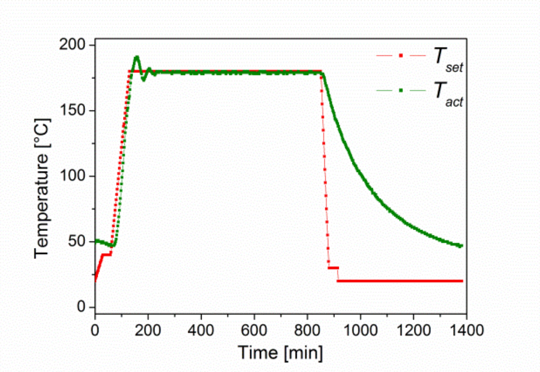

Figure 44 Typical temperature program using the BR-2000 high pressure reactor.

To prevent a deformation of the PFTE inlet the reaction was started with an increased initial pressure of 2 bar by adding compressed air via one of three available sampling ports (2x gas and 1x liquid sampling possible). The maximum allowed temperature was given with 230 °C (using the PTFE) and a pressure of 200 bar with an installed blow-out disc (Monel, 200 bar) connected to a blow-off tube.

Besides two available reactor setups, the hydrochars were also synthesized using two different approaches. The first one (htc_A) was based on the works of Fechler *et al.*[11]. Their procedure is characterized by high amounts of salt-additives compared to rather small amounts of substrate. Overall not more than 24 g of solution were used in each of their experiments. In the present work, the reactions by this method were conducted only in the small 200 mL autoclaves.

Based on the results and experiences of using method htc_A, an optimized version was developed (htc_B). For this, the amount of salt was comparable low and rather used as salt-water mixtures with different weight percentages than fixed amounts as done in the procedure of Fechler *et al.* Usually, a ratio of substrate to salt-water-mixture of one to two was chosen with a 60 wt% salt solution. These experiments allowed the use of higher substrate amounts (e.g. 100 g) and were therefore done using the 2 L autoclave.

Mostly the results from the optimized procedure (htc_B) are presented in this work but since not all experiments of htc_A were reproduced, some of those are shown for comparison.

All samples were given names that allow easy understanding of the procedure they are based on. The nomenclature starts with the three letters for the used substrate, followed by an underline and A or B for the used method (htc_A or htc_B), a description of the used time and temperature within the hydrothermal carbonization and, if a water-salt mixture was used, a abbreviation for the additive. Furthermore, if the hydrochar was used for activation, an additional A together with the activation time and temperature is attached at the end of the nomenclature. Table 4 shows two examples for further understanding the used sample nomenclature.

Table 4 Examples for the understanding of the used sample nomenclature.

Nomenclature	**Explanation**	**Meaning**
Ccn_B12h180C60Zn		
Ccn	Substrate	Coconut shell powder
_B	Approach	htc_B
12h	HTC time	12 hours
180C	HTC temperature	180 °C
60Zn	Wt% salt-water mixture	60 wt% zinc chloride solution
Dnd_A12h180CLi(0.23)ZnA60m500C		
Dnd	Substrate	Dried dandelion leaves
_A	Approach	htc_A
12h	HTC time	12 hours
180C	HTC temperature	180 °C
Li(0.23)Zn	Salt-water mixture	LiCl (23 mol%) and $ZnCl_2$
A	Activation	Activated hydrochar
60m	Activation time	60 minutes
500C	Activation temperature	500 °C

In addition, further letters in the nomenclature used to describe parameter variations will be explained in the corresponding chapters of the result and discussion part.

3.2.1.1 Procedure htc_A

The production of the hydrochars with procedure htc_A consisted of mixing the corresponding substrate (9 g) with either water (180 mL) only (e.g. Ccn_A12h180C) or with 22.5 g of a freshly grinded salt mixture of an alkali metal chloride (e.g. LiCl, NaCl or KCl) and zinc chloride at a certain molar ratio with e.g. 23 mol% LiCl and only 9 mL of water (e.g. Ccn_A12h180CLi(0.23)Zn). The mixture was then filled into a 200 mL PTFE inlet and placed into a stainless steel autoclave, which was put in a preheated oven (e.g. 180 °C) for the desired time (e.g. 12 h). After cooling to room temperature, the solid product was removed from the PTFE inlet, ground and stirred in 1 L of water overnight to remove any residual salts.

Afterwards, the samples were collected by vacuum filtration, washed with 1 L water and dried at 105 °C overnight. The samples were ground one last time and collected over a sieve with a mesh size of 0.63 mm.

Variations of this method beside the change in substrate, temperature, time or additive included different ratios of substrate to water and/or salt as well as salt mixture composition, which will be described in more detail in the corresponding section of the result and discussion chapter.

3.2.1.2 Procedure htc_B

In a typically experiment following procedure htc_B firstly the desired salt-water mixture was prepared by solving the needed amount of salt in water (e.g. 60 wt% salt). Then, a certain amount of the salt-water mixture depending on the desired substrate to solvent ration (e.g. 200 mL) was mixed with the substrate (e.g. 100 g) and filled into the 2 L PTFE inlet, which was placed into the BR-2000 high pressure reactor and sealed. After setting an initial pressure of 2 bar with compressed air, the temperature aim was reached with a programmed ramp of 2 $°C \cdot min^{-1}$. After the chosen reaction time and cooling of the autoclave, the wet solid product was removed from the PTFE inlet, ground and stirred in 1 L of water overnight to remove any residual salts. Afterwards, the samples were collected by vacuum filtration, washed with 1 L water and dried at 105 °C overnight. The samples were ground one last time and collected over a sieve with a mesh size of 0.63 mm.

Same as with for htc_A, variations of process parameters will be described in more detail in the corresponding section of the result and discussion chapter.

3.2.2 Activation of hydrochars

For the steam activation of the hydrochars, 2-3 g of each sample obtained by HTC were loaded into a perforated ceramic crucible and placed into a glass inlet, which was located in a tube furnace and heated. The temperature was adjusted with a simple temperature controller which was connected to a PT100 thermoelement that measured the temperature in the middle of the tube furnace. Upon reaching the desired temperature (e.g. 500 °C), steam, which originated from a simple heating of water in a connected 500 mL Erlenmeyer flask, was allowed to flow through the glass inlet for a fixed time ranging from 10 to 60 minutes. After cooling down, the obtained samples were analyzed without further treatment expect if otherwise noted under the specific characterization techniques. Figure 45 shows a scheme of the used apparatus for hydrochar activation.

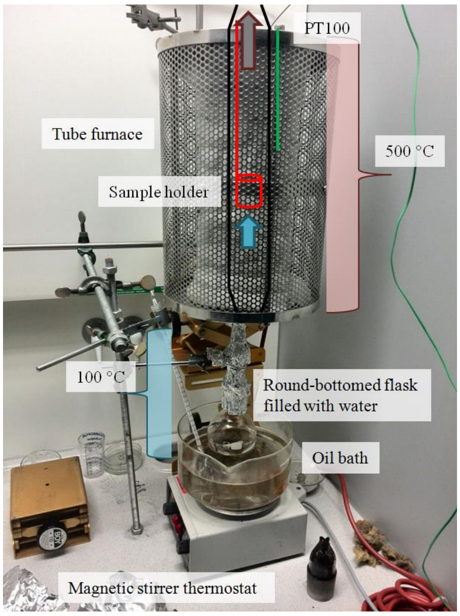

Figure 45 Image of the apparatus used for the steam activation of hydrochars.

3.2.3 Dye sorption experiments

3.2.3.1 Initial dye sorption studies

The adsorption experiments with methylene blue (MB) and methyl orange (MO) were performed for selected samples using a modified procedure based on works published in literature[226, 227]. For the first comparison of adsorption capacities of hydrochars and their activated forms, 40 mL of methylene blue or methyl orange solution (initial concentration of 100 mg/L) were added to a small amount (50 mg) of char in a 50 mL plastic tube and shaken for 24 h at room temperature (250 rpm) with a Dual-Action Shaker KL 2 (Edmund Buehler GmbH). After 24 hours the samples were filtered with Sarstedt syringe filters (0.2 µm) to make it carbon-free and diluting it by a factor of 20. The residual concentration in the solution was analyzed using a Varian Cary 4000 spectrophotometer (for a description of the UV-Vis spectroscopy see chapter 3.3.8). A prior made calibration curve enabled the calculation of the concentration from the absorbance maximum at a wavelength of 664 and 464 nm for methylene blue and methyl orange, respectively. Figure 46 shows the calibration curves for both dyes. Due to limitations of the Beer-Lambert Law (compare 3.3.8) for higher absorbances, two fits were used for the methylene blue data at low and higher concentrations that are noted in the figures.

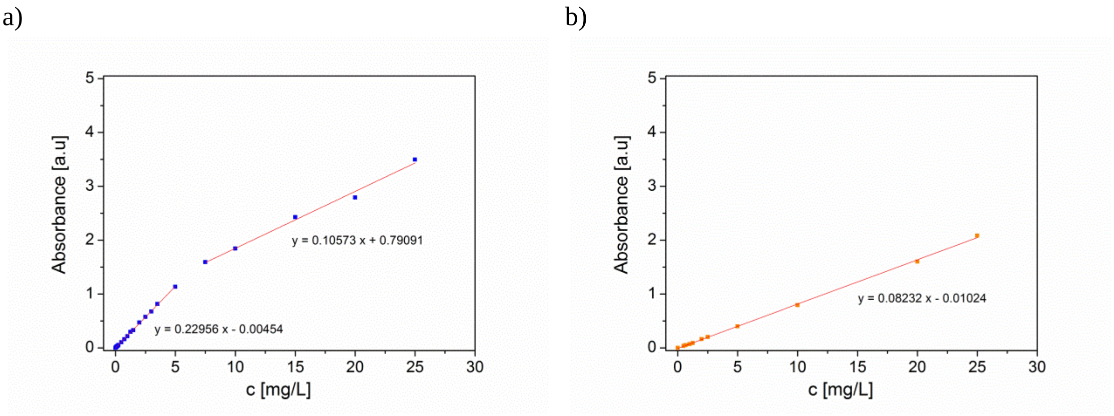

Figure 46 Calibration curves for the absorbance to concentration relation of the dyes methylene blue (a) and methyl orange (b).

The amount of dye removed from solution was reported as q_e in mg·g^{-1}, which was calculated using equation 1,

$$q_e = \frac{(c_0 - c_e)V}{m} \qquad [1]$$

where c_0 and c_e are the initial and equilibrium dye concentrations (mg/L), respectively, V is the volume of used dye solution (L), and m is the weight of the adsorbent (g). In order to reduce the error of the adsorption data, each sample was tested two times, and the average was reported.

3.2.3.2 Detailed study of methylene blue adsorption

For the detailed studies of methylene blue adsorption, a slight variation of the used amounts described under 3.2.3.1 was done. Here, the removal of dye was studied using 12.5 mg of hydrochar and 0.5 L of a MB solution with known concentration (further described in the following subchapters). Instead of 50 mL plastic tubes, 1 L Erlenmeyer flasks were used. Shaking and measurement of the residual concentration were done accordingly to as previously described, just with no sample dilution.

3.2.3.2.1 Adsorption kinetics

To study the residence time required for completing the adsorption of MB onto the solid samples, the solute uptake rate can be determined from the kinetic analysis. For this, a methylene blue solution with an initial concentration of 5 mg/L was used. After certain time intervals, samples were taken and the concentration at the specific time (c_t) was determined by UV-VIS as previously described. The capacity was calculated as q_t according to equation 2:

$$q_t = \frac{(c_0 - c_t)V}{m} \qquad [2]$$

where c_0 and c_t are the initial dye concentration and that at the time t (mg/L), respectively, V is the volume of used dye solution (L), and m is the weight of the adsorbent (g).

The obtained data were fitted using three different kinetic models that try to formulate a general expression to describe the kinetics of adsorption on solid surfaces for the liquid-solid adsorption system, including pseudo-first-order (P1st) and pseudo-second-order (P2nd) kinetic models, as well as Elovich kinetic model (Elovich). Table 5 shows the non-linear and linear form of these.

The pseudo-first-order equation was proposed in 1898 by Lagergren as first order rate equation, who described the adsorption of ocalic acid and malonic acid onto charcoal.[228] He obtained a linear form after integration and applying of boundary conditions (t = 0 to t = t and q_t = 0 to q_t = q_t).[229] It was named pseudo-first-order to differentiate between kinetics equation based on concentration of solution and those of adsorption capacity of solid.[230]

It also differs from a true first order equation in terms of the parameter $k_1(q_e - q_t)$ not representing the number of available sites as well as the parameter $\log(q_e)$ differing from the intercept of the plot $\log(q_e - q_t)$ versus t.[229] If the observed kinetics follow the pseudo-first-order equation, it can be an indication that the adsorption is preceded by diffusion through a boundary.[231] A problem of the pseudo-first-order equation is the fact that the equilibrium sorption capacity is unknown in many cases, because the chemisorption tends to become immeasurably slow and the measured amount adsorbed is still smaller than the actual equilibrium amount.[229]

Table 5 Linear and non-linear forms of pseudo-first-order (P1st), pseudo-second-order (P2nd) and Elovich kinetic models.[227]

Model	**Non-linear form**	**Linear form**	**Plot**
P1st	$q_t = q_e[1 - \exp(-k_1 t)]$	$\log(q_e - q_t) = log q_e - \frac{k_1 t}{2.303}$	$\log(q_e - q_t)$ versus t
P2nd	$q_t = \frac{k_2 q_e^2 t}{1 + k_2 q_e t}$	$\frac{t}{q_t} = \frac{t}{q_e} + \frac{1}{k_2 q_e^2}$	$\frac{t}{q_t}$ versus t
Elovich	$q_t = bln(abt)$	$q_t = \frac{1}{b}\ln(ab) + \frac{1}{b} lnt$	q_t versus lnt

k_1 (min^{-1}) and k_2 (g·mg^{-1}·min^{-1}) - adsorption rate constants of the pseudo-first-order and pseudo-second-order equation, respectively; a - initial sorption rate (mg·g^{-1}·min^{-1}); b- coefficient related to the extent of surface coverage and activation energy for chemisorption (g·mg^{-1}).

By using the pseudo-second-order equation, the disadvantage of the pseudo-first-order equation in terms of that it does not fit well for the whole range of the adsorption process can be overcome.[229] The same boundary conditions as with the pseudo-first-order model are applied to receive the linear form.

The Elovich equation is described with a general application to chemisorption kinetics with a more general validity than other equations.[232, 233] From the determination of the parameters in the equation, the number of available adsorption sites can be determined as $(1 \cdot b^{-1})$.[231]

3.2.3.2.2 Equilibrium isotherms

Different isotherm models can be used to describe the relation between the adsorption capacity and the concentration at equilibrium. The data for these were obtained using different starting concentrations of MB, ranging from 1 to 25 mg/L. Experimental procedure and measurement of concentration was done as described in the kinetic studies but only with the equilibrium concentration (24 hours) measured. Three different two-parameter isotherm models were tested for describing the experimental data, including Langmuir, Freundlich and Temkin isotherm models (table 6). The suitability of the isotherm equation to describe the adsorption of methylene blue onto the hydrochar was judged by the value of the correlation coefficients R^2, with the highest showing the most promising model for the process.

Table 6 Linear and non-linear forms of Langmuir, Freundlich and Temkin isotherm model.[227]

Model	Non-linear form	Linear form	Plot
Langmuir	$q_e = \frac{q_m K_L C_e}{1 + K_L C_e}$	$\frac{C_e}{q_e} = \frac{C_e}{q_m} + \frac{1}{K_L q_m}$	$\frac{C_e}{q_e}$ versus C_e
Freundlich	$q_e = K_F C_e^{1/n}$	$logq_e = logK_F + \frac{1}{n} logC_e$	$logq_e$ versus $logC_e$
Temkin	$q_e = \frac{RT}{b} ln(A_T C_e)$	$q_e = \frac{RT}{b} lnA_T + \frac{RT}{b} lnC_e$	q_e versus lnC_e

q_m - maximum monolayer adsorption capacity of the sorbent ($mg \cdot g^{-1}$); K_L - Langmuir constant related to the free energy of the sorption ($L \cdot mg^{-1}$); K_F - Freundlich adsorption constant ($(mg \cdot g^{-1})(L \cdot mg^{-1})^{1/n}$); $1/n$ - measure of adsorption intensity; b and A_T - Temkin constant related to heat of sorption ($J \cdot mol^{-1}$) and equilibrium binding constant ($L \cdot g^{-1}$),respectively; R - gas constant (8.314 $J \cdot mol^{-1} \cdot K^{-1}$); T - absolute temperature (K).

The Langmuir adsorption model assumes that the adsorbate will adsorb onto a homogenous surface as a monolayer. The interaction between those molecules is negligible, with all adsorption sites having uniform energies.[234] Multilayer formation of adsorbate on a heterogeneous surface with diverse adsorption sites are better described with the empirical Freundlich isotherm model.[235] A higher fractional value of 1/n [0<(1/n)<1] can signify stronger adsorptives forces on the solid surface.[236] Furthermore, the Temkin model considers also effects of indirect interaction between the adsorbed molecules, leading to a linear decrease of heat of adsorption of all molecules in the layer with increasing coverage.[237]

3.2.3.2.3 Adsorption mechanism

For the adsorption of the dye onto the hydrochar surface not only the interaction between the MB molecules on the solid surface is important to describe the whole process but also the mechanisms of diffusion into possible pores of the adsorbents. Webber and Morris proposed an intraparticle diffusion mechanism for the adsorption process, which allows estimating if the process followed the intraparticle diffusion or not.[238] They expressed the intra particle diffusion as:

$$q_e = k_{di} t^{0.5} + C_i \qquad [3]$$

with the intraparticle diffusion rate constant k_{di} ($mg \cdot g \cdot min^{1/2}$) and an expression C_i that can describe the boundary layer effect. A greater value of C_i indicates a greater contribution of the surface sorption in the rate-controlling step. By plotting the experimental data for q_t versus $t^{0.5}$ insight if intraparticle diffusion is involved besides external diffusion can be obtained. If the fitted data pass through the origin, intraparticle diffusion is the only rate limiting step. Otherwise both diffusions contribute to the whole adsorption process.[227]

3.3 Characterization methods

The following chapter will give insight into the different characterization methods used in this work. The basics of each method will be shortly summarized together with specific settings or variations from usual procedures done for the characterization of the hydrochars and their activated forms as well as the substrates and side products. It is divided into different sections with each focusing onto another part of the properties such as composition (3.3.1), morphology (3.3.2), structure (3.3.3), functionality (3.3.4), gas sorption (3.3.5) and stability (3.3.6). This chapter will close with discussing the analysis of the liquid phase (3.3.7) and the procedure for the UV-Vis-spectroscopy (3.3.8).

3.3.1 Composition

3.3.1.1 Reaction yield

The reaction yield is reported as amount of obtained sample (m [g]) in percentage of amount of sample initially used for the process (m_0 [g]), as described by equation [4]:

$$\text{Yield} = \frac{m}{m_0} \cdot 100 \ [\%] \qquad [4]$$

In the case of the hydrothermal carbonization, the obtained sample was the dried hydrochar and the used sample the corresponding substrate. For the activation process the initially used sample was a hydrochar and the obtained its resulting activated hydrochar.

3.3.1.2 Ash content

The amount of inorganic residue as ash in the substrates, hydrochars and their activated forms were determined using the ASTM D3174-02 method for coals[239].
It is determined by weighing the residue remaining after burning the sample under rigidly controlled conditions. For this, approximately 1 g of the thoroughly mixed sample was transferred into a small, weighed ceramic crucible. The filled crucible was placed into a cold furnace and heated gradually at such a rate that the temperature reached 500 °C in 1 hour. The final temperature of 750 °C was reached by the end of the second hour and hold for an additional 2 hours.

After cooling down the residual weight was measured and the ash content calculated using equation [5]:

$$\mathrm{Ash} = \frac{m}{m_0} \cdot 100\ [\%] \qquad [5]$$

with the residual and initial weight m and m_0 in g, respectively.

3.3.1.3 Elemental composition

For the quantitative determination of the elemental composition (C, H, N) of the samples a EuroEA Elemental Analyser (HEKAtech GmbH) was used. Here, the regarding sample was burned in an oxygen atmosphere and the decomposition products of carbon, hydrogen and nitrogen were detected through thermal conductivity measurement. The amount of oxygen in the sample was then estimated as the difference of the elements detected (C, H, N) together with the ash content (equation [5]) to 100 %, as described by equation [6]:

$$O(\%) = 100 - C(\%) - H(\%) - N(\%) - Ash(\%)\ [\%] \qquad [6]$$

3.3.2 Morphology

3.3.2.1 Electron microscopy

To get an understanding of the surface morphologies and particle sizes in the different samples, scanning electron microscopy (SEM) and transmission electron microscopy (TEM) were applied. Usually, a SEM can provide images with a resolution up to about 1 to 10 nm while the TEM can reach higher resolutions of about 0.2 nm.[240] In both cases, electrons produced by a hot cathode are accelerated through the evacuated microscope with the help of a potential difference and emitted on the sample. In case of the TEM, these electrons ideally penetrate through the sample and the transmitted electrons are detected. From this, especially particle sizes and pore systems can be visualized. Since the contrast depends on the sample thickness it is important to have small or thin particles. Thicker structures like particle aggregates can result in a low transmittance and appear as black spots on the TEM images.

For the obtained TEM images, the samples in this work were dissolved in propan-2-ol (about a spatula tip full of sample in about 50 mL solvent) and ultrasonicated in an ultrasonic bath or with an ultrasonic rod.

About one or two drops of the solution were added from a small glass pipette onto a TEM grid. After evaporation of the solvent, the sample grid was inserted into a Zeiss EM 902A TEM and the images were recorded with a connected Proscan High Speed SSCCD camera (1x1k) that was operated with the software iTEM Five.

To get an actual image of the samples and to analyze their morphology, scanning electron microscopy was used. Here, instead of measuring transmitted electrons, those reflected (backscattered) or emitted out of the sample (secondary) due to excitation of the particle energy by the primary electrons of the electron beam are of interest. A Hitachi S3200N SEM was used with an Everhart-Thornley secondary electron detector to obtain images of different samples. Prior to imaging, the samples were placed on carbon sample holders and sputtered with gold (thickness about 15 nm) by a SCD 005 sputter coater from Bal Tec for sample conductivity. An Oxford INCA EDX system with a 10 mm^2 SDD detector (PentaFET Precision INCA X-act) allowed elemental analysis by Energy-dispersive X-ray spectroscopy (EDX) of non-sputtered samples. Here, the energy of X-rays that are emitted when electrons from outer shells fill holes created by ejecting electrons on inner shells by the initial electron beam is measured.

3.3.3 Structure

3.3.3.1 X-ray diffraction

To identify crystalline phases inside different powder materials, X-ray diffraction (XRD) can be conducted. This method allows to reveal locations of ions within a structure from the distribution of monochromatic X-rays scattered by the array of these ions.[241] A diffraction takes places since the interatomic distances in solids are usually in the order of angstrom (10^{-8} cm), corresponding to wavelengths related to the X-ray energies. Intense peaks of scattered radiation can be observed if the rays specularly reflected on the different parallel planes of ions in a crystal interfere constructively. For this, the path difference between two rays must be an integral number of wavelengths, as described by Bragg's law:

$$n\lambda = 2dsin\theta \tag{7}$$

with an integer value for the order of the corresponding reflection, n, the wavelength of the X-ray, λ, the distance of two parallel planes of ions in a crystal, d, and the angle of incidence, θ. The term $2dsin\theta$ describes the path difference between two rays.[242] A detector measures the intensity of the diffracted X-rays as a function of the angle of X-ray source, sample and detector (2θ). The detector moves to different angles while the sample is rotated.

Because the lattice planes and signal intensities are powder characteristic, the obtained diffractogram can be compared to references found in data bases (e.g. International Centre for Diffraction Data (ICDD)).

The X-rays are created from an X-ray tube in which electrons are emitted by an cathode (tungsten filament) and accelerated towards and anode (copper). The X-rays result from two different processes. Firstly, the primary electrons slowed down by the anode emit a continuous background spectrum of so called Bremsstrahlung. Superimposed to this is the generation of an X-ray quantum created by X-ray fluorescence, where the hole created by a primary electron hitting an atom shell is filled by an electron from a subsequent shell. Cu Kα radiation and Kβ radiation result from the filling of the hole in the K-shell from either the L-shell or M-shell, respectively.[243] Monochromatic Cu Kα X-rays (wavelength of 0.154 nm and energy of 8.04 keV) are achieved by using a nickel X-ray filter, which adsorbs the higher energy Cu Kβ radiation.

In this work, a PANalytical Empyrean Series 2 diffractometer was used to measure the diffraction patterns of different samples. A 2θ range of 10-80° in Bragg-Brentano geometry with a step size of 0.013° (time per step 450.075 seconds) was chosen for data collection using Cu Kα radiation (λ = 0.154 nm). A PIXcel1D-Medipix3 detector was used to count the diffracted radiation. Soller slits and anti-scatter slits were used to reduce scattered radiation.

3.3.3.2 Solid state nuclear magnetic resonance spectroscopy

To get insights about actual carbon structures inside the substrates and hydrochars, solid state NMR (nuclear magnetic resonance) spectroscopy was conducted. In this method the sample is placed in a magnet pole gap and subjected to a radio-frequency (rf) field of an oscillator. In the presence of the magnetic field, atom nuclei in the sample that have a magnetic moment can align in different states (magnetic quantum states), e.g. either with or against the field. The magnetic moment usually results from a circulation of the nuclear charge (spinning). Since the natural common isotope of carbon, ^{12}C, behaves like a non-spinning spherical body, with the nuclear charge distributed evenly over its surface, it cannot be used when characterizing carbon materials. Here, even while at low natural concentration, the ^{13}C isotope is used since it acts like a spinning nucleus with spherical charge distribution (figure 47a). Such nuclei were assigned to a nuclear spin value, I, of 1/2. Their magnetic moment vectors along the axis of a magnetic field have certain permitted values (figure 47b) that are expressed by their magnetic quantum numbers, m. For a nuclear spin of 1/2 the possible magnetic quantum numbers are +1/2 and -1/2, describing two different energy states.[244]

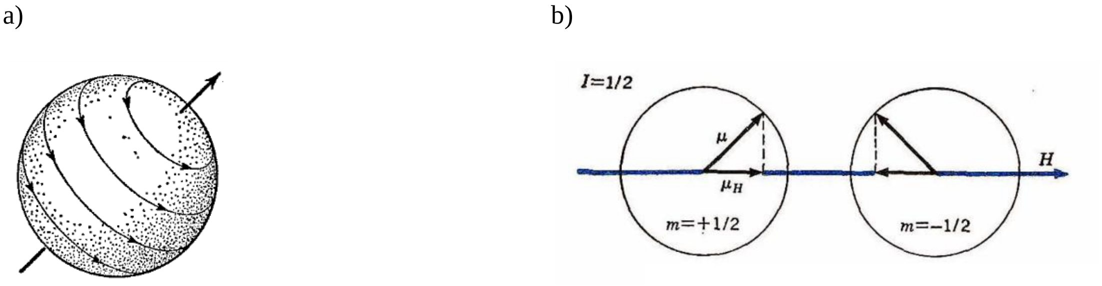

Figure 47 a) Scheme for a spherical spinning nucleus; b) Magnetic moment vectors (μ - magnetic moment; H - magnetic field). Both images taken and altered from Roberts[244].

The two states are separated by a field dependent energy difference $\varDelta E$, described by:

$$\varDelta E = h\gamma B_0/2\pi \qquad [8]$$

where γ is the magnetogyric ratio that connects the magnetic moment to the nuclear spin values, B_0 is the magnitude of an applied static magnetic field and h is the Planck constant. The lower state (α state) corresponds to the magnetic quantum number m = +1/2, where the magnetic moment is parallel to the applied magnetic state. The higher state (β state) is therefore expressed as m = -1/2 and corresponds to an antiparallel magnetic moment. The two states are unequally occupied, dependent on the field and also the nuclear species, with the ratio of the population given by the Boltzmann equation:

$$\frac{N_\beta}{N_\alpha} = e^{(-\frac{\varDelta E}{k_B T})} \qquad [9]$$

with the population of the upper and lower state, N_β and N_α, respectively, the Boltzmann constant, k_B, and the temperature, T.[245]

By applying a second magnetic field, B_1, which oscillates at an appropriate radio frequency, the magnetization can be moved away from its equilibrium position by excitation. Since the nuclei strive for equilibrium distribution between these different magnetic quantum states, processes summarized as nuclear relaxations take place. These come with absorption of an rf energy, that is measured by a detector. This absorption, which occurs at particular combinations of the magnetic field strength with the oscillator frequency, depends on the chemical and magnetic environment of the nuclei. Therefore, by inducing resonance of them with the fixed-frequency oscillator at different values of the applied magnetic field, characterization of the atom nuclei in the sample is possible.[244, 245]

Anisotropic magnetic interactions of crystallites inside the sample like dipolar couplings (through-space interaction related to the internuclear distance) and chemical shift anisotropies (related to the chemical environment of the nuclei) can be an issue for the measurements, leading to a significant signal broadening. For this, the technique known as magic angle spinning (MAS) is used. Here, the angle θ between the principal axis of the spinning sample holder (commonly a zirconia rotor) and the static magnetic field B_0 is set to 54.74° (the so called *magic angle*; see figure 48a), and the sample is rotated around the magic angle at a rate faster than the anisotropy of the interaction. This leads to the reduction of the line broadening. Additionally, by using the method of cross polarization (CP), where magnetization is transferred from abundant protons to ^{13}C nuclear spins close in space, the sensitivity of the spectra can be improved further. Figure 48b shows a classical pulse sequence for a CP-NMR experiment where t_{CP} is the cross polarization contact time between the ^{1}H and ^{13}C nuclei, whose manipulation can give information about the structure and chemistry of the sample that controls the magnetization transfer.[246, 247]

Figure 48 a) Rotor at the magic angle[247]; b) Classical pulse sequence for a basic CP-NMR experiment[246].

To overcome the challenges caused by the structural complexity of biomass derived hydrochars in solid state NMR analysis, various NMR techniques and pulse sequences can be combined to allow a characterization, as described by e.g. Baccile *et al.*[246, 248] or Falco *et al.*[53]

For this work, a Bruker Avance 500 MHz (11.75 T) spectrometer was used for the characterization of different hydrochars with 4 mm zirconia rotors as sample holders, spinning at MAS rate ν_{MAS} up to 15 kHz. The chemical shift reference was tetramethylsilane (TMS; $\delta = 0$ ppm). ^{1}H T_1 relaxation time was set to 3 s. Proton-to-carbon CP MAS was used to enhance carbon sensitivity with a cross polarisation time equal to 1 ms. Assignment of peaks and peak areas was done by comparing parts found in biomass building units (cellulose and lignin) to those found in the structural complex biomass. Additionally, they were compared and assigned with the help of data of other works.[53, 246, 248]

3.3.4 Functionality

3.3.4.1 Fourier transform infrared spectroscopy

The adsorption of infrared (IR) energy by bonds within molecules can activate vibrations and rotations of these. This adsorption can be measured directly for IR spectra or indirectly as scattered radiation in the Raman spectroscopy.[249, 250] An IR spectrometer measures the change of adsorption over a range of wavelengths, usually from 4000 to 500 cm^{-1}. Instead of running a time consuming wavelength scan, the Fourier transform infrared spectroscopy (FTIR) allows a detection of all frequencies simultaneously. For this, an interferometer (e.g. Michelson interferometer) converts the polyfrequent IR radiation of the light source into a time dependent interferogram before the radiation is brought onto the sample. The interfering is achieved through splitting, distraction and reflection of the light by a beamsplitter and different mirrors into two rays. Convergence of those two rays results into an interferometrically combined amplitude, including the interferograms of all frequencies. After the selective adsorption from the sample, a detector registers the arriving infrared light as an interferogram. The mathematical Fourier transformation then changes the interferogram back into a frequency dependent spectrum.[249] Most functional groups of organic molecules show adsorption of IR energy at a certain wavelength which allows the determination of the chemical nature of the bond. Different data bases or tables found in literature help with the assignment to a certain type of functional group through their position, size and intensity.

In this work, FTIR was conducted using a Bruker Tensor FT-IR spectrometer. Additionally, a MKII Golden Gate Single Reflection Diamond ATR-System was used for easy sample measurement without additional preparation. In this attenuated total reflection (ATR) setup, an infrared beam that passes through an optically dense crystal, which is in contact with the sample, is measured.[251] The internal reflectance in the ATR crystal creates an evanescent wave that extends beyond the surface of the crystal a few microns into the sample held in contact with the crystal (figure 49). The wave will be altered or attenuated when the sample absorbs regions of the IR spectrum. The resulting IR beam is passed to a detector from which the system generates an infrared spectrum through Fourier transformation.

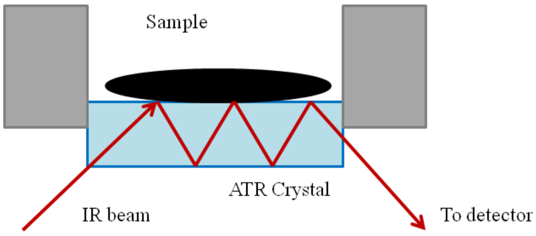

Figure 49 Principle of multiple reflection ATR system.

3.3.4.2 X-ray photoelectron spectroscopy

X-ray photoelectron spectroscopy (XPS) was conducted to obtain qualitative and quantitative information about the elements on the sample surface as well as their chemical states. For this, the sample is irradiated with X-ray photons of energy $h\nu$ in an ultra-high vacuum. The resulting photoelectrons released from a core level of molecules on the surface of the sample are analyzed by the spectrometer according to their kinetic energy (E_K) which is characteristic for each element together with its chemical and electronic environment. The resulting data are typically plotted as intensity versus electron energy. Because the measured E_K is dependent on the used photon energy $h\nu$, usually the binding energy of the electron (E_B) is used, which can be calculated using equation 10:

$$E_B = h\nu - E_K - W \qquad [10]$$

where $h\nu$ is the photon energy, E_K is the kinetic energy of the electron and W is the spectrometer work function.[252] Monochromatic X-rays with defined energy are needed to fulfill the conditions of equation 10. The spectrometer work function is equal to the work function of the sample holder material and applied to include Fermi level equilibration of the solid sample and the sample holder, which are in electric contact. The binding energy is calculated by the data system connected to the spectrometer and identifies the electron specifically. All electrons with a binding energy less than the photon energy can be featured in a photoelectron spectrum which helps to reproduce the electronic structure of an element. In this, electrons that are excited and emitted without energy loss present characteristic peaks in the spectrum while those that suffer energy loss due to inelastic scattering contribute to the background noise. Therefore only electrons located near the top of the surface are measured and studying bulk materials shows limitations of the XPS.[253] Depending on the kinetic energy, the depth of detection is usually between approximately 5 to 10 nm.

As a side effect, the needed relaxation of the atom ionized from the photoemission of the electron results in emission of an X-ray photon, which can be used in X-ray fluorescence spectroscopy (XRF). It is also possible that the energy of the photon is transferred after internal relaxation events onto another electron of the atom. This ejected electron is known as an Auger electron whose emission is used in the X-ray induced Auger electron spectroscopy (X-AES). The advantage of AES is its high spatial resolution (10 to 15 nm) compared to XPS (3 to 10 µm) while the latter offers better ease for quantitative analysis and information about the chemical state.[252] While survey spectra over a whole range of binding energies provide information about the elements present, high-resolution scans in narrow E_B ranges can give chemical shift data. Different electronic environments of the ejected photoelectrons can result in small shifts in the binding energy peak position.

The oxidation state of the considered element species can also be determined since the binding energy increases with higher oxidation number due to the greater coulomb interaction of the more positive nucleus to a core electron with the obtained survey spectra giving information about the present elements while high resolution spectra can give more detailed information about their different binding states.[253]

For this work, X-ray photoelectron spectroscopy (XPS) measurements were carried out in an ultra-high vacuum set-up equipped with a monochromatic Al Kα X-ray source ($h\nu$ = 1486.6 eV) with a double-focusing full 180° spherical analyzer (ESCALAB 250 Xi, Thermo Fischer Scientific). The electron binding energies of the measured elements were referenced to adventitious C 1s of hydrocarbon contaminations at 284.8 eV. High resolution XPS core level spectra for C, O, and Zn were collected and analyzed using the Avantage software (version 5.951).

3.3.5 Gas sorption

The physical sorption of a gas (adsorptive) with a known size onto the surface of a solid (adsorbent) with known mass offers the possibility to calculate the specific surface area (SSA, surface area of unit mass of powder) in $m^2 \cdot g^{-1}$ from the amount of gas physical adsorbed using different mathematical models. For this, different gases have been effectively used over the last century by various workgroups to describe the surface areas of different compounds. For active carbons, these include mostly nitrogen, carbon dioxide, water vapor, organic vapors (e.g. methane, ethane, *n*-hexane and benzene) or noble gases (helium, argon and krypton).[254] The change of gas can result in changed adsorptive behavior due to different adsorptive-adsorbent interactions. Additionally, pore accessibility can also differ for one adsorptive when compared to another. On top of that, each adsorptive requires a specific measurement temperature that has to be applied, affecting the speed of reaching a state of equilibrium between the free and adsorbed gas. These facts can ultimately lead to varying values of the calculated surface area when comparing different gases to each other.

Typically, the porosity of hydrochars or active carbons is characterized using nitrogen at a measurement temperature of 77 K (cooled with liquid nitrogen). Furthermore, the sorption of carbon dioxide at 273 K (cooled with an ice bath) is sometimes reported and compared along to those obtained for N_2.[254]

The physisorption of the gas is caused by van der Waals forces and leaves the chemical species of the adsorbate and surface intact. Contrary, a chemisorption would include a chemical reaction between the surface and the adsorbate with electronic bonds formed, which is usually used as a characterization tool in samples for heterogeneous catalysis.

Most commercial available systems for gas sorption work statically volumetric. In these, the adsorptive is expanded from a chamber with exact know volume (manifold) onto the sample tube. The amount adsorbed is calculated from the pressure drop after equilibrium is formed.

Here it is important to consider the void volume of the tube (free space), which is measured prior or after the sorption experiment by an inert gas, e.g. helium.

3.3.5.1 Sorption isotherms

Since the quantity of gas adsorbed is related to the pressure, the adsorption is characterized by an isotherm that shows the amount adsorbed at varying partial pressure p/p_0 (p - equilibrium pressure; p_0 saturation vapor pressure of the adsorptive). Depending on the pore structure of the sample to be examined and the used adsorptive gas, different isotherms shapes are obtained. These were grouped into six different types by the International Union of Pure and Applied Chemistry (IUPAC) (see figure 50), allowing classification of the sample to certain pore characteristics.[255]

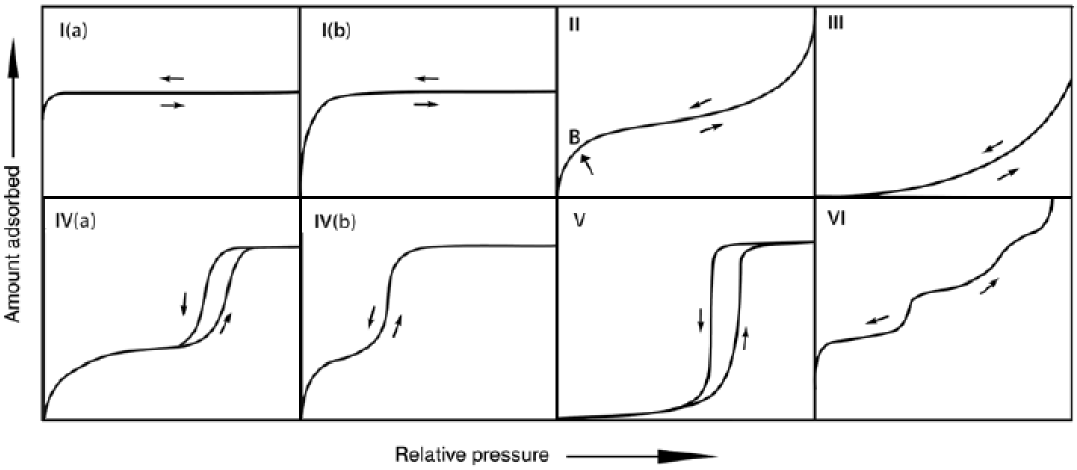

Figure 50 IUPAC classification of physisorption isotherms (altered from Thommes *et al.*[255]).

Type I isotherms are found usually for microporous solids, with an abrupt uptake at low relative pressures, quickly reaching a plateau depending on the accessible micropore volume. They are subdivided depending on their pore size distributions with Type I(a) having mainly narrow micropores while for Type I(b) a broader pore size distribution can be found. Type II isotherms are found for most nonporous or macroporous adsorbents, with an unrestricted monolayer-multilayer adsorption. If the interactions between the adsorptive and the adsorbent are rather weak, a Type III isotherm shape can be observed. Here, the gas adsorbs only onto the most favorable sites on the surface, leaving many parts of the nonporous or macroporous sample uncovered. Mesoporous samples result into Type IV isotherms with a typical hysteresis between the adsorption and desorption curve caused by pore condensation. Depending on the size of the mesopores, two different types (a and b) can be found for this isotherm. In some cases, an initial weak interaction between gas and solid similar to a Type III isotherm is followed by an increased uptake due to pore filling.

This is characterized by a Type V isotherm. An example for this isotherm is the adsorption of water onto hydrophobic micro- and mesoporous samples. The last group is represented by a Type VI isotherm, which is observed if different layers are adsorbed onto the surface one after another found in e.g. the adsorption of argon or krypton at low temperature on graphitized carbon blacks.

If a hysteresis, as mentioned for the Type IV isotherms, is observed, the shape of it can give additional information about the pore structure, as described in the IUPAC technical report.[255] Figure 51 shows six characteristic hysteresis loop types, each related to a particular sorption process caused by a specific pore structure.

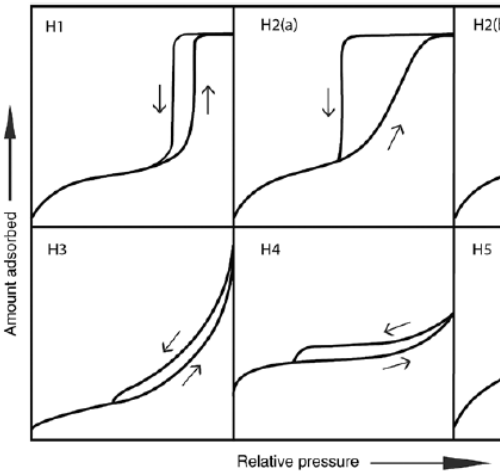

Figure 51 IUPAC classification of hysteresis loops.[255]

A Type H1 loop is found in samples with a rather uniform mesoporous system, as seen in e.g. templated silicas. If the gas cannot leave the pores easily due to pore-blocking a Type H2 loop is observed. A narrow range of pore necks results in a Type H2(a) loop (desorption after a plateau happens suddenly at a critical relative pressure) and a larger size distribution in Type H2(b) loop (slow continuous emptying of pores). Examples for a sample types with a H2(a) loop are many silica gels, while Type H2(b) has been observed with e.g. mesocellular silica foams. Type H3 loops and Type H4 loops can results from cavitation effects, indication a pore network with macropores that are not completely filled with pore condensate (Type H3 loop) or aggregated crystals of zeolites and micro-mesoporous carbons (Type H4 loop). A Type H5 loop is usually found in samples with a distinct pore structure containing open and partially blocked mesopores.

3.3.5.2 Calculation of the surface area

A general mathematical relation for an isotherm was first proposed by Freundlich in 1907, followed by Langmuir in 1916 who introduced the theory of the formation of a monomolecular layer based on the conclusions of Lord Rayleigh.[254, 256, 257]

Furthermore, the Brunauer-Emmett-Teller (BET) theory from 1938 extended the Langmuir mechanism with the empirical approach that a nearly linear section of the adsorption isotherm after an initial gas uptake characterizes the completion of the monolayer. After this designated Point B (compare figure 50 (Type II isotherm)), a multilayer coverage of the surface begins.[258] Emmet and Brunauer determined the completion of a close-packed monolayer at this point B in their study of the surface area of iron synthetic ammonia catalysts, after calculating the hypothetical surface areas at four characteristic points (A, B, C and D) on the adsorption isotherm of different gases.[259] Since then, the BET method has become a standard procedure for the determination of the surface area for a wide range of different powders and porous materials.[254, 260]

The original isotherm equation described by Brunauer, Emmet and Teller in 1938 is given by equation 11:

$$v = \frac{v_m c p}{(p_0 - p)[1 + (c-1)(\frac{p}{p_0})]} \tag{11}$$

with the total volume adsorbed, v, the volume of gas adsorbed when the entire adsorbent surface is covered with a complete unimolecular layer, v_m, the saturation pressure of the gas, p_0, and the equilibrium pressure, p.[258] The appropriate constant c gives a relation of the heat of adsorption and heat of liquefaction of the adsorbed molecules, describing that the evaporation-condensation properties of the molecules in the second and higher adsorbed layers are the same as those of the liquid state as expressed by equation 12:

$$c = \frac{a_1 g}{b_1} e^{E_1 - E_L/RT} \tag{12}$$

with a_1, b_1 and g given as appropriate constants, the heat of adsorption of the first layer and heat of liquefaction, E_1 and E_L, respectively, as well as the ideal gas constant, R, and the temperature, T.[258]

Usually equation 11 is written in the linear form:

$$\frac{p}{v(p_0 - p)} = \frac{1}{v_m c} + \frac{c-1}{v_m c}\frac{p}{p_0} \tag{13}$$

allowing the determination of v_m and c from experimental data by plotting $p/v(p_0-p)$ against p/p_0.

The specific surface area, *SSA*, can then be calculated through equation 14:

$$SSA = v_m L\sigma \qquad [14]$$

where L is the Avogrado constant and σ the average area occupied by each molecule in the completed monolayer (molecular cross-sectional area).[260] The latter is described as:

$$\sigma = f\left(\frac{M}{\rho L}\right)^{2/3} \qquad [15]$$

with f as an packing factor (1.091 for hexagonal close-packing), M the molar mass of the adsorptive and p the absolute density of the liquid adsorptive at the operational temperature.[260] Values for the used gas are usually included in the used apparatus files with e.g. $\sigma(N_2) = 0.162\ nm^2$ and $\sigma(CO_2) = 0.170\ nm^2$ (data from the sorption apparatus ASAP 2020 by Micromeritics).

To apply the BET method to a linear section of the sorption isotherm and to calculate the surface area, Rouquerol *et al.*[261] proposed some criteria that help to determine an appropriate pressure range, including:

- the selected linear part of the data when plotting $p/v(p_0-p)$ against p/p_0 should have an positive intercept on the ordinate, i.e. no negative value of the c constant;
- the value of $v(p_0-p)$ or $v(1-p/p_0)$ for the selected data continuously increase with the relative pressure;
- the calculated BET monolayer capacity should correspond to a relative pressure located within the pressure range used for the calculation;
- the relative pressure for the monolayer capacity calculated from the c constant and the experimental one should not differ by, say, more than 10%.

Furthermore, the DIN norm DIN ISO 9277 from 2014 describes the determination of the specific surface area from solids by the BET method.[262] The norm recommends using the methodology only for adsorption isotherms of Type II and Type IV, with an additional approach for Type I isotherms (microporous materials). For the calculation of v_m and c from the linear plotting of the BET equation (equation [13]) the relative pressure range between $p/p_0 = 0.05 - 0.3$ should be used, with the linear part of the data having an positive intercept on the ordinate, which is in accordance with the criteria described by Rouquerol *et al.*[261] For the application to microporous materials, the relative pressure range is shifted significantly towards lower partial pressures, with the surface area calculated in respect to the additional criteria from Rouquerol *et al.*[261, 262]

3.3.5.3 Pore size distribution

Besides the calculation of the surface area and the classification of the isotherm and its hysteresis (if present), it is possible to determine a distribution of the different pore sizes. For this, different methods have been used over the years including e.g. the method developed by Barrett, Joyner and Halenda (BJH), which is based on the Kelvin equation. The pores are classified by IUPAC[255] according to their size:

- pores with widths exceeding about 50 nm are called macropores;
- pores of widths between 2 nm and 50 nm are called mesopores;
- pores with widths not exceeding about 2 nm are called micropores.

Micropores can then be further divided into ultramicropores (approximate width < 0.7 nm) and supermicropores.[255]

Recently, a method based on the computational quantum mechanical modeling density functional theory (DFT) is used, which is independent of capillary condensation and can therefore be applied over the whole micro- and mesopore range.[263] Furthermore, the nonlocal density functional theory (NLDFT) includes various smoothing approximations to the DFT, improving the obtained data to better describe the adsorption and phase transition in different pores. These methods calculate a series of theoretical isotherms, the so called kernel, and calculate the pore size distribution after integration over a finite range of pore sizes using regularization algorithms.[263] Since these methods are based on idealized theoretical models its application has to be taken with caution.

3.3.5.4 Experimental procedure

The determination of the specific surface areas (SSA) and pore size distributions of samples in this work were done using a Micromeritics TRISTAR II (N_2 at 77 K) apparatus. The data were collected usually over a pressure range of p/p_0 = 0.005-0.95 (36 points, distribution geometrical to lower pressures) and p/p_0 = 0.95-0.1 (19 points, linear distribution) for the adsorption and desorption, respectively. The free space was measured using helium. The SSA was calculated using the BET model in accordance with the Rouquerol criteria. The pore size distributions and pore volumes were obtained by NLDFT model for slit pores using the MicroActive Interactive Data Analysis Software adjusting the goodness of fit towards the best accordance of RMS Error of Fit (cm^3/g STP) and Roughness of Distribution.

Low pressure experiments were conducted using a Micromeritics ASAP 2020 with N_2 at 77 K in the range of p/p_0 = 0.000001-0.95 (16 points) for the adsorption and p/p_0 = 0.95-0.05 (4 points) for the desorption.

Sorption of CO_2 was conducted to compare the SSA values to those obtained from N_2, enabling the characterization of pores in the lower micropore regime.[264] These experiments were done on a Micromeritics ASAP 2020 with CO_2 at 273 K in the range similar to those done at the TRISTAR II.

Before measurement, the samples were filled in sorption tubes, weighed, degassed in vacuum for 1 hour at 80 °C and overnight at 150 °C, flushed with nitrogen and weighed again to determine the lost mass, prior to installing them to the corresponding sorption apparatus.

3.3.5.5 Water sorption experiments

Water sorption experiments were conducted to get information about the sample capability of water uptake as well as a possible hydrophobicity or hydrophilicity of the samples. They were determined volumetrically similar as to a typical gas sorption. The main difference lays in the usage of water vapor instead of a gas and the important that the used apparatus is internally heated, thus no condensation of the water takes place inside the machine, potentially altering the results. For this, a Quantachrome Hydrosorb-1000 was used that could be operated at an internal temperature of 100 °C. A water bath allowed the tempering of the external connected sample tube, enabling sorption experiments at temperatures of 25 °C. Data were recorded from p/p_0 = 0.01 - 0.95 (25 points) and p/p_0 = 0.95 - 0.01 (30 points) for the adsorption and desorption, respectively.

3.3.6 Stability

3.3.6.1 Thermogravimetric analysis

To test the thermal stability of the hydrochars and its substrates, thermogravimetric analysis (TGA) was conducted. This method allows to follow the temperature dependent decomposition of a material in either inert or oxygen atmosphere. For this, a Perkin Elmer TGA 4000 system was used. Around 10-20 mg of the sample was placed in a ceramic crucible in the furnace of the apparatus, which was connected to a balance that allowed constant measurement of the sample weight. The sample was then heated in a constant flow of nitrogen (40 mL/min) from 30 °C to 750 °C with a rate of 10 °C/min. The weight loss of the sample due to the production of volatile species was recorded as a function of temperature and time and displayed on a connected computer. Usually, the mass of the sample [%] is plotted against the temperature [°C]. For better determination of critical temperature ranges of the mass loss, the first derivative (DTG [a.u.]) is also plotted against the temperature.

3.3.7 Analysis of the liquid phase

3.3.7.1 Total organic carbon

For the determination of the total organic carbon content (TOC) of the liquid phases obtained in the HTC process, a TOC-VCPH total organic carbon analyzer from Shimadzu was used. Here, about 3 mL of the sample were oxidized by a $Pt/CuO/Al_2O_3$ catalyst at a temperature of 680 °C. The CO_2 that was formed out of the sample was detected by a nondispersive infrared sensor (NDIR) and an analyzing program on a connected computer calculated the TOC value from intern calibration data. Prior to measurement, the liquid phases resulting by vacuum filtration of the wet coals formed in the HTC process were diluted with water by a factor of 100 to obtain TOC values in the range of the detection limit. Each liquid phase was measured three times and the average reported (error < 10 %).

3.3.7.2 High-performance liquid chromatography

The composition of the liquid phase was analyzed using high-performance liquid chromatography (HPLC). With this, compounds of the liquid phase obtained in the HTC process are detected after being separated by a column filled with an adsorption material (stationary phase). For this, the sample is dissolved in portions in an eluent (mobile phase), before being pumped through the column at constant flow rate. The various compounds of the sample are restrained by interaction with the stationary phase. Since the degree of restraint depends on the physical and chemical properties of the different compounds, the detected concentration varies with time. With either weak or no interactions, the compounds can usually be detected after a few minutes while those with strong affinity to the adsorbent leave the column towards later analysis times. The detector then determines their concentration in relation to the volume of eluent.[265]

For the analysis of the liquid phases from the HTC process the samples (20.0 µl injection volume) were dissolved in an acetonitrile/water (20/80) mixture (isocratic elution mode) and pumped through a Merck LiChrospher 100 RP-18 (reversed phase; length: 250 mm; inner diameter: 4.0 mm; particle size: 3.0 µm) column at 25 °C by a Shimadzu LC-20 AT pump at a flow rate of 1.25 ml/min with a Shimadzu SPD-M20A Diode Array Detector determining the different compounds after leaving the column.

3.3.8 UV-Vis-spectroscopy

Ultraviolet-visible spectroscopy (UV-Vis) can be used to record a spectra of the wavelengths absorbed by a colored substance (e.g. dye). A characteristic portion of the mixed wavelengths of white light passed through a sample is absorbed with the absorbance of the remaining light measured by the spectrometer.[266] The technique can be used to measure the concentration of a sample in solution since according to the Beer-Lambert Law the concentration is proportional to the absorbance:

$$A = \varepsilon \cdot c \cdot l \qquad [16]$$

with the absorbance A, the molar extinction ε ($L \cdot mol^{-1} \cdot cm^{-1}$), the concentration of the solution c ($mol \cdot L^{-1}$) and the optical path length l (cm).

In this work, a Varian Cary 4000 spectrophotometer was used for recording the spectra, which worked similar to the schematic diagram shown in figure 52.

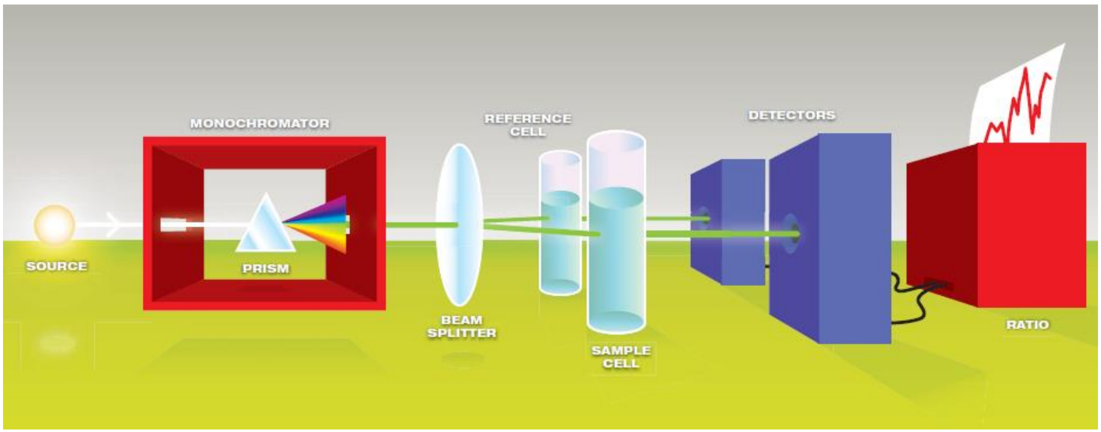

Figure 52 Schematic diagram of a UV-visible spectrometer.[266]

Here, a halogen (visible light region) and deuterium (UV light region) lamp emit light that passes through a prism towards a reference cell and the sample cell. A detector detects the arriving light after passing through the sample, resulting in a spectrum (absorbance vs. wavelength) shown on a connected computer.

For this work, no reference cell was used but rather a baseline correction with water before each measurement run. A calibration graph was used to determine the concentration of the samples, as described in the dye sorption studies section (chapter 3.2.3). To ensure the validity of the Beer-Lambert Law, only the range where the plot absorbance versus concentration showed linear behavior was considered.

Chapter 4

Results and discussion

The following chapter will start the discussion of the obtained results in this work with a detailed investigation of the hydrochars received from hydrothermal carbonization of various substrates. The main goal is to determine how certain characteristics change if a salt-water mixture, primarily those containing zinc chloride, was present in the reaction mixture. For this, the hydrochars received by a conventional hydrothermal carbonization in terms of biomass in water (HTC) are compared to those received if the salt was present in the water (salt-HTC). Ideally an understanding of the interaction mechanism between the salt (e.g. zinc chloride) and the biomass can be developed. Therefore, seven different biomass feedstocks in different cut sizes were used, which are summarized along four additional substrates (see below) in table 7.

Table 7 List of substrates used in this work together with their abbreviation and assigned color.

Substrate	**Abbreviation**	**Assigned color**
Glucose	Glu	■ Blue
Hydroxymethylfurfural	HMF	■ Dark turquoise
α-Cellulose	Cel	■ Red
Lignin	Lig	■ Black
Mixture of different grasses and rushes	Gnr	■ Purple
Broken coconut shell pieces	Crw	■ Brown
Coconut shell powder	Ccn	■ Orange
Rice husks	Rce	■ Gray
Dried dandelion leaves	Dnd	■ Yellow
Spirulina algae	Alg	■ Green
Sawdust	Saw	■ Pink

Each has a specifically assigned color that will be used in all of the figures of this chapter, if not stated otherwise. These used substrates included a mixture of different grasses and rushes (Gnr), broken coconut shell pieces (Crw), coconut shell powder (Ccn), rice husks (Rce), dried dandelion leaves (Dnd), spirulina algae (Alg) and sawdust (Saw). Subsequent, the influence of some of the major reaction conditions like time, temperature, feedstock to water ratio as well as salt amount and type could be conducted for the as most suitable determined biomass with the goal of a process optimization for hydrochars with desired properties.

To develop an understanding of a possible mechanism for the role of the salts within the carbonization reactions, the complicated chemical nature of the substrates represents an obstacle. Therefore, two less complex but major biomass components (α-cellulose (Cel) and lignin (Lig)), one biomass framework molecule (glucose (Glu)) and one possible reaction intermediate (hydroxymethylfurfural (HMF)) were also carbonized under similar conditions and analyzed accordingly.

To discuss the hydrochar properties, first the experimental yield as well as the main char composition (elemental composition and ash content) will be shown since they provide a first glance of the reaction outcome. Images of scanning electron microscopy and transmission electron microscopy give information about the structural changes on a microscopic level while results of the solid state nuclear magnetic resonance spectroscopy provide more in depth insight at the molecular level. Additionally, Fourier transformation infrared spectroscopy and X-ray photoelectron spectroscopy offer information about the nature of surface functional groups. Finally, the results for either nitrogen or carbon dioxide sorption provide with the specific surface areas and pore volumes some of the most crucial parameters for a possible application.

For an imaginable industrial utilization, a cost efficient process includes the determination of all possibilities and risks. For this, a simple look at the results of the liquid waste phase of the carbonization is also included in terms of composition as seen by total organic carbon and high-performance liquid chromatography. For this, the waste water phase after a normal carbonization was compared to that obtained by salt-HTC. A potential recycle loop by using the waste water phase as the reaction medium for the next HTC is also discussed.

The activation of hydrochars by means of physical activation with steam will show an improving of certain char characteristics to make them more suitable for applications in active carbon like fields.

Closing, the dye sorption of two different dyes on various hydrochars and activated hydrochars will be shown.

4.1 Hydrothermal carbonization in the presence of salt-water mixtures

4.1.1 Hydrochars from different substrates obtained in the presence of zinc chloride

The carbonization of biomass with different additives showed to alter several hydrochar characteristics, as reported in various literature sources. To study the effect of adding a salt-water mixture containing zinc chloride to the carbonization of various biomass substrates, all substrates listed in table 7 were carbonized for 12 hours at 180 °C (if not stated otherwise) in either water (HTC) or a zinc chloride containing salt-water mixture (salt-HTC). Most HTC and salt-HTC reactions were carried out by HTC method B using either water or a 60 wt% zinc chloride solution (e.g. Glu_B12h180C60Zn). Only the reactions of the mixture of different grasses and rushes, as well as those with sawdust followed procedure HTC method A for the salt-HTC in which either water or a mixture of zinc chloride with traces of another chloride (e.g. lithium chloride) was used (e.g. Gnr_A12h180CLi(0.23)Zn). While the latter had two salts instead of one present, their results are shown for integrity. For a detailed description of the HTC method A or B consult chapter 3.2.1 of the material and methods part.

4.1.1.1 Reaction yield and ash content

By carbonizing various substrates for 12 hours at 180 °C in either water (HTC) or a zinc chloride containing water mixture (salt-HTC), different hydrochars were obtained. Depending on the nature of the starting material, some of the obtained samples shared similar characteristics for which they could be divided into certain groups. For this, the reaction yield (amount of g received from g substrate used in %) and ash content (amount of sample remaining after heat treatment at a maximum temperature of 750 °C) gave two quick and easy methods for a first classification. A higher yield points to a substrate with structures more resistant to a hydrothermal treatment at the chosen process time and temperature. As seen in figure 53a and table A1 all chars were obtained with a yield of less than 65 wt%. Half of them even lost 50 wt% of the initial used substrate. The highest yields were received when carbonizing sawdust, rice husks or broken coconut shell pieces without the salt. Considerably less hydrochar remains if algae, HMF or glucose were used. All other samples had a yield between 40 to around 60 wt%. The trend from HTC to salt-HTC usually showed a decrease in yield between 3 to 8 wt%.

The yield for the samples from lignin (difference 0.2 wt%) and dried dandelion leaves (difference 1.5 wt%) showed similar values when comparing their HTC and salt-HTC samples. Only those received from glucose, the mixtures of different grasses and rushes or algae had a higher yield when synthesized via salt-HTC method, with around 8 to more than 20 wt%.

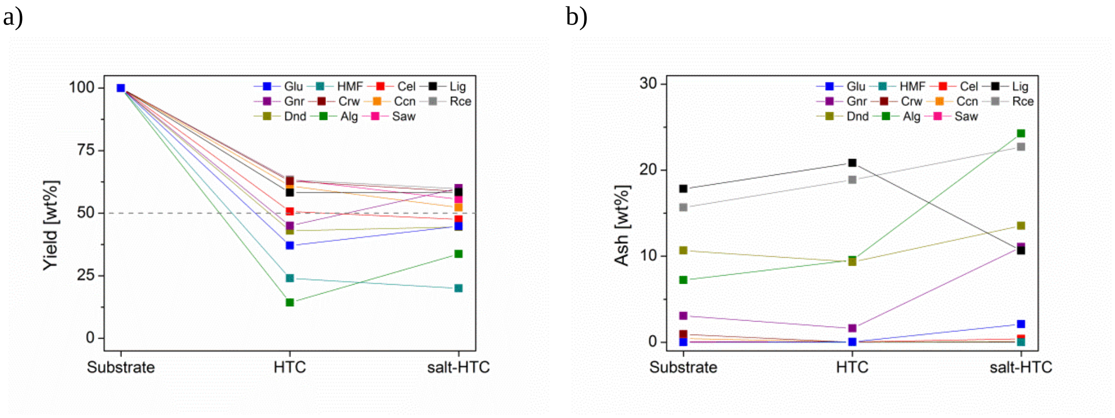

Figure 53 Yield (a) and ash content (b) of different substrates and their resulting hydrochars obtained by HTC for 12 h at 180 °C with either no salt present (HTC) or a zinc chloride containing one present (salt-HTC).

To conclude from these results onto the stability of the substrates under HTC conditions, it is also important to discuss the amount of inorganic components in the substrates and more importantly in the hydrochars, since these give additional weight when calculating the yield. High inorganic contents in the received chars would indicate an increased yield and may lead to false conclusions. Figure 53b and table A1 show the ash content of the substrates and their hydrochars. For the substrates, especially lignin and rice husks showed high amounts of non-organic compounds present with nearly 20 wt% ash. The dried dandelion and spirulina algae also had a comparable high ash content around 10 wt%. The mixture of different grasses and rushes with 3 wt% ash formed the last substrate with increased ash content, while all other substrates showed comparable low values of < 1 wt%. Figure 53b also illustrates that the ash content increased in all cases from the substrate over hydrochar to those received in the salt-HTC reactions except for those received by lignin. This trend could be explained if an excess amount of reaction salt was left in the char, but since not all samples showed a similar high increase of ash amount in the salt-HTC char it is questionable. In the cases of low initial ash content in the substrates, the difference in ash from HTC to salt-HTC was minimal, usually less than 1 wt%. Only glucose showed around 2 wt% in the salt-HTC with 0 wt% in the substrate. If the biomass had a high initial content of inorganic matter present, the salt-HTC chars mostly contained an increased amount of ash if compared to those received by the normal HTC method. On top of that, the observation that the yield usually decreases from HTC to salt-HTC, as discussed before, also suggested that the increased ash content does not result from the added zinc chloride.

To verify that the washing steps solved all zinc chloride from the hydrochars, an unwashed sample is compared to a normally washed one by XPS (Figure 54). Figure 54a shows an XPS survey spectrum of an unwashed sample (Ccn_B12h180C60Zn) that had an ash content of about 10 wt% (while the substrate had an initial ash content of 0.44 wt% (coconut shell powder)) and figure 54c a washed sample, that had only 0.10 wt% ash left after burning. The survey spectrum of the unwashed sample showed a clear signal at an binding energy of 1022-1023 eV, referring to either zinc oxide or zinc metal. An XRD of the ash from this sample is also given in figure 54b, showing good agreement with the database diffractrogram ICSD 98-006-5121, also resembling ZnO. The decrease in ash content after washing and the absence of a zinc compounds signal in the XPS survey spectra of the washed sample (figure 54c) underline that the initial used salt, which would stay in an unwashed hydrochar as ZnO, was removed in the washing process after the HTC. While zinc oxide is typically insoluble in water, it is imaginably that the soluble compounds of the hydrochar create an acidic environment in which the ZnO can be removed from the sample. This further indicates that the increased inorganic matter is based off the substrate rather than the added zinc chloride.

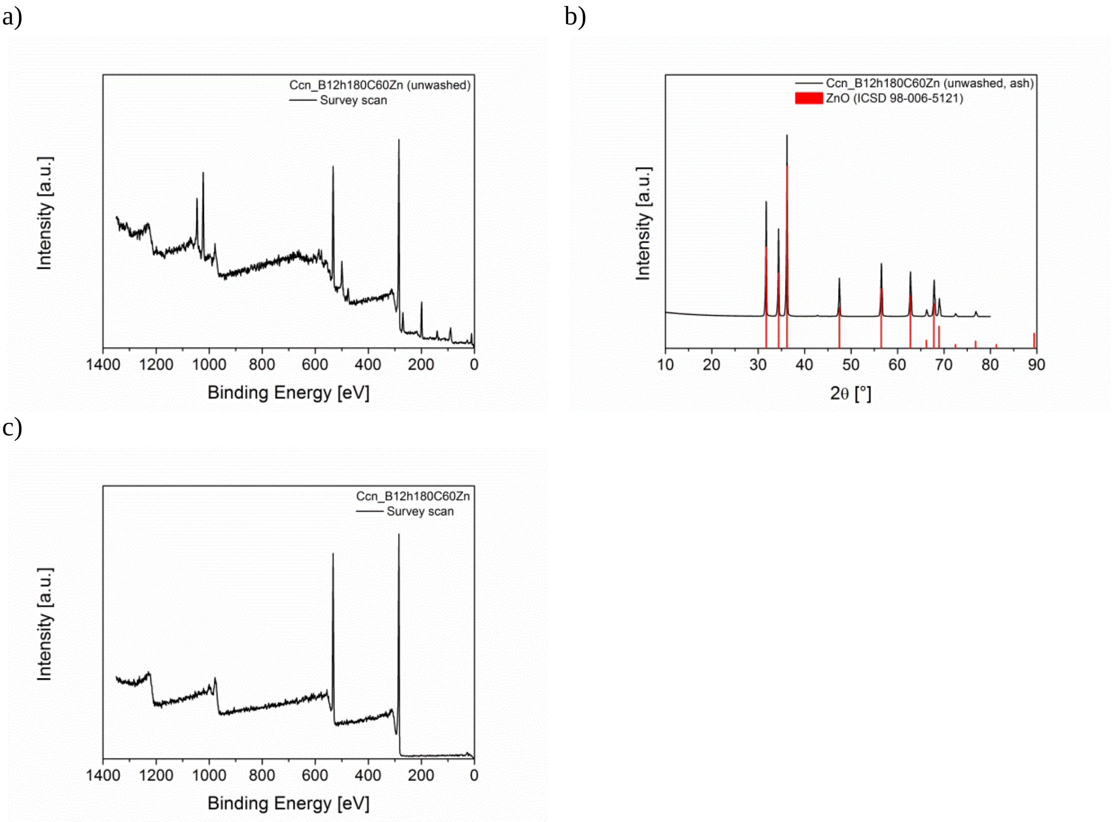

Figure 54 a) XPS survey spectrum of an unwashed hydrochar (Ccn_B12h180C60Zn), together with b) an XRD of its residual ash and c) an XPS survey spectrum of the washed sample (Ccn_B12h180C60Zn).

In case of a substrate with high initial content of inorganic compounds like rice husks (15.67 wt%), the nature of the ash from the salt-HTC char (Rce_B12h180C60Zn) was not easily determinable like in the previous case, as seen in figure 55a. The figure shows no clear signals in the XRD. An investigation by EDX showed prominent peaks of silicon with 6.67 wt% and 3.31 at% as Si-K, probably from SiO_2, as shown in figure 55b (compare table A2). The ashes of other substrates (spirulina algae, cellulose or broken coconut shell pieces) were also investigated by XRD but they could also not be assigned to one specific compound.

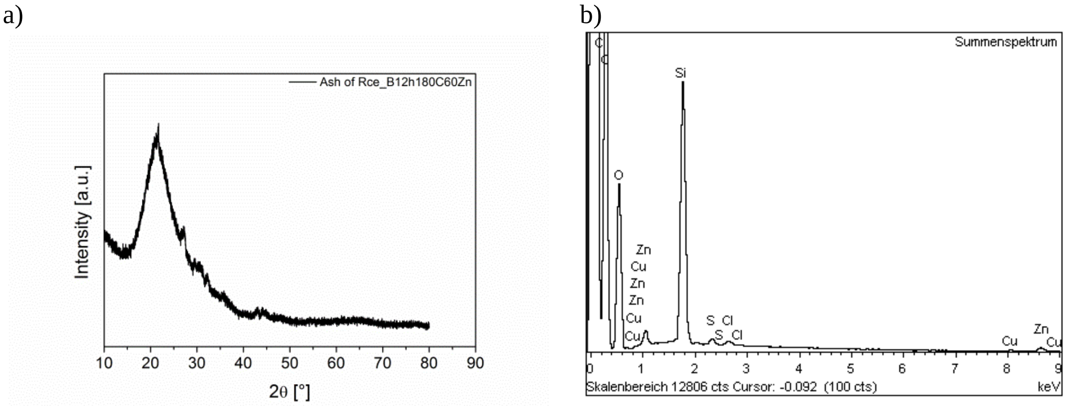

Figure 55 XRD of the ash of Rce_B12h180C60Zn (a) and an EDX spectrum of the hydrochar (b).

Since in the process of the HTC a huge amount of liquid and gaseous side products is formed mostly the hydrogen and oxygen content of the sample decrease (as discussed later in chapter 4.1.1.3), increasing the percentage of inorganic compounds. The yield is in most cases decreased, even further for the salt-HTC, suggesting a raise in degradation reactions induced by the zinc chloride, which would increase the amount of ash percentage. These results already hint that the zinc chloride can potentially perform or enable reactions within the hydrothermal carbonization that usually don't take place under the used conditions (12 hours at 180 °C) acting as an catalyzing agent for the HTC.

By keeping the ash content in mind, the substrates can now be grouped into three possible classes with the sugar (glucose) and its degrading product HMF kept out:

a) stable or hard, wood like biomass with high yield and low ash content (cellulose, broken coconut shell pieces, coconut shell powder and sawdust);
b) stable ones with rather high ash content (lignin, rice husks) and
c) soft biomass with low yield and high ash (mixture of different grasses and rushes, dried dandelion leaves and spirulina algae).

4.1.1.2 Hydrochar morphology

To investigate the formation of hydrothermal carbons from complex lignocellulosic biomass, first the morphology change for the framework molecule glucose is discussed. Figure 56 shows the hydrochars obtained from carbonization of the sugar for 12 hours at 180 °C in either water (a) or a zinc chloride containing salt-water mixture (htc_A) (b). In both cases, big agglomerates were build of smaller particles. In the case of the simple HTC reaction the agglomerates were in the size range of 50 µm while in the salt-HTC much smaller agglomerates are formed (0.6 to 6.5 µm). Further insight can be drawn from the size of the aggregates forming those agglomerates. For a simple hydrothermal carbonization the aggregates build well shaped spheres in the range of a radius about 2 to 15 µm (figure 56a-I). Much smaller particles were formed in the salt-HTC with no distinct visible aggregates since the agglomerates seem to be formed only by primary particles (figure 56b).

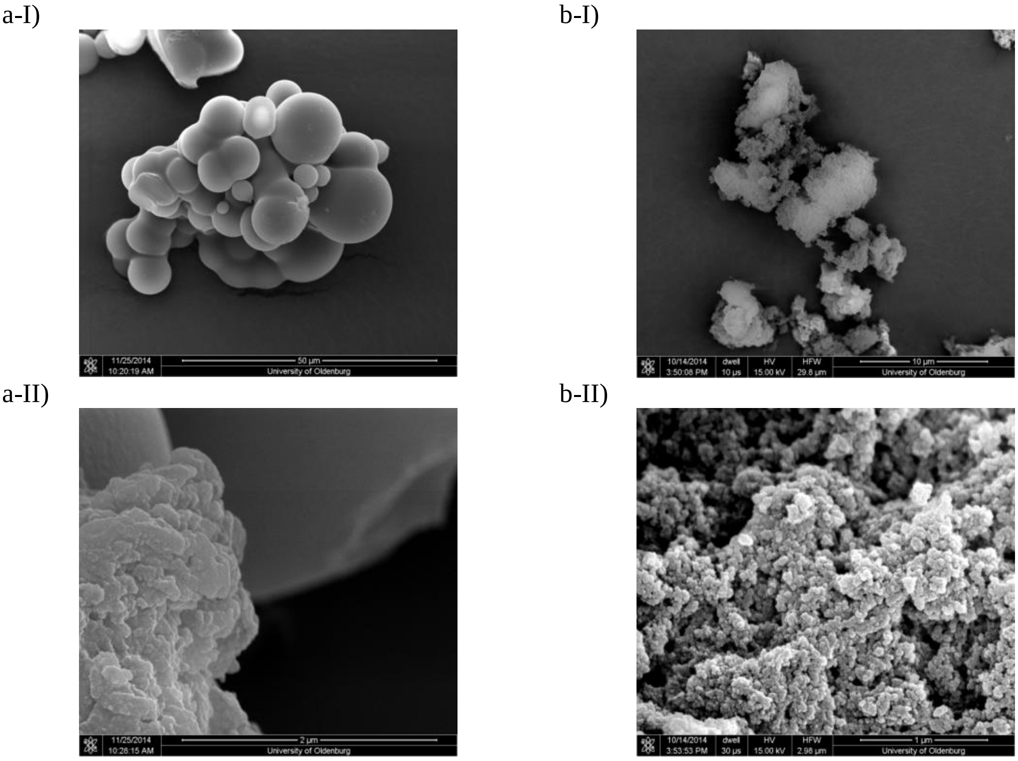

Figure 56 SEM images of hydrochars received by glucose (Glu_A12h180C (a) and Glu_A12h180CLi(0.23)Zn (b)) with smaller (I) and higher (II) magnification.

However, not only the aggregate and agglomerate sizes were different as also the roughness was strongly increased in the sample synthesized with the salt as seen in figure 56b-II. While the surface of the nuclei in case of the HTC hydrochar also looked quite rough at closer look (figure 56a-II), the salt-HTC sample showed a roughness increased to a high extent, probably due to smaller primary particles.

Usually, the char formation from glucose takes place through a nucleation growth process. In this the glucose molecules react to HMF which transforms to the hydrothermal carbon by a wide range of chemical reactions like polymerisation from which they nucleate and form spherical carbon particles. Since the agglomerates in the case of the salt-HTC don't have a spherical form no typical nucleation growth seems to have taken place. Thus, the salt mixture seems to inhibit a particle growth and the formation of large spherical structures. By that, a surface made out of many small primary particles instead of grown ones is obtained resulting in increased roughness.

The conclusions from the SEM images of glucose hydrochars is supported by observations from the TEM images as seen in figure 57. The hydrochars received by HTC of glucose showed round spherical particles with nearly no interparticle spaces for which it was difficult to determine the primary particle sizes (figure 57a). Those received by salt-HTC on the other hand showed a lot of free spaces between the particles in the range of around less than 100 nm with primary particles of around 50 nm in size (figure 57b-II).

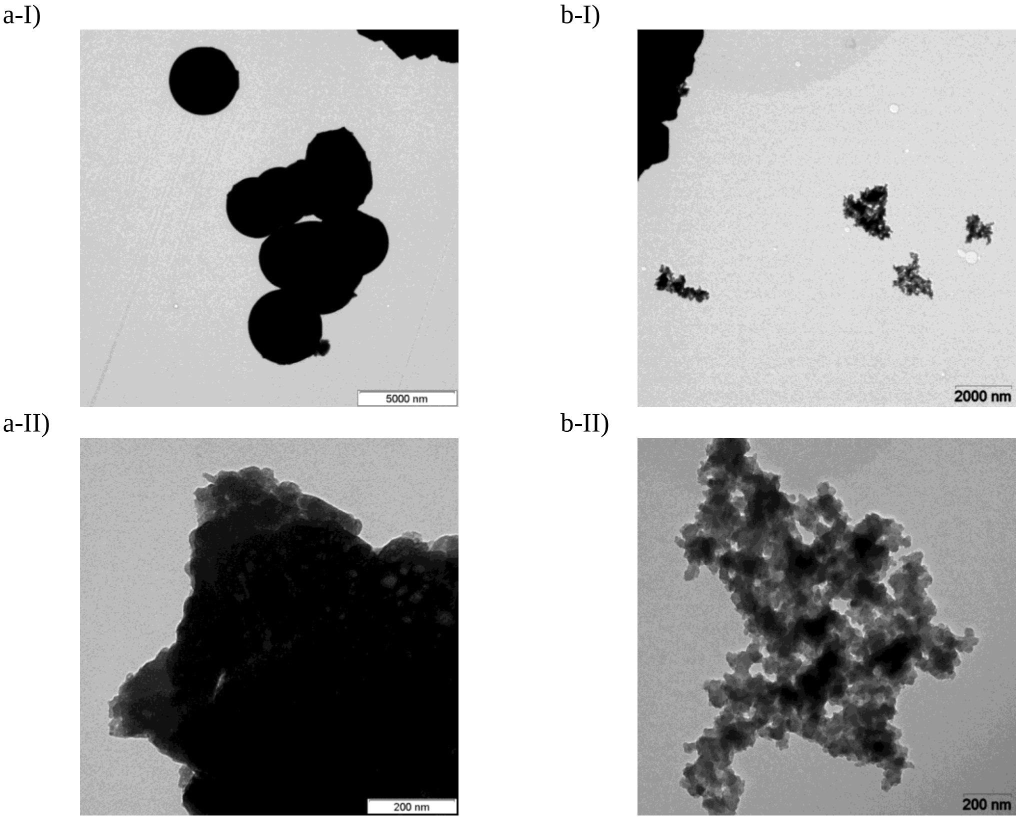

Figure 57 TEM images of hydrochars received by glucose (Glu_A12h180C (a) and Glu_A12h180CLi(0.23)Zn (b)) with smaller (I) and higher (II) magnification.

In the next step, to discuss the morphological changes from the biomass materials as seen by SEM and TEM, one substrate from each of the previously determined classes (see 4.1.1.1) will be shown representatively: Coconut shell powder as a stable/hard biomass (figure 58), rice husks as a stable biomass with high ash content (figure 59) and the mixture of grasses and rushes as a rather soft biomass with high ash content (figure 60). TEM images support the gathered information and are shown in figure 61.

In case of the coconut shell powder at magnifications of around 45 times no significant difference was visible between the substrate, its HTC and salt-HTC char (figure 58-I). Only in the latter bigger structures were obtained that were not present in the initial substrate (figure 58c-I).

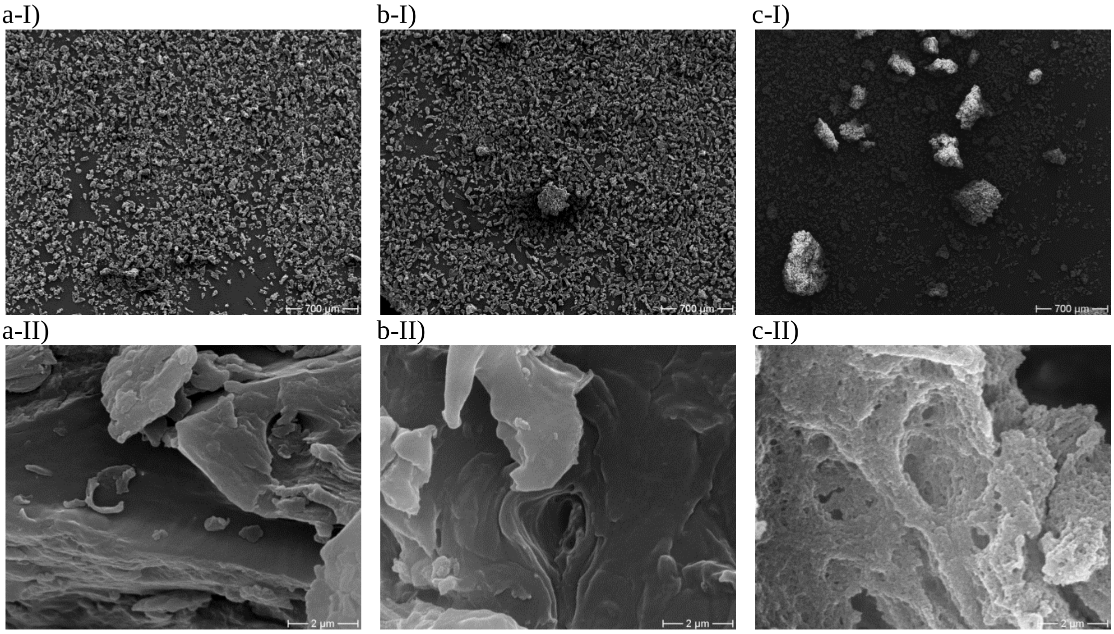

Figure 58 SEM images of coconut shell powder (a) and its HTC (b, Ccn_B12h180C) and salt-HTC hydrochar (c, Ccn_B12h180C60Zn) with magnifications of around 45x (I) and 12,000x (II).

From a magnification of at least 12,000 times, the differences in the samples were clearer. While the substrate and the HTC sample showed a similar structure to each other with different layers of smooth surfaces, the salt-HTC sample showed a much rougher surface. The previously rather smooth surface was spotted to a high extent with a lot of holes in the structure similar to those seen for the glucose salt-HTC sample (compare figure 56b-II).

These results indicate that the substrate was not much attacked at a carbonization temperature of 180 °C and stays mostly intact under normal conditions. When the zinc chloride was present, the surface of the biomass was attacked and holes were formed and therefore the roughness created by the degradation of compounds in the structure increased. Since the main macrostructure stayed intact some framework parts seem to be resistant to the hydrothermal treatment at the chosen, rather low HTC conditions even with the salt mixture present. Biomass is usually built by a combination of the three components cellulose, hemicellulose and lignin which all have different stabilities when hydrothermally carbonized. Since lignin is usually resistant to the HTC reactions at lower temperatures like 180 °C it is possible that the preserved macrostructures consist mostly of the lignin from the biomass and the holes and roughness were created by dissolution or reaction of the cellulose and/or hemicellulose to compounds going into the liquid phase. Because most these fragments are not soluble in water they might form spherical shaped carbon particles to minimize the contact area with its surroundings, which can settle on the carbon surface, creating additional roughness.[53] Similar reactions to that observed for glucose are also imaginable if sugars formed from the degradation of the biomass form spherical carbon particles which also move and stick to the initial biomass surface.

For the rice husks, which were used as received (non-milled), the initial particles were much bigger compared to those found for the coconut shell powder substrate and therefore the effects of the HTC reaction are clearer already at a lower magnification. The rice husks substrate is built of big, scaly structures with thinner fibers on top of them (figure 59a). The hydrothermal carbonization leads to a breakup of the bigger structures as seen in figure 59b-I. Some remaining bigger structures are reminiscent of the substrate and look just like smaller pieces broken out of it. Also, by comparing figure 59a-II and 59b-II, smaller particles are seen on top of the bigger structures that didn't exist in the substrate. By using the zinc chloride in the carbonization, the breakup increased to a high extent so that there are no similarities between the hydrochar and the substrate visible anymore (figure 59c-I).

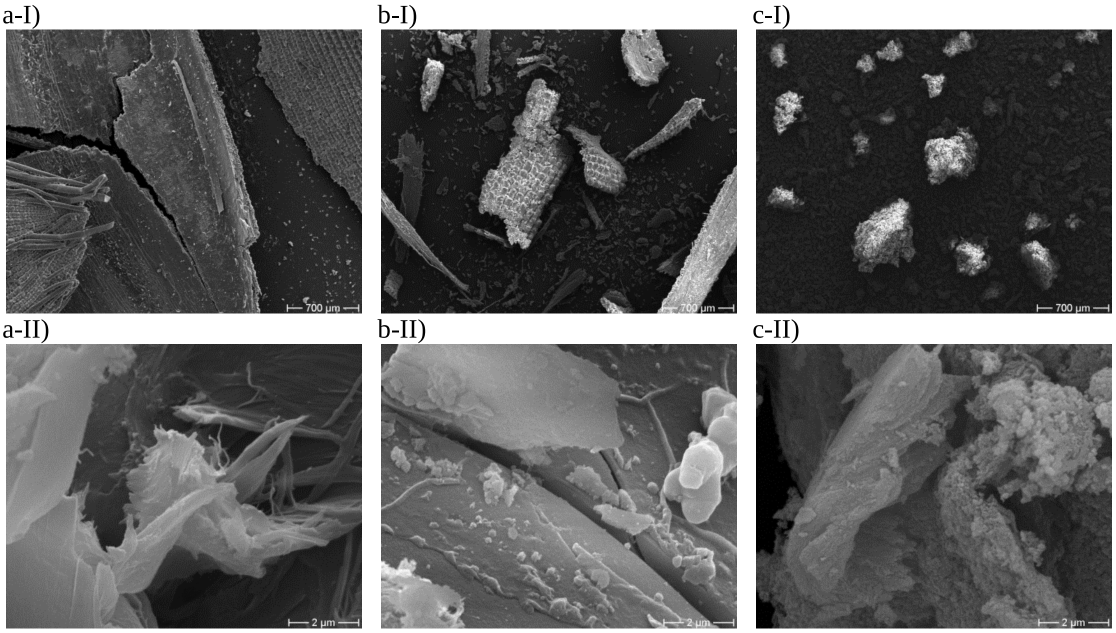
a-I) b-I) c-I)

a-II) b-II) c-II)

Figure 59 SEM images of rice husks (a) and its HTC (b, Rce_B12h180C) and salt-HTC hydrochar (c, Rce_B12h180C60Zn) with magnifications of around 45x (I) and 12,000x (II).

The average particle size is decreased by several orders of magnitude and also the surface roughness increases to a great extent (figure 59c-II) as seen also for the coconut shell powder sample (figure 58c-II).

For the samples obtained from the mixture of different grasses and rushes similar observations to those from the coconut shell powder and rice husks were made as seen in figure 60. The difference in the substrate and the carbonized sample is minimal, with carbonized particles visible on the former substrate (figure 60b-II). By using the salt-water mixture the bigger substrate particles breakup into many small particles (figure 60c-I), which show an increased amount of carbonized particles on their surface (figure 60c-II).

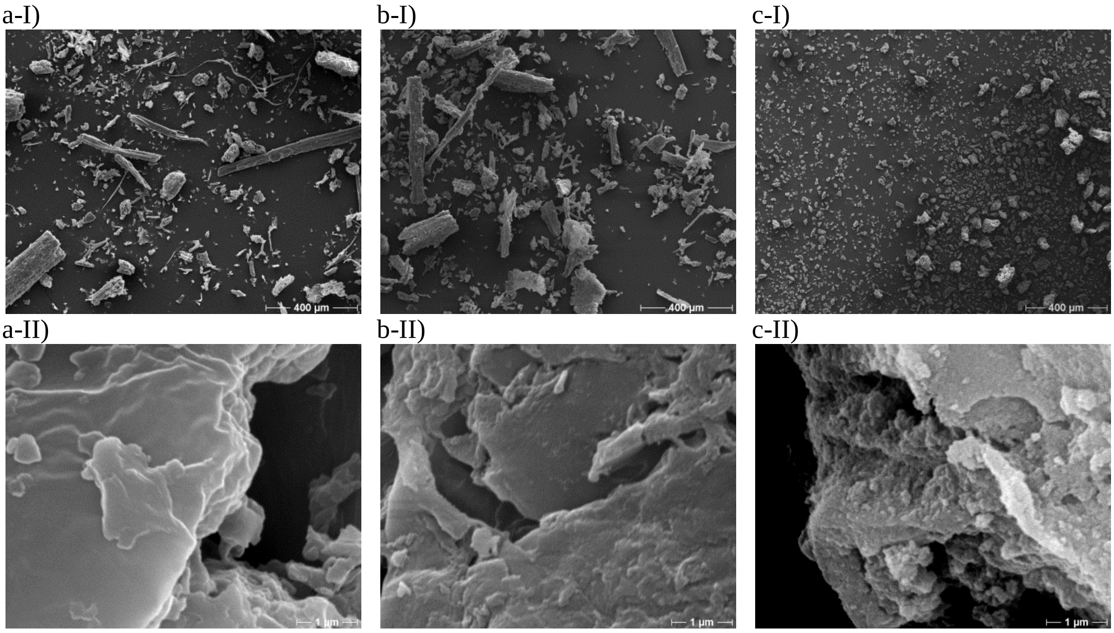

Figure 60 SEM images of a mixture of different grasses and rushes (a) and its HTC (b, Gnr_A8h180C) and salt-HTC hydrochar (c, Gnr_A8h180CLi(0.23)Zn) with magnifications of around 45x (I) and 12,000x (II).

The TEM images of all six carbonized samples, either by HTC or salt-HTC and with the three substrates coconut shell powder, rice husks and the mixture of different grasses and rushes, further point out the information gathered by SEM, as seen in figure 61. Since no image could be obtained for the salt-HTC sample of the mixture of different grasses and rushes discussed for the SEM images (Gnr_A12h180 CLi(0.23)Zn), an image of a comparable sample (Gnr_A12h180CK(0.51)Zn) is shown instead. Compared to the carbonized samples, which show a rather smooth surface with no distinct primary particles, the samples carbonized with a salt mixture present show smaller primary particles in the size range of 20-50 nm. Only the sample obtained from the mixture of different grasses and rushes shows bigger structures together with bigger holes (figure 61c-II). This might be related to the previously mentioned presence of the second cation (potassium from KCl). The influence of the salts in the mixtures besides the zinc chloride will be discussed at a later point in this work (see 4.1.5).

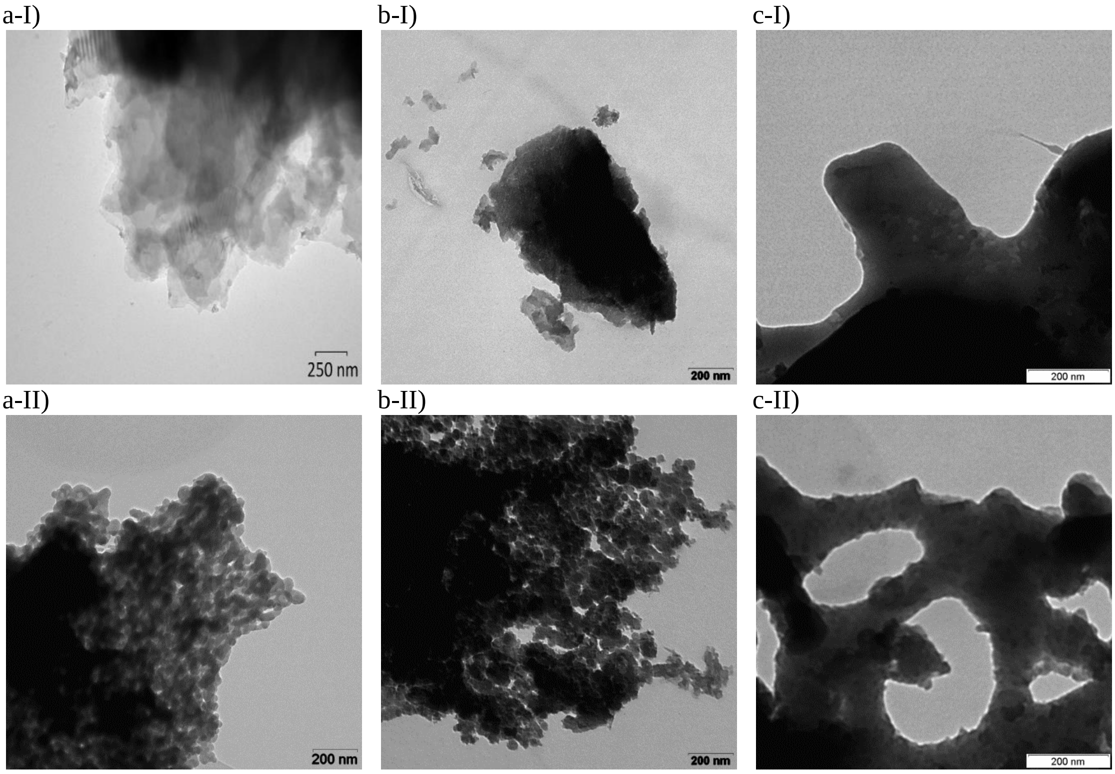

a-I) b-I) c-I)

a-II) b-II) c-II)

Figure 61 TEM images of hydrochars received from different substrates: a) coconut shell powder (Ccn_B12h180C (I) and Ccn_B12h180C60Zn (II)), b) rice husks (Rce_B12h180C60Zn (II)) and c) the mixture of different grasses and rushes (Gnr_A12h180C (I) and Gnr_A12h180CK(0.51)Zn (II)).

4.1.1.3 Elemental composition

While the yield and ash content gave some information about the reaction course as well as the substrate suitability and SEM/TEM images visuals of the morphology, the first information about the actual chemical sample properties can be obtained from elemental analysis. The results for the carbon, hydrogen, nitrogen and oxygen content are summarized in table A1.

Only three substrates had a noteworthy presence of nitrogen, namely the mixture of different grasses and rushes, the dried dandelion leaves and the spirulina algae. Depending on the substrate, the nitrogen content either increases or decreases after the HTC or salt-HTC which does not give any detailed information about a general trend. While the general level of nitrogen amount stays the same for the Gnr and Dnd samples, the one with the highest initial value, the substrate spirulina algae, showed the highest change with declining from about 34.77 (Alg) over 13.29 (Alg_B12h180C) to 3.93 % (Alg_B12h180C60Zn). The high amount of ash in the last sample (Alg_B12h180C60Zn) suggests that a lot of nitrogen was lost into the liquid or gaseous phase. Interestingly, traces of nitrogen were also found in hydrochars whose substrates did not have any nitrogen present (e.g. Glu_B12h180C60Zn), indicating a small cross-contamination from the reaction vessels by previous experiments.

But since all the nitrogen contents in those hydrochars were under < 1 % it is possible that they also simply lay within the apparatus error.

The change in carbon content from the substrate over HTC to salt-HTC char is graphically shown for all samples along with a resulting van Krevelen diagram in figure 62.

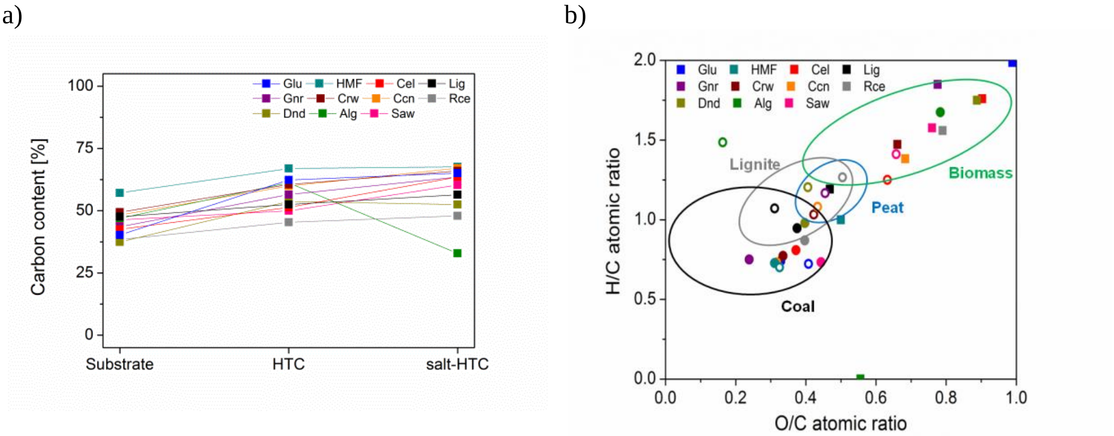

Figure 62 Carbon content (a) of various substrates and their hydrochars as well as a van Krevelen diagram (b) obtained from elemental analysis (square - substrate; empty circle - HTC; full circle - salt-HTC). The areas for biomass, peat, lignite or coal are collected from literature[40, 96, 267].

As seen in figure 62a, the carbon content increases significant from the substrates to the hydrochars in all cases. The majority of the substrates had an initial carbon content of around 40-50 % present with the only exception being the HMF (57.14 %) whose value was calculated from the theoretical chemical formula. The broken coconut shell pieces and the coconut shell powder had the highest initial values with 49.40 and 49.07 %, respectively. The rice husks and the dried dandelion leaves contained the lowest carbon percentages with less than 40 %, precisely 38.44 and 37.47 %, respectively. After carbonizing at 180 °C for 12 hours the average carbon content rose to around 50-60 % with the highest found for the HMF with 66.95 %. With the exception of the algae samples the increase of carbon content is mainly due to a loss of oxygen and hydrogen (table A1). The biggest change occurred in the case of glucose from 40.25 (Glucose) to 62.34 % (Glu_B12h180C) with a change of 22.09 %. The dried dandelion leaves followed with an increase of 16.21 %. The smallest increases were found for lignin and sawdust with a small increase by 4.92 and 3.63 %, respectively.

Some of the results underline the classification as discussed from the yield and ash content. Lignin or sawdust, but also cellulose (+8.80 %) and the rice husks (+6.91 %) seem to have a harder structure more resistant to the HTC. Interestingly, the coconut shell pieces and coconut shell powder, which were classified as stable biomass before due to their yield and ash, show high carbon content increase (+11.13 % (Crw) and +10.83 % (Ccn)).

The three substrates in the soft category show not only a high yield loss and high ash but also a higher change in carbon content with the mixture of different grasses and rushes changing from 43.56 to 56.48 % (+12.92 %), the dried dandelion leaves from 37.47 to 53.68 % (+16.21 %) and the spirulina algae from 46.93 to 61.23 % (+14.30 %). The results indicate that these substrates lost a lot of their composition from either hydrogen or oxygen (since the nitrogen content is stable for the mixture of different grasses and rushes and the dried dandelion leaves) and/or nitrogen (in the case of spirulina algae as discussed above).

With the addition of zinc chloride to the reaction a further increase in carbon content can be observed in most cases. While the carbon content present in the HMF samples increased by just 0.65 %, other samples showed values from nearly +3 up to nearly +13 % (from Cel_B12h180C to Cel_B12h180C60Zn). Since the cellulose showed the highest increase, the zinc chloride seems to be especially useful for the converting of cellulose. Because cellulose is also part of most used biomass, their cellulose parts could have been similar suitable for reaction. Besides in the cellulose the carbon content also increased significantly when comparing the HTC and salt-HTC char for the sawdust (+ 10.33 %) and coconut shell powder (+ 7.21 %). Surprisingly, the carbon content of the lignin sample, which was not only increased by a normal HTC reaction, could be further optimized by the use of the salt-water mixture. While the dried dandelion leaves as a soft biomass with high ash content showed a minor decrease in carbon content from HTC to salt-HTC of around 1 % another substrate from this class showed a significant decrease in carbon content, namely the spirulina algae. The zinc chloride might have solved a lot of organic compounds into the liquid phase for this biomass, preventing the formation of a significant carbon phase, as supported by the observations of the yield for this sample.

The van Krevelen diagram in figure 62b shows the evolution of the different samples from the substrate to coal-like hydrochars. As to be expected, most substrates fall in the area usually attributed to biomass. Since the van Krevelen diagram is usually used for coals from biomass, the glucose and hydroxymethylfurfural are not well represented. The high nitrogen amount in the spirulina algae samples also lead to an unreasonable distribution of their points. The lignin with its low amount of hydrogen (4.76 % compared to usually 5-7 %) and oxygen (29.70 % compared to usually 40-50 %) falls in the lignite section. The carbonized samples (HTC) tend to leave to the peat or lignite areas but for most samples, the conditions 180 °C for 12 hours seem not to be enough to push them into the coal region. Only when the salt was present in the reaction, the obtained hydrochars show H/C and O/C atomic rations similar to those usually found for coals. The different sample colors, mainly resulting from aromatic carbon compounds, underline the evolution since most HTC chars are light brown to brown as typical with peat-like chars, while the salt-HTC samples are of dark brown to black color, as seen in figure 63a (overview) and 63b (detail) for samples received from coconut shell powder.

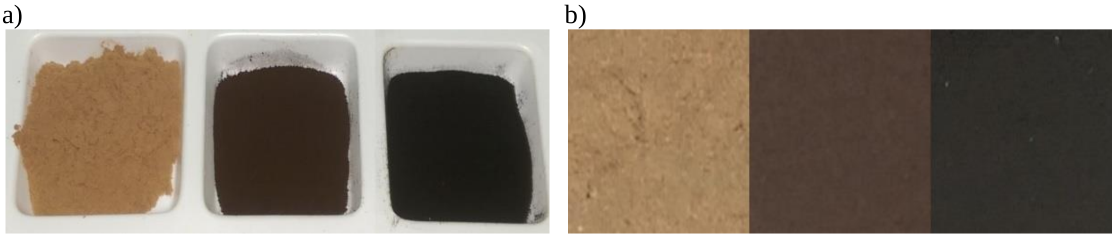

Figure 63 Coconut shell powder (light brown), its HTC (brown, Ccn_B12h180C) and salt-HTC coal (black, Ccn_B12h180C60Zn).

Since the change from substrate to hydrochar as well as to those received by salt-HTC usually follows the dehydration line within the van Krevelen diagram, two main information are obtained: the reactions within the hydrothermal carbonization are mainly dehydration reactions and zinc chloride catalyzes these reactions. The latter is derived from the extent of change for the substrate to hydrochar, which is more prominent for the salt-HTC samples because more hydrogen is lost overall. Comparing the hydrochars with the salt-HTC chars the latter ones are also more shifted to lower H/C atomic ratios, so they not only follow the dehydration lines but also the demethylation line. Since nearly no shift on the demethylation line took place from the substrate to the normal HTC chars it can be assumed that the zinc chloride also enables demethylation reactions within the hydrothermal carbonization.
Interestingly, the van Krevelen diagram shows the sample received from salt-HTC of the mixture of different grasses and rushes (Gnr_B12h180C60Zn) as the most evolved sample in regards with it being the one nearest to the lower left corner of the diagram. Otherwise the stable or hard biomass (Crw, Ccn and Saw) seem to be more dehydrated than others (Rce, Dnd). The demethylation is most prominent for the char from salt-HTC of sawdust (Saw_B12h180C60Zn), additionally to a moderately high amount of dehydration. In case of the lignin and dried dandelion leaves the difference of HTC and salt-HTC chars is not seen as an increase in dehydration but rather in demethylation. This indicates that the zinc chloride seems not to act the same way in each substrate. Some include compounds that are more easily demethylated or all those who can be dehydrated already followed these reactions, while in other substrates not all are dehydrated in normal reactions so the salt can still increase the amount of those. There are also differences in the extent of dehydration. The samples from cellulose, the mixture of different grasses and rushes and sawdust show the biggest increase from HTC to salt-HTC. Another interesting point is visible from the glucose and HMF where the HTC and salt-HTC samples are relatively close to each other, in case of the HMF nearly on top of each other. Here, the reactions are already possible in the normal HTC since no biomass structures need to be broken and therefore the substrates are much easier accessible for carbonization.

4.1.1.4 Hydrochar structure and its order

From the discussion of the change in elemental composition two of the major reaction pathways, dehydration and demethylation, with the latter mostly only in case of salt-HTC samples, were identified. However, no clues about which parts of the substrate actually changed were gathered from these. Patterns obtained by XRD give a first glimpse of the change in hydrochar structure in terms of structural order when comparing the substrate with those received by HTC and salt-HTC. Figure 64a shows exemplary the XRD diffractograms for the case of coconut shell powder. After a simple hydrothermal treatment the initial signals from the substrate are not changed but only increase in intensity. A possible explanation could be the removal of impurities from the initial substrate without changing the crystalline structures of the biomass.[12] The reflections at 16° (101) and 22° (002) could be caused by transverse arrangement of the crystallites in cellulose I, while the reflection at 34° (004) can be related to the longitudinal structure of the polymer.[57] When the zinc chloride was used in the reaction the sample becomes amorphous with a very broad reflection signal, suggesting a very disordered structure. The only signal at 22° could be related to a highly disturbed (002) interlayer carbon packing in aromatics.[246]

More detailed information about the actual structure change within the hydrochars can be derived from data received by ^{13}C solid state NMR spectroscopy. Figure 64b-d shows the data for samples from three different substrates with two of the main biomass components, cellulose (fig. 64b) and lignin (fig. 64c), as well as one biomass, namely coconut shell powder (fig. 64d). Since the biomass is partly build from cellulose and lignin their signals are found in the spectra for the biomass. These are highlighted by colored squares (red: cellulose; black: lignin) in figure 64d. The assignment of the other signals found in the ^{13}C NMR spectra of the biomass derived hydrochars was done with help from data found in literature by different work groups that intensely studied hydrochars using various NMR methods.[53, 248]

The typical cellulose resonance area is found at around roughly 55 to 105 ppm (fig. 64b, red line) whose signals are mainly from aliphatic carbons (typical region 0-80 ppm) and sp^2 hybridized aromatic carbons (typical region 100-160 ppm). After carbonizing the cellulose 12 hours at 180 °C nearly the exact same pattern is found with the only difference of a very small plateau around 15-55 and 142-164 ppm (fig. 64b, gray line). Since these are barely visible they could be assigned as background noise. However, as discussed later in this section, the salt-HTC sample (Cel_B12h180C60Zn) develops broad signals in these regions and therefore it is possible that in the normal HTC these formations also take place even when they are nearly negligible. Otherwise, the reaction conditions seem too low to induce a structural change as already supported by previous results, e.g. with the SEM and TEM images of the substrate and hydrochars from normal HTC showing similar morphologies. The signals of the cellulose region are nearly not present in the cellulose salt-HTC sample and a variety of new signals appear (fig. 64b, black line).

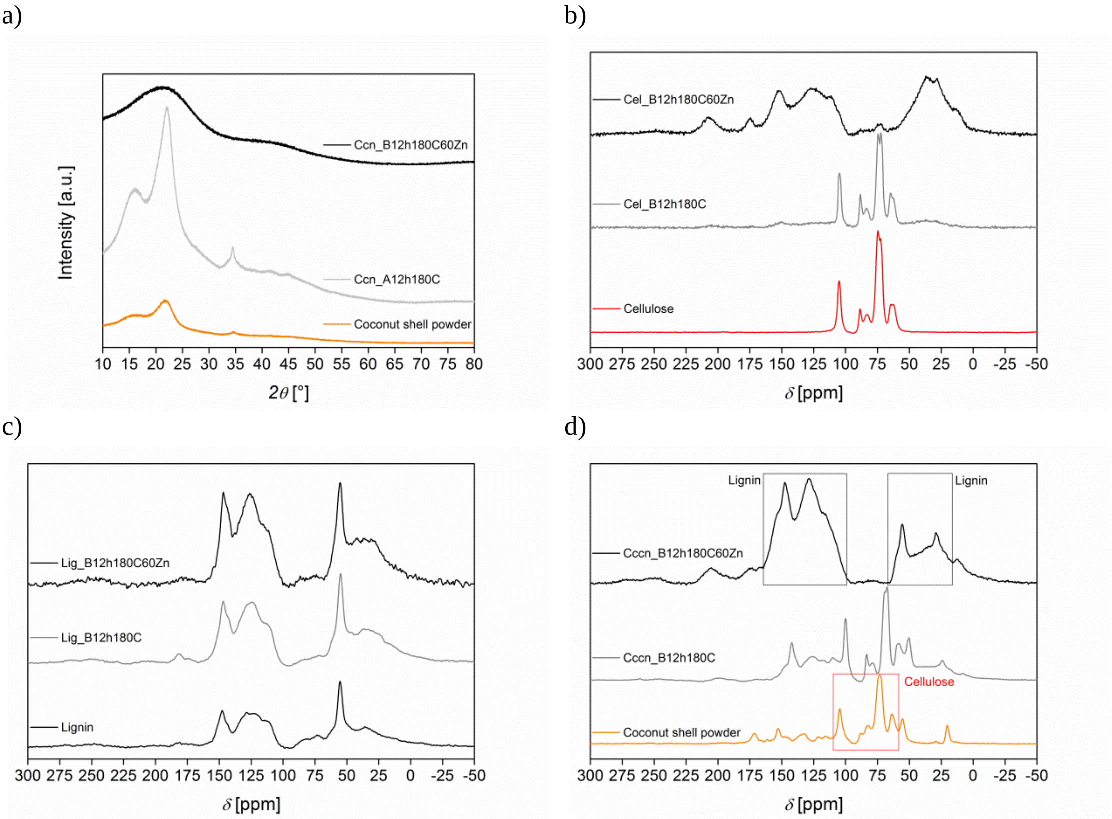

Figure 64 XRD patterns of coconut shell powder and its HTC (Ccn_A12h180C) and salt-HTC (Ccn_B12h180C60Zn) carbons (a) together with ^{13}C SS-NMR spectra for different substrates and their hydrochars (cellulose (b), lignin (c) and coconut shell powder (d)).

This indicates that almost a complete structural change after the hydrothermal carbonization was induced by the addition of the zinc chloride. The broad signal from around 0 to 60 ppm results mostly from aliphatic carbons. The wide distribution indicates the presence of a variety of different CH_x sites. Two peaks at 28 and 37 ppm, as well as a shoulder at 13 ppm can be seen as the main signals which can be attributed to rigid CH_2, mobile CH_2 and mobile CH_3, respectively. The last signal in the area of the sp_3 carbons, one small peak at around 73 ppm, could result from CH. This peak is the only one that can possibly be attributed to remains of the initial cellulose. A quite high number of new signals appear in the aromatic (100-160 ppm) and carbonyl region (175-225 ppm), which can be attributed to $C{=}\underline{C}{-}C$ (112 ppm), sp^2 hybridized carbons (126 ppm), $O{-}\underline{C}{=}C$ (152 ppm) and carbonyl groups (174 and 208 ppm), respectively.

The results show that a temperature of 180 °C is not sufficient to carbonize cellulose in simple water. By using the salt-water mixture (60 wt% zinc chloride), the disruption of cellulose, which usually starts at 200 °C (Falco *et al.*[53]), is achieved already at 180 °C. The influence of temperature will be discussed in the next chapter (see chapter 4.1.2). It seems that the zinc chloride therefore enables the structural changes of the cellulose to the carbon, acting as a kind of activation agent.

Similar result were found for HTC experiments in the presence of strong mineral acids (i.e., H_2SO_4) were cellulose reacts fully at 180 °C.[246] Here, the extent of cellulose hydrolysis to glucose is enhanced.

Figure 64c shows the ^{13}C solid state NMR spectra of lignin and its hydrochars. It can be seen that the substrate is resistant in the hydrothermal carbonization since no significant change in peaks is seen towards the HTC (fig. 64c, gray line) or the salt-HTC char (fig. 64c, upper black line). The characteristic peaks at 55, 126 and 146 ppm can be contributed to lignin methoxy groups, sp^2 hybridized carbons and aromatic carbons bound to lignin methoxy groups, respectively. The area of the sp^2 hybridized carbons develops sharped peaks in the salt-HTC char compared to the substrate, indicating some minor structural changes. As already discussed for the XRD patterns, such a small increase in signal clarity could also be caused from the loss of impurities in a normal hydrothermal carbonization process.

Combining the results of the cellulose and lignin, the structural changes for the complex lignocellulosic biomass, the coconut shell powder, can be discussed. Figure 64d shows the signals received from the substrate (orange line), the HTC (gray line) and salt-HTC char (black line). The characteristic signals from cellulose (red box) and lignin (black box) are inserted for better visualization. The cellulose in the biomass behaves similar as the raw cellulose with a normal HTC reaction changing its characteristic signals only minimal (55-105 ppm), while they disappear completely, if the zinc chloride was present. Since lignin is nearly completely resistant to the carbonization at 180 °C even with the salt present, its signals still occur for the black line. The results hint that the structure of the salt-HTC char from coconut shell powder is mainly made out of carbon structures that originated in the lignin parts of the biomass. Therefore it can be assumed that the hydrochar is constructed nearly only out of partly carbonized lignin structures while all the cellulose from the substrate underwent major changes. The lignin parts can still maintain the macrostructure of the biomass as seen in the SEM and TEM images while the holes and roughness is created by breaking of the cellulose particles.

4.1.1.5 Surface functionality

Information about the surface functionality of hydrochars in terms of functional groups can be obtained by Fourier transform infrared spectroscopy (FTIR) and X-ray photoelectron spectroscopy (XPS). The FTIR spectra of most hydrochars are shown in figures 65 to 69 and are discussed separately for different pairs of substrates or biomass. To determine the surface functionality further, also in terms of quantification besides qualification, the XPS data from the samples obtained from coconut shell powder are shown in figure 70 along with a signal assignment in table 8. The assignment of the peaks found in the FTIR spectra were done by several work groups and are found for a general classification in the work of Zeeh *et al.*[249], while Baccile *et al.*[246] looked more detailed into hydrochars, with a determination of typical XPS signals of those mentioned as well.

While the signals in the substrates vary due to their different biomass nature, some peaks are found in most of them, with differences standing out especially in the finger print area. All measured samples share a broad absorption band between 3500 and 3000 cm^{-1} corresponding to the stretching vibration of O-H from hydrogen bonds. This peak weakens in the hydrochars, indicating a loss of OH-functions. A weak signal between 3000 to 2800 cm^{-1} for CH_x (x = 1-3) valence stretching, shows a similar trend as well. The most obvious changes always happen in the fingerprint area, with a huge part of surface functionality getting lost from the substrate to the hydrochars. The latter often consists of three major signals at 1700, 1600 and 1200 cm^{-1}, corresponding to carbonyl C=O stretching, aromatic C=C stretching and ether C-O stretching, respectively.

For the simple sugar glucose, the prior described trend is seen ideally. The substrate with a rather complex fingerprint region is converted into a hydrochar with just the three prior described, for HTC carbons characteristic, signals at around 1700, 1600 and 1200 cm^{-1}. No significant difference between the HTC and salt-HTC sample is seen. In case of those chars received from its first HTC reaction intermediate HMF, a very similar FTIR pattern is received. Here, some signals from the fingerprint area of glucose are more distinct in the HTC sample than in the salt-HTC sample. This indicates a higher loss of surface functionality if the zinc chloride is used in the reaction.

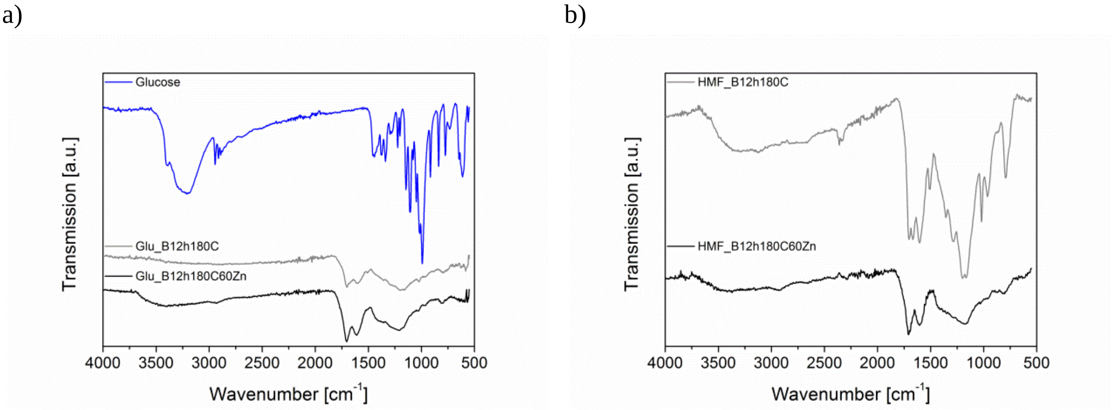

Figure 65 FTIR spectra of glucose and its hydrochars (a) as well as the hydrochars obtained by HMF (b).

In the FTIR spectra from the samples of the two biomass building units, cellulose and lignin, only the first one shows a similar trend like the glucose with just different changes in the fingerprint region. If the cellulose is carbonized at 180 °C a high extent of its surface functionality still maintains, with the C=O, C=C and C-O signals emerging. Interestingly, the signal from C-O changed from around 1000 cm^{-1} to around 1200 cm^{-1}, which can be seen also for glucose and most other tested biomass. Clearly a change from the groups including the C-O signal takes place. While the lignin seemed to be stable in the prior results, a small loss in surface functionality is observed when comparing the lignin with its hydrochar (Lig_B12h180C).

No further change is observed when the salt was present (Lig_B12h180C60Zn), indicating the resistance of lignin to the salt-HTC, as also seen from the NMR results.

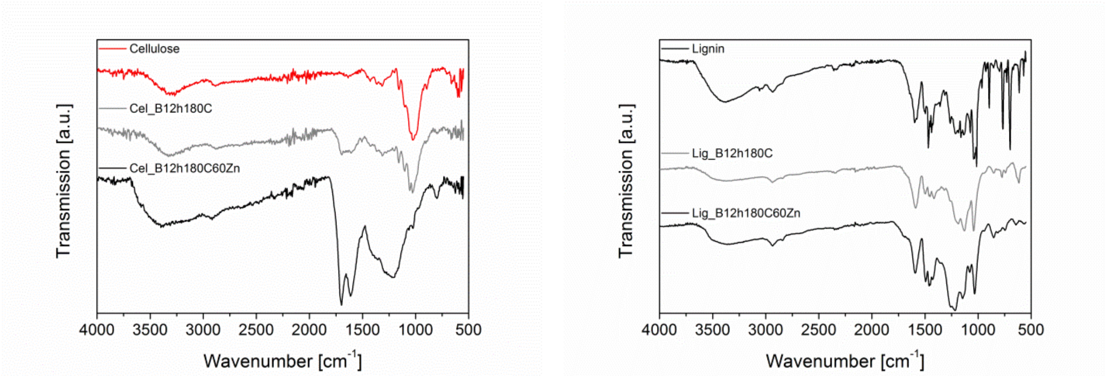
a) b)

Figure 66 FTIR spectra of cellulose (a) and lignin (b) together with those of their hydrochars.

The two biomass coconut shell powder and sawdust show a mixed behavior when compared to cellulose and lignin. While the carbonization at 180 °C for 12 hours leaves most of the surface functionality intact, the lines at 1700 and 1600 cm^{-1} develop more clearly. The signal at 1000 cm^{-1} splits into more small signals wandering towards 1200 cm^{-1}. If the salt is present the shift of the ether band is more developed like in the case of cellulose, indicating the effect of zinc chloride mostly in the reactions including ether bands.

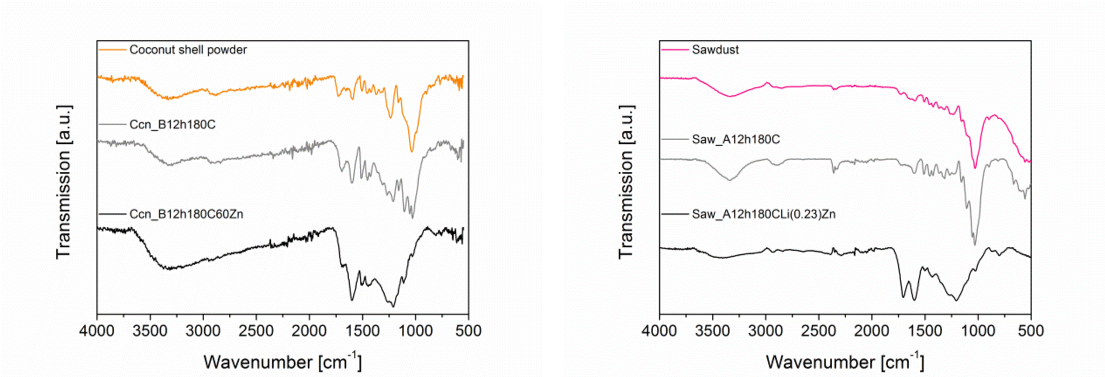
a) b)

Figure 67 FTIR spectra of coconut shell powder (a) and sawdust (b) together with those of their hydrochars.

For the rice husks and the mixture of different grasses and rushes the ether bands around 1000 or 1200 cm^{-1} have a higher intensity than the C=C and C=O signals at 1600 and 1700 cm^{-1}, respectively. While the rice husks seemed to have stable C-O groups even with salt present, the one with the mixture of different grasses and rushes changed in the salt-HTC as with previous samples. The ether groups in the rice husks therefore seemed to be more stable than in other samples.

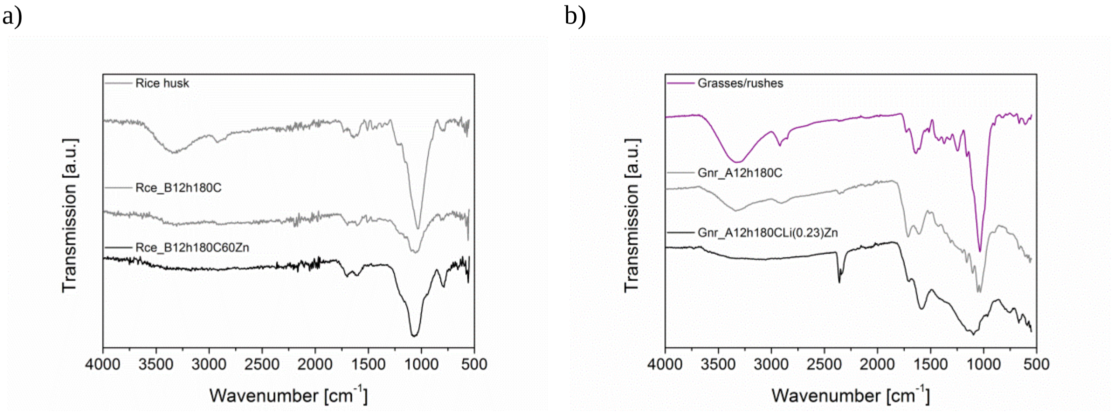

Figure 68 FTIR spectra of rice husks (a) and the mixture of different grasses and rushes (b) together with those of their hydrochars.

The hydrochars from the dried dandelion leaves showed the biggest difference between HTC and salt-HTC samples with the first having rather high signals for ether groups and the latter for carbonyl groups with a broad ether signal. Since the dandelion leaves and algae had a rather high amount of nitrogen present in their substrate and hydrochars the signals at 1600 and 1400 cm^{-1} could also results from N-H and C-N stretching vibrations, respectively.

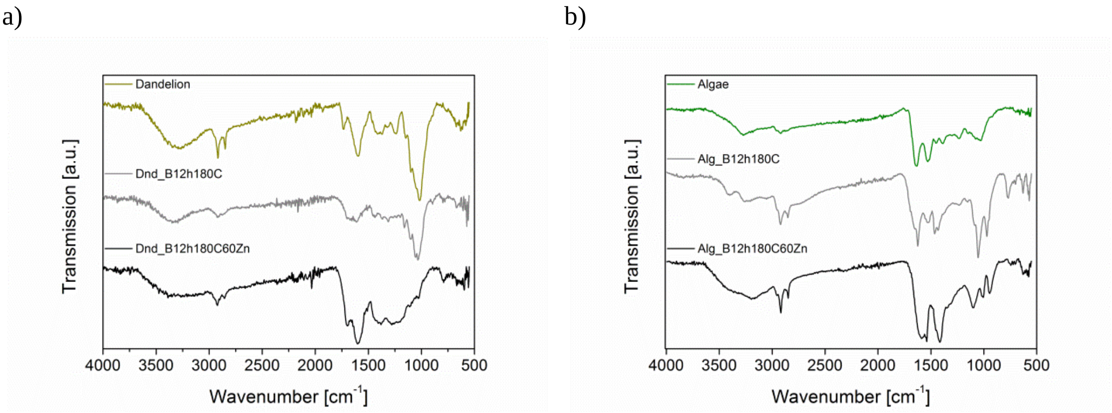

Figure 69 FTIR spectra of dried dandelion leaves (a) and spirulina algae (b) together with those of their hydrochars.

The obtained FTIR spectra for most of the samples showed a similar trend in change of functional surface groups with a decreasing variety and an emerging of three distinct signals (carbonyl, aromatic, ether). While the kind of surface groups can be determined it is difficult to obtained information about the quantity of the groups by this method. Therefore measurements by XPS were conducted on the hydrochars obtained from the coconut shell powder. Figure 70 shows the survey spectra along the C1(s) and O1(s) photoelectron envelope for the HTC and salt-HTC sample obtained from coconut shell powder.

The assignment of the experimental binding energies to different chemical states is done in table 8 together with the peak rations to get an idea of the quantity of certain groups.

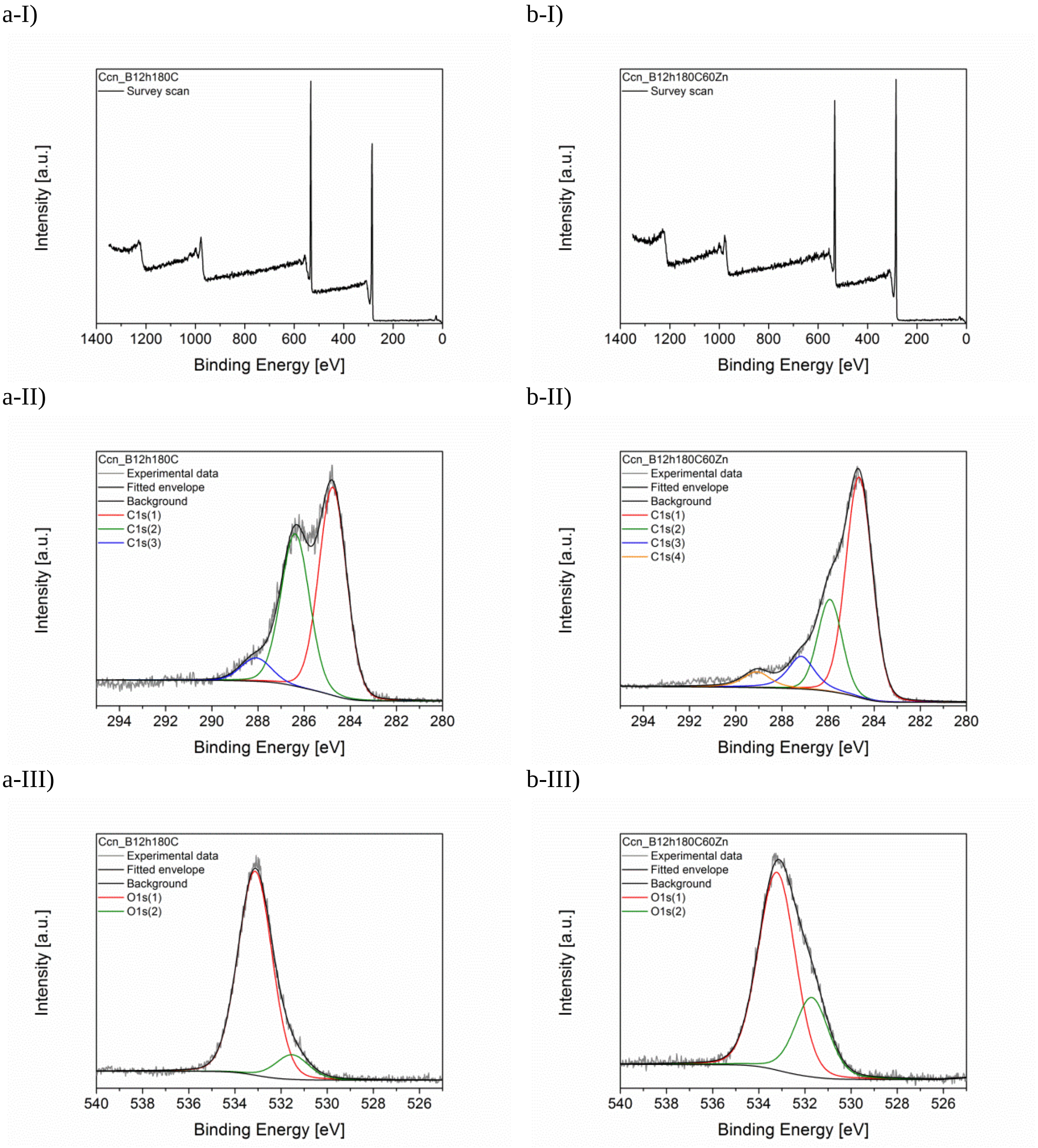
a-I) b-I) a-II) b-II) a-III) b-III)

Figure 70 XPS survey scans (I), C1(s) (II) and O1(s) (III) photoelectron envelope for the hydrochars obtained from coconut shell powder by HTC (a) and salt-HTC (b).

The survey scans of both hydrochars show two distinct signals at around 285 and 533 eV resulting from oxygen and carbon atoms in the samples, respectively. While the survey spectra did provide information about what atoms are mainly prominent, the differences of the samples become clearer from the fitted envelope of the carbon signal as seen in figure 70a-II and b-II. The hydrochar (Ccn_B12h180C) has mainly carbon signals from those bound to other carbon or hydrogen carbons (53.2 %) with some bound to oxygen in a single (40.3 %) or double bond (6.5 %). When the zinc chloride was present in the reaction (Ccn_B12h180C60Zn) the C2 signal decreases by half in peak ratio when compared to the HTC sample with the C1 and C3 signals increasing. Another peak becomes visible at a binding energy of 289.1 eV resulting from the carbon bound to two oxygen atoms (O=C-O). The O1(s) envelope of both samples is characterized by two signals with the main peak at 531.5/531.7 eV (C-O) and a minor shoulder at 533.1/533.2 eV (C=O). Both samples have a higher amount of oxygen double bound to a carbon than one with only a single bond. While the HTC sample showed a higher signal for carbon single bonds to oxygen than the salt-HTC sample (40.3 % to 23.3 %), oxygen single bound to a carbon atom is more present in the salt-HTC sample.

Table 8 Chemical state assignment of the experimental C1(s) and O1(s) binding energies [eV] with their peak area ratios [%] for two hydrochars obtained from coconut shell powder.

Assignment	**Ccn_B12h180C**	**Ccn_B12h180C60Zn**
C1 (C-C, C-H_x)	284.8/53.2 %	284.7/60.5 %
C2 (C-O)	286.4/40.3 %	285.9/23.3 %
C3 (C=O)	288.1/6.5 %	287.2/10.9 %
C4 (O=C-O)	-	289.1/5.3 %
O1 (C-O)	531.5/11.1 %	531.7/27.9 %
O2 (C=O)	533.1/88.9 %	533.2/72.1 %

Together with the information obtained by FTIR the results indicate that if the zinc chloride is present in the HTC reaction a lot of oxygenated functional groups change. Many carbons primary bound to one oxygen atom either change to a bond with a carbon or hydrogen atom or higher oxygen bond.

4.1.1.6 Porosity analysis

For the analysis of the porosity of the obtained samples and to judge their potential for a possible application as a sorption material comparable to activated carbons (e.g. dye sorption, chapter 4.3) two different gases (nitrogen and carbon dioxide) were used for the gas sorption experiments. While nitrogen sorption is common for determination of specific surface areas (SSA) of carbon materials, carbon dioxide sorption experiments were conducted for comparison with the most promising samples judged by N_2-sorption results. The calculated surface areas from both gases are listed along their pore volumes in table 9. Figure 71 visually highlights the trend from HTC to salt-HTC hydrochar.

Typical sorption isotherms together with the resulting pore volume distributions for both gases onto the hydrochars obtained from coconut shell powder are shown in figure 72. Additionally, this section will end with a view at the active sites on the surface from results obtained by nitrogen sorption towards very low pressures ($p/p_0 = 1\cdot10^{-5}$).

Table 9 and figure 71 show that in nearly all cases the surface area increases drastically if the zinc chloride was present in the reaction.

Table 9 Specific surface areas obtained by sorption experiments and calculated by BET theorem together with the pore volumes for different hydrochars.

Sample	**Specific surface area [$m^2\cdot g^{-1}$]**		**Pore volume [$cm^3\cdot g^{-1}$]**	
	N_2	**CO_2**	**N_2**	**CO_2**
Glu_B12h180C	0.00[a], (83.90)[b]	40.01	0.00[a]	0.02
Glu_B12h180C60Zn	125.42, (714.01)[b]	59.89	0.02	0.03
HMF_B12h180C	(0.00)[a,b]	-	(0.00)[a,b]	-
HMF_B12h180C60Zn	(528.73)[b]	-	(0.46)[b]	-
Cel_B12h180C	9.79	19.24	0.02	0.01
Cel_B12h180C60Zn	104.12	48.57	0.16	0.02
Lig_B12h180C	0.00[a]	-	0.00[a]	-
Lig_B12h180C60Zn	0.00[a]	-	0.00[a]	-
Gnr_A12h180C	0.00[a]	36.02	0.00[a]	0.02
Gnr_A12h180CLi(0.23)Zn	95.49	79.36	0.04	0.04
Ccn_B12h180C	4.19	28.22	0.00[a]	0.01
Ccn_B12h180C60Zn	97.84, (107.17)[b]	47.94	0.28	0.02
Rce_B12h180C	11.19	29.15	0.02	0.01
Rce_B12h180C60Zn	65.38	46.20	0.11	0.02
Dnd_B12h180C	5.17	-	0.01	-
Dnd_B12h180C60Zn	19.51	-	0.05	-
Saw_A12h180C	2.32	-	0.00[a]	-
Saw_A12h180CLi(0.23)Zn	32.60	-	0.03	-
Alg_B12h180C	1.49	-	0.00[a]	-
Alg_B12h180C60Zn	0.00[a]	-	0.00[a]	-

[a] 0.00 - at detection limit

[b] () - synthezied in small autoclaves

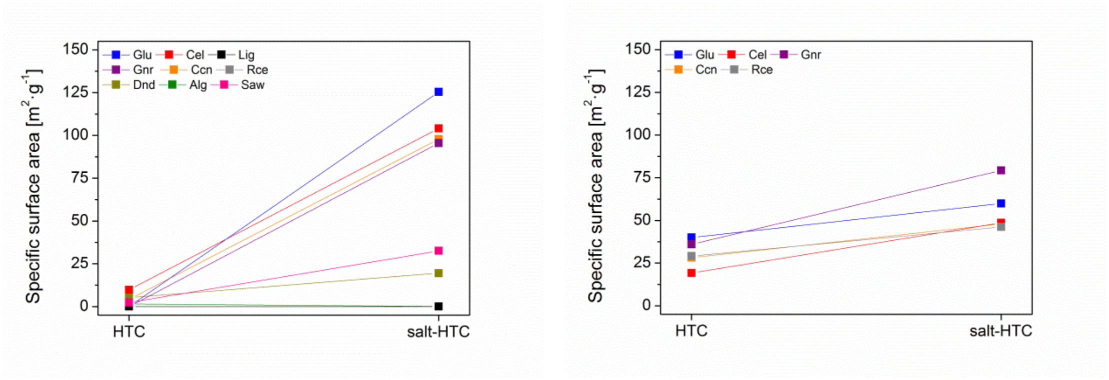
a)

b)

Figure 71 Specific surface areas for various hydrochars from different substrates (used gas: N_2 (a) and CO_2 (b)).

When using nitrogen as the sorption gas, most of the normal HTC samples were either at detection limit (0.00 $m^2 \cdot g^{-1}$) like glucose, HMF, lignin, the mixture of different grasses and rushes and spirulina algae or less than 20 $m^2 \cdot g^{-1}$ with the highest measured surface area received from rice husk hydrochar with 11.19 $m^2 \cdot g^{-1}$. By having the zinc chloride present, the surface area increased up to values of around 100 $m^2 \cdot g^{-1}$, depending on the nature of the substrate used. The sample received from coconut shell powder by salt-HTC (Ccn_B12h180C60Zn) had the highest SSA of all used biomass (97.49 $m^2 \cdot g^{-1}$). This sample also shows the only considerably pore volume with 0.28 $cm^3 \cdot g^{-1}$.

The samples from HMF were produced on a very small scale due to substrate price and availability. While in the htc_B procedure usually 100 g of substrate were used, for the production of hydrochars from HMF only 5 g were used. Surprisingly, their salt-HTC hydrochars resulted in very high surface areas above 500 $m^2 \cdot g^{-1}$. Similar results were also obtained from glucose if its reactions were undertaken on a very small scale, showing the issues of a scale-up. However, for a biomass like the coconut shell powder, the differences in the production of small or large scale were minor (compare table 9).

When using carbon dioxide as the gas for the sorption experiments, usually higher surface areas are obtained for the normal HTC samples. Due to the smaller size and higher sorption experiment temperature this gas adsorbs more easily onto the surface, even if only low surface areas samples are present. Interestingly, when used for the salt-HTC samples, lower values are received than with nitrogen. The previous explanation therefore might prove not true since more surface area is present for the gas to get adsorbed, for which the difference in measured SSA gets clearer. The highest value is obtained for those from salt-HTC of the mixture of different grasses and rushes (79.36 $m^2 \cdot g^{-1}$). Interestingly this sample can adsorb more carbon dioxide than those from coconut shell powder, while exhibiting a similar surface area calculated from nitrogen.

For the samples received from lignin and algae no specific surface areas could be found. Since lignin showed to be nearly resistant at HTC conditions even with the zinc chloride present these results were to be expected. Cellulose hydrochars had low surface areas from HTC (9.79 $m^2 \cdot g^{-1}$) which increases by use of zinc chloride in the reaction to over 100 $m^2 \cdot g^{-1}$ (104.12 $m^2 \cdot g^{-1}$). For this, the previously made statement about the development of porosity for the biomass, dissolution and degradation of cellulose to spherical carbonized particles which settle on the remaining lignin, remains comprehensible. From lignin alone a porous structure cannot be produced by hydrothermal carbonization under the used conditions. The use of pure cellulose can result in hydrochars with increased surface areas by use of zinc chloride. The combination of lignin and cellulose, as in a typical biomass, results in nearly the same SSA like the cellulose (in the case of coconut shell powder) by salt-HTC. It could be expected that the values are lower since the parts of the lignin usually should not add to the porosity. But since the disintegrated cellulose parts could create holes in the structure, the lignin parts could remain as skeletal structure and therefore the lignin would add in fact a part to the porosity. This was confirmed from the SEM and TEM images were a porous macrostructure remained, presumably from the lignin parts, with carbonized particles on them. Those images showed also that the big macrostructures are broken into smaller parts for the salt-HTC, from which some part of the increased surface area, but not directly porosity, could result.

Figure 72 shows representatively the sorption isotherms of nitrogen (fig. 72a-I) and carbon dioxide (fig. 72b-I) for the hydrochars received from coconut shell powder, together with the resulting pore size distributions.

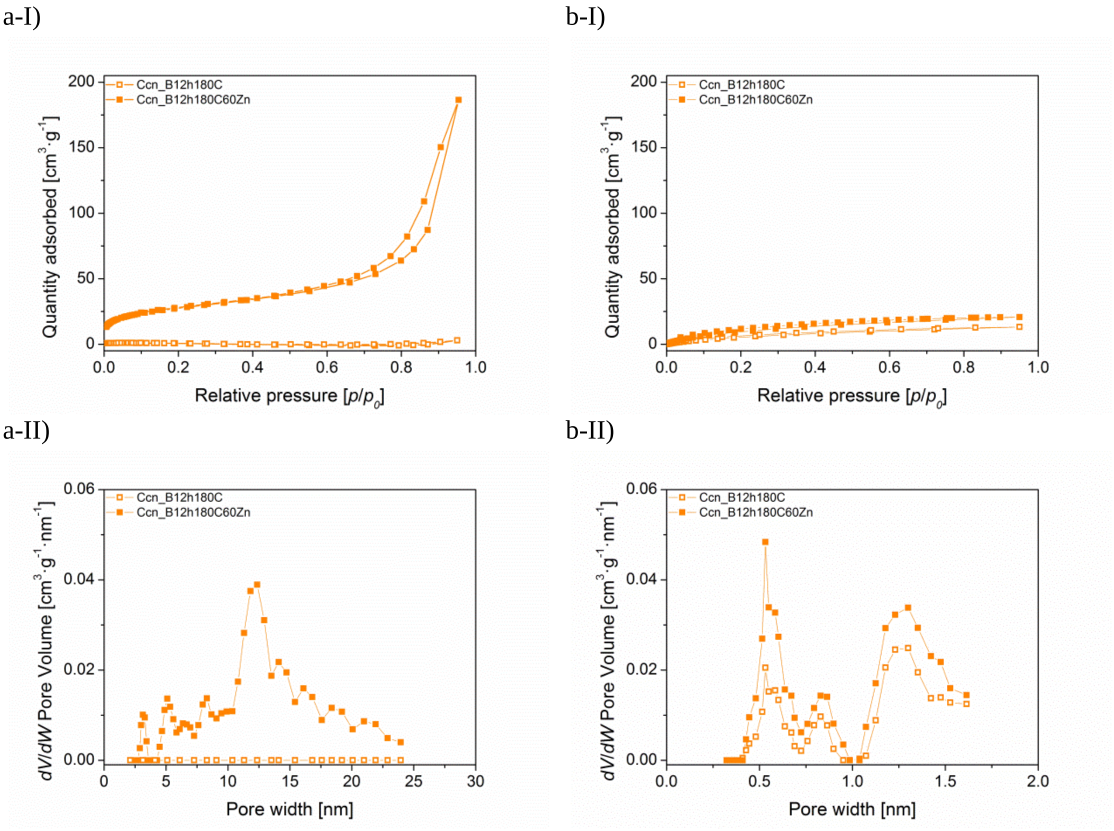

Figure 72 Sorption isotherms (I) for nitrogen (a) and carbon dioxide (b) onto hydrochars obtained from coconut shell powder together with the resulting pore size distributions (II).

The nitrogen sorption isotherms for the HTC sample (Ccn_B12h180C) show no noticeable adsorption of the gas as with all hydrochars created without salt present, resulting in the low specific surface areas calculated. For the salt-HTC sample (Ccn_B12h180C60Zn) a sorption following a typical Type II isotherm is observed, indicating a nonporous or macroporous adsorbent[255]. These results indicate that the hydrothermal carbonization with zinc chloride does not create distinct porosity. However, the pore volume distribution (fig. 72a-II) shows the presence of pore sizes in the range of mesopores with 2-25 nm, even when the quantity adsorbed in those is at a really low level. Macroporosity can be caused from pores or holes bigger than 50 nm, which could also be interparticle voids, which are also indicated by the small hysteresis loops in the isotherm. The Type H3 loop like hysteresis loop also points to macropores which are not completely filled with pore condensate[255]. Therefore the main reasons for the increase in surface area could be derived from breakup of macrostructures into smaller pieces (increase of external surface area and interparticle spaces), formation of carbon spheres from the cellulose parts of the biomass (creation of external surface area - especially roughness - and maybe creation of minor porosity) and/or holes left in the resistant lignin skeleton structure (creation of macroporosity).

When carbon dioxide is used as the gas for the sorption experiments, no distinct uptake of adsorbed quantity is observed for neither the HTC (Ccn_B12h180C) nor the salt-HTC hydrochar (Ccn_B12h180C60Zn). Still, the amount adsorbed onto the HTC sample is higher than for nitrogen, while remaining at low values. This indicates that carbon dioxide is initially easier adsorbed onto the hydrochars but can't enter any porous systems the salt-HTC sample might have. Since only a small amount of gas was adsorbed in the low pressure range, the pore size distribution shows pore widths lower than 2 nm, indicating a minor presence of micropores. Comparing the results of the nitrogen and carbon dioxide sorption experiments shows that the latter seems less suitable for the discussion of the surface areas of hydrochars. Thus, e.g. discussing the influence of process parameters onto the SSA will be done for results obtained with nitrogen only.

To compare the active sites available on the surfaces of the hydrochars and not only the areas, the nitrogen sorption was undertaken also towards very low pressures ($p/p_0 = 1 \cdot 10^{-5}$). By normalizing the monolayer to a value of $V_m = 1$ and plotting the obtained data logarithmic, more active sites should be shifted towards higher adsorbed amounts. Figure 73 shows that hydrochars obtained by the salt-HTC route have a less sharp curve (filled squares), indicating the presence of more active sites on these compared to the samples produced by the normal HTC route.

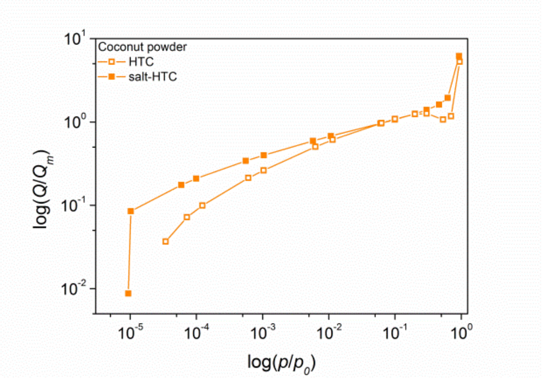

Figure 73 Determination of active sites on surfaces of hydrochars from coconut shell powder by HTC or salt-HTC by low pressure nitrogen sorption.

4.1.2 Influence of temperature and time onto the hydrothermal carbonization of coconut shell powder in the presence of zinc chloride

To discuss the influence of various process parameters onto the hydrothermal carbonization of one selected substrate, coconut shell powder, first the parameter temperature and time will be discussed. The coconut shell powder was chosen since it showed the most promising surface areas while proving as the most easily manageable in the whole reaction process and sample processing. Therefore, the substrate was carbonized either in water (HTC) or a 60 wt% zinc chloride solution (salt-HTC). To study the effect of time, it was carbonized at either 4, 12 or 20 hours at a constant temperature of 180 °C. For the effect of the temperature 180, 200 and 220 °C were used while the carbonization time was kept the same for each experiment (12 hours). To test also the extremes and search for potential resulting maxima, two additional experimental runs were conducted at 220 °C with either 20 or 36 hours of carbonization time.

4.1.2.1 Reaction yield and ash content

Following, the change in yield and ash content of the hydrochars received either at different times with constant temperature (fig. 74, T = 180 °C) or at different temperatures with constant time (fig 75, t = 12 hours) are shown. The results for the extremes (220 °C for 20 or 36 hours) are shown in figure 76. All values can also be found in table A3.

The initial discussion of the substrates showed that the coconut shell powder has one of the lowest tested inorganic contents with less than 1 wt% ash. It could also be shown that the ash which would result from the initial zinc chloride used is usually washed out completely (ash < 1 wt%). Here also no enrichment of ash could be observed in the different experiments for the time or temperature, suggesting its independence of these parameters. Slightly more information could be obtained from the yield. In most cases the yield of the normal HTC reaction without the zinc chloride present was a little bit higher, indicative of an increased reactive behavior due to the presence of the salt, equivalent to what was seen in previous results. At a temperature of 180 °C the yield changes slightly from 4 to 20 hours with values around 52 to 56 wt%. A slightly higher amount of the sample received at 12 hours with no salt present (60.9 wt%) was obtained, probably resulting from slight reaction deviations but inside the error tolerance.

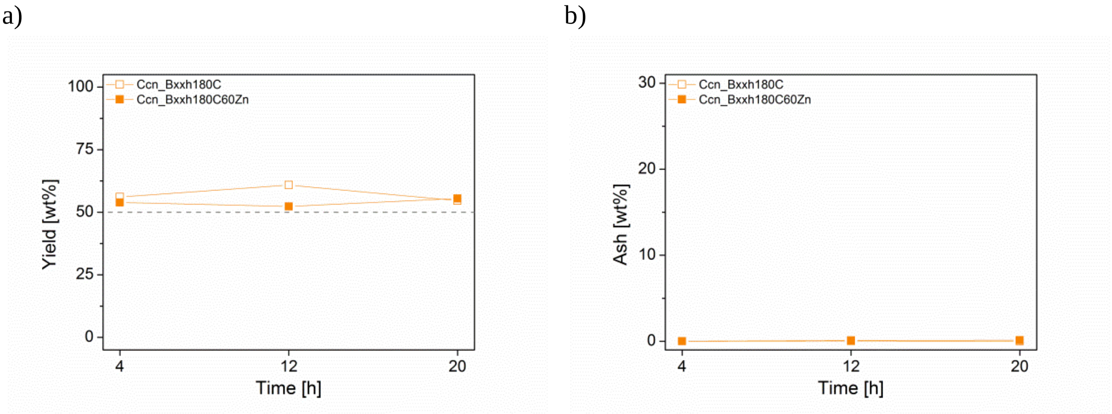

Figure 74 Yield (a) and ash content (b) of hydrochars obtained after 4, 12 or 20 hours at 180 °C.

Keeping the time constant and changing the temperature from 180 to 220 over 200 °C the yield changes to values around 47 to 49 wt%. Only at 180 °C a yield over 50 wt% was received, showing a temperature dependence of the carbonization process. Still, the samples received from normal HTC or salt-HTC both show a similar weak decrease of yield.

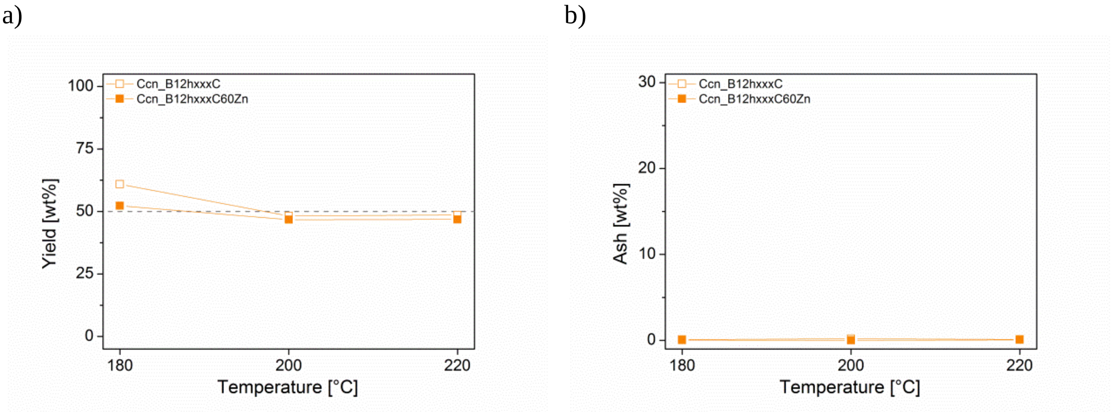

Figure 75 Yield (a) and ash content (b) of hydrochars obtained after 12 hours at 180, 220 or 220 °C.

Checking the extremes of temperature and time with 220 °C and at 12, 20 and 36 hours no significant change of yield is observed. As seen in figure 76, the time dependence of the yield seems to less important than the temperature. Since the recommended temperature maximum of the supplier for the PTFE inlet was 220 °C, no higher temperature was tested.

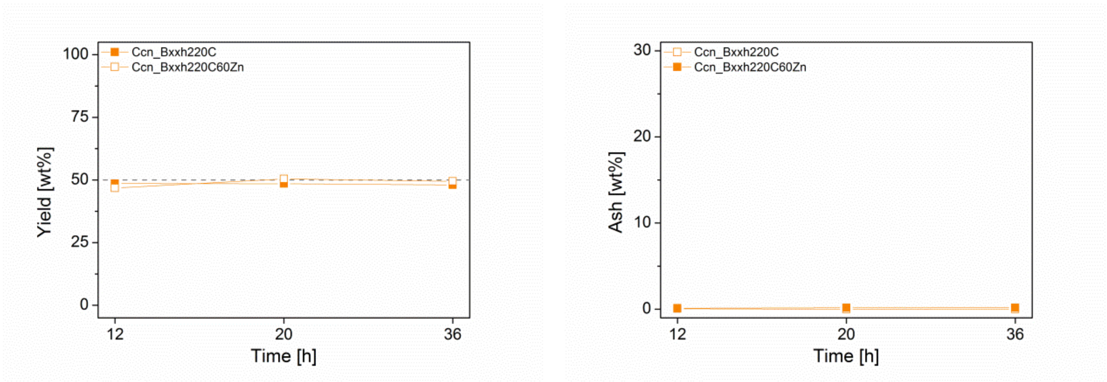
a)

b)

Figure 76 Yield (a) and ash content (b) of hydrochars obtained after 12, 20 or 36 hours at 220 °C.

4.1.2.2 Hydrochar morphology

Since the results from the discussion of the yield showed the biggest influence of the reaction temperature, the SEM images of the samples received at 180 °C or 220 °C (t = 12 h) are shown exemplarily in figure 77. For comparison the images of the sample received after 20 hours at 220 °C are shown as well. The minor influences of the reaction parameters as seen in the results of the yield and the ash are supported by the images received by SEM with the samples looking very similar in shape and size.

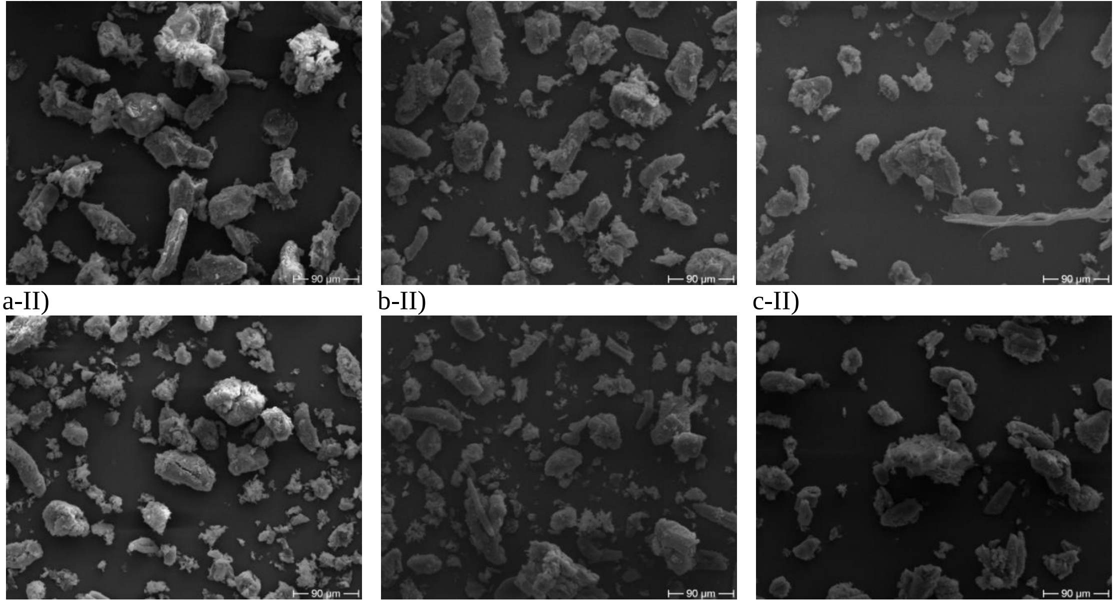
a-I)

b-I)

c-I)

a-II)

b-II)

c-II)

Figure 77 SEM images of hydrochars received from coconut shell powder at 180 °C for 12 hours (a) or at 220 °C for 12 (b) and 20 hours (c) with no salt (I) or zinc chloride present (II) at a magnification of 450x.

4.1.2.3 Elemental composition

The change in carbon content from varying the time or temperature for the reactions of the coconut shell powder is shown in figure 78a-c. A van Krevelen diagram in figure 78d supports the discussion about the changes in elemental composition. Similar as seen in the discussion of the different substrates the carbon content is always higher if zinc chloride was present in the reaction compared to a normal HTC reaction. The main change usually occurs between the substrate and any carbonized sample, showing that the highest influence is the carbonization itself and not so much the reaction conditions. By changing the time from 4 to 12 and 20 hours at a constant temperature of 180 °C the carbon content of the HTC samples stays at a flat level of around 59 (HTC) and 67 % (salt-HTC). More impact can be seen from the variation of the temperature with a jump from 59.90 % at 180 °C to 66.76 % at 200 °C for the reaction without additive, raising the carbon content to the level of those received with zinc chloride present. Another increase of temperature to 220 °C does not result in a noticeable increase of carbon content (66.73 %).

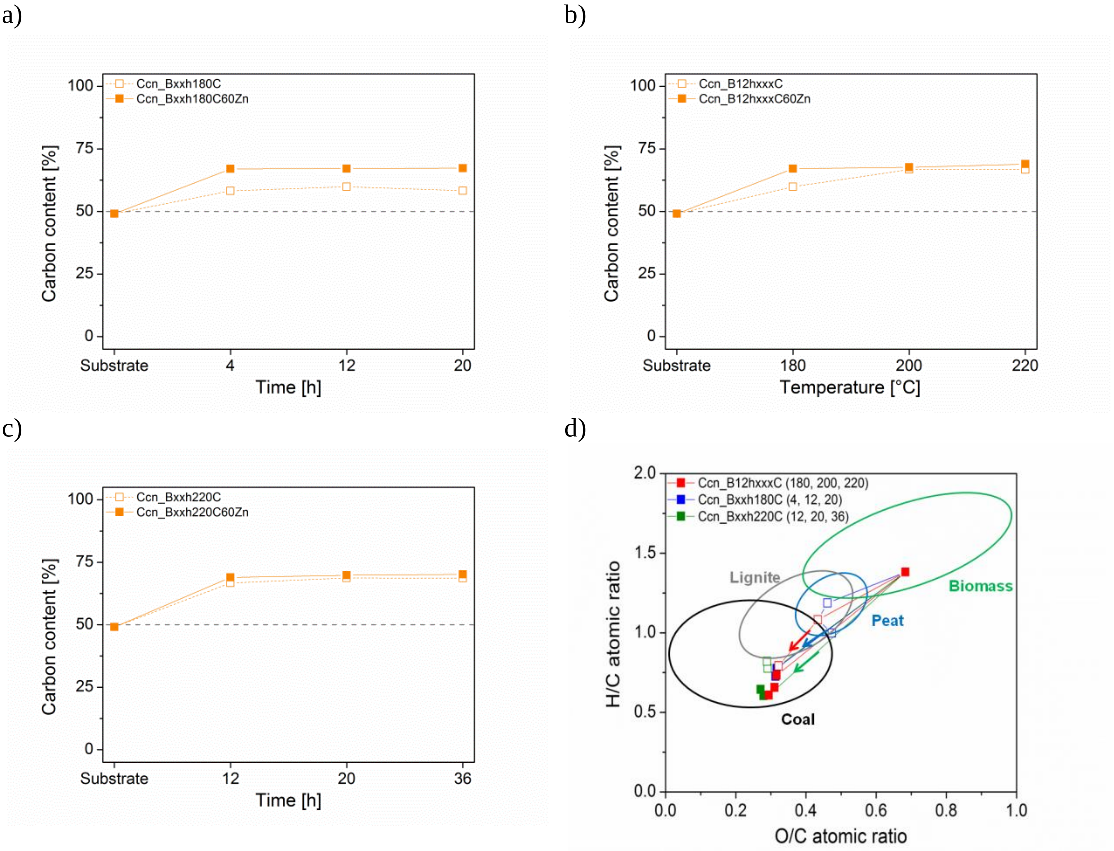

Figure 78 Carbon content of hydrochars received under different conditions (a: T = 180 °C, t = 4, 12, 20 h; b: T = 180, 200, 220 °C, t = 12 h; c: T = 220 °C, t = 12, 20, 36 h) from coconut shell powder and the resulting van Krevelen diagram (d). Empty squares are for the HTC and filled for the salt-HTC hydrochars. Arrows show increased reaction conditions. The areas for biomass, peat, lignite or coal are collected from literature[40, 96, 267].

As for the reactions with additive present the temperature did not have such an impact with the carbon content increasing slightly from 67.11 (180 °C) over 67.65 (200 °C) to 68.93 % (220 °C). As will be also seen and further discussed with the NMR results the most crucial change for the HTC reaction seems to happen around 200 °C. This temperature seems to be the threshold for certain reactions that are not possible at 180 °C (e.g. the degradation of cellulose; compare discussion in chapter 4.1.1.4). The presence of the zinc chloride enables these reactions by either lowering the pH to a highly acidic environment or catalyzing the reactions, lowering the temperature threshold. A further increase in temperature therefore has no significant effect on the reactions with the additive. It is also possible that another temperature threshold would be at a much higher temperature since all compounds stable at 200 °C are also stable at 220 °C. When testing a further increase of reaction time at the highest reaction temperature (220 °C) from 12 to 20 and 36 hours, the carbon content increases further but only by up to 2 %. The sample for the normal carbonization takes 20 hours at 220 °C so that the reactions increase the carbon content to 68.72 %. A further increase in reaction time keeps the carbon content at a similar level (68.64 %). At the same temperature, a comparable carbon content (68.93 %) is obtained in 12 hours if zinc chloride was present in the reaction. Increasing the reaction time to 20 or 36 hours for the salt-HTC leads to the highest observed carbon contents in this work from a hydrothermal carbonization reaction with 69.81 and 70.18 %, respectively. The increase in carbon content results from a loss of hydrogen and oxygen atoms, as common for the hydrothermal carbonization and as already described for the substrates. The change in hydrogen and oxygen shows the same but contrarious trend like the carbon content. The initial hydrogen and oxygen contents of around 6 and 45 % decrease in the carbonized samples up to nearly 4 and 25 %, respectively. The biggest changes again take place with increasing temperature from 180 to 200 °C at 12 hours for the carbonization without salt present. The other changes in time or temperature lead only to slight changes with a decrease in both hydrogen and oxygen with increasing reaction conditions. The loss in both elements is also always higher with zinc chloride present at same reaction conditions. This supports the idea that especially dehydration reactions are taking place to a higher extent if the zinc chloride is present; potentially the zinc catalyzes those reactions.

The initial small amount of nitrogen present (0.13 %) increases slightly with rising reaction parameters up to 0.52 %. This supports the idea that nitrogen atoms stay in their compounds and are not lost in the carbonization reactions and, thus, increase in percentage.

The van Krevelen diagram shown in figure 78d underlines the results discussed for the change of carbon, hydrogen and oxygen content. With increasing reaction conditions (symbolized with an arrow in figure 78d) the hydrochar properties change from peat (mild conditions (HTC)) over lignite like samples to those comparable with coal (higher temperatures (HTC) or salt-HTC). The change in H/C and O/C atomic ratios takes only place in the direction to the lower left corner, indicating dehydration reactions.

This additionally supports the idea that the zinc chloride catalyzes dehydration reactions that usually take place at 200 °C, enabling them at already 180 °C.

4.1.2.4 Hydrochar structure

The influence of the temperature and time onto the structure of the obtained hydrochars was studied by ^{13}C solid state NMR spectroscopy. The results are shown in figure 79 with the typical regions for cellulose and lignin as received in the analysis of the substrates highlighted with a red and black square, respectively. Figure 79a shows the change in structure if the carbonization time was changed from 4 to 12 and 20 hours at a constant temperature of 180 °C for the HTC (I) and salt-HTC (II) of coconut shell powder. In case for the normal HTC reaction many of the initial signals from the cellulose or lignin parts of the biomass are still present as seen in figure 79a-I. A slight overall increase but flattening of small signals can be found in the region from 110 to 150 ppm characteristic for sp^2 hybridized aromatic carbons. If the zinc chloride was present in the reactions the change in signals with increasing time also does not show a significant change compared to the initial one already described in the substrate section as seen in fig. 79a-II.

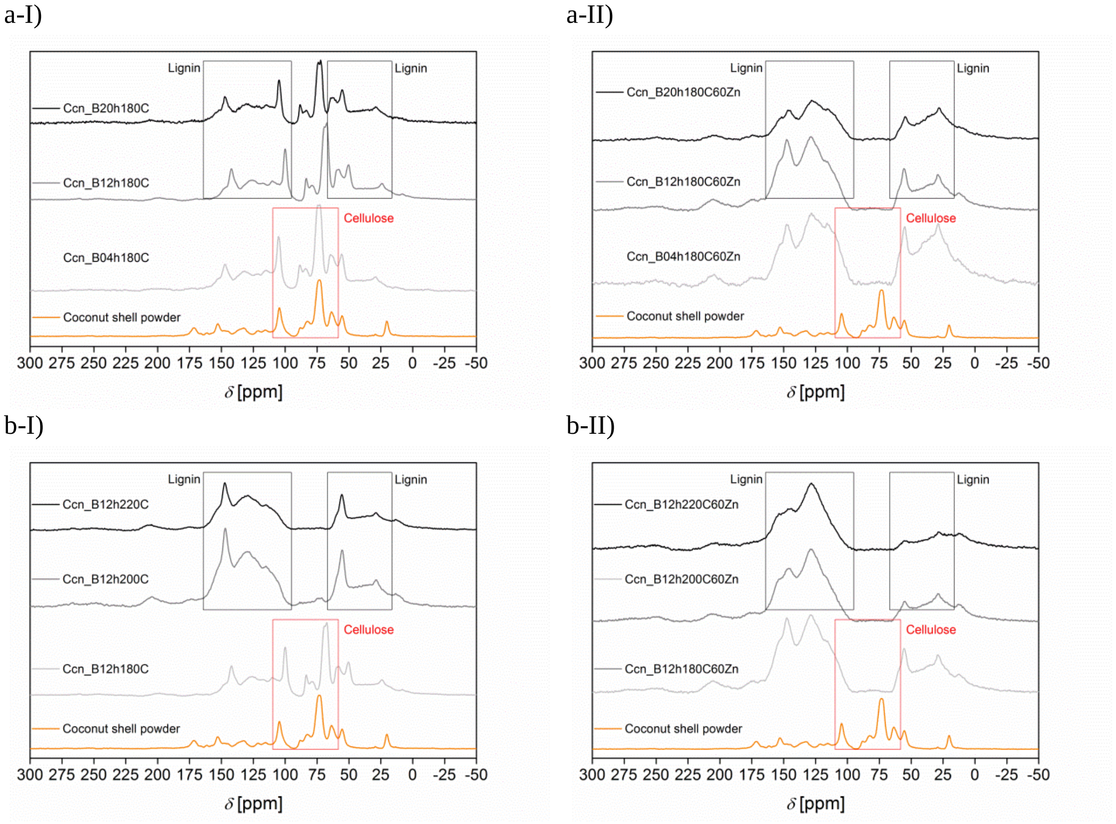
a-I)

a-II)

b-I)

b-II)

Figure 79 ^{13}C SS-NMR spectra of hydrochars obtained from coconut shell powder by HTC (I) or salt-HTC (II) at different reaction conditions (a: changing time, b: changing temperature).

More interesting information are seen from changing the temperature. As already discussed in the previous sections the zinc chloride seems to enable or catalyze reactions at 180 °C that are only possible at temperatures of at least 200 °C in the normal HTC reaction since the signals for Ccn_B12h200C show a similar pattern to Ccn_B12h180C60Zn. A small difference can be seen in the intensities of the signals. In case of the HTC reaction two signals at around 55 and 147 ppm are distinct that can be attributed to lignin methoxy groups and aromatic carbons bound to those[53], respectively. Two additional small signals in the aromatic carbon region at 114 and 129 ppm get smaller with increasing temperature, as also seen with two signals at 12 and 29 ppm in the aliphatic region, showing that the increasing temperature seems to have a small effect. The salt-HTC samples on the other hand have their most significant signal at around 128 ppm resulting from sp^2 hybridized carbons[53]. The signals that were prominent in the normal HTC samples were also visible at 180 and 200 °C but are only shoulder peaks in the 220 °C sample, indicating that the methoxy groups from the lignin are broken with increasing temperature. This shows that the lignin structures, which are always seen as a problem compound in the biomass with its resistance to the HTC reaction, can in fact be affected by the addition of the zinc chloride. The salt therefore not only catalyzes the degradation of cellulose but also opens up possibilities for reactions with the lignin compounds in the biomass at higher temperatures that are resistant in normal HTC reactions. Therefore, while before the change from 180 to 200 °C was described as the most crucial part for the biomass, an additional temperature dependence up to higher temperatures, especially with the salt present, can be supposed.

4.1.2.5 Surface functionality

To determine the effect of the temperature and time on the nature of functional surface groups, FTIR spectra were recorded for the samples from coconut shell powder with different process conditions, always either with no additive (HTC) or a 60 wt% zinc chloride solution present (salt-HTC). The results for changing the time from 4 to 12 and 20 hours at a fixed temperature of 180 °C are shown in figures 80a (HTC) and 80b (salt-HTC). The difference between a normal carbonization and the one with the salt present was discussed in the first chapter of the results and here only the process conditions are in focus. A change from 4 hours at 180 °C to 20 hours at the same temperature did not have a distinct influence on the surface functionality of the hydrochars received by HTC or salt-HTC. In all cases the spectra of the normal HTC coals look similar to that of the substrate with the signal of around 1000 cm^{-1} decreasing in intensity. The change from substrate to hydrochar was a lot more significant for the salt-HTC samples with the signals at 1700, 1600 and 1200 cm^{-1} emerging, which correspond to carbonyl C=O stretching, aromatic C=C stretching and ether C-O stretching, respectively. Figure 80b shows that already 4 hours seem to be enough time for the change in surface functionality to happen at 180 °C.

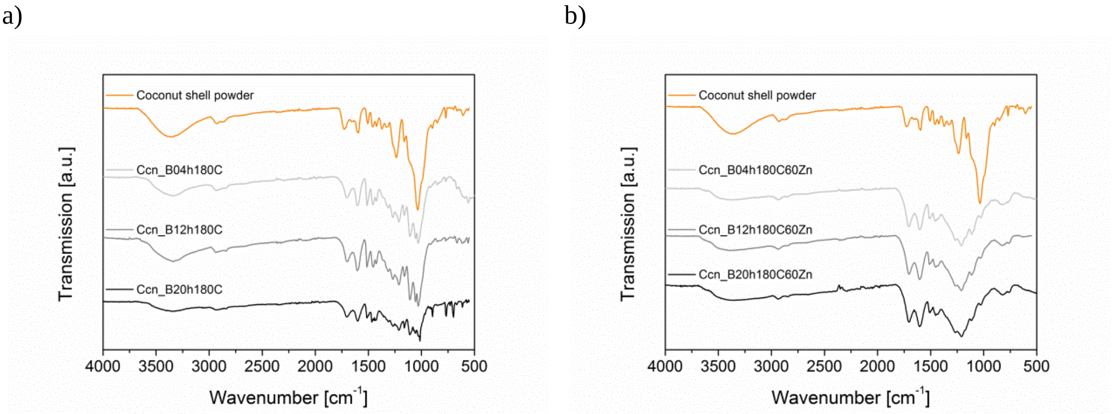

Figure 80 FTIR spectra coconut shell powder and its hydrochars obtained after 4, 12 or 20 hours at 180 °C with no additive (a) or a 60 wt% zinc chloride solution (b).

Increasing the time to 12 or 20 hours at the same temperature did not result in any major change in the functional groups present on the hydrochar surface.

The change of temperature from 180 over 200 to 220 °C at a constant time (12 hours) proved to be of more importance for changing the surface functionality as seen in figure 81.

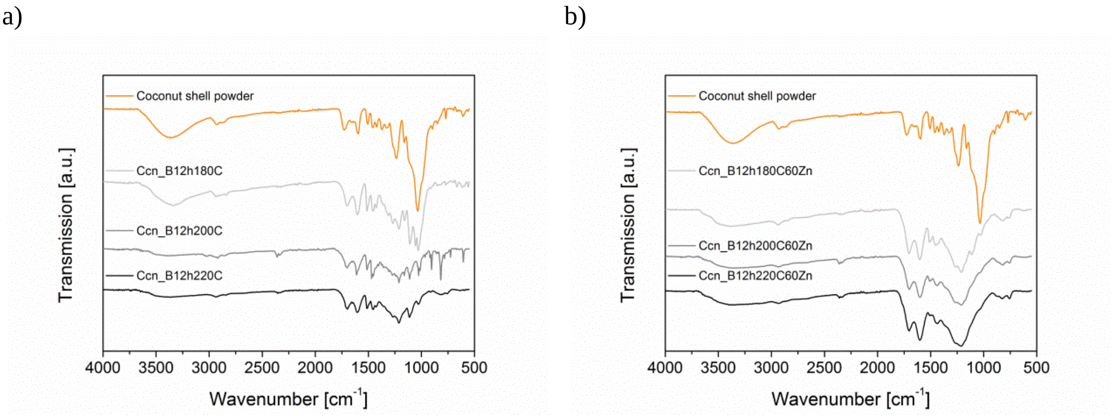

Figure 81 FTIR spectra coconut shell powder and its hydrochars obtained after 12 hours at 180, 200 or 220 °C with no additive (a) or a 60 wt% zinc chloride solution (b).

Similar as with the previous characteristics, the influence of the temperature was higher for the HTC samples than those received by salt-HTC. By increasing the temperature the surface functionality of the salt-HTC samples showed nearly the same spectrum at all temperatures measured. Only a loss of a very minor peak at around 1500 cm^{-1} can be observed, indicating a small loss of surface functionality. In the case of the HTC reactions the change showed more crucial. With increasing time more and more surface groups seem to get lost. The spectrum of the hydrochar from coconut shell powder at 220 °C for 12 hours showed similarities with the one obtained in the presence of zinc chloride at 180 °C for the same time.

A few more peaks are seen in the HTC sample but this result underlines the previous stated understanding of the zinc chloride enabling reactions at lower temperatures of what they usually take place at.

Testing the longer times at 220 °C showed nearly no change in surface functionality for all samples received either by HTC or salt-HTC (figure 82). Even after 36 hours at 220 °C some surface groups seem to be stable on the HTC coal that are lost in the variant with the additive present. This indicates that the temperature is the most crucial parameter in changing the surface functionality and that the zinc chloride leads to a change that not only lowers the required temperature but also those that are not possible even at higher temperatures or times with the normal carbonization reactions.

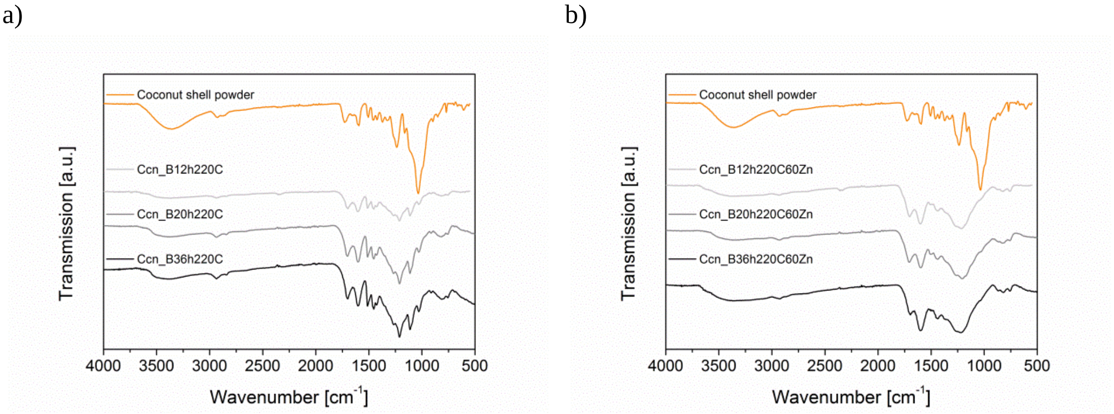

Figure 82 FTIR spectra coconut shell powder and its hydrochars obtained after 12, 20 or 36 hours at 220 °C with no additive (a) or a 60 wt% zinc chloride solution (b).

To get more insight into the quality and quantity of the surface functionality of the hydrochars and since the temperature was seen as the most crucial parameter by FTIR the data recorded by XPS for the samples received at 220 °C for 20 hours are shown in figure 83. Their peak data are listed in table 10 together with those received for the samples of 12 hours at 180 °C that were discussed in the substrate section (see 4.1.1.5) for comparison. The survey spectra of both samples show a similar trend as those seen in figure 70 (see 4.1.1.5) with the signals for oxygen and carbon at a similar level for the HTC samples and a decreased signal for oxygen in the salt-HTC sample. The C2 signal decreases in both samples (Ccn_B20h220C & Ccn_B20h220C60Zn) when compared to those received at 180 °C for 12 hours in line with increasing values for the C1 and C3 peaks. The carbon atoms single bound to an oxygen atom further change to carbon-carbon or carbon-oxygen double bounds. In the salt-HTC sample a fourth peak at 290.5 eV appears. This signal usually results from adsorbed carbon dioxide.

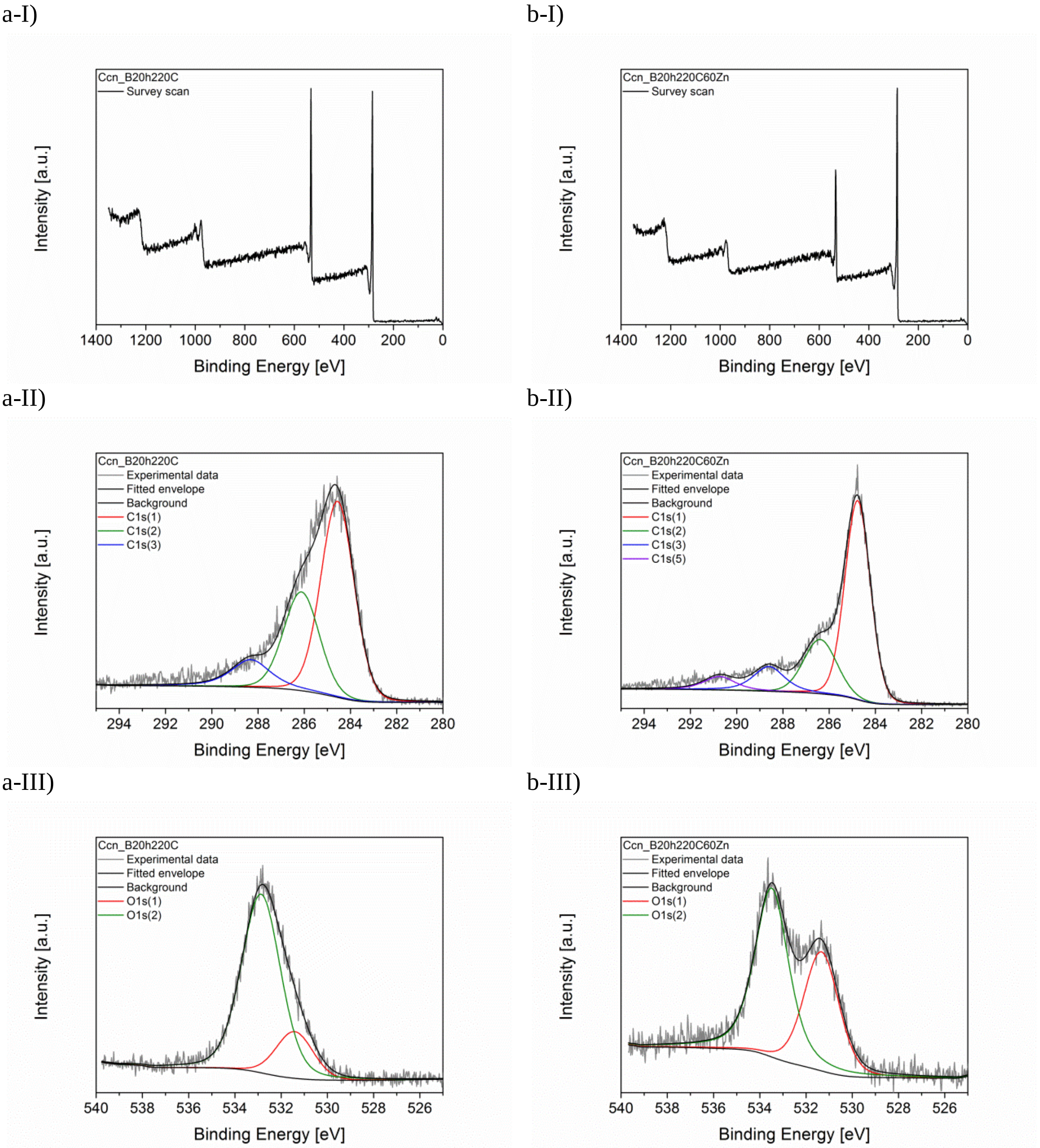
a-I) b-I) a-II) b-II) a-III) b-III)

Figure 83 XPS survey scans (I), C1(s) (II) and O1(s) (III) photoelectron envelope for the hydrochars obtained from coconut shell powder by HTC (a) and salt-HTC (b).

Table 10 Chemical state assignment of the experimental C1(s) and O1(s) binding energies [eV] with their peak area ratios [%] for different hydrochars obtained from coconut shell powder.

Assignment	**Ccn_B12h180C**	**Ccn_B12h180C60Zn**	**Ccn_B20h220C**	**Ccn_B20h220C60Zn**
C1 (C-C, C-H$_x$)	284.8/53.2%	284.7/60.5%	284.6/57.7%	284.8/62.6%
C2 (C-O)	286.4/40.3%	285.9/23.3%	286.1/31.0%	286.4/19.9%
C3 (C=O)	288.1/6.5%	287.2/10.9%	288.3/11.3%	288.4/9.2%
C4 (O=C-O)	-	289.1/5.3%	-	(290.5/8.3%)
O1 (C-O)	531.5/11.1%	531.7/27.9%	531.4/19.1%	531.3/39.2%
O2 (C=O)	533.1/88.9%	533.2/72.1%	532.9/80.9%	533.5/60.8%

4.1.2.6 Porosity analysis

The influences of the process parameters temperature and time on the porosity of the hydrochars received from coconut shell powder are shown in figures 84 to 86 and table A4. The trend so far observed for the variation of the time is confirmed also with the surface areas and pore volumes, as no major influence on most of the previous shown characteristics could have been observed. Without the zinc chloride present the surface area stays at values below 10 $m^2 \cdot g^{-1}$. The salt-HTC reaction can be increased slightly from around 98 $m^2 \cdot g^{-1}$ (4 hours) to almost 105 $m^2 \cdot g^{-1}$ (20 hours). The pore volumes stay at a small level with values at the detection limit for the normal HTC reactions and around 0.28-0.29 $cm^3 \cdot g^{-1}$ for the hydrochars received by salt-HTC.

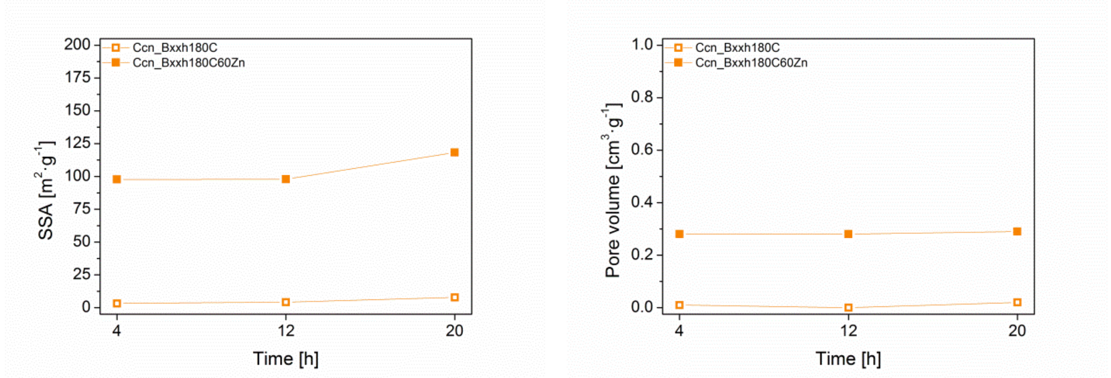
a)
b)

Figure 84 Specific surface areas (SSA) and pore volumes from hydrochars received from coconut shell powder (Ccn) at 180 °C for different times (4, 12, 20 hours) with either no salt (empty squares) or a 60 wt% zinc chloride solution present (full squares).

The increase in temperature, which proved the most significant parameter in the so far discussed results, leads to an increase in surface area for the normal HTC reaction. By increasing the temperature to 200 °C a surface area of around 50 $m^2 \cdot g^{-1}$ and pore volumes up to 0.16 $cm^3 \cdot g^{-1}$ can be obtained. A further increase to 220 °C does not result in a noticeable improvement of the SSA. As seen in the previous shown results, but especially in those discussed in the NMR section, a temperature of at least 200 °C seems to be necessary for the reactions of certain biomass parts to take place, especially cellulose. Since the increase in SSA seems to be connected to these reactions, the development in surface area can be connected to the degradation reactions of the cellulose. Still, the increase in temperature does not lead to those values of SSA received by the reactions with zinc chloride present. Therefore, the salt must play the important role in developing the porosity and not only in catalyzing the temperature dependent reactions. The influence of increasing temperature on the SSA for the hydrochars received by salt-HTC shows a slight increase up to nearly 120 $m^2 \cdot g^{-1}$ at 220 °C.

a) b)

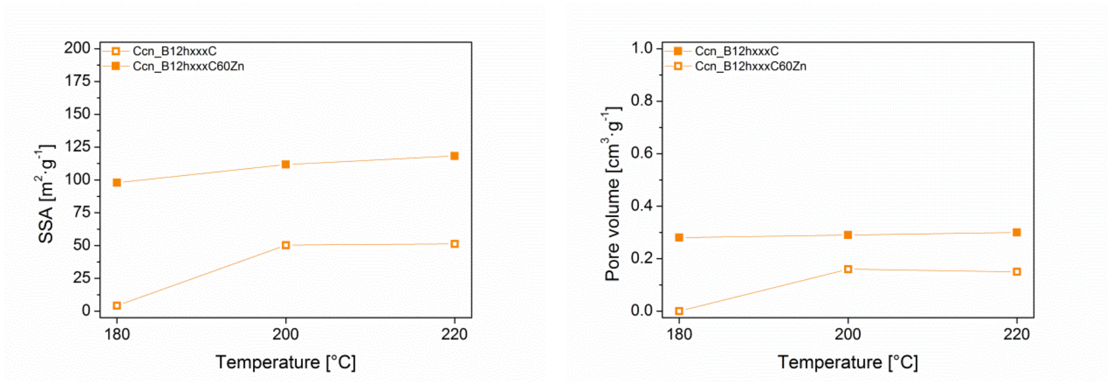

Figure 85 Specific surface areas (SSA) and pore volumes from hydrochars received from coconut shell powder (Ccn) after 12 hours at different temperatures (180, 200, 220 °C) with either no salt (empty squares) or a 60 wt% zinc chloride solution present (full squares).

The hydrochars with the highest surface areas were obtained by increasing the time at 220 °C to 36 hours in the reaction with zinc chloride present. With nearly 200 m^2·g^{-1} a significant increase of surface area compared to the initial hydrochars could be obtained. Interestingly, the increase in SSA did not result in higher pore volumes. Contrary, in the normal HTC reactions the SSA could not be further improved and stayed at values of around 50 m^2·g^{-1}, while it even decreased a little at 36 hours.

a) b)

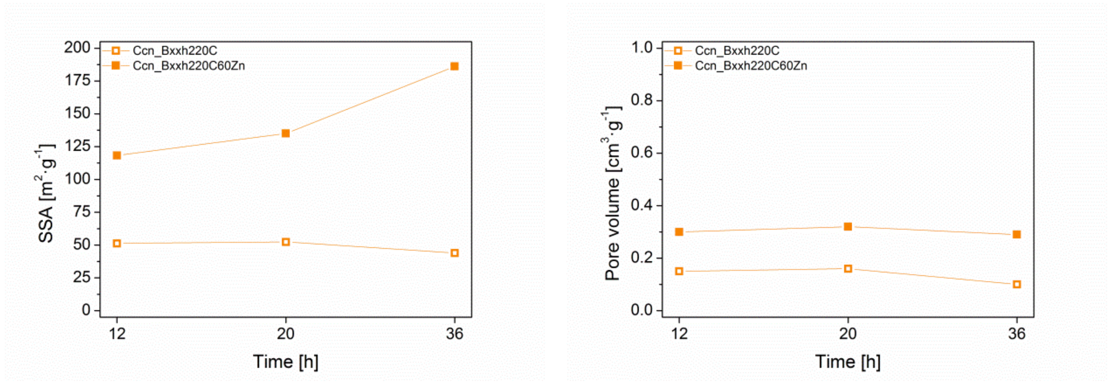

Figure 86 Specific surface areas (SSA) and pore volumes from hydrochars received from coconut shell powder (Ccn) at 220 °C for different times (12, 20, 36 hours) with either no salt (empty squares) or a 60 wt% zinc chloride solution present (full squares).

For a better understanding of the SSA values figure 87 shows exemplary six isotherms from the samples received at low (4 hours at 180 °C (light gray line)), normal (12 hours at 180 °C (gray line)) and high (36 hours at 220 °C (black line)) conditions by the normal (empty squares) or salt-HTC (filled squares). While the HTC samples usually show no uptake of nitrogen, a type II shaped isotherm could be obtained for the high conditioned sample (Ccn_B36h220C). This type is also found for the salt-HTC samples. A change happened in the high salt-HTC sample (Ccn_B36h220C60h) were some of the increased surface area seems to come from the increased presence of micropores in the relative pressure range below $p/p_0 = 0.1$ since an additional uptake is found in that region when compared to the other two salt-HTC samples that are nearly on top of each other. This sample also had a desorption curve which seemed a little bit off the adsorption curve, indicating that interparticle spaces could have added a portion to the high measured surface area.

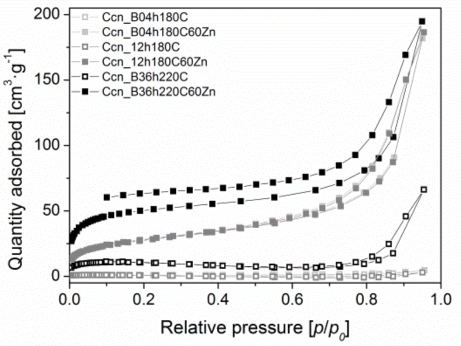

Figure 87 Nitrogen sorption isotherms from different hydrochars received from coconut shell powder (Ccn).

4.1.3 Influence of water and salt content onto the hydrothermal carbonization of coconut shell powder in the presence of a salt-water mixture containing zinc chloride

The reaction medium in the hydrothermal carbonization is typically water. Therefore it is of important interest to check the influence of the substrate to water ratio on the characteristics of the hydrochars. Since in this study mainly salt-water mixtures are used, they will be compared to those received by pure water. On top of that, the water to salt ratio is also of interest. For that a total of four different reaction series have been conducted to study the effect of water and salt ratio. These included two with a mixture of zinc chloride and lithium chloride (50-50 mol%) at conditions htc_A at three different substrate to water (mass to volume) ratios (1:0, 1:2 and 1:20) or three different substrate to water to salt ratios (1:20:1, 1:1:10, 1:20:10). Another series studied also the effect of substrate to water (mass to water) ratio (1:1, 1:2 and 1:4) but in the reaction setup htc_B. Additionally to study the effect of amount of zinc chloride in the water-salt mixture another approach was chosen where a 10, 20, 40, 60 or 80 wt% $ZnCl_2$ solution in the substrate to solvent (mass to volume) ratio 1:2 (typical htc_B approach) was used. For all of the above mentioned reactions coconut shell powder was used as the biomass and the reaction was conducted at 180 °C for 12 hours.

To discuss the influence onto the main interest, the porosity of the obtained hydrochars, first an overview over the reaction by change in yield, ash and carbon content of the samples will be shown (compare table A5). Subsequently, the specific surface areas will be discussed (see also table A6).

4.1.3.1 Reaction yield and ash content

The change in reaction yield and ash content for the different reactions varying the water and salt content are shown in figure 88 to 91. Figure 88a shows that by varying the substrate to water ratio in the setup htc_A the yield is affected. The ash content stayed at a typical low level of less than 1 wt% (figure 88b). If no water was present in the reaction (substrate to water ratio 1:0) a yield of around 41 wt% is obtained. This shows that the coconut shell powder and salt mixture (lithium chloride/zinc chloride) do react even without the typical reaction medium (water) present. The temperature of 180 °C seems therefore already sufficient to indicate a coalification of the biomass, comparable to a chemical activation process which usually takes place at higher temperatures. At the ratio 1:2 the yield increases to nearly 50 wt%, commonly seen for these reactions as indicated by most of the previous results. Increasing the water ratio by a factor 10 the yield drops to nearly 39 wt%. The increased amount of solvent leads to more compounds being solved into the liquid phase resulting in a loss of obtained solid hydrochar. The results indicate that the ratio of 1:2, which is used in most of the prior discussed reactions, showed the most promising results regarding the yield.

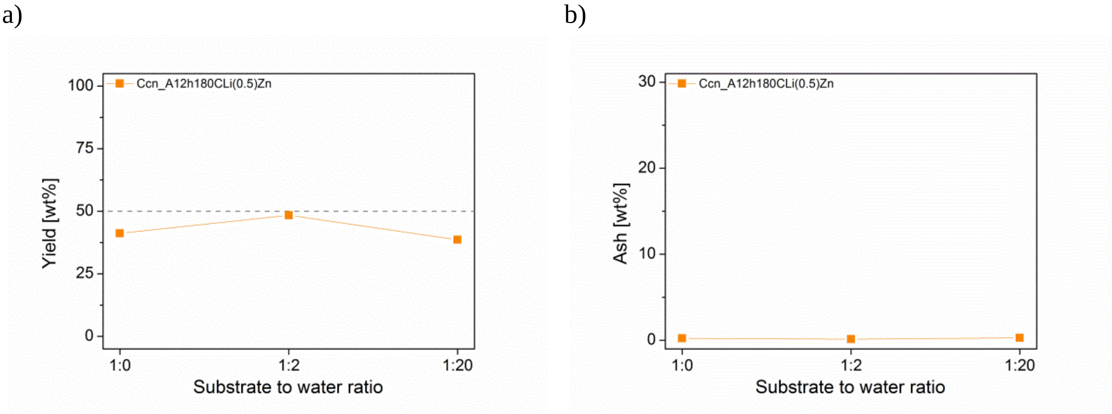

Figure 88 Yield and ash content of hydrochars received at different substrate to water-salt mixture ratio.

When the salt ratio is changed an increase in yield is observable, as seen in figure 89a. The ash content increased by a factor 2.5 but still stayed under 1 wt%. A high salt amount can potentially increase the formation of solid compounds by catalyzing the reactions involved in the formation of those. By increasing the water and salt ratio at the same time, the yield drops again (figure 89a), similar as seen for the increase of only the water ratio (figure 88a).

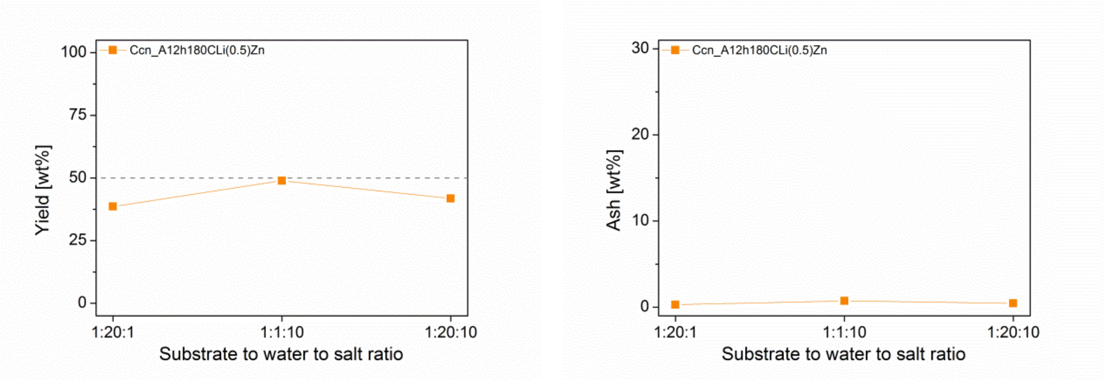
a)
b)

Figure 89 Yield and ash content of hydrochars received at different substrate to water to salt mixture ratio.

In case of reaction setup htc_B similar observations for the variation of the water content are seen, for both a normal HTC and the salt-HTC reaction (figure 90). The ash content stays at a low level of < 1 wt% and the yield increases from a 1:1 substrate to water or water/salt-mixture ratio to that with a 1:2 ratio. Increasing the amount of solvent further, a small loss in yield takes place. Therefore, the ratio of substrate to solvent of 1:2 seems in both cases the optimal condition for receiving a solid hydrochar. Increasing the amount of water leads to a loss of compounds into the liquid phase and an increase in salt counteracts a potential application if the amount of used salt is considered on a technical scale.

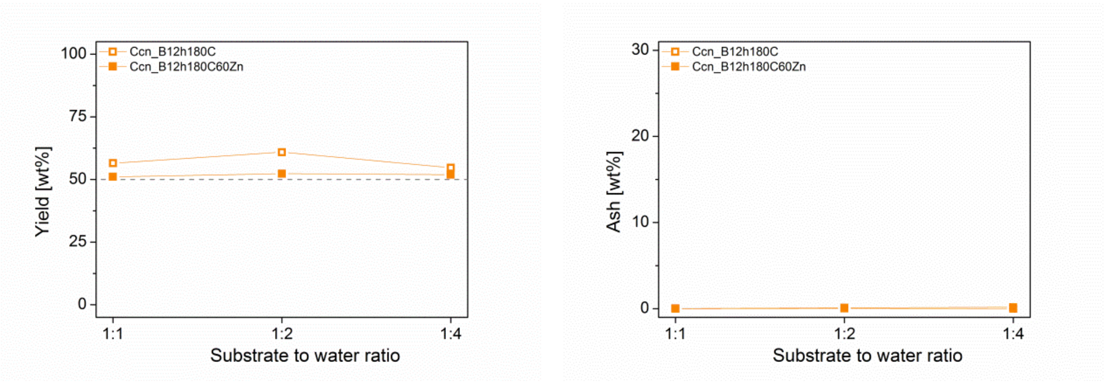
a)
b)

Figure 90 Yield and ash content of hydrochars received at different substrate to water-salt mixture ratio.

To check the influence of salt wt% in the salt-water-mixture, five different wt%'s ranging from 10 to 80 wt% were chosen for reactions in the setup htc_B at a substrate to solvent ratio of 1:2. Ideally, the amount of used zinc chloride is lower than 60 wt%, resulting in lower material, application and process recycling costs. The results shown in figure 91a indicate a small rise in reaction yield from 50.8 (Ccn_B12h180C10Zn) to 52.8 wt% (Ccn_B12h180C80Zn). The ash content stays at a low level but increases at a $ZnCl_2$ wt% of 80 to 3.18 wt%.

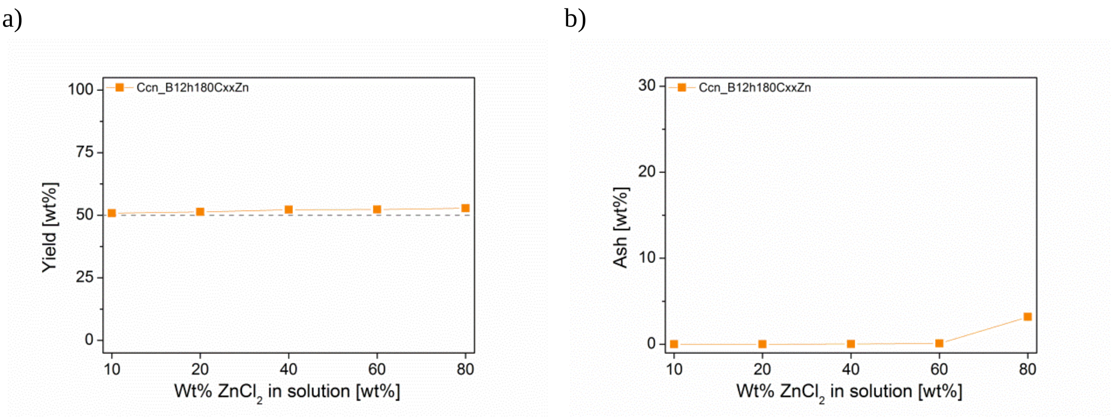

Figure 91 Yield and ash content of hydrochars received at different wt% of zinc chloride in the salt-water mixture.

The increased yield for this sample could therefore be caused by leftover salt from the reaction due to the high initial amount. The typically used washing procedure of this work was therefore not sufficient enough to remove the entire high initial amount of salt by washing for the last sample of the salt content series (80 wt%). Furthermore, it indicates that the salt content in the salt-water mixture does not play a significant role in the reaction yield. Increased amounts of salt do not lead to a loss in solid yield but small ones also did not result in a decreased reaction process if judged by the yield loss. Therefore a 10-20 wt% $ZnCl_2$ solution seems to be a good choice for the hydrothermal carbonization, which would nicely reduce the initially used salt.

4.1.3.2 Elemental composition

The changes in carbon content from the variation of substrate to water or substrate to water salt ratio as well as the weight percentage of zinc chloride are seen in figure 92 and 93.

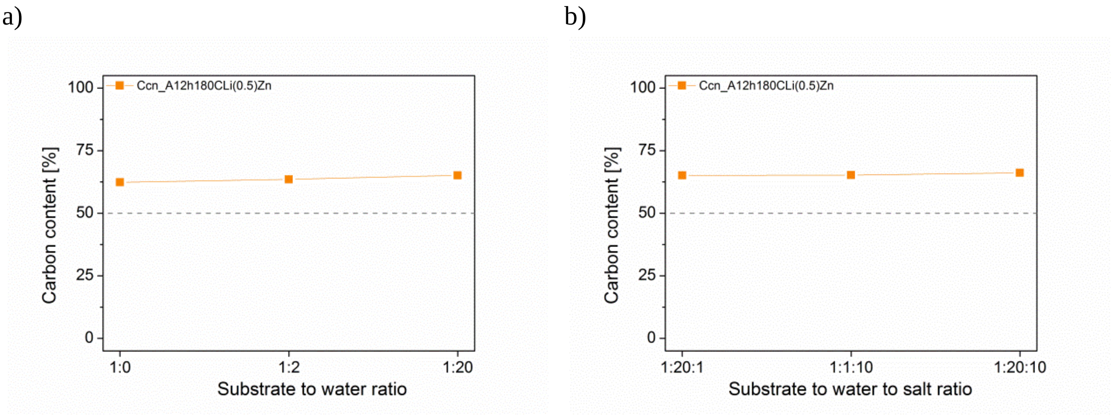

Figure 92 Carbon content of hydrochars received at different substrate to water or substrate to water to salt ratios.

The changes when using setup htc_A proved minimal with the carbon content increasing only slightly (figure 92a). By using more water an increase from 62.3 (1:0) over 63.5 (1:20) to 65.1 % (1:20) is observed (figure 92b). In the discussion of the yield a loss of compounds, probably into the liquid phase, was discussed. Here it seems the loss occurs mainly for hydrogen and oxygen as probably water. Using also a high concentration of salt in the high water ratio results in a further increase up to 66.2 carbon percentage.

Testing the water ratio as well as the amount of zinc chloride in solution with the main setup used for most hydrochars in this work (htc_B) no direct correlation between the varying factor and the carbon content was found (figure 93a). The carbon content stayed at a stabile value of around 57-59 % (HTC) or 66-68 % (salt-HTC).

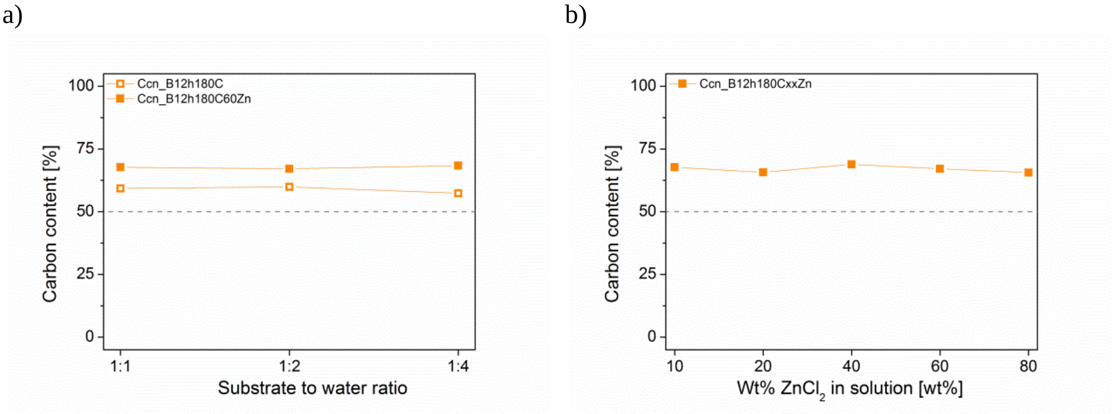

Figure 93 Carbon content of hydrochars received at different substrate to water ratios or different wt% of zinc chloride in the solution.

While the yield and ash content showed that a substrate to solvent ratio of 1:2 and a low zinc chloride content (e.g. 10-20 wt%) would be ideally, no distinct influence onto the carbon content was found (figure 93b). Therefore the optima from the yield discussion could be used if those also result in sufficient surface areas, as discussed in the next subchapter.

4.1.3.3 Porosity analysis

The development of possible porosity by varying the amount of water and salt in the hydrothermal carbonization will be discussed with the data received by nitrogen sorption on the samples. The results are presented in figures 94 and 95 (see also table A6).

With no water present (substrate to water ratio 1:0) the specific surface area is at the detection limit. While arguable not being a hydrothermal carbonization anymore the result is not surprising since there is no medium available for the reaction to take place in. At the usual ratio used in most previous described experiments (1:2) a typical value between 100-130 $m^2 \cdot g^{-1}$ is obtained in both setups (htc_A and htc_B). By increasing the water amount to values of 20 times in ratio to the substrate by keeping the salt amount the same a decrease in surface area is visible. The reaction medium is not concentrated enough in additive anymore and therefore having a decreased catalyzing effect. By increasing the amount of salt at a low water to substrate ratio (1:1:10) the surface does also not reach the values for the typical reactions as seen in figure 94b. At high water and salt amounts (1:20:10) no desirable influence could be observed as well.

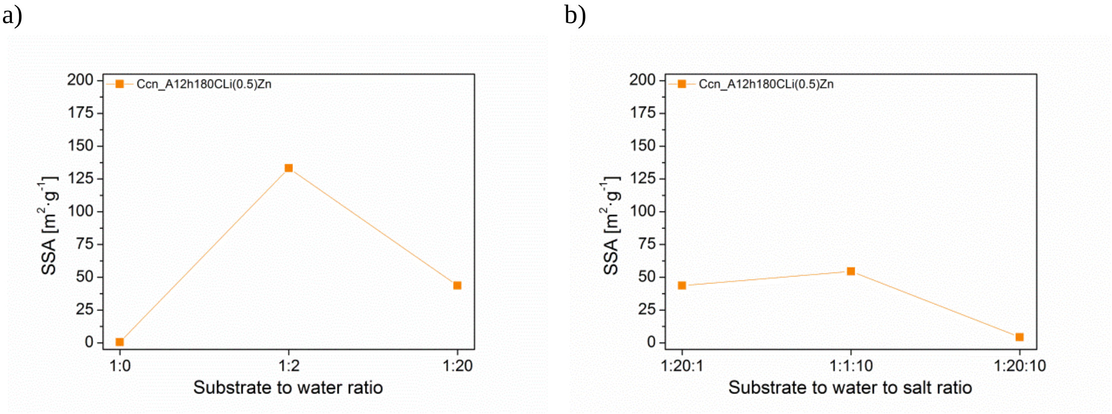

Figure 94 Specific surface areas (SSA) of hydrochars received from different substrate to water (a) and substrate to water to salt ratios (b) as measured with nitrogen.

In the setup htc_B the influence of water was studied in ratios 1:1, 1:2 and 1:4 with no distinct influence on the SSA in both cases, with HTC or salt-HTC (results shown in figure 95a). On the other hand, the amount of salt in the salt-water solution plays a critical role as seen in figure 95b.

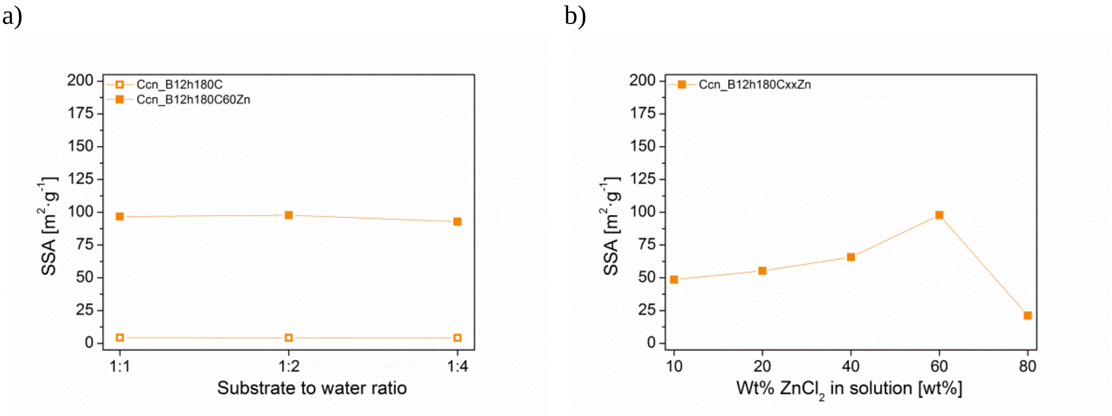

Figure 95 Specific surface areas (SSA) of hydrochars received from different substrate to water ratios or from different wt% of zinc chloride in the solution as measured with nitrogen.

By increasing the amount of zinc chloride from 10 to 60 wt% nearly a doubling in surface area is observed. However, increasing the salt amount further to 80 wt%, a decrease in surface area under the values of 10 wt% is observed. The amount of water in the reaction medium was too low in this reaction comparable to the reaction without water present as seen in figure 95a.

The results of the surface area determination showed that the best results were obtained with a substrate to solvent ratio of 1:2 using a 60 wt% zinc chloride solution. This setup was used in most experiments already presented in this study.

4.1.4 Influence of lithium chloride and zinc chloride onto the hydrothermal carbonization of coconut shell powder

The use of a mixture of lithium chloride with zinc chloride at the eutectic ratio for the HTC of glucose as reported by Fechler *et al.* resulted in, for the HTC unusual, high surface areas.[11] In their work, using the LiCl/$ZnCl_2$ eutectic mixture resulted in higher SSA than pure zinc chloride. In this study so far the effect of zinc chloride was in the focus. However, some samples received by method htc_A, which was a similar approach to the one found in the work by Fechler *et al.*, had lithium chloride present but its effect was considered negligible to this point. The difference to the literature work was not only the substrates being complex biomasses but also the salt composition was not always in the eutectic ratio (LiCl 23 mol%) but at e.g. LiCl to $ZnCl_2$ ratio of 50:50 mol%. To determine the effect of each salt in the hydrothermal carbonization, different salt compositions ranging from pure lithium chloride over different LiCl to $ZnCl_2$ ratios to pure zinc chloride were used. The coconut shell powder was also tested in setup htc_B, while here the typical weight percentage of zinc chloride was decreased from 60 to 40 wt%. Since lithium chloride is only soluble in water up to containing content of around 40 wt% LiCl, the change in zinc chloride solution was done for better comparison of the two salts. The mixtures of the two salts were therefore also used as 40 wt% salt-water mixtures.

This chapter will show that the major factor in the development of porosity is caused by the zinc chloride and that the lithium chloride does not play a major role in the HTC of different substrates. For that, at first a look into the reaction yield, ash content, visible morphology, structural order and elemental composition will be taken, before the results from the nitrogen sorption experiments will be shown.

4.1.4.1 Reaction yield and ash content

The different yields together with the ash content of the samples are shown in figure 96 and table A7. No distinct difference in yield is visible when changing the salt composition. Only a jump from the normal HTC reaction (indicated as HTC in figure 96) to the salt-HTC is visible, but different depending on the setup.

The coconut shell powder has a higher yield loss in the salt-HTC in setup htc_B than in htc_A when compared to the normal HTC. The yield stays around 50 wt% but not high enough to get any clues from it towards the reaction progress. However, in the setup htc_A the lowest yield was found with the pure lithium chloride.

The amount of inorganic compounds rose to nearly 3 wt% in some cases for the Ccn_A series, while Ccn_B stayed below 1 wt%, as seen in most of the previous results for this substrate. This indicates that some of the higher initial amount of salt used in the htc_A setup remained after the washing procedure. These might explain some of the higher yields seen for htc_A in figure 96a.

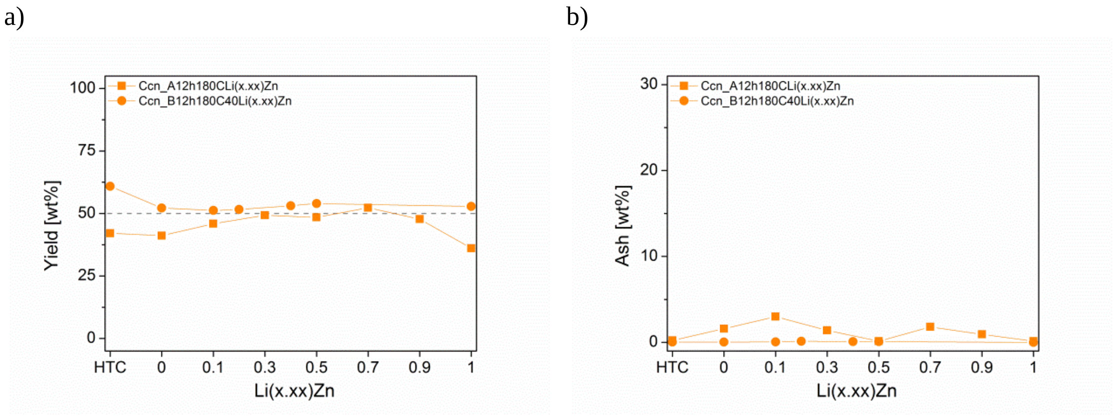

Figure 96 Yield and ash content of hydrochars received by coconut shell powder (Ccn) after 12 h at 180 °C.

4.1.4.2 Hydrochar morphology and structural order

The change in morphology will be exemplary discussed based on the SEM images shown in figure 97. These resulted from three different hydrochars obtained from coconut shell powder with the lithium chloride to zinc chloride ratios 1:0 (a), 1:1 (b) and 0:1 (c). On a low magnification (fig. 97-I) not much difference in each sample can be seen. A variety of different particle sizes seem to be present. By looking at the images received at a higher magnification the differences get clearer. If only the lithium chloride was used as an additive to the hydrothermal carbonization of the coconut shell powder the surface seems rather smoothed as seen also for normal HTC reactions (see discussion of the substrates chapter 4.1.1.2). By mixing zinc chloride to the additive or by using the pure $ZnCl_2$ the surface is covered with small particles, possibly creating a lot of surface roughness, as seen in figure 97b-II and c-II. These results indicate that the lithium chloride alone does not lead to a change in surface morphology and that the zinc chloride is needed as an additive to trigger a morphology change.

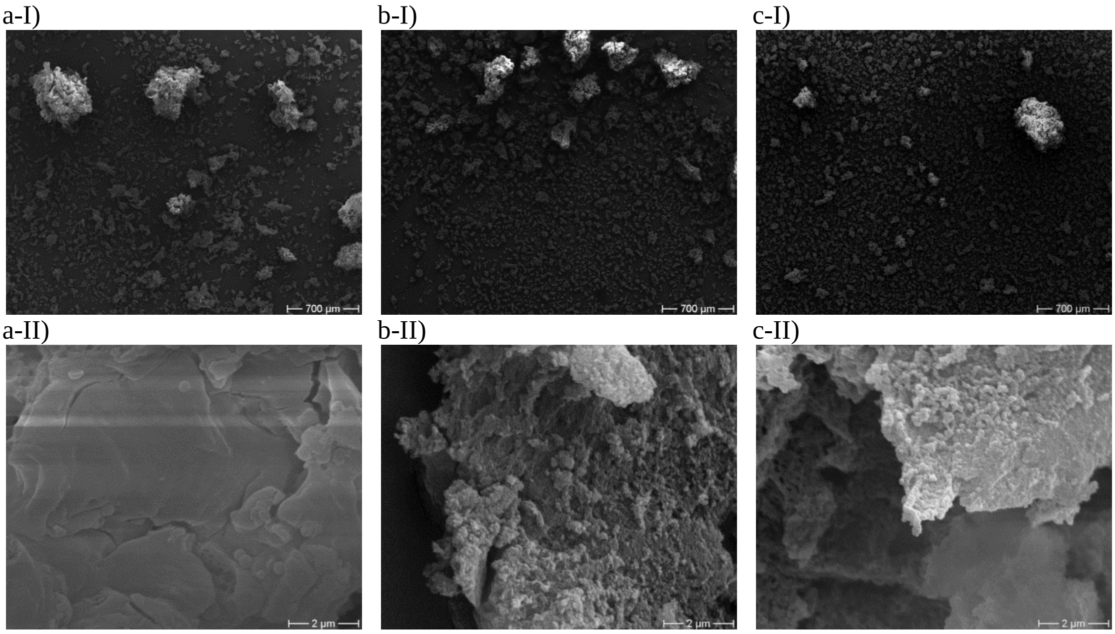

Figure 97 SEM pictures of hydrochars obtained from coconut shell powder with varying lithium chloride to zinc chloride ratios (a: Li(1.0)Zn; b: Li(0.5)Zn; c: Li(0.0)Zn) after 12 hours at 180 °C with low (I) and high (II) magnifications.

Additionally for a better understanding of the sample structure, XRD patterns were recorded for all three samples that are presented in figure 98. Interestingly, the change in structural order towards an amorphous sample with the appearance of a very broad reflection signal, suggesting a very disordered structure, already happens with only lithium chloride present (Ccn_B12h180C40Li). This indicates that while the lithium chloride does not lead to a rough visible surface, it can indeed initiate structural changes that don't take place during a normal HTC reaction.

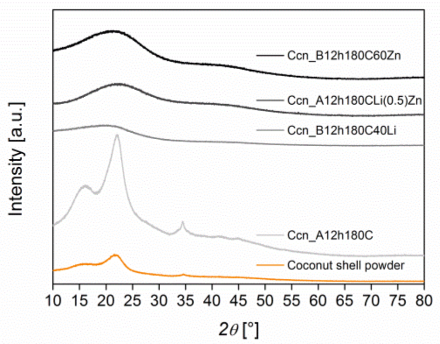

Figure 98 XRD of different hydrochars obtained from coconut shell powder and the original substrate.

4.1.4.3 Elemental composition

The change in elemental composition will be discussed from the change in carbon content of the hydrochars received from coconut shell powder. As seen in figure 99 no distinct influence of the salt composition is visible onto the carbon content. The initial increase from HTC to salt-HTC is followed by a stable trend around 63 (Ccn_A) or 68 % (Ccn_B). Setup htc_B resulted in an additional higher carbon content, possible due to a higher amount of inorganic compounds found in those received by htc_A.

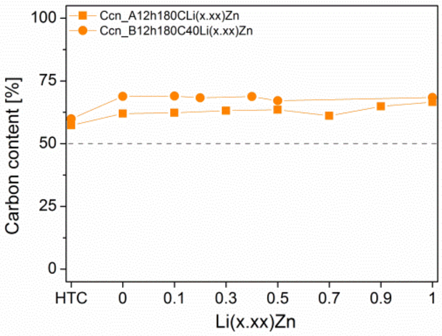

Figure 99 Carbon content of different hydrochars obtained after 12 h at 180 °C starting from coconut shell powder (Ccn) with different salt compositions present.

4.1.4.4 Porosity analysis

When testing the nitrogen sorption onto the different hydrochars it was found that only if zinc chloride was present in the reaction mixture, a surface area of around 100 $m^2 \cdot g^{-1}$ was obtained in setup htc_A (compare figure 100 and table A8). Since for htc_B a 40 wt% salt-solution was used, the values for the SSA didn't reach their optima (see discussion of salt to water ratio). However, with increasing content of lithium chloride, the SSA was decreasing for both series. Interestingly, the use of lithium chloride did in fact also lead to a small increase of surface area (< 25 $m^2 \cdot g^{-1}$) when compared to the normal HTC reaction (< 10 $m^2 \cdot g^{-1}$). Still, it seems that the reason of the creation of increased surface area is caused mainly by the zinc chloride.

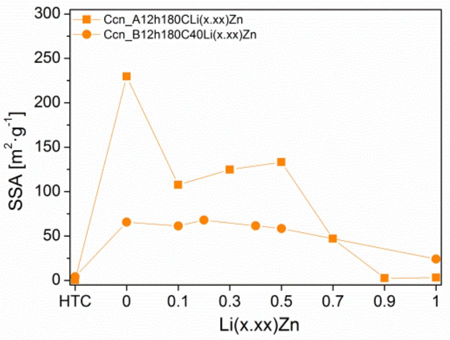

Figure 100 Specific surface areas (SSA) of hydrochars received from different salt compositions as measured with nitrogen.

4.1.5 Influence of different types of salts and their mixtures onto the hydrothermal carbonization of coconut shell powder

In the last chapter it was shown that the main reason for the creation of porosity within the hydrothermal carbonization of coconut shell powder is the presence of zinc chloride. Lithium chloride did not increase the surface area significantly. Since both salts have a chloride ion, it is possible that the cation plays the important role in the process. Therefore, chloride salts with different cations (sodium, potassium and magnesium) were tested. For the variation of the anion zinc sulfate, sodium sulfate and sodium carbonate were used. Additionally, lithium perchlorate was tested as an oxidizing agent.

First this chapter will give a general reaction overview by discussion the change in reaction yield, ash content and elemental composition before the porosity will be in focus.

4.1.5.1 Reaction yield and ash content

The change in reaction yield and ash content with different additives is shown in figure 101 (compare table A9). Most samples were received with yields of around 50 wt%. Noticeably, if sodium salts (without zinc chloride present) were used nearly 60 wt% of the used substrate was obtained as a solid hydrochar. Surprisingly, if magnesium chloride or lithium perchlorate were used the yield dropped to nearly 30 wt%. This indicates that especially in these two cases increased degradation with more compounds changing into the liquid or gaseous phase take place. The highest carbon yield was received for the sodium carbonate, which also resulted in the only hydrochar from this series with an ash content of greater than 1 wt% (1.33 wt%).

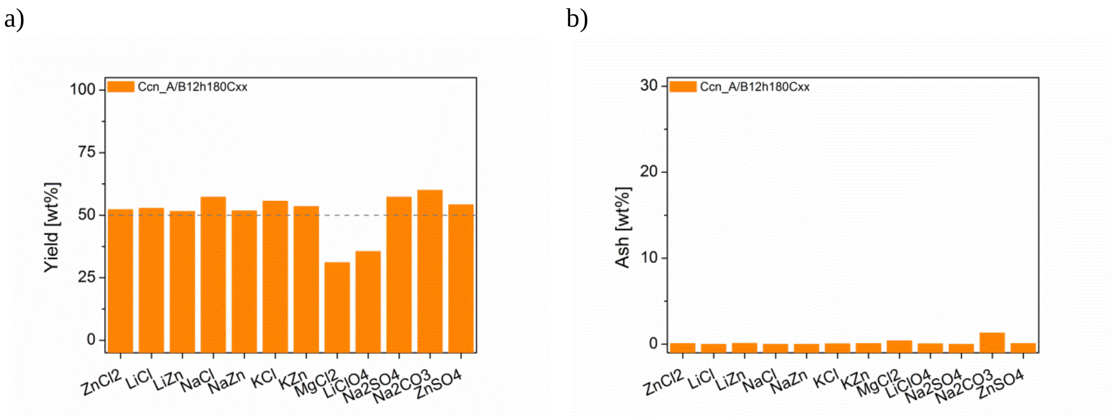

Figure 101 Reaction yield and ash content of hydrochars received from coconut shell powder using different additives.

4.1.5.2 Hydrochar morphology

Since the samples received from magnesium chloride and lithium perchlorate showed a very low product yield, SEM images were made of them which are shown in figure 102.

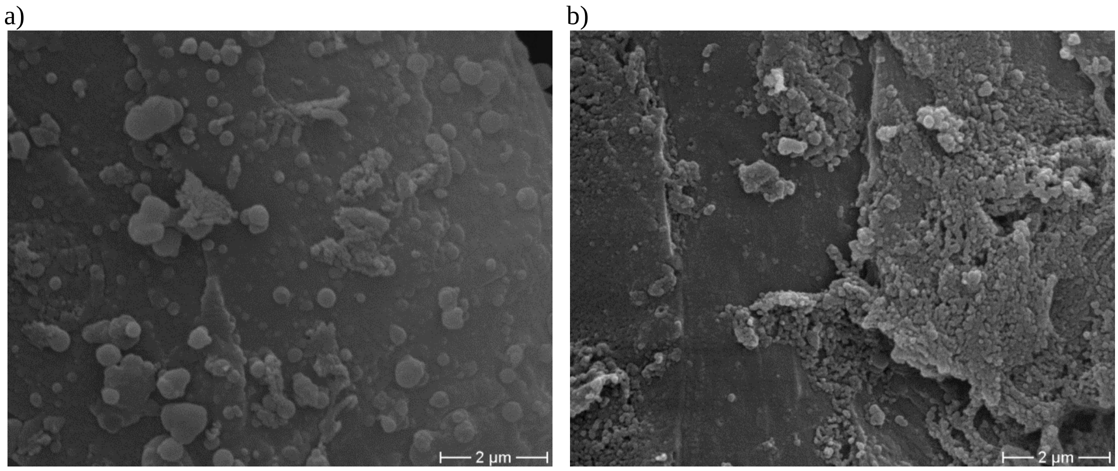

Figure 102 SEM images from hydrochars obtained at 180 °C for 12 hours with magnesium chloride (a) or lithium perchlorate (b) present.

The images show that the hydrochar produced with magnesium chloride has a rather smooth surface with bigger carbonized particles present and that the weight loss is probably not accompanied with the production of a lot of surface roughness or porosity. The hydrochar received with lithium perchlorate on the other hand showed a lot of very small holes or tunnels etched into the surface creating a lot of visible roughness and therefore possible porosity.

4.1.5.3 Elemental composition

Changing the additive did not result in a major change in carbon content as shown in figure 103. The most promising additive was the perchlorate, which already resulted in nearly the highest yield loss, raising the carbon content to more than 69 %. Two of the three sodium salts tested had the lowest carbon contents, underlining the weaker reactive behavior seen from the yield. Unexpectedly, the carbon content from the hydrochar received with zinc sulfate was more in the lower region towards 60 % than those usually received from zinc chloride, which goes towards 70 %. Here, it is possible that not only the zinc ion is important, as discussed in the chapter for the influence of lithium chloride and zinc chloride, but also that the anion plays an important role for a possible catalyzing effect.

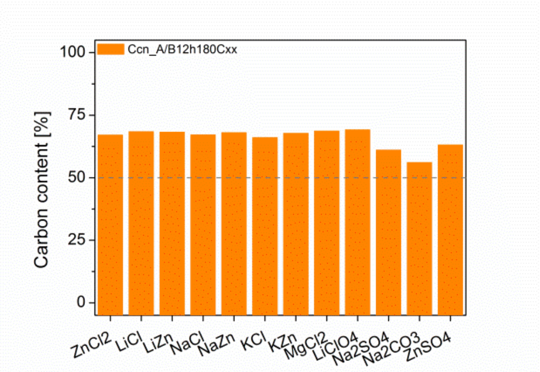

Figure 103 Carbon content of hydrochars received from coconut shell powder using different additives.

4.1.5.4 Porosity analysis

When calculating the specific surface areas for the different hydrochars using the BET theorem from nitrogen sorption data, nearly all additives showed lower potential of increasing the SSA than zinc chloride (see figure 104 and table A10). However, the lithium perchlorate which already showed the highest yield loss and carbon content also resulted in the highest surface area. The oxidizing agent can oxidize a lot of the biomass compounds, resulting in increased porosity and a higher surface area.

For the zinc chloride it can be seen again that the addition of another chloride salt, which results in only a small increase of surface area if used alone, decreases the suitability for creation of higher surface areas.

Changing the anion for the zinc does not result in any improved surface area with the tested additive ($ZnSO_4$), underlining the importance of not only the zinc cation, but also its anion for its effect in the hydrothermal carbonization to take place.

The two sodium salts (Na_2SO_4, Na_2CO_3) that already did not show promising results in the yield and carbon content discussion have both surface areas well below 10 $m^2 \cdot g^{-1}$.

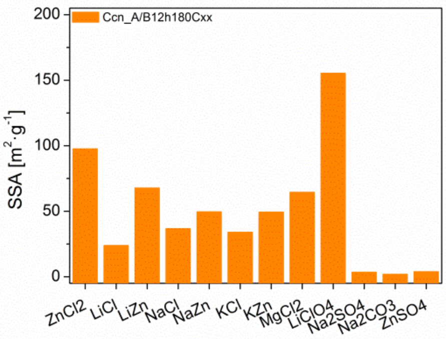

Figure 104 Specific surface areas of hydrochars received from coconut shell powder using different additives as measured by nitrogen sorption.

The results underlined the so far established importance of the presence of the zinc chloride. Additionally, with the $LiClO_4$ another interesting additive was found. Its high explosive nature in mixtures with organic matter however limits the potential for being used within the HTC.

4.1.6 Possibilities for a process recycling towards a cycle loop

In the process of the salt-HTC all the zinc from the initial used zinc chloride should be either in the coal as zinc oxide or in the liquid phase as either zinc chloride or zinc hydroxide. In the discussion of the different substrates it could be shown that without sufficient washing indeed ZnO can be found by XRD as the ash of the obtained hydrochar from coconut shell powder (compare 4.1.1.1). But since the washing was carried out so nearly no zinc could be found in the ash, it stands to reason that all zinc will be in the liquid phase. By atomic absorption spectroscopy measurements only a decreased amount of zinc was found in the waste and washing water (together around 50 %). By using minimal extra water for washing the obtained coals and rinsing the filtrated hydrochar three additional times with the filtrated wash water, around 74 % of the initial used zinc can be found in the waste water. An additional 6 % were found as ash (ZnO) in the hydrochar since this washing step did not provide enough water to solve all into the liquid phase. So overall, only around 80 % of the initial zinc could be found. Since the PTFE liner is a porous material some of the zinc compounds might have sticked to the inlet. Therefore it proved difficult to receive the whole initial used zinc back while some mass is lost with every processing step. Since the zinc was found as ZnO in the unwashed samples it can be assumed that it will be in the solution as zinc chloride since the usually water insoluble oxide is dissolved in the acidic water, whose pH is set by the HTC degradation products. By taking the weight of a determined amount of the solution and with the former assumption, that all zinc is present as its chloride, a washing solution of around 40-50 wt% $ZnCl_2$ can be obtained by using minimal additional water. Since the usual washing step includes washing with 200 mL of additional water and 1 L over night the actual used solution has a lower wt% of zinc chloride, decreasing with every recycle step. An evaporation of the excess water for increasing of salt amount in percentage is thinkable but it proved difficult to evaporate the water from the formed hydrate and was therefore not further considered in the here shown results. The waste solutions can then be used in a following carbonization step to ideally receive a hydrochar with properties of those received with a fresh zinc chloride solution with the certain weight percentage. This process was repeated two (Series 1) or one (Series 2) additional time(s) to have an overview of four process cycles and its resulting hydrochars. Since a lot of organic products from the HTC reactions are present in the waste solution which possibly sum up with each step and not all zinc chloride can be transferred into the wash solutions a decrease in characteristic optima is to be expected. Therefore, Cycle 1 should be comparable to an initial solution of between 40-60 wt% zinc chloride and each further cycle step should be comparable to a lower $ZnCl_2$ concentration.

For the following discussion the data received in the test of salt concentration is presented in orange along those received for the recycled hydrochars to compare the influence of leftover salt onto the yield, ash content, carbon content and finally the porosity (compare figure 105-107).

4.1.6.1 Reaction yield and ash content

Figure 105 and table A11 show the change in yield and ash content if coconut shell powder was hydrothermally carbonized at 180 °C for 12 hours in either a fresh 60 wt% zinc chloride solution, or the waste and washing water obtained by the prior reaction (e.g. Cycle1 uses the waste and washing water from the reaction with the fresh solution, Cycle2 the one from Cycle1, etc.). The orange points show the values obtained in the study of the weight percentage of zinc chloride in solution (compare 4.1.3) to give a possibility to estimate the zinc chloride amount in the solution used in the recycle series.

The results indicate that the yield does not significantly change with each cycle loop, showing that no crucial difference in reactive behavior seems to take place. On top of that, no concentrating of inorganic compounds into hydrochars from e.g. the waste water takes place since the ash content stays at a low level (figure 105b).

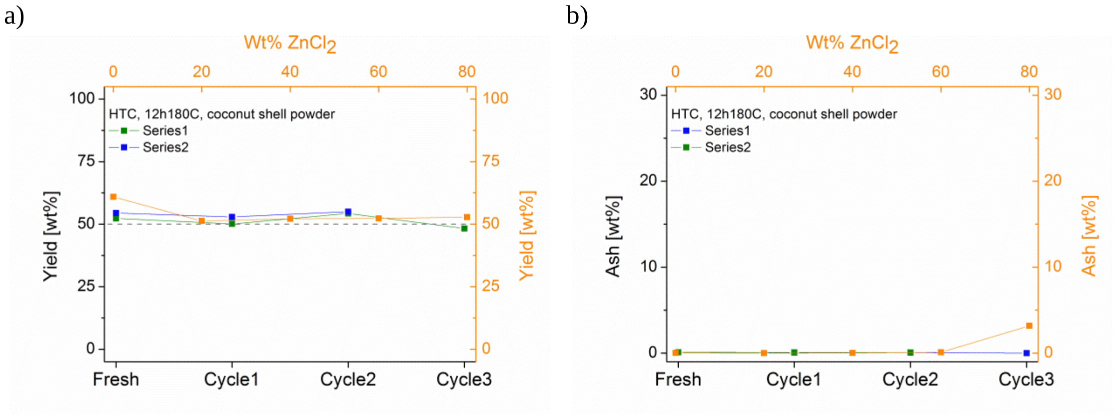

Figure 105 Reaction yield and ash content of hydrochars received by the recycle series together with those from the amount of zinc chloride study (orange).

4.1.6.2 Elemental composition

The carbon content, as shown in figure 106 and table A11, stays at a stable level of around 68 % even after three recycling steps of the waste and washing water phase. The carbon content does not sink in any case to those found for a normal carbonization (first orange point in figure 106, presenting the carbon content from a hydrochar received with pure water). This indicates that there is always sufficient zinc chloride present in the reaction mixture that catalysis of the reactions in the hydrothermal carbonization can take place.

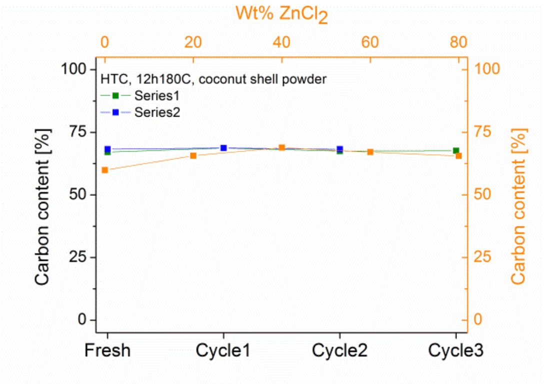

Figure 106 Carbon content of hydrochars received by the recycle series together with those from the amount of zinc chloride study (orange).

4.1.6.3 Porosity analysis

When measuring the specific surface areas of the hydrochars received from using the recycled waste and washing water in the hydrothermal carbonization of coconut shell powder a decrease of surface area takes place, as seen in figure 107 and table A12. Using a fresh, 60 wt% zinc chloride solution for the HTC at 180 °C for 12 hours usually results in hydrochars with a SSA of around 100 $m^2 \cdot g^{-1}$. This can be seen in both series of the recycling experiments (figure 107 fresh), as well as for the 60 wt% solution of the zinc chloride content series (figure 107 orange point at 60 wt%). Using the waste and wash water, which contains around 40-50 wt% $ZnCl_2$ (Cycle1), the received hydrochars have a surface area of around 70 $m^2 \cdot g^{-1}$, which is in good agreement with the point of the orange line for a surface area of a hydrochar produced with a 40 wt% fresh solution.

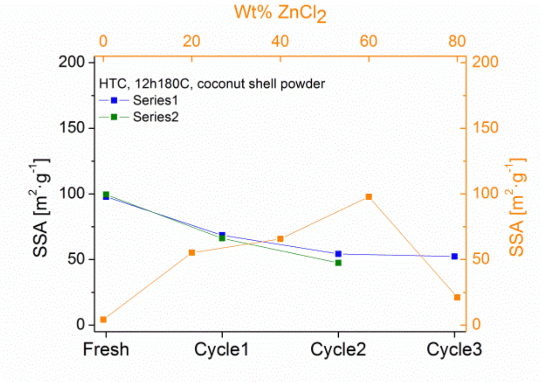

Figure 107 Specific surface areas of hydrochars received by the recycle series together with those from the amount of zinc chloride study (orange).

The decreasing amount of salt in the liquid phase therefore leads to a lower resulting surface area. Using the waste and wash water phase received from Cycle1 for another run, the surface area decreases further to about the values received from a fresh 20 wt% solution. This was to be expected since the extra washing water decreases the weight percentage of the zinc chloride in each step. At a third cycle (Cycle3) the surface area seems not to decrease further. It seems that the zinc chloride amount still did not fall under the critical amount needed for the observed effects to take place.

The results therefore indicate that a recycling of the waste and wash water phase is possible to receive hydrochars with increased surface areas. To reach those values obtained with a fresh solution, additional treatment like adding of new zinc chloride or the evaporation of excess water could be imagined.

4.1.7 Waste water phase of the hydrothermal carbonization in the presence of salt-water mixtures

The analysis of the liquid phase of the hydrothermal carbonization often proves a big issue due to the huge amount of compound variety present. Here, only a short analysis of the liquid phase of the normal carbonization of coconut shell powder and that received with a 60 wt% zinc chloride solution will be discussed. Both reactions were done at 180 °C for 12 hours. The waste phases are obtained after vacuum filtration of the wet coals as obtained by either HTC or salt-HTC, without any additional water than the one used for the reaction added. A total organic carbon analysis showed that in the normal hydrothermal carbonization about 18 g/L of carbon are obtained (compare table 11). If the salt was present in the reaction less carbon is found in the waste water phase (10.55 g/L). While the lower yield for the salt-HTC (compared to the HTC reaction; see discussion of different substrates chapter 4.1.1.1) would indicate that more of the sample is lost into the waste water phase, the elemental analysis showed that the carbon in the hydrochars received by salt-HTC is notably higher than those received by normal HTC. Therefore the higher yield loss but also higher C% indicates that the additional more water out of the substrate present dilutes the organic compounds in the water phase. It is also possible on the other hand that the loss of carbon into the waste water phase is higher in the normal HTC reactions.

Table 11 Total organic carbon content of the waste waters received in the process of hydrothermal carbonization.

Sample	**Total carbon [g·L^{-1}]**
Ccn_B12h180C	18.24
Ccn_B12h180C60Zn	10.55

While the relative amount of carbon is higher in the normal HTC reaction, the figures obtained by HPLC of the reaction waste waters (WW) show an additional interesting observation (figure 108).

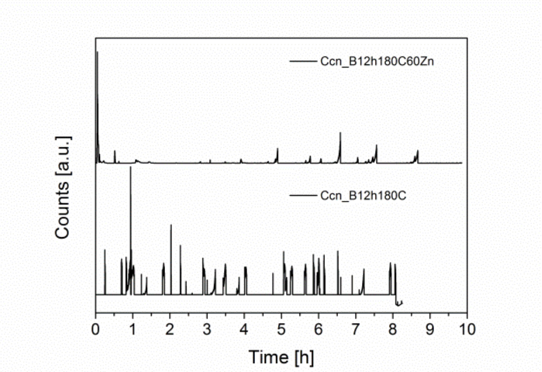

Figure 108 Chromatogram received by HPLC of the waste water phases of two different HTC reactions from coconut shell powder.

The variety of organic compounds is increased in the waste water from the salt-HTC reaction. The HPLC chromatogram clearly shows an increased amount of peaks for the salt-HTC waste water compared to that from the normal HTC. While no further peak assignment to a specific compound was done, the amount of peaks and overlap of signals in the salt-HTC sample is significant. It seems that for the normal HTC certain compounds are formed in the end, which leave the column after 5 to 9 hours with the used HPLC setup, indicating more polar compounds since a polar column was used. A lot of compounds that leave at lower retention times are found in the salt-HTC sample. Therefore a lot of more apolar compounds are formed in this case. Additionally, it is imaginable that the zinc chloride catalyzes not only reactions from the solid biomass but also those in the solution. Due to this the bigger compounds could react to shorter ones, leaving the HPLC column at lower retention times.

4.2 Activation of hydrochars received in the presence of salt-water mixtures

Usually, high surface area carbons are received by a traditional physical or chemical activation route to values of four digit surface areas like e.g. 1000 $m^2 \cdot g^{-1}$ or even higher. The studies of the reaction temperature in this work showed the strongest relation of this parameter to the surface area of the obtained hydrochars besides the use of an additive but the temperatures used in a typical HTC reaction are still to low to compare them to those used in activation processes. However, studies in literature have shown that by an additional physical activation step the surface areas of various hydrochars can be increased. Compared to usual activated carbons some positive characteristics of the hydrochars could be taken onto the activated forms (compare chapter 2.5). This work also took a look into the activation of those hydrochars received by hydrothermal carbonization. Especially those received by salt-HTC are of interest since these had different characteristics to the usual hydrochars.

For a physical activation using steam at increased temperatures, first the thermal stability of the hydrochars obtained from coconut shell powder were tested by thermogravimetrical analysis (TGA) under nitrogen as seen in figure 109. The substrate (black line) and its hydrochars have a small weight loss around 100 °C, mostly from leftover water or volatile compounds. At 300 °C the substrate has a weight loss not prominent in the hydrochars, probably resulting from compounds changed or lost in the carbonization reactions within the HTC. The most change in all samples occurs around 350 to 450 °C with the hydrochars received with a salt present shifted to higher temperatures, indicating a more resistant structure (orange and green line). If traces of zinc chloride would be present in the hydrochars, their weight loss would be seen around 550-600 °C (blue line).

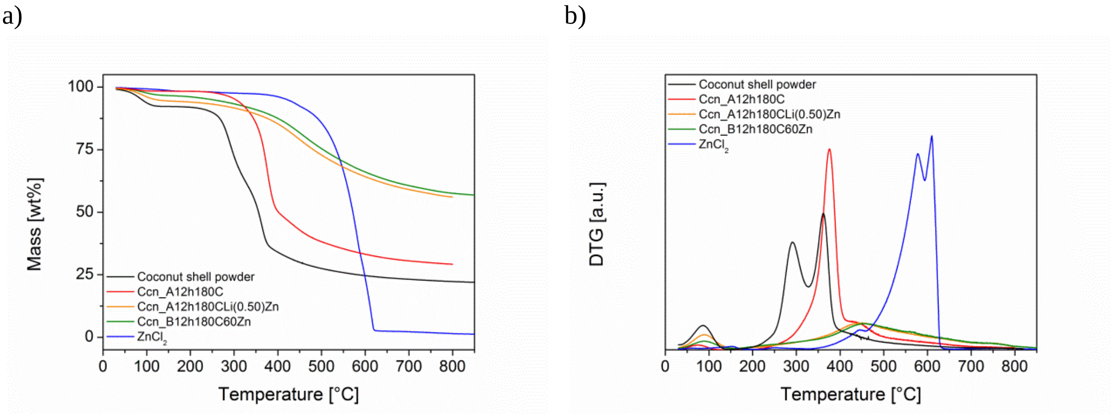

Figure 109 TGA (a) and DTG (b) results of coconut shell powder and three of its hydrochars, as well as zinc chloride for comparison.

Based on the observations seen in TGA an activation temperature of 500 °C was chosen as the standard temperature for the steam activation of the different hydrochars. The samples were therefore kept at this temperature in a tubular furnace (see 3.2.2), which had a constant flow of steam, for 60 minutes. The used hydrochars for the activation included those obtained from either HTC or salt-HTC (use of a mixture of lithium chloride and zinc chloride) of three different substrates, namely coconut shell powder, dried dandelion leaves or sawdust with the setup htc_A (compare 3.2.1.1).

To get a better understanding of the activation process itself, four different temperatures (200, 350, 500, 650 °C) at constant time (60 minutes) and three different times (10, 30, 60 minutes) at constant temperature (500 °C) were tested for the activation of the hydrochars obtained from coconut shell powder.

The results will be discussed based on the yield (obtained solid in weight percentage of initially used hydrochar), ash content, carbon content, morphology, surface functionality and porosity.

4.2.1 Activation of hydrochars obtained from different substrates

The results of previous chapters showed that coconut shell powder proved as the most suitable substrate of those tested for the hydrothermal carbonization as well as the one with the salt-water mixture used. So the hydrochars of this substrate were chosen along those of two additional biomasses (dried dandelion leaves and sawdust) for the activation tests. For the discussion the results for the activated hydrochars will be compared to those from the hydrothermal carbonization as well as to the substrate.

4.2.1.1 Reaction yield and ash content

Figure 110 and table A13 show the yields and ash contents for the different biomasses, their hydrochars and activated hydrochars. The empty squares indicate those received without an additive present in the HTC while the filled squares show the data for the salt-HTC samples together with the ones activated out of these. The yield in case of the activation is in relation to 1 g hydrochar used for this step, therefore the points in the figure can lay higher than those for the hydrochar (which is in relation of total biomass used). As seen already in the discussion of the different substrates in the HTC process the sawdust had the highest stability in the HTC reaction, followed by the coconut shell powder and the dried dandelion leaves. In the activation step however, the type of biomass does not seem as the significant factor, since the hydrochars from all three biomasses have a similar low yield for this step. As seen in the TGA results (figure 109a), the hydrochars received by salt-HTC have an increased stability compared to those received by HTC, for which their yields are significantly higher, as seen in figure 110a. The little initial ash content in the coconut shell powder and sawdust concentrated in the activated hydrochar to values of nearly 3 wt%, which is understandably due to the loss in carbon from the physical activation. The dried dandelion leaves contained a high amount of inorganic compounds, as already seen in the substrate discussion for the HTC step, whose ratio increases in the activated hydrochar.

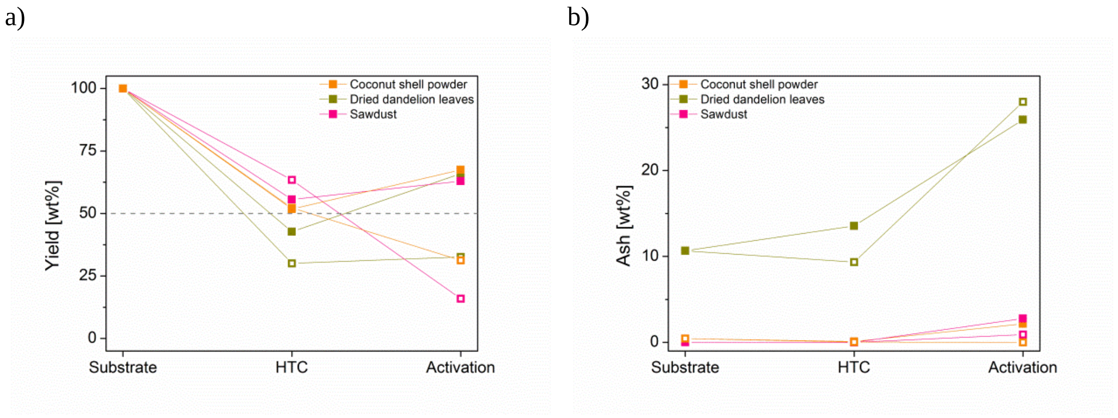

Figure 110 Yield (a) and ash content (b) of different substrates and their hydrochars (HTC) and activated hydrochars (Activation). Empty squares HTC and filled salt-HTC.

The higher stability of the activated salt-HTC samples could possibly result from the remains of a porous structure, which is lost in the normal HTC samples. The high ash content of the dried dandelion leaves samples will probably be a hindrance for the porosity.

4.2.1.2 Morphology of activated hydrochars

The activation of the hydrochars with steam at high temperatures resulted in a strong loss of solid, so a stronger change in morphology is expected. The SEM images in figures 111-113 show the morphologies of the substrate, hydrochars (HTC/salt-HTC) and its activated hydrochars in two different magnifications (overview and detail). The change from substrate to hydrochar from HTC or salt-HTC was discussed already extensively in prior chapters but the images are shown for better understanding of the changes towards the activated hydrochars. In each case the morphology changes only little from the substrate to those received by HTC, while the salt-HTC results in a breakup of biomass macrostructures, increasing the external surface area while also creating roughness from small carbonized particles which settle on the carbon surface. After physical activation for 1 hour at 500 °C also the normal HTC samples are broken into smaller pieces with increasing visible surface roughness. If the hydrochars activated originated from the salt-HTC route the amount of broken pieces increases significantly. Since the salt-HTC process creates hydrochars with smaller particles than the normal HTC route, these smaller particles are further split in the activation process, leading to the observed phenomena. For every biomass tested the activated hydrochars possessed a higher visible roughness, indicating a possible higher surface area.

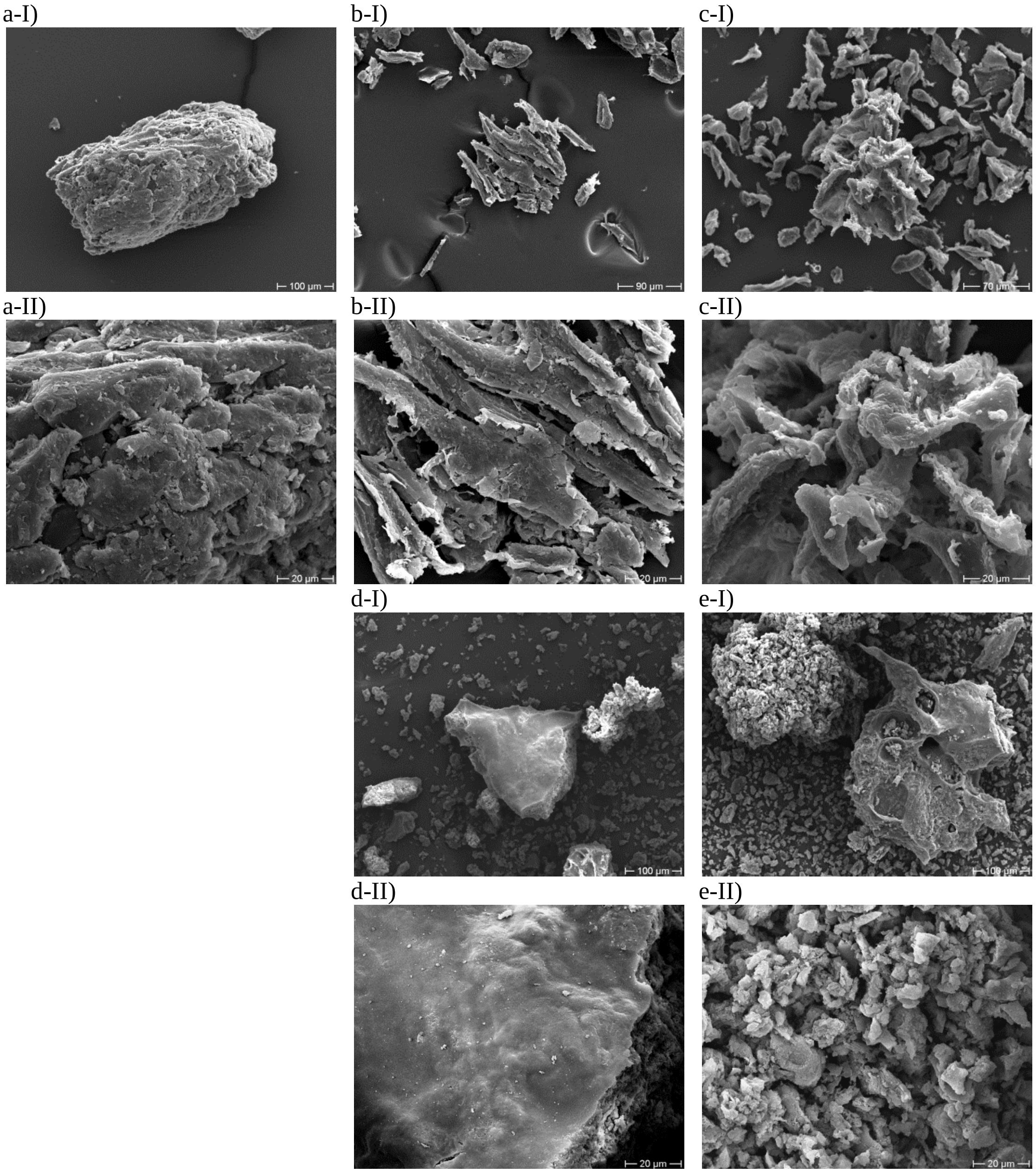
a-I) b-I) c-I)
a-II) b-II) c-II)
d-I) e-I)
d-II) e-II)

Figure 111 SEM images of coconut shell powder together with its HTC/salt-HTC and activated hydrochars (a - substrate; b - HTC (12 h, 180 °C); c - HTC activated (1 h, 500 °C); d - salt-HTC (12 h, 180 °C, Li(0.23)Zn); e - salt-HTC activated (1 h, 500 °C). Magnification: I - 120-200 times; II - 600-700 times.

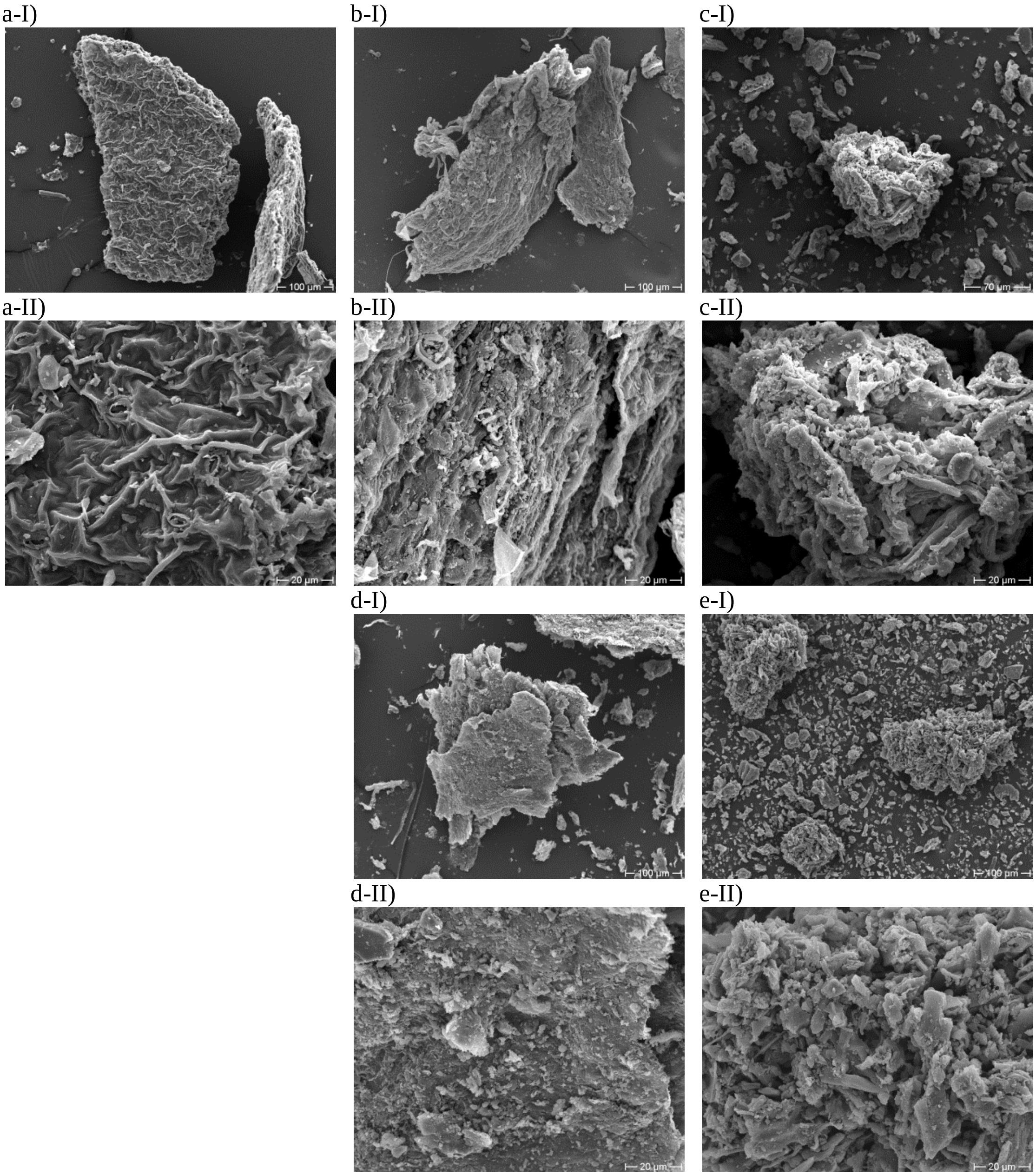

Figure 112 SEM images of dried dandelion leaves together with its HTC/salt-HTC and activated hydrochars (a - substrate; b - HTC (12 h, 180 °C); c - HTC activated (1 h, 500 °C); d - salt-HTC (12 h, 180 °C, Li(0.23)Zn); e - salt-HTC activated (1 h, 500 °C). Magnification: I - 120 times; II - 600 times.

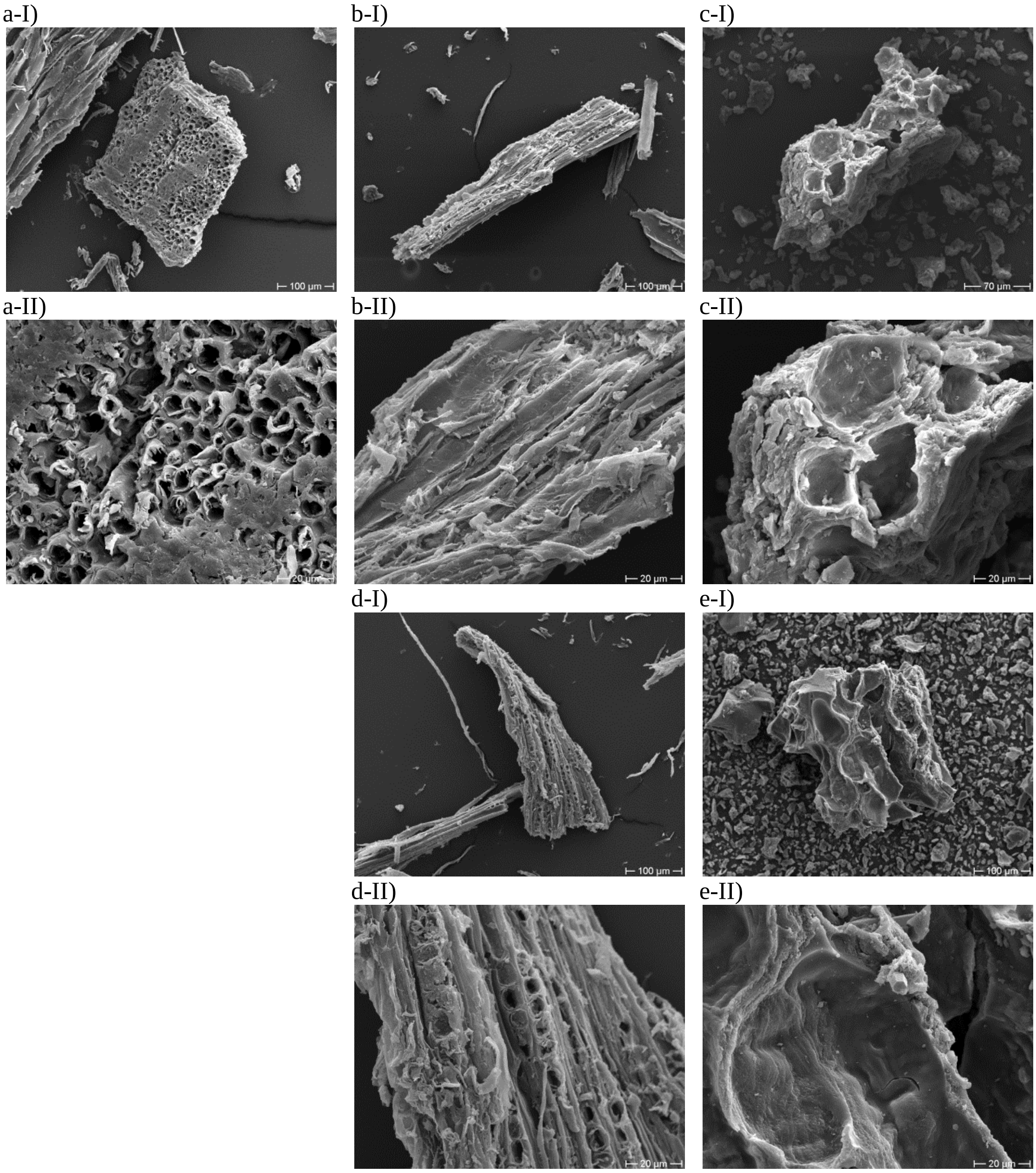

Figure 113 SEM images of sawdust together with its HTC/salt-HTC and activated hydrochars (a - substrate; b - HTC (12 h, 180 °C); c - HTC activated (1 h, 500 °C); d - salt-HTC (12 h, 180 °C, Li(0.23)Zn); e - salt-HTC activated (1 h, 500 °C). Magnification: I - 120-200 times; II - 600 times.

4.2.1.3 Elemental composition

The change in carbon content is shown in figure 114 and table A13 for the three substrates coconut shell powder, dried dandelion leaves and sawdust together with their hydrochars (HTC - empty square; salt-HTC - filled square) and activated hydrochars. The increase in carbon content from substrate to hydrochar was already described in prior chapters, always resulting in higher contents when the salt was present in the HTC reaction. By activating the hydrochars, the carbon content could be increased further for the coconut shell powder and sawdust. Up to around 77 % for both Ccn hydrochars and 66 or 72 % for the HTC and salt-HTC activated sample from sawdust, respectively. Only those received from dried dandelion leaves stayed at a level of around 50 % originating from a low carbon and high ash containing substrate.

The van Krevelen diagram (fig. 114b) resulting from the measurements of the elemental composition showed that the activated samples moved to compositions reminding of anthracite, whose region is around the lower left corner of the diagram.

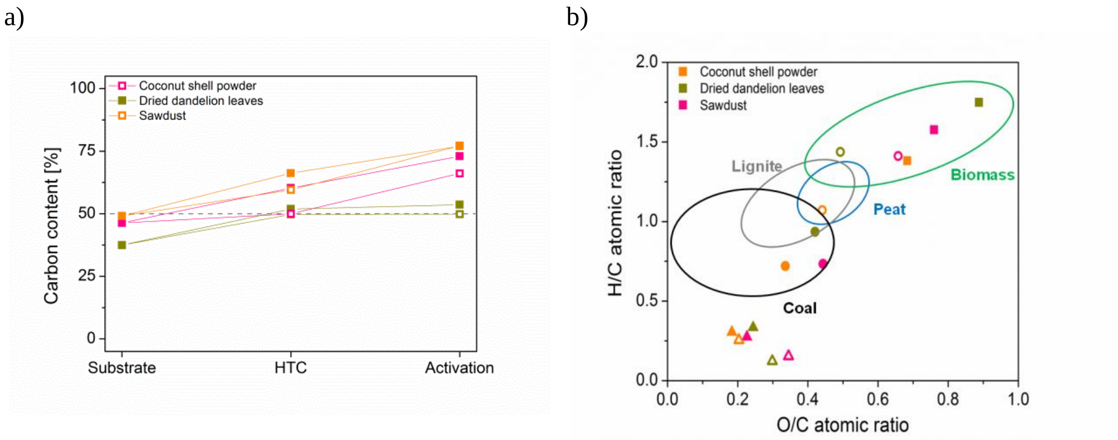

Figure 114 Carbon content and the resulting van Krevelen diagram. Empty signs are for the HTC and filled for the salt-HTC hydrochars (square - biomass; circle - hydrochars; triangle - activated hydrochars). The areas for biomass, peat, lignite or coal are collected from literature[40, 96, 267].

4.2.1.4 Surface functionality

It was shown before in this work that in the process of the hydrothermal carbonization some of the functional groups initially present on the biomass surface vanish towards the hydrochars with the emerging of three hydrochar typical signals at 1700, 1600 and 1200 cm^{-1}, corresponding to carbonyl C=O stretching, aromatic C=C stretching and ether C-O stretching, respectively. Some of the original functionality is more present in the HTC chars produced without salt mixture present, which gets nearly completely lost after the activation step (see figure 115).

The activated hydrochars received from either activation of the HTC or salt-HTC sample showed a very similar pattern with only the three previous mentioned signals present, showing similarities to the salt-HTC hydrochar. On top of that, those received from the activation of the salt-HTC hydrochar were less intense than those from the normal hydrochars. It can be imagined that the high temperatures together with the steam remove a lot of the functionality of the surface. But it is interesting to note that still some of the surface functionality originated from the biomasses can be found on the activated hydrochars since commercial activated carbons, which are mostly produced with the goal towards a carbon-carbon network free of especially oxygen, often have a surface without any functionality. The samples received in this work still have oxygenated functional groups present after physical activation with steam at 500 °C for 1 hour, possible increasing their interactive behavior for different technical applications.

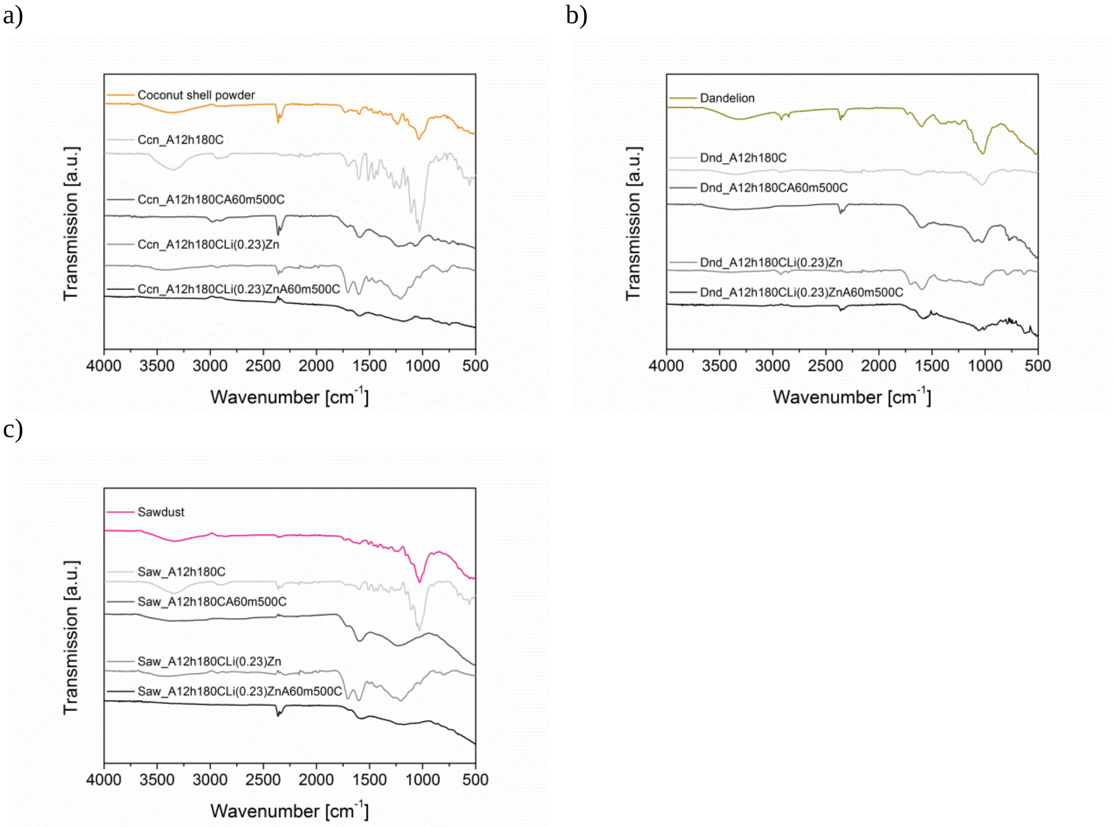

Figure 115 FTIR spectra of different substrates together with their hydrochars and activated hydrochars (a - coconut shell powder; b - dried dandelion leaves; c - sawdust).

4.2.1.5 Porosity analysis

The surface areas as measured with nitrogen for the different hydrochars and their activated forms are shown in figure 116a and table A14. Typical sorption isotherms are shown exemplarily from those originating on coconut shell powder can be found in figure 116b. It can be seen that the additional step of a steam activation increases the specific surface area of all hydrochars by a considerably factor. The highest measured surface area with well over 700 $m^2 \cdot g^{-1}$, was obtained by activating the hydrochar from sawdust for 1 hour at 500 °C with steam. Surprisingly, the samples obtained from dried dandelion, which showed a high amount of ash present and did not improve significantly by the use of the salt-HTC route in terms of SSA, could also be tuned towards increased surface areas by steam activation. All activated samples showed an increased uptake of nitrogen in the pressure region $p/p_0 < 0.1$ with a type I(b) isotherm, indicating the high measured areas being due to the presence of micropores and possibly narrow mesopores (< ~ 2.5 nm)[255].

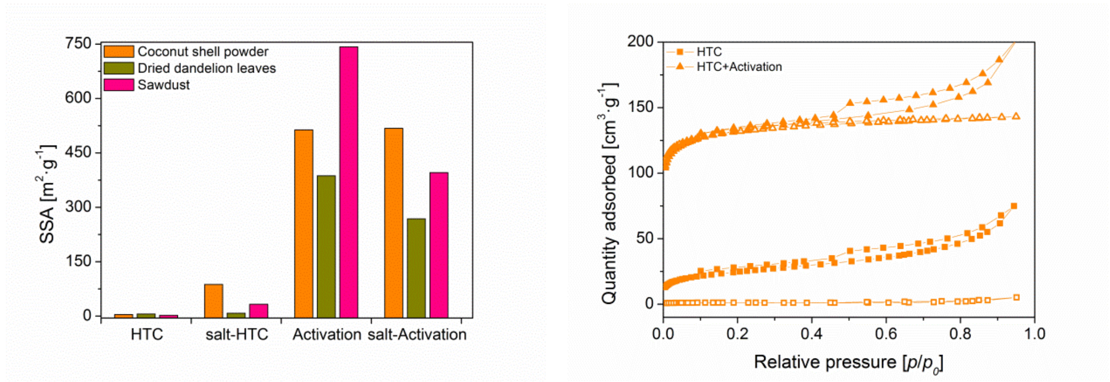
a)

b)

Figure 116 Specific surface areas (SSA) of different samples (a) together with sorption isotherms from hydrochars and activated hydrochars from coconut shell powder (empty points - no salt present; filled points - Li(0.23)Zn present in the salt-HTC).

Interestingly, those activated chars obtained from the salt-HTC hydrochars showed a lower surface area than those from the normal HTC chars in the cases of sawdust and dried dandelion. Only in the case of the coconut shell powder both had a similar specific surface area around 500 $m^2 \cdot g^{-1}$. It could be argued that the bigger structures of the normal HTC samples give more space to introduce microporosity, building a larger skeletal structure than the small parts found in the salt-HTC samples. No explanation why the coconut shell powder behaves differently could be found in this study.

An additional difference between the activated and salt-activated samples can be seen in the high relative pressure region from the sorption isotherms representatively shown for those from coconut shell powder (figure 116b). The isotherm from the sample received by activation of the salt-HTC char had an additional uptake of nitrogen over the relative pressure range from around 0.4 to 0.95 together with a visible hysteresis.

These possible Type H3 or H4 loops could indicate pore networks consisting of macropores which are not completely filled with pore condensate or point to micro-mesoporous carbons, respectively. Both were already found partly in the salt-HTC hydrochars, putting the idea near that those meso- or macropores were formed initially in the hydrothermal carbonization step. The activation is able to introduce only microporosity but the possible meso/macroporosity of the salt-HTC hydrochar remains and is not lost in the activation step. This observation shows an interesting, possible strength of the activated hydrochars from the salt-HTC samples when compared to those from normal HTC, which have a higher values of SSA, but only micropores present.

4.2.2 Influence of activation temperature and time onto the activation of hydrochars obtained from coconut shell powder

In the prior subchapter it was shown that activation in terms of physical activation with steam can increase the specific surface areas of hydrochars significantly by the introduction of microporosity. This comes with the drawback of the need of a high temperature (> 500 °C) and a loss in yield and surface functionality. It is therefore interesting to see which temperature is sufficient enough to increase the SSA but maybe does not fully remove the surface functionality as seen partly in the discussion of the activation of the three different substrates. For this, the hydrochars obtained from coconut shell powder (HTC/salt-HTC, 12 hours at 180 °C) were activated with steam at either constant time or temperature. The activation time was changed from 10 over 30 to 60 minutes at an activation temperature of 500 °C. The activation temperature was changed in 150 °C steps, starting with 200 and ending with 650 °C at a constant time of 60 minutes. The change in yield and ash content, as well as the carbon content are discussed first before the influence onto the surface functionality and porosity is in focus.

4.2.2.1 Reaction yield and ash content

The change in activation parameters is expected to strongly influence the yield. The ash content is shown to exclude its portion of the yield. As seen in figure 117a and table A15, the change in activation time did not change the yield to a notable amount, with those received by activation of the salt-HTC hydrochar around 70 wt% remaining of the hydrochar used, while those received from the activation of the normal hydrochar around 30 wt%. Again, much more solid is lost by the activation of the HTC hydrochar than the salt-HTC one, as seen in the discussion of the activation of the different substrates.

The ash remaining in the activated hydrochars stays also at a relative low level, underlining the stability of the salt-HTC chars being not connected to high inorganic compound contents. From these results it can be imagined that an activation time of 10 minutes seems to be enough to activate most of the hydrochar, decreasing the process time significantly.

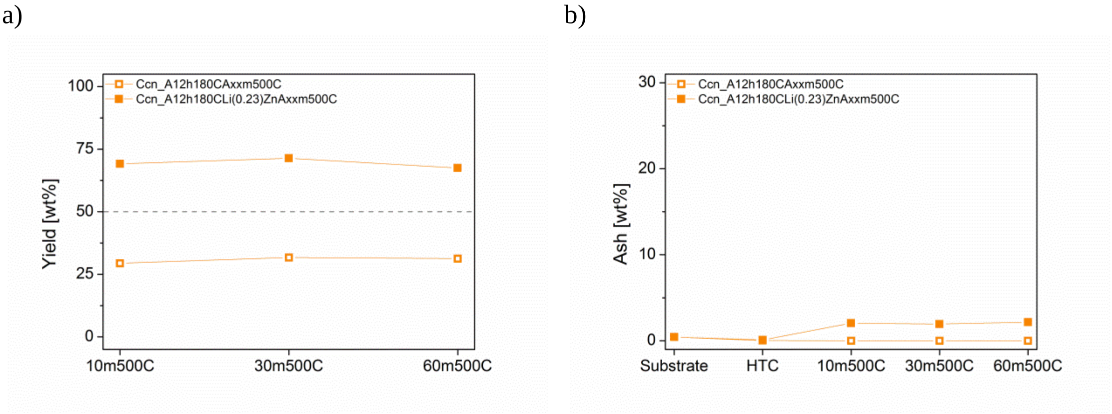
a)

b)

Figure 117 Reaction yield (a) and ash content (b) of different samples from the change in activation time (t = 10, 30 or 60 minutes) at constant temperature (500 °C).

The change in activation temperature was observed to have a higher influence than the time (figure 118). A temperature of 200 °C seems not to be sufficient enough to change the hydrochar structure, since nearly no amount of it is lost (as would be typically seen in a successful activation).

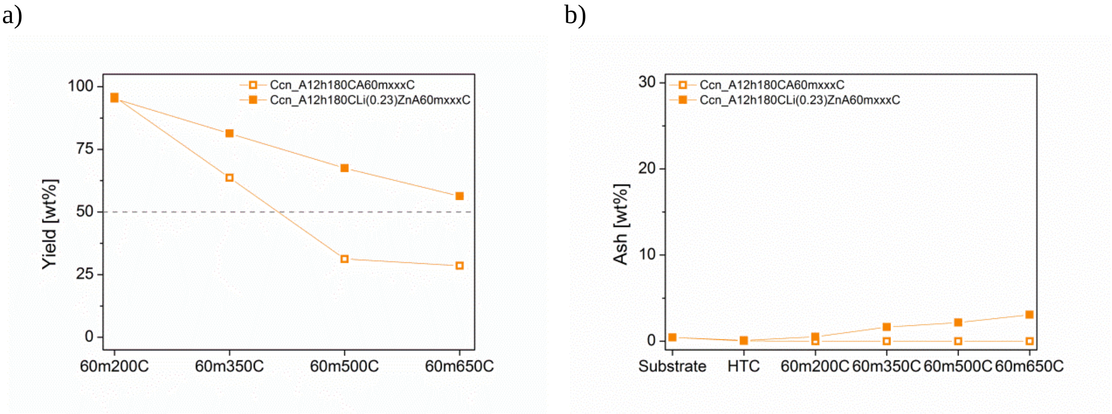
a)

b)

Figure 118 Reaction yield (a) and ash content (b) of different samples from the change in activation temperature (T = 200, 350, 500 or 650 °C) at constant time (60 minutes).

By increasing the temperature via 350 and 500 to 650 °C a straight trend in yield loss is seen. The change from 500 to 650 °C resulted only in a change from a yield of around 32 to 29 wt% for the HTC samples, indicating that most of the sample was activated already (compare TGA, figure 109). A more crucial change was seen for those received from salt-HTC samples.

An additional loss of nearly 12 wt% (from 68 to 56 wt%) took place when increasing to the highest temperature compared to those at 500 °C. As indicated by the TGA results, the initial higher stable salt-HTC hydrochars have more initial solid present that will react at higher temperatures due to its higher stability. The ash content increases slightly, due to an increase in ratio in the solid.

4.2.2.2 Elemental composition

The change in carbon content with changing activation parameters can be seen in figure 119 (a - constant temperature (500 °C); b - constant time (60 minutes)) and table A15. As already seen in the discussion of the yield, the temperature seems not to result in any major structural changes, with the carbon content staying at relatively stable level of around 75 %. With increasing temperature the carbon content raises up to values of 86 or 82 % for those received by activation of HTC or salt-HTC, respectively. Surprisingly, the highest carbon content found was for the sample received without salt present in the HTC reaction.

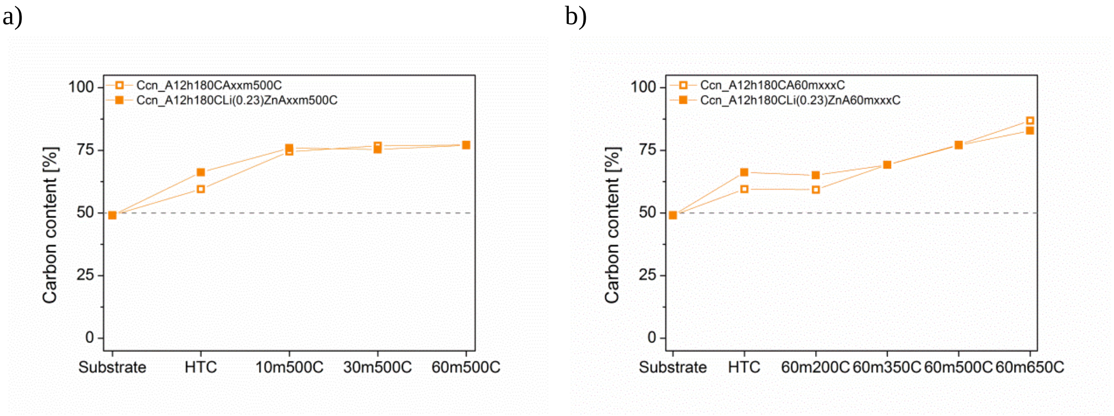

Figure 119 Carbon content of samples of the activation series at either constant temperature (a) or time (b).

4.2.2.3 Surface functionality

In the discussion of the different substrates used in the hydrothermal carbonization, whose resulting hydrochars were activated, it could be seen that the physical activation results in a loss of most surface functionality with three characteristic signals remaining. In fact, the increase in activation time does not result in a higher loss of surface functionality, neither for those received by the HTC (fig. 120a) nor the salt-HTC chars (fig. 120b).

As seen in prior results, the temperature seems to be the more crucial parameter of the activation (compare figure 121). While at 200 °C most of the initial surface functionality found in the hydrochars is also on the activated hydrochar surface, these vanish with increasing activation temperature.

At 500 °C only small signals are found, while a temperature of 650 °C seems to remove nearly all of the initial surface functionality. Only a signal at around 2300 cm^{-1} can be seen in the spectra, resulting from adsorbed CO_2.

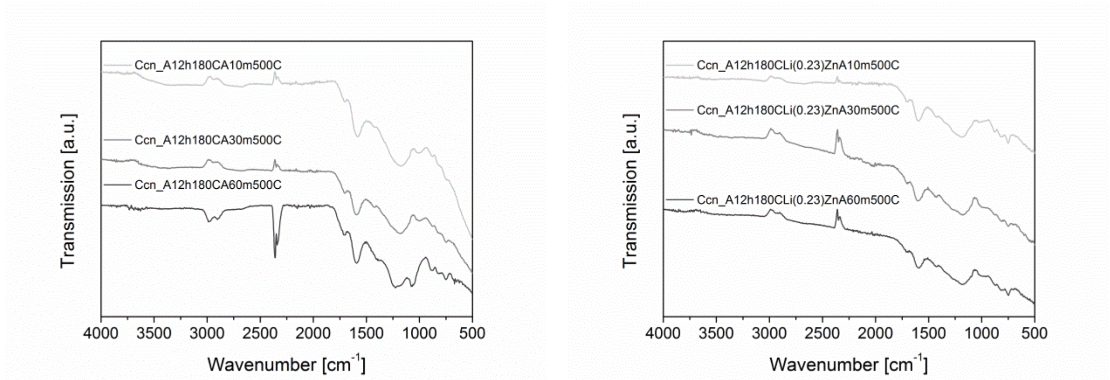
a)
b)

Figure 120 FTIR spectra of activated hydrochars at different activation times (*T* = 500 °C). The hydrochars were obtained by HTC (a) or salt-HTC (b).

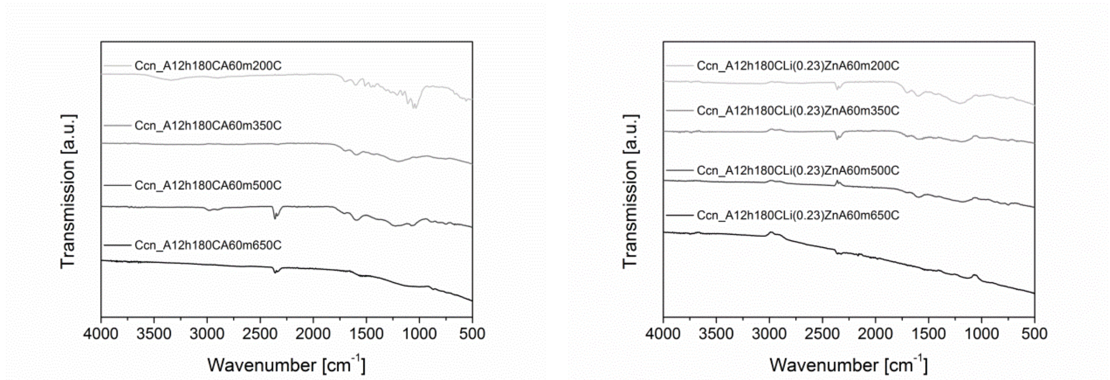
a)
b)

Figure 121 FTIR spectra of activated hydrochars at different activation temperatures (*t* = 60 minutes). The hydrochars were obtained by HTC (a) or salt-HTC (b).

4.2.2.4 Porosity analysis

Figure 122 and table A16 show how the specific surface area (SSA) of the activated hydrochars changes with varying activation parameters. At a constant temperature of 500 °C the SSA stays nearly at all tested times (10, 30 or 60 minutes) at a similar level of around 500 $m^2 \cdot g^{-1}$. Only one sample, the one received after 10 minutes from the normal hydrochar, resulted in a value of nearly 600 $m^2 \cdot g^{-1}$. There was no further examination why this sample had such a high SSA and was more seen as a deviant from the average 500 $m^2 \cdot g^{-1}$.

A strong dependency of the surface areas was seen with the temperature, which also showed to be the crucial parameter on the previous discussed characteristics.

While only a small to nearly no change compared to the hydrochar was observed, if the activation temperature was at it two lowest tested values (200 or 350 °C), an increase to 500 or 650 °C gave a sudden jump in the SSA. The highest recorded value was from the salt-HTC char, reaching over about 625 $m^2 \cdot g^{-1}$. The TGA results from figure 109 showed that a temperature of at least 350 °C is needed for a mass loss to take place in case of the normal hydrochars, and of around 450 °C for those received by salt-HTC method.

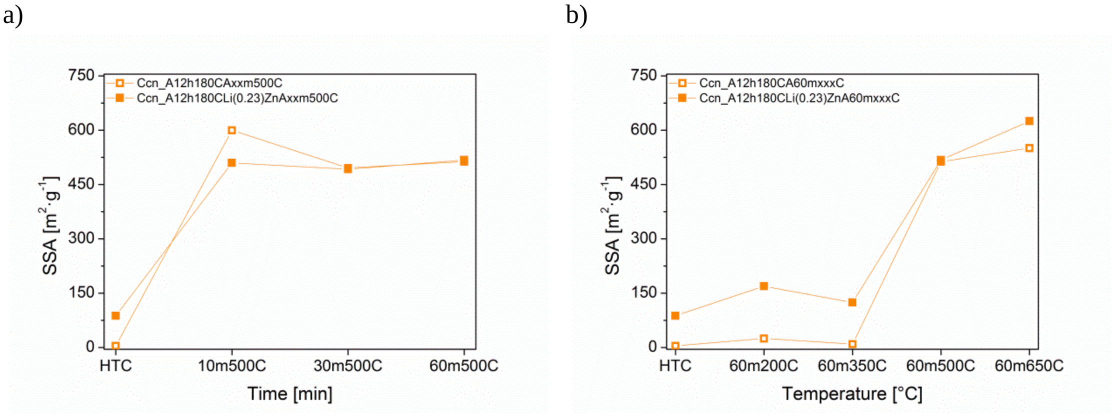

Figure 122 Values of the specific surface areas (SSA) of different hydrochars or their activated forms at varying activation time (a) or temperature (b).

4.3 Removal of dyes from aqueous solutions with hydrochars and their resulting activated carbons

4.3.1 Influence of hydrochar and activated carbon properties onto dye removal

For the removal of dyes from aqueous solutions by the hydrochars and their activated forms synthesized in this work at first the adsorption of methylene blue onto the salt-HTC hydrochars (12 h, 180 °C) and their activated forms (60 minutes, 500 °C) was studied since these showed the highest SSA. Figure 123a and table A17 show the adsorption capacity q_e of the salt-HTC hydrochars and their activated forms received from the three different substrates (coconut shell powder, dried dandelion leaves and sawdust). Surprisingly, the hydrochars could remove more dye from the solution than their activated forms. The adsorption capacity for the salt-HTC samples were between 60-70 $mg \cdot g^{-1}$ but those for the activated forms only around 34 $mg \cdot g^{-1}$ for the coconut shell powder derived char and below 15 $mg \cdot g^{-1}$ for the other two substrates. It would have been supposed, that the higher surface areas of the activated hydrochars (up to over 700 $m^2 \cdot g^{-1}$ (Saw_A12h180CA60m500C)) would offer more available space for the dye to be adsorb onto and therefore higher adsorption capacities. Even the salt-HTC hydrochars with partial very low SSA could remove over 50 mg of methylene per 1 g of char.

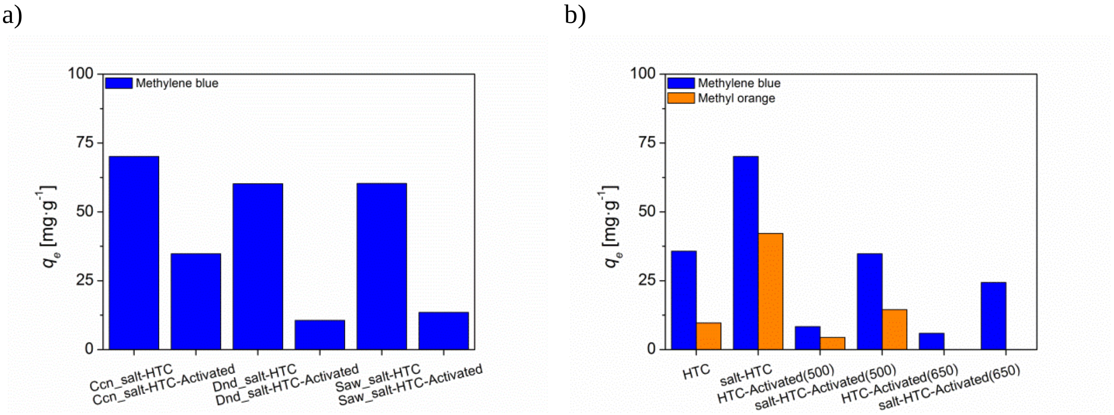

Figure 123 Adsorption capacity at equilibrium (q_e) of dyes onto different hydrochars and their activated carbons from different substrates (a) or coconut shell powder (b).

For the samples received from coconut shell powder additionally methylene blue was removed with the normal HTC sample and its activated version as well as the activated hydrochars received at 650 °C, which had an even higher SSA than those received at 500 °C. The normal hydrochar showed also a higher adsorption capacity for methylene blue than the activated sample (see figure 123b and table A17).

Its q_e was nearly at the same level like the activated carbon from the salt-HTC char. Even when 650 °C were used as the activation temperature, resulting in an increased specific surface area, the adsorption capacity did not increase any further for methylene blue but even decreased a little.

It could be possible, that the microporosity, which was introduced by the activation step, is not accessible by the methylene blue. Interestingly, the activated carbons from the salt-HTC sample result in a decrease of dye adsorption capacity when compared to their hydrochars. Here, it is possible that parts of the meso- and macropores in the activated forms are lost through the activation or constrained by the introduced micropores. To test the influence of adsorptive size onto q_e, methyl orange was additionally used as an adsorptive. Methyl orange has a molecular size of 11.9 x 6.7 Å while methylene blue is longer but thinner with around 13.8 x 5.91 Å.[268, 269] As seen in figure 123b, the amount of methyl orange removed from solution and adsorbed onto the carbon samples was always considerable less than that for the initial used dye.

Since no correlation of the actual surface areas, neither through micro- nor meso- or macroporosity, to the adsorption of the two tested dyes was found it seems that another characteristic of the chars must be the decisive factor of the dye sorption. In the discussion of the activation of the hydrochars it was shown that a lot of surface functionality is lost from that treatment. In chapter 2.6 it was shown that the functional surface groups present play an important role onto the interaction of the dye and the surface. Since the salt-HTC hydrochar had less variety of surface groups present than the normal hydrochar (compare chapter 4.1.1.5 and figure 124a) but could remove a higher amount of methylene blue from the solution, the type of surface group is important as well. Since the salt-HTC hydrochar mainly contains carbonyl or ether groups, it is possible that these are crucial for the adsorption of the dye onto the surface. Since the salt-HTC had an increased SSA compared to its hydrochar, with still much surface functionality present, it could remove the most dye. While the activated carbons had an higher surface area but less to none surface functionality, the amount of dye removed decreased significantly. Since those received from activation of the salt-HTC char still had at least half the adsorption capacity than the highest samples and their significant parameter was their mesoporosity, it is very likely that especially the surface groups found in the surface making up the mesopores are those mainly taking place in the dye sorption onto the sample.

Besides the surface areas, available pore size types and surface functionality, another factor could be the interaction with the water of the dye solutions. If the carbons would be hydrophilic, the interaction with the aqueous dye solution could prove better than with a hydrophobic adsorbate. For this, water sorption data were collected, with their isotherms shown in figure 124b. It can be seen that the salt-HTC hydrochars have the highest uptake in water and its normal HTC char the lowest. The activated char lies in between those two. It is also visible that all three tested samples have a rather steady but low uptake, contrary to typical water sorption isotherms.

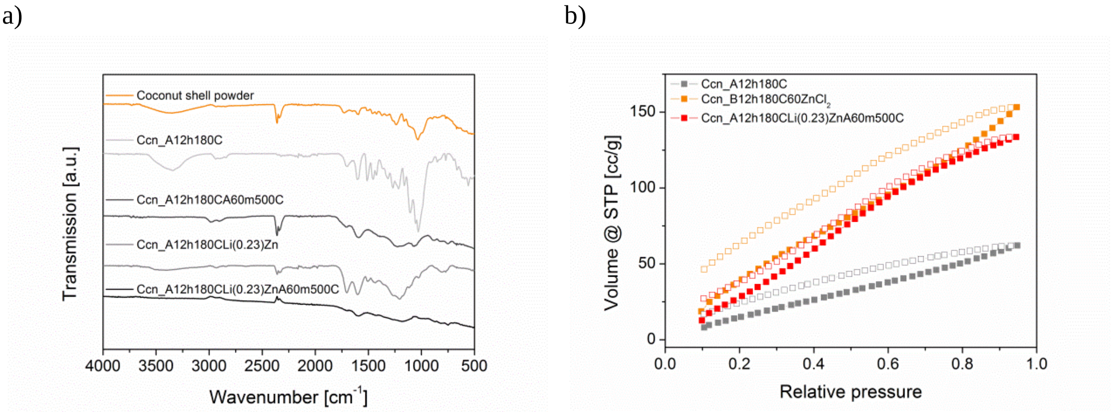

Figure 124 FTIR spectra (a) and water sorption isotherms (b) from different hydrochars and their activated forms.

To get further insight into the removal of methylene blue from the aqueous solution, the adsorption equilibrium, isotherms, kinetics and mechanism was further studied and will be discussed subsequent. Figure 125 shows how the color of a methylene blue solution changes from deep blue (0 min) to colorless after 24 hours (1440 min) with the resulting UV-Vis. With increasing contact time of the solution and the hydrochar or activated carbon (indicated towards less intense grey graph color), the signals in the UV-Vis spectra decrease in intensity, with the most prominent peak at the characteristic wavelength for methylene blue at 664 nm.

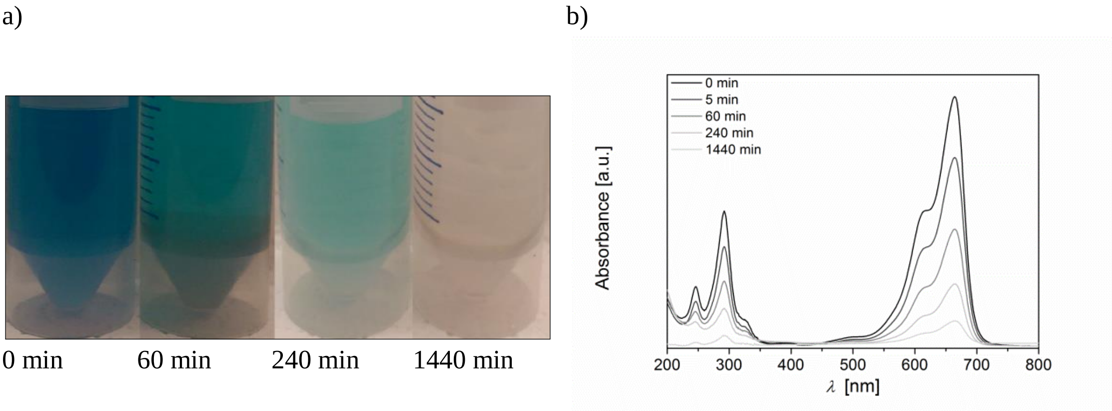

Figure 125 Image of MB solutions after different contact times (a) and the resulting UV-Vis spectra (b).

Figure 126 and table A18 show how the amount adsorbed onto different samples increases with contact time. Data for the substrate coconut shell powder, its HTC and salt-HTC hydrochar (12 h at 180 °C; salt: $ZnCl_2$) as well as one activated carbon received from the salt-HTC. Additionally, a hydrochar from salt-HTC with an increased surface area (Ccn_B20h220C60Zn) was used to further determine the influence of surface area onto the dye adsorption. As discussed previously, the activated char has a really low adsorption capacity (orange line), comparable to that of the pure substrate (black line).

The hydrochar (green line) showed a little higher capacity than the previous two, contrary to the results shown in figure 123 (see also table A18), where the values only after 24 hours were compared and the HTC hydrochar and the activated carbon from the salt-HTC char had nearly the same value. Again, the salt-HTC hydrochar showed the highest uptake of methylene blue (blue line). When the hydrochar received after 20 hours at 220 °C, that also had a higher surface area, was used, an additional adsorption of methylene blue was observed (red line). The increased surface area and changed structure of the sample received after 20 hours at 220 °C therefore seemed beneficial for the removal of methylene blue from the aqueous solution. This sample was therefore chosen for further adsorption studies.

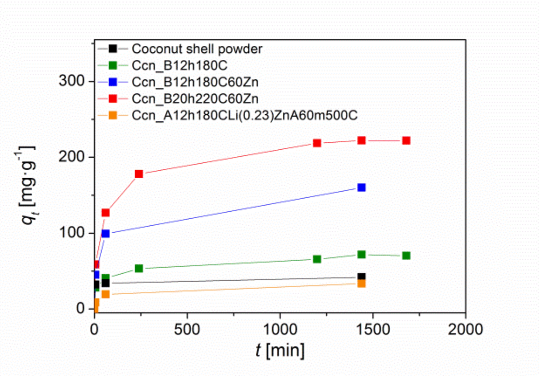

Figure 126 Kinetic studies on the adsorption of methylene blue onto different samples.

4.3.2 Adsorption studies of methylene blue

Since the salt-HTC sample after 20 hours at 220 °C showed the highest values for q_e, all further determination of the adsorption equilibrium, isotherms, kinetics and mechanism were done on this sample. Various groups have studied the adsorption of different dyes onto activated carbons[227], whose reported methods were applied accordingly for the adsorption of methylene blue onto the hydrochar.

4.3.2.1 Adsorption kinetics

A first look onto the adsorption kinetic of methylene blue onto various samples was already done in the previous segment and shown in figure 126. It could be seen that the majority of the dye was removed in first few hours, even minutes, with the curve in the graph steadily decreasing in slope. The last three points of the red and green curve in figure 126 showed that equilibrium was reached after around 20 hours, since no change to about 30 hours took place. Since the data in the lower time segment were few, the sample times were increased in a new experimental run, resulting in the graph shown in figure 127 as a black curve.

The data for the chosen hydrochar from figure 126 are also shown in red, showing good agreement with the new data of the kinetic studies. The studies resulted in a maximum adsorption capacity for the hydrochar obtained by salt-HTC of coconut shell powder with zinc chloride at 220 °C for 20 hours with a value of $q_e = 207\ \text{mg·g}^{-1}$. After just 5 minutes, already around a quarter of this capacity ($q_e = 47\ \text{mg·g}^{-1}$) was achieved. After 30 minutes already nearly 50% of the capacity were reached ($q_e = 94\ \text{mg·g}^{-1}$), showing that the major part of methylene blue is removed in the first few minutes of the experiment. The last point measured before equilibrium shows that after 8 hours a value of 185 is reached ($q_e = 185\ \text{mg·g}^{-1}$), showing that the remaining 16 hours increased the capacity only slightly.

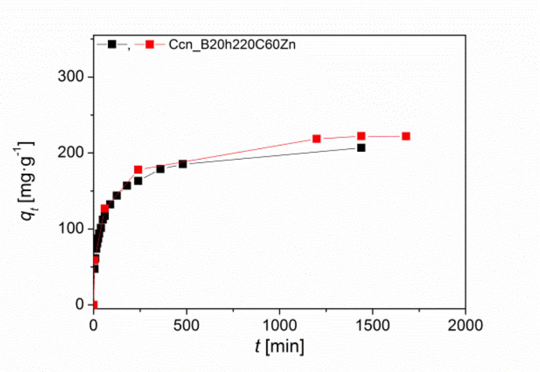

Figure 127 Effect of contact time on the adsorption of MB onto a hydrochar.

To characterize the adsorption process, three kinetic models were used for the fitting of the data (pseudo-first-order and pseudo-second-order as well as Elovich kinetic model). The resulting plots are shown in figure 128b-d with the parameters of the different kinetic models found in table 12. The correlation coefficient R^2 of the different fittings implies that the pseudo-second-order model suits best for describing the adsorption of methylene blue onto the hydrochar. The three correlation coefficients all show a value of over 0.9, with the lowest for the pseudo-first-order model ($R^2 = 0.9192$), followed by the Elovich model ($R^2 = 0.9924$) with the highest for the pseudo-second-order model ($R^2 = 0.9979$). Therefore, the rate of adsorption probably depends less on the concentration of the adsorbate in the aqueous dye solution but more on the availability of the adsorption sites, as described by the pseudo-second-order model.[227]

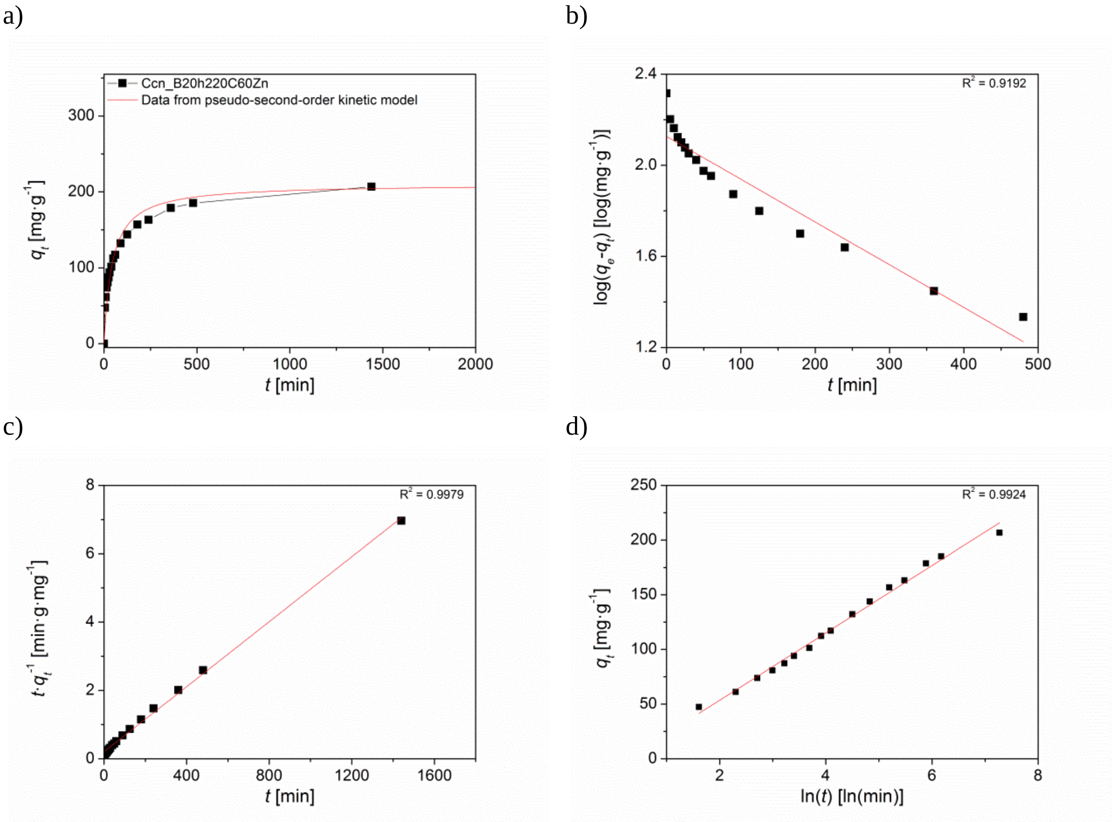

Figure 128 Effect of contact time on the adsorption of MB onto a hydrochar (a) the resulting pseudo-first-order kinetic plot (b), pseudo-second-order kinetic plot (c), and Elovich kinetic plot (d).

Table 12 Parameters of the different kinetic models for the adsorption of MB onto a hydrochar.

Model	**Parameter**	**Value**
Experimental	q_e(exp) [mg·g^{-1}]	206.79
Pseudo-first-order	q_{e1}(calc) [mg·g^{-1}]	133.81
	k_1 [min^{-1}]	0.0041
	R^2	0.9192
Pseudo-second-order	q_{e2}(calc) [mg·g^{-1}]	210.53
	k_2 [min^{-1}]	0.0001
	R^2	0.9979
Elovich	q_{eE}(calc) [mg·g^{-1}]	215.89
	a [mg·g^{-1}·min^{-1}]	23.6975
	b [g mg^{-1}]	0.0325
	R^2	0.9924

4.3.2.2 Equilibrium isotherms

While the kinetic studies showed that the adsorption seems to be more dependent on the available adsorption sites and less on the dye concentration in solution, the initial concentration can be an important driving force for the mass transfer between the solution onto the solid. Therefore, the dependency of the initial dye concentration onto the adsorption capacity was tested. The initial concentration ranged from 1 to 25 mg·L^{-1} where with increasing c_0 the adsorption capacity q_e increased from 48 to 200-350 mg·g^{-1} (see figure 129a and table A19). While the data show a strong spreading of data points due to the low weights and high dilutions of the different compounds, a quick saturation trend is visible. The obtained data points were fitted using three different isotherm models: Langmuir, Freundlich and Temkin. The data are shown in figure 129b-d and table 13 with the isotherm parameters determined from the slopes and intercepts of the linear fitting. The data could be best fitted to the Langmuir isotherm model, with a correlation coefficient of 0.9682. The other two models showed a very poor representation of the data, with values for R^2 of around 0.5 (Freundlich: R^2 = 0.5436; Temkin R^2 = 0.5031). The good fitting to the Langmuir isotherm indicates rather homogenous adsorption places on which the methylene blue will be adsorbed in a monolayer.[227]

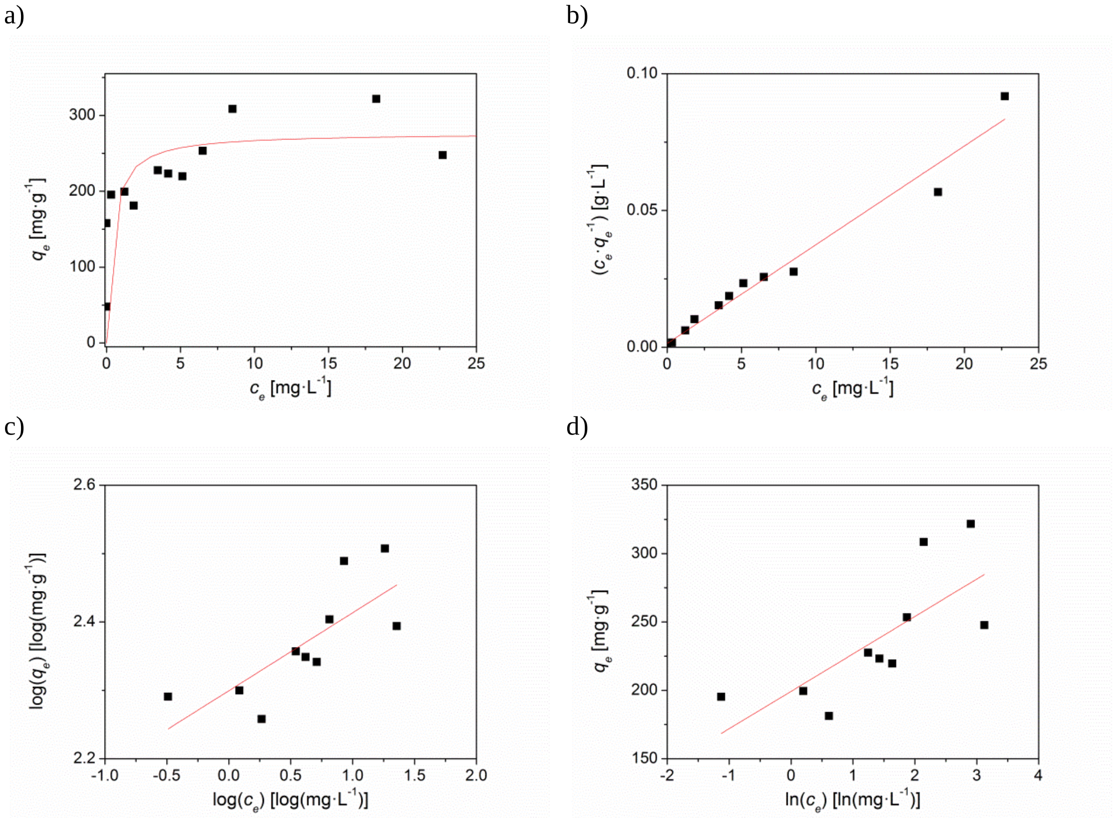

Figure 129 Equilibrium study on the adsorption of MB onto a hydrochar (a) and the resulting Langmuir equilibrium isotherm (b), Freundlich isotherm (c) and Temkin isotherm (d).

Table 13 Parameters of the different isotherm models for the adsorption of MB onto a hydrochar.

Model	Parameter	Value
Langmuir	q_m [mg·g^{-1}]	277.01
	K_L [L·mg^{-1}]	2.6159
	R^2	0.9682
Freundlich	K_F [(mg·g^{-1})(L·mg^{-1})$^{1/n}$]	199.29
	$1/n$	0.1140
	R^2	0.5436
Temkin	A_T [L·g^{-1}]	1455.59
	B	90.5810
	R^2	0.5031

The maximum monolayer adsorption capacity of the methylene blue (q_m) found from the Langmuir isotherm was determined at 277.01 mg·g^{-1} and was therefore in the range of other reported hydrochars (compare chapter 2.6 and table 3).

4.3.2.3 Adsorption mechanism

To further check the removal of methylene blue by the hydrochar and understand if the solution and especially dye particles diffuse into possible pores of the solid, the intraparticle diffusion model can be used. The data from the kinetic studies was therefore fitted by the intraparticle diffusion model, whose data are shown in figure 130 and table 14. The curve was divided into three different sections, with an initial sharp rise in the first hour ($t^{0.5}$ = 0-8 min$^{0.5}$), a less steep part between 1-4 hours ($t^{0.5}$ = 9-16 min$^{0.5}$) and nearly a plateau in the final section ranging from 4 to 24 hours ($t^{0.5}$ = 18-42 min$^{0.5}$). Since all lines do not pass through the origin, the intraparticle diffusion is not the only rate-limiting step.[227] Therefore, both, the external diffusion and the intraparticle diffusion, are probably important parts for the whole adsorption process. With increasing time the values for C_i increase, indicating a raising importance of the boundary layer effects onto the diffusion.[227]

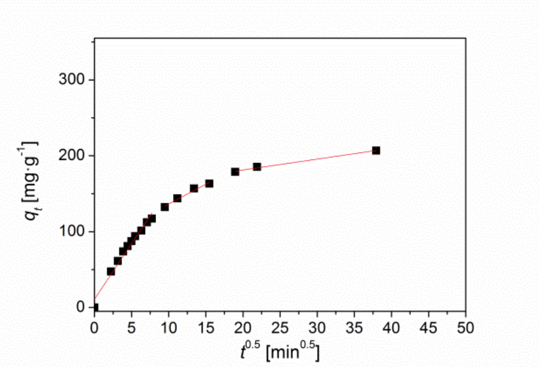

Figure 130 Plot for the intraparticle diffusion model for the adsorption of MB onto the hydrochar.

Table 14 Intraparticle diffusion model parameters for the adsorption of MB onto a hydrochar.

Fitting range [min$^{0.5}$]	**Parameter**	**Value**
0-8	k_{di} [mg·g^{-1}min$^{-0.5}$]	14.69
	C_i	10.91
	R^2	0.9702
9-16	k_{di} [mg·g^{-1}min$^{-0.5}$]	5.21
	C_i	84.40
	R^2	0.9641
18-42	k_{di} [mg·g^{-1}min$^{-0.5}$]	1.43
	C_i	152.61
	R^2	0.9879

Chapter 5

Conclusion and outlook

Within this work, the carbon product (hydrochar) of the hydrothermal carbonization (HTC) of lignocellulosic biomass was studied in terms of its material properties such as morphology as seen by electron microscopy, elemental composition, molecular structure, surface functionality and especially surface area. The main goal was to understand how the previously mentioned characteristics can be changed to specific material desires and needs by the use of an additive in the reaction process. Ideally, with the knowledge of its function the right choice of additive can lead to wanted material properties. Here, special interest lies in the modification of the specific surface areas (SSA) of the hydrochars since these are usually too small (e.g. $< 10\ m^2 \cdot g^{-1}$) for promising industrial applications leading to the combustion of the chars for energy production, counteracting the background thoughts of an environmental friendly process for the limitation of carbon dioxide emissions. Many studies found in literature describe the use of additives in the HTC but especially metal chlorides, mainly eutectic mixtures of alkali metal salts with zinc chloride, proved to be promising as additives in the HTC of biomass building units like glucose and fructose, leading to carbon materials with surface areas around 400 to nearly 700 $m^2 \cdot g^{-1}$.[11, 13] The salts have also the advantage that they are easily removed by washing with water. However, it was also shown that when using more complex biomass substrates, the desired effects for an increase of surface area are much less pronounced with values for the SSA less than 100 $m^2 \cdot g^{-1}$.[12] Unfortunately, no further results of how the salts function in the HTC process were published. The main ideas are shortly mentioned as stabilization of primary particles formed[11, 13] or catalyzing effects[12]. This work therefore studied the effects of various salts as additives in the hydrothermal carbonization for a range of different substrates onto the initial mentioned properties of the obtained hydrochars, with main focus on the specific surface areas as determined by nitrogen sorption. Additionally, process parameters such as reaction time and temperature, compound ratios (biomass, water or additive) as well as waste water recycling steps were examined. Since hydrochars have become more and more interesting as precursors for the production of activated carbons[17] an additional activation step of the hydrochars obtained in this work in terms of a physical activation with steam at elevated temperatures was conducted.

Furthermore, for a possible and interesting industrial application, the most promising of the obtained hydrochars and their activated forms were tested in waste water treatment, more detailed in the removal of dyes from aqueous solutions.

This thesis showed that salts can be used as additives in the HTC from biomass to increase the otherwise low specific surface areas of the hydrochars. The main reasons for the increase in surface area could be derived from breakup of macrostructures into smaller pieces (increase of external surface area and interparticle spaces), formation of carbon spheres from the cellulose parts of the biomass (creation of external surface area - especially roughness - and possibly creation of minor porosity) and/or holes left in the resistant lignin skeleton structure (creation of macroporosity). The highest SSA for a biomass based hydrochar with nearly 200 $m^2 \cdot g^{-1}$ was obtained when using coconut shell powder with zinc chloride. It was shown that various effects like stabilization of formed primary particles, enhanced reactivity by improved biomass dissolution and catalysis of HTC reactions are triggered by the additive, resulting in the increased SSA. From the elemental analysis it was concluded that the zinc chloride catalyzes especially the dehydration reactions but also enables demethylation reactions in some cases. The most crucial change for the HTC reaction seems to happen around 200 °C since this temperature seems to be the threshold for certain reactions that are not possible at 180 °C (e.g. the degradation of cellulose). The presence of the zinc chloride enables these reactions by either lowering the pH to a highly acidic environment or catalyzing the reactions, lowering the temperature threshold. Evidences from electron microscopy showed that while in a normal hydrothermal carbonization often the macroscopic biomass structure maintains due to stable lignin compounds being present, by use of zinc chloride these can be broken into smaller parts. This gives not only the possibility of bound water in the biomass structures to escape, raising the percentage in carbon content, but also increase the external surface area. While the effect of reaction time seems to be less significant, the influence of the reaction temperature seems crucial. The standard experiments were carried out at 12 hours but for future investigations a shorter time between 2-4 hours might be sufficient. An increase in temperature from 180 to 220 °C lead to an increase of carbon content and surface areas for both normal HTC and HTC with a salt present. However, with around 50 $m^2 \cdot g^{-1}$ the limit of possible surface area for a normal HTC char seems to be reached, while it was possible to obtain hydrochars with areas of nearly 200 $m^2 \cdot g^{-1}$ in the salt-HTC. Most interestingly, the use of the $ZnCl_2$ enables the conversion of cellulose parts of the biomass at lower temperatures (180 °C) than those usually needed (200 °C), as seen by ^{13}C SS-NMR spectra. Additionally, at higher temperatures (220 °C) the carbon compounds resulting from the usually resistant lignin parts could be changed with the use of the zinc chloride towards a more aromatic hydrochar with carbon contents of nearly over 70 %. While the increase in surface area by the salt was partly achieved due to the particle breakup, nitrogen sorption isotherms indicated introduction of micro-, meso- and macroporosity to a high extent as well. If simple sugars like glucose are used, carbon materials with SSA over 500 $m^2 \cdot g^{-1}$ can be obtained, as also reported when using eutectic salt mixtures.[11, 13]

However, due to the complexity of the lignocellulosic biomass materials a lower SSA was to be expected for the products from the biowaste materials. Some surface functionality originating from the biomass that still persisted in the hydrochars is lost in those from the salt-HTC, with mainly carbonyl and ether as well as aromatic groups remaining. The results from XPS indicate together with the information obtained by FTIR that if the zinc chloride is present in the HTC reaction a lot of oxygenated functional groups change. Many carbons primary bound to one oxygen atom either change to a bond with a carbon or hydrogen atom or higher oxygen bond. An optimum for the amount of water used was not clearly determined, it seems however crucial, to have enough water present so that the hydrothermal carbonization can take place, but also not too much in order to ensure sufficient concentration of the salt. It could be shown that a recycling of the additive by reusing the waste phase after washing is in principle possible, but it is important to find a way to remain the desired salt concentration.

By an additional activation step in terms of physical activation with steam it is possible to introduce mainly microporosity into the biomass based hydrochars, resulting in surface areas between 400 to 600 $m^2 \cdot g^{-1}$. Additionally, the meso- and macroporosity in the hydrochars obtained by salt-HTC remained, resulting in activated carbons with micro, meso- and macroporosity. However, due to the high activation temperatures, a lot of the surface functionality was lost.

It was also shown that the salt-HTC chars possess high potential for the removal of dyes from waste waters. Their activated forms however removed only little dye even after 24 hours. The amount of adsorbed dye proved to depend on a combination of available surface area and pore sizes, surface functionality and hydrophilicity. Sorption studies showed that the rate of adsorption probably depends less on the concentration of the adsorbate in the aqueous dye solution but more on the availability of the adsorption sites, as described by the pseudo-second-order model. Additionally, a good fit to the Langmuir isotherm indicated rather homogenous adsorption places on which the methylene blue could adsorb in a monolayer. The maximum monolayer adsorption capacity of the methylene blue (q_m) for a hydrochar from coconut shell powder obtained in the presence of zinc chloride was found from the Langmuir isotherm with 277.01 $mg \cdot g^{-1}$, well in the range of other reported hydrochars. It was also shown that a possible intraparticle diffusion is not the only rate-limiting step. Therefore, both, the external diffusion and the intraparticle diffusion, are probably important parts for the whole adsorption process. With increasing time a raising importance of the boundary layer effects onto the diffusion was indicated.

While a lot of promising results could be obtained and showed in this thesis, there is still a lot of potential currently not used for the hydrothermal carbonization. Especially the utilization of the hydrochar in industrial applications is often limited to combustion for energy generation. Since the tests as an adsorptive material for the removal of dyes from waste waters proved successful especially for the hydrochars obtained from the salt-HTC more research should be done in this field. This could include the test for the adsorption of other contaminants in waste waters.

But most interestingly, the implementation and testing in a real waste water treatment facility could raise awareness for this hydrochar use. As for the substrates used in the HTC, often wet biomass like liquid manure or sewage sludge are beneficial due to their availability and price. The concept of using zinc chloride as an additive therefore should be expanded to these substrates. Ideally, the resulting hydrochars are also optimized in terms of surface area, structure and functionality. However, due to their highly water containing nature, the dilution of the salt might be too high, resulting in needs of excess amount of the additive. Thus, a lot of potential further research can be done here. Furthermore, since the zinc chloride is highly corrosive and also very toxic to aquatic life with long lasting effects, the search for a less problematic additive is essential. While other salts like the pure alkali metal chlorides did not increase the surface area dramatically, the small increase still might be beneficial for an application in waste water treatment. While the activated hydrochars did not proof to be very effective for the adsorption of the dyes the possible cost intensive activation step seems not being necessary. Since the main reason for this seems to be the lost surface functionality, it would be highly interesting to see if a post-introduction of certain oxygenated functionality onto these micro-, meso- and macroporous hydrochars with higher specific surface areas would lead to materials with even higher contaminant removal capacities.

References

1. P. Gerland, A. E. Raftery, H. Sevcikova, N. Li, D. A. Gu, T. Spoorenberg, L. Alkema, B. K. Fosdick, J. Chunn, N. Lalic, G. Bay, T. Buettner, G. K. Heilig and J. Wilmoth, *Science*, 2014, **346**, 234-237.
2. C. Schar and G. Jendritzky, *Nature*, 2004, **432**, 559-560.
3. *Climate change 2001: The scientific basis*, Cambridge University Press, Cambridge, 2001.
4. W. Keim, in *Methanol: The Basic Chemical and Energy Feedstock of the Future*, eds. M. Bertau, H. Offermanns, L. Plass, F. Schmidt and H. J. Wernicke, Springer-Verlag, Berlin, 2014, ch. 2, pp. 23-37.
5. L. Perez-Lombard, J. Ortiz and C. Pout, *Energ Buildings*, 2008, **40**, 394-398.
6. *World Energy Outlook 2010*, IEA Publications, France, 2010.
7. *Adoption of the Paris Agreement*, United Nations, Paris, 2015.
8. H. Lieth and R. H. Whittaker, *Primary Productivity of the Biosphere*, Springer-Verlag, Berlin, 1975.
9. M. M. Titirici, A. Thomas and M. Antonietti, *New Journal of Chemistry*, 2007, **31**, 787-789.
10. S. Reiche, N. Kowalew and R. Schloegl, *Chemphyschem*, 2015, **16**, 579-587.
11. N. Fechler, S. A. Wohlgemuth, P. Jaker and M. Antonietti, *Journal of Materials Chemistry A*, 2013, **1**, 9418-9421.
12. H. Ma, J. B. Li, W. W. Liu, M. Miao, B. J. Cheng and S. W. Zhu, *Bioresource Technology*, 2015, **190**, 13-20.
13. S. M. Alatalo, E. Makila, E. Repo, M. Heinonen, J. Salonen, E. Kukk, M. Sillanpaa and M. M. Titirici, *Green Chemistry*, 2016, **18**, 1137-1146.
14. S. J. Teh, S. B. A. Hamid, C. W. Lai and Y. S. Lim, *Nanosci Nanotech Let*, 2015, **7**, 611-615.
15. C. J. Coronella, J. G. Lynam, M. T. Reza and M. H. Uddin, in *Application of Hydrothermal Reactions to Biomass Conversion*, ed. F. Jin, Springer-Verlag, Berlin, 2014, ch. 12, pp. 275-311.
16. M. M. Titirici and M. Antonietti, *Chemical Society Reviews*, 2010, **39**, 103-116.
17. A. Jain, R. Balasubramanian and M. P. Srinivasan, *Chemical Engineering Journal*, 2016, **283**, 789-805.
18. T. P. Fellinger, *Hydrothermal and Ionothermal Carbon Structures: From carbon negative materials to energy applications - Dissertation*, Potsdam, 2011.
19. Berghof, *Product brochure - High pressure reactors*.
20. T. Rebling, P. von Frieling, J. Buchholz and T. Greve, *Journal of Thermal Analysis and Calorimetry*, 2015, **119**, 1941-1953.
21. A. Kruse and N. Dahmen, *J Supercrit Fluid*, 2015, **96**, 36-45.
22. J. Ohlert, *Hydrothermale Carbonisierung (HTC) von Klär- und Faulschlämmen*, Oldenburg, 2015.
23. C. He, A. Giannis and J. Y. Wang, *Appl Energ*, 2013, **111**, 257-266.
24. C. He, K. Wang, Y. H. Yang and J. Y. Wang, *Energ Fuel*, 2014, **28**, 6140-6150.

25. S. M. Heilmann, J. S. Molde, J. G. Timler, B. M. Wood, A. L. Mikula, G. V. Vozhdayev, E. C. Colosky, K. A. Spokas and K. J. Valentas, *Environmental Science & Technology*, 2014, **48**, 10323-10329.
26. Z. L. Jiang, D. W. Meng, H. Y. Mu and K. Yoshikawa, *Sci China Technol Sc*, 2010, **53**, 160-163.
27. F. Bergius, *Anwendung hoher Drucke bei chemischen Vorgängen und die Nachbildung des Entstehungsprozesses der Steinkohle*, Halle, 1913.
28. F. Bergius, *Die Naturwissenschaften*, 1928, **16**, 1-10.
29. E. Berl and A. Schmidt, *Justus Liebigs Annalen der Chemie*, 1932, **493**, 97-123.
30. M. M. Titirici, in *Sustainable Carbon Materials from Hydrothermal Processes*, ed. M. M. Titirici, John Wiley & Sons, Ltd., 2013, ch. 1, pp. 1-36.
31. K. Yoshikawa and P. Prawisudha, in *Application of Hydrothermal Reactions to Biomass Conversion*, ed. F. Jin, Springer-Verlag, Berlin, 2014, ch. 14, pp. 355-383.
32. A. Funke and F. Ziegler, *Biofuel Bioprod Bior*, 2010, **4**, 160-177.
33. S. Karagoz, T. Bhaskar, A. Muto and Y. Sakata, *Fuel*, 2005, **84**, 875-884.
34. K. Tekin and S. Karagoz, *Res Chem Intermediat*, 2013, **39**, 485-498.
35. M. Tymchyshyn and C. B. Xu, *Bioresource Technology*, 2010, **101**, 2483-2490.
36. M. H. Waldner and F. Vogel, *Ind Eng Chem Res*, 2005, **44**, 4543-4551.
37. P. T. Williams and J. Onwudili, *Energ Fuel*, 2006, **20**, 1259-1265.
38. C. B. Xu and N. Lad, *Energ Fuel*, 2008, **22**, 635-642.
39. M. Moller, P. Nilges, F. Harnisch and U. Schroder, *Chemsuschem*, 2011, **4**, 566-579.
40. M. T. Reza, B. Wirth, U. Luder and M. Werner, *Bioresource Technology*, 2014, **169**, 352-361.
41. J. A. Libra, K. S. Ro, C. Kammann, A. Funke, N. D. Berge, Y. Neubauer, M. M. Titirici, C. Fühner, O. Bens, J. Kern and K. H. Emmerich, *Biofuels* 2011, **2**, 89-124.
42. I. Oliveira, D. Blohse and H. G. Ramke, *Bioresource Technology*, 2013, **142**, 138-146.
43. E. M. Rubin, *Nature*, 2008, **454**, 841-845.
44. L. J. Gibson, *J R Soc Interface*, 2012, **9**, 2749-2766.
45. A. Cabiac, E. Guillon, F. Chambon, C. Pinel, F. Rataboul and N. Essayem, *Appl Catal a-Gen*, 2011, **402**, 1-10.
46. K. Tekin, S. Karagoz and S. Bektas, *Renew Sust Energ Rev*, 2014, **40**, 673-687.
47. H. S. Kambo and A. Dutta, *Renew Sust Energ Rev*, 2015, **45**, 359-378.
48. J. R. M. Almeida, T. Modig, A. Petersson, B. Hahn-Hagerdal, G. Liden and M. F. Gorwa-Grauslund, *Journal of Chemical Technology and Biotechnology*, 2007, **82**, 340-349.
49. H. P. Yang, R. Yan, H. P. Chen, C. G. Zheng, D. H. Lee and D. T. Liang, *Energ Fuel*, 2006, **20**, 388-393.
50. S. M. Kang, X. H. Li, J. Fan and J. Chang, *Ind Eng Chem Res*, 2012, **51**, 9023-9031.
51. M. M. Titirici, A. Thomas, S. H. Yu, J. O. Muller and M. Antonietti, *Chemistry of Materials*, 2007, **19**, 4205-4212.
52. A. J. Romero-Anaya, M. A. Lillo-Rodenas, C. S. M. de Lecea and A. Linares-Solano, *Carbon*, 2012, **50**, 3158-3169.
53. C. Falco, N. Baccile and M. M. Titirici, *Green Chemistry*, 2011, **13**, 3273-3281.
54. M. M. Titirici, M. Antonietti and N. Baccile, *Green Chemistry*, 2008, **10**, 1204-1212.
55. A. Funke, *Hydrothermale Karbonisierung von Biomasse - Dissertation*, Berlin, 2012.

56. A. Kruse, A. Funke and M. M. Titirici, *Curr Opin Chem Biol*, 2013, **17**, 515-521.
57. M. Sevilla and A. B. Fuertes, *Carbon*, 2009, **47**, 2281-2289.
58. M. Sasaki, Z. Fang, Y. Fukushima, T. Adschiri and K. Arai, *Ind Eng Chem Res*, 2000, **39**, 2883-2890.
59. M. Sasaki, B. Kabyemela, R. Malaluan, S. Hirose, N. Takeda, T. Adschiri and K. Arai, *J Supercrit Fluid*, 1998, **13**, 261-268.
60. Y. Ogihara, R. L. Smith, H. Inomata and K. Arai, *Cellulose*, 2005, **12**, 595-606.
61. Y. Yu and H. W. Wu, *Ind Eng Chem Res*, 2010, **49**, 3919-3925.
62. Y. Yu, X. Lou and H. W. Wu, *Energ Fuel*, 2008, **22**, 46-60.
63. Y. Yu and H. W. Wu, *Ind Eng Chem Res*, 2010, **49**, 3902-3909.
64. W. Schwald and O. Bobleter, *J Carbohyd Chem*, 1989, **8**, 565-578.
65. A. Ebringerova, *Macromol Symp*, 2006, **232**, 1-12.
66. H. Pinkowska, P. Wolak and A. Zlocinska, *Biomass Bioenerg*, 2011, **35**, 3902-3912.
67. E. Dinjus, A. Kruse and N. Troger, *Chem Eng Technol*, 2011, **34**, 2037-2043.
68. M. T. Reza, J. G. Lynam, M. H. Uddin and C. J. Coronella, *Biomass Bioenerg*, 2013, **49**, 86-94.
69. R. Hashaikeh, Z. Fang, I. S. Butler, J. Hawari and J. A. Kozinski, *Fuel*, 2007, **86**, 1614-1622.
70. H. Wikberg, T. Ohra-aho, F. Pileidis and M. M. Titirici, *Acs Sustainable Chemistry & Engineering*, 2015, **3**, 2737-2745.
71. Z. G. Liu, A. Quek, S. K. Hoekman and R. Balasubramanian, *Fuel*, 2013, **103**, 943-949.
72. Z. Fang, T. Sato, R. L. Smith, H. Inomata, K. Arai and J. A. Kozinski, *Bioresource Technology*, 2008, **99**, 3424-3430.
73. H. Pinkowska, P. Wolak and A. Zlocinska, *Chemical Engineering Journal*, 2012, **187**, 410-414.
74. A. A. Peterson, F. Vogel, R. P. Lachance, M. Froling, M. J. Antal and J. W. Tester, *Energ Environ Sci*, 2008, **1**, 32-65.
75. Y. Shin, L. Q. Wang, I. T. Bae, B. W. Arey and G. J. Exarhos, *J Phys Chem C*, 2008, **112**, 14236-14240.
76. N. Baccile, C. Falco and M. M. Titirici, *Green Chemistry*, 2014, **16**, 4839-4869.
77. C. Yao, Y. Shin, L. Q. Wang, C. F. Windisch, W. D. Samuels, B. W. Arey, C. Wang, W. M. Risen and G. J. Exarhos, *J Phys Chem C*, 2007, **111**, 15141-15145.
78. V. K. Lamer, *Ind Eng Chem*, 1952, **44**, 1270-1277.
79. X. M. Sun and Y. D. Li, *Angewandte Chemie-International Edition*, 2004, **43**, 597-601.
80. T. Karayildirim, A. Sinag and A. Kruse, *Chem Eng Technol*, 2008, **31**, 1561-1568.
81. Y. N. Sun, B. Gao, Y. Yao, J. N. Fang, M. Zhang, Y. M. Zhou, H. Chen and L. Y. Yang, *Chemical Engineering Journal*, 2014, **240**, 574-578.
82. A. B. Fuertes, M. C. Arbestain, M. Sevilla, J. A. Macia-Agullo, S. Fiol, R. Lopez, R. J. Smernik, W. P. Aitkenhead, F. Arce and F. Macias, *Aust J Soil Res*, 2010, **48**, 618-626.
83. Z. G. Liu and F. S. Zhang, *Journal of Hazardous Materials*, 2009, **167**, 933-939.
84. K. Wiedner, C. Rumpel, C. Steiner, A. Pozzi, R. Maas and B. Glaser, *Biomass Bioenerg*, 2013, **59**, 264-278.
85. K. Wiedner, in *Hydrothermale Prozesse*, eds. M. Klemm and R. Glowacki, 2015, pp. 38-43.
86. Z. G. Liu, F. S. Zhang and J. Z. Wu, *Fuel*, 2010, **89**, 510-514.

87. V. K. Gupta and A. Nayak, *Chemical Engineering Journal*, 2012, **180**, 81-90.
88. K. Wiedner, C. Naisse, C. Rumpel, A. Pozzi, P. Wieczorek and B. Glaser, *Org Geochem*, 2013, **54**, 91-100.
89. Z. G. Liu and R. Balasubramanian, *Appl Energ*, 2014, **114**, 857-864.
90. S. Q. Guo, X. Y. Dong, K. T. Liu, H. L. Yu and C. X. Zhu, *Bioresources*, 2015, **10**, 4613-4625.
91. S. Roman, J. M. V. Nabais, B. Ledesma, J. F. Gonzalez, C. Laginhas and M. M. Titirici, *Microporous and Mesoporous Materials*, 2013, **165**, 127-133.
92. G. K. Parshetti, S. K. Hoekman and R. Balasubramanian, *Bioresource Technology*, 2013, **135**, 683-689.
93. K. Aydincak, T. Yumak, A. Sinag and B. Esen, *Ind Eng Chem Res*, 2012, **51**, 9145-9152.
94. Y. W. Xue, B. Gao, Y. Yao, M. Inyang, M. Zhang, A. R. Zimmerman and K. S. Ro, *Chemical Engineering Journal*, 2012, **200**, 673-680.
95. M. Sevilla, J. A. Macia-Agullo and A. B. Fuertes, *Biomass Bioenerg*, 2011, **35**, 3152-3159.
96. J. Mumme, L. Eckervogt, J. Pielert, M. Diakite, F. Rupp and J. Kern, *Bioresource Technology*, 2011, **102**, 9255-9260.
97. J. Fang, B. Gao, J. J. Chen and A. R. Zimmerman, *Chemical Engineering Journal*, 2015, **267**, 253-259.
98. F. Y. Liu and M. H. Guo, *Journal of Materials Science*, 2015, **50**, 1624-1631.
99. W. S. L. Mok, M. J. Antal, P. Szabo, G. Varhegyi and B. Zelei, *Ind Eng Chem Res*, 1992, **31**, 1162-1166.
100. E. Leibnitz, H. G. Konnecke and M. Schroter, *J Prakt Chem*, 1958, **6**, 18-24.
101. P. G. Hatcher, K. A. Wenzel and G. D. Cody, in *Vitrinite Reflectance as a Maturity Parameter*, eds. P. K. Mukhopadhyay and W. G. Dow, American Chemical Society, 1994, ch. 8, pp. 112-135.
102. M. Siskin and A. R. Katritzky, *Chem Rev*, 2001, **101**, 825-835.
103. X. W. Lu, J. R. V. Flora and N. D. Berge, *Bioresource Technology*, 2014, **154**, 229-239.
104. B. F. M. Kuster, *Starch-Starke*, 1990, **42**, 314-321.
105. A. Funke, F. Reebs and A. Kruse, *Fuel Process Technol*, 2013, **115**, 261-269.
106. D. S. Ross, B. H. Loo, D. S. Tse and A. S. Hirschon, *Fuel*, 1991, **70**, 289-295.
107. P. Landais, R. Michels and M. Elie, *Org Geochem*, 1994, **22**, 617-630.
108. C. Falco, *Sustainable biomass-derived hydrothermal carbons for energy applications - Dissertation*, Potsdam, 2012.
109. A. J. Romero-Anaya, M. Ouzzine, M. A. Lillo-Rodenas and A. Linares-Solano, *Carbon*, 2014, **68**, 296-307.
110. S. Inoue, S. Uno and T. Minowa, *J Chem Eng Jpn*, 2008, **41**, 210-215.
111. S. S. Jamari, J. R. Howse and A. A. Bakar, *Internation Journal of Chemical Engineering and Applications*, 2013, **4**, 149-152.
112. X. Y. Cao, K. S. Ro, J. A. Libra, C. I. Kammann, I. Lima, N. Berge, L. Li, Y. Li, N. Chen, J. Yang, B. L. Deng and J. D. Mao, *J Agr Food Chem*, 2013, **61**, 9401-9411.
113. H. S. Kambo and A. Dutta, *Appl Energ*, 2014, **135**, 182-191.
114. S. K. Hoekman, A. Broch and C. Robbins, *Energ Fuel*, 2011, **25**, 1802-1810.
115. S. K. Hoekman, A. Broch, C. Robbins, B. Zielinska and L. Felix, *Biomass Conversion and Biorefinery*, 2013, **3**, 113-126.

116. Z. L. Yao, X. Q. Ma and Y. S. Lin, *Appl Therm Eng*, 2016, **104**, 678-686.
117. J. G. Lynam, M. T. Reza, W. Yan, V. R. Vasquez and C. J. Coronella, *Biomass Conversion and Biorefinery*, 2015, **5**, 173–181.
118. S. Roman, J. M. V. Nabais, C. Laginhas, B. Ledesma and J. F. Gonzalez, *Fuel Process Technol*, 2012, **103**, 78-83.
119. E. Sermyagina, J. Saari, J. Kaikko and E. Vakkilainen, *J Anal Appl Pyrol*, 2015, **113**, 551-556.
120. X. W. Lu, P. J. Pellechia, J. R. V. Flora and N. D. Berge, *Bioresource Technology*, 2013, **138**, 180-190.
121. M. T. Reza, M. H. Uddin, J. G. Lynam, S. K. Hoekman and C. J. Coronella, *Biomass Conversion and Biorefinery*, 2014, **4**, 311–321.
122. M. Sevilla and A. B. Fuertes, *Chem-Eur J*, 2009, **15**, 4195-4203.
123. R. Demir-Cakan, N. Baccile, M. Antonietti and M. M. Titirici, *Chemistry of Materials*, 2009, **21**, 484-490.
124. S. M. Heilmann, H. T. Davis, L. R. Jader, P. A. Lefebvre, M. J. Sadowsky, F. J. Schendel, M. G. von Keitz and K. J. Valentas, *Biomass Bioenerg*, 2010, **34**, 875-882.
125. V. Benavente, E. Calabuig and A. Fullana, *J Anal Appl Pyrol*, 2015, **113**, 89-98.
126. M. T. Reza, W. Yan, M. H. Uddin, J. G. Lynam, S. K. Hoekman, C. J. Coronella and V. R. Vasquez, *Bioresource Technology*, 2013, **139**, 161-169.
127. Y. Gao, X. H. Wang, J. Wang, X. P. Li, J. J. Cheng, H. P. Yang and H. P. Chen, *Energy*, 2013, **58**, 376-383.
128. Y. Q. Lei, H. Q. Su and R. K. Tian, *Rsc Advances*, 2016, **6**, 107829-107835.
129. J. H. Zhang, Q. M. Lin and X. R. Zhao, *J Integr Agr*, 2014, **13**, 471-482.
130. S. W. McKibbins, J. F. Harris, J. F. Saeman and W. K. Neill, *Forest Products Journal*, 1962, **12**, 17-23.
131. Y. H. Li, X. Y. Lu, L. Yuan and X. Liu, *Biomass Bioenerg*, 2009, **33**, 1182-1187.
132. R. A. Schraufnagel and H. F. Rase, *Ind Eng Chem Prod Rd*, 1975, **14**, 40-44.
133. X. H. Qi, M. Watanabe, T. M. Aida and R. L. Smith, *Green Chemistry*, 2008, **10**, 799-805.
134. R. L. Huang, W. Qi, R. X. Su and Z. M. He, *Chem Commun*, 2010, **46**, 1115-1117.
135. H. B. Zhao, J. E. Holladay, H. Brown and Z. C. Zhang, *Science*, 2007, **316**, 1597-1600.
136. S. Q. Hu, Z. F. Zhang, J. L. Song, Y. X. Zhou and B. X. Han, *Green Chemistry*, 2009, **11**, 1746-1749.
137. I. Jimenez-Morales, M. Moreno-Recio, J. Santamaria-Gonzalez, P. Maireles-Torres and A. Jimenez-Lopez, *Appl Catal B-Environ*, 2015, **164**, 70-76.
138. K. Lourvanij and G. L. Rorrer, *Ind Eng Chem Res*, 1993, **32**, 11-19.
139. Y. Takeuchi, F. M. Jin, K. Tohji and H. Enomoto, *Journal of Materials Science*, 2008, **43**, 2472-2475.
140. F. S. Asghari and H. Yoshida, *Ind Eng Chem Res*, 2006, **45**, 2163-2173.
141. X. F. Cao, X. W. Peng, S. N. Sun, L. X. Zhong, W. Chen, S. Wang and R. C. Sun, *Carbohyd Polym*, 2015, **118**, 44-51.
142. K. Seri, Y. Inoue and H. Ishida, *B Chem Soc Jpn*, 2001, **74**, 1145-1150.
143. T. Stahlberg, M. G. Sorensen and A. Riisager, *Green Chemistry*, 2010, **12**, 321-325.
144. H. H. Szmant and D. D. Chundury, *Journal of Chemical Technology and Biotechnology*, 1981, **31**, 135-145.

145. M. Watanabe, Y. Aizawa, T. Iida, T. M. Aida, C. Levy, K. Sue and H. Inomata, *Carbohyd Res*, 2005, **340**, 1925-1930.
146. A. Takagaki, M. Ohara, S. Nishimura and K. Ebitani, *Chem Commun*, 2009, DOI: 10.1039/b914087e, 6276-6278.
147. A. Chareonlimkun, V. Champreda, A. Shotipruk and N. Laosiripojana, *Fuel*, 2010, **89**, 2873-2880.
148. R. Rinaldi and F. Schuth, *Chemsuschem*, 2009, **2**, 1096-1107.
149. F. M. Jin and H. Enomoto, *Energ Environ Sci*, 2011, **4**, 382-397.
150. S. Van De Vyver, J. Geboers, P. A. Jacobs and B. F. Sels, *Chemcatchem*, 2011, **3**, 82-94.
151. Y. B. Huang and Y. Fu, *Green Chemistry*, 2013, **15**, 1095-1111.
152. N. S. Mosier, C. M. Ladisch and M. R. Ladisch, *Biotechnol Bioeng*, 2002, **79**, 610-618.
153. K. Shimizu, H. Furukawa, N. Kobayashi, Y. Itaya and A. Satsuma, *Green Chemistry*, 2009, **11**, 1627-1632.
154. K. M. Pan, H. Ming, Y. Liu and Z. H. Kong, *New Journal of Chemistry*, 2012, **36**, 113-118.
155. X. H. Qi, M. Watanabe, T. M. Aida and R. L. Smith, *Cellulose*, 2011, **18**, 1327-1333.
156. T. Minowa, F. Zhen and T. Ogi, *J Supercrit Fluid*, 1998, **13**, 253-259.
157. S. Karagoz, T. Bhaskar, A. Muto, Y. Sakata, T. Oshiki and T. Kishimoto, *Chemical Engineering Journal*, 2005, **108**, 127-137.
158. T. Bhaskar, A. Sera, A. Muto and Y. Sakata, *Fuel*, 2008, **87**, 2236-2242.
159. Y. J. Pagan-Torres, T. F. Wang, J. M. R. Gallo, B. H. Shanks and J. A. Dumesic, *Acs Catalysis*, 2012, **2**, 930-934.
160. Y. Yang, C. W. Hu and M. M. Abu-Omar, *Green Chemistry*, 2012, **14**, 509-513.
161. S. Fischer, *Lenzinger Berichte*, 2004, **83**, 71-78.
162. H. Leipner, S. Fischer, E. Brendler and W. Voigt, *Macromol Chem Physic*, 2000, **201**, 2041-2049.
163. N. J. Cao, Q. Xu, C. S. Chen, C. S. Gong and L. F. Chen, *Appl Biochem Biotech*, 1994, **45-6**, 521-530.
164. N. J. Cao, Q. Xu and L. F. Chen, *Appl Biochem Biotech*, 1995, **51-2**, 21-28.
165. T. S. Deng, X. J. Cui, Y. Q. Qi, Y. X. Wang, X. L. Hou and Y. L. Zhu, *Chem Commun*, 2012, **48**, 5494-5496.
166. Q. Xu and L. F. Chen, *J Appl Polym Sci*, 1999, **71**, 1441-1446.
167. N. J. Richards and D. G. Williams, *Carbohyd Res*, 1970, **12**, 409-&.
168. Y. X. Wang, C. M. Pedersen, T. S. Deng, Y. Qiao and X. L. Hou, *Bioresource Technology*, 2013, **143**, 384-390.
169. S. H. Yu, X. J. Cui, L. L. Li, K. Li, B. Yu, M. Antonietti and H. Colfen, *Advanced Materials*, 2004, **16**, 1636-1640.
170. X. J. Cui, M. Antonietti and S. H. Yu, *Small*, 2006, **2**, 756-759.
171. X. M. Sun and Y. D. Li, *J Colloid Interf Sci*, 2005, **291**, 7-12.
172. R. Demir-Cakan, M. M. Titirici, M. Antonietti, G. L. Cui, J. Maier and Y. S. Hu, *Chem Commun*, 2008, DOI: 10.1039/b805671b, 3759-3761.
173. M. M. Tusi, M. Brandalise, O. V. Correa, A. O. Neto, M. Linardi and E. V. Spinace, *Materials Research*, 2007, **10**, 171-175.

174. M. M. Tusi, N. S. O. Polanco, M. Brandalise, O. V. Correa, A. C. Silva, V. A. Ribeiro, A. O. Neto and E. V. Spinace, *Ionics*, 2012, **18**, 215-222.
175. L. Peng, Y. Q. Ren, J. D. Gu, P. F. Qin, Q. R. Zeng, J. H. Shao, M. Lei and L. Y. Chai, *Environ Sci Pollut R*, 2014, **21**, 7631-7640.
176. Y. Yan, H. F. Yang, F. Q. Zhang, B. Tu and D. Y. Zhao, *Small*, 2006, **2**, 517-521.
177. M. M. Titirici, A. Thomas and M. Antonietti, *Advanced Functional Materials*, 2007, **17**, 1010-1018.
178. S. Ikeda, K. Tachi, Y. H. Ng, Y. Ikoma, T. Sakata, H. Mori, T. Harada and M. Matsumura, *Chemistry of Materials*, 2007, **19**, 4335-4340.
179. M. M. Titirici, A. Thomas and M. Antonietti, *J Mater Chem*, 2007, **17**, 3412-3418.
180. R. Demir-Cakan, P. Makowski, M. Antonietti, F. Goettmann and M. M. Titirici, *Catal Today*, 2010, **150**, 115-118.
181. M. M. Titirici, M. Antonietti and A. Thomas, *Chemistry of Materials*, 2006, **18**, 3808-3812.
182. S. Kubo, R. Demir-Cakan, L. Zhao, R. J. White and M. M. Titirici, *Chemsuschem*, 2010, **3**, 188-194.
183. M. T. Reza, E. Rottler, L. Herklotz and B. Wirth, *Bioresource Technology*, 2015, **182**, 336-344.
184. L. L. Wang, Y. P. Guo, Y. C. Zhu, Y. Li, Y. N. Qu, C. G. Rong, X. Y. Ma and Z. C. Wang, *Bioresource Technology*, 2010, **101**, 9807-9810.
185. H. Q. Xiao, Y. X. Guo, X. Z. Liang and C. Z. Qi, *Monatsh Chem*, 2010, **141**, 929-932.
186. N. Baccile, M. Antonietti and M. M. Titirici, *Chemsuschem*, 2010, **3**, 246-253.
187. R. J. White, N. Yoshizawa, M. Antonietti and M. M. Titirici, *Green Chemistry*, 2011, **13**, 2428-2434.
188. S. A. Wohlgemuth, R. J. White, M. G. Willinger, M. M. Titirici and M. Antonietti, *Green Chemistry*, 2012, **14**, 1515-1523.
189. S. Wohlgemuth, H. Urakami, L. Zhao and M. M. Titirici, in *Sustainable Carbon Materials from Hydrothermal Processes*, ed. M. M. Titirici, John Wiley & Sons, Ltd., 2013, ch. 5, pp. 125-149.
190. H. L. Wang, L. B. Zhang, T. S. Deng, H. Ruan, X. L. Hou, J. R. Cort and B. Yang, *Green Chemistry*, 2016, **18**, 2802-2810.
191. D. D. Mai, R. Wen, W. M. Cao, B. Yuan, Y. Liu, Q. Liu and G. R. Qian, *Acs Sustainable Chemistry & Engineering*, 2017, **5**, 3499-3508.
192. J. Ming, Y. Q. Wu, G. F. Liang, J. B. Park, F. Y. Zhao and Y. K. Sun, *Green Chemistry*, 2013, **15**, 2722-2726.
193. J. G. Lynam, C. J. Coronella, W. Yan, M. T. Reza and V. R. Vasquez, *Bioresource Technology*, 2011, **102**, 6192-6199.
194. J. G. Lynam, M. T. Reza, V. R. Vasquez and C. J. Coronella, *Fuel*, 2012, **99**, 271-273.
195. M. T. Reza, J. Nover, B. Wirth and C. J. Coronella, *Aims Energy*, 2016, **4**, 173-189.
196. C. Y. Zhang, S. Lin, J. J. Peng, Y. Z. Hong, Z. Y. Wang and X. B. Jin, *Rsc Advances*, 2017, **7**, 6486-6491.
197. T. P. Fellinger, R. J. White, M. M. Titirici and M. Antonietti, *Advanced Functional Materials*, 2012, **22**, 3254-3260.
198. S. A. Wohlgemuth, T. P. Fellinger, P. Jaker and M. Antonietti, *Journal of Materials Chemistry A*, 2013, **1**, 4002-4009.

199. J. Ryu, Y. W. Suh, D. J. Suh and D. J. Ahn, *Carbon*, 2010, **48**, 1990-1998.
200. A. Jain, S. Jayaraman, R. Balasubramanian and M. P. Srinivasan, *Journal of Materials Chemistry A*, 2014, **2**, 520-528.
201. A. Jain, V. Aravindan, S. Jayaraman, P. S. Kumar, R. Balasubramanian, S. Ramakrishna, S. Madhavi and M. P. Srinivasan, *Sci Rep-Uk*, 2013, **3**.
202. G. K. Parshetti, S. Chowdhury and R. Balasubramanian, *Fuel*, 2015, **148**, 246-254.
203. G. B. Barin, I. D. Gimenez, L. P. da Costa, A. G. Souza and L. S. Barreto, *Carbon*, 2014, **78**, 609-612.
204. A. Jain, R. Balasubramanian and M. P. Srinivasan, *Chemical Engineering Journal*, 2015, **273**, 622-629.
205. C. Falco, J. P. Marco-Lozar, D. Salinas-Torres, E. Morallon, D. Cazorla-Amoros, M. M. Titirici and D. Lozano-Castello, *Carbon*, 2013, **62**, 346-355.
206. C. A. Toles, W. E. Marshall, L. H. Wartelle and A. McAloon, *Bioresource Technology*, 2000, **75**, 197-203.
207. R. Azargohar and A. K. Dalai, *Microporous and Mesoporous Materials*, 2008, **110**, 413-421.
208. P. Saetea and N. Tippayawong, presented in part at the World Congress on Engineering, London, U.K., 2013.
209. J. S. Cha, S. H. Park, S. C. Jung, C. Ryu, J. K. Jeon, M. C. Shin and Y. K. Park, *J Ind Eng Chem*, 2016, **40**, 1-15.
210. K. Mochidzuki, N. Sato and A. Sakoda, *Adsorption*, 2005, **11**, 669-673.
211. H. Y. Zhao, X. A. Lu, Y. Wang, B. Sun, X. H. Wu and H. F. Lu, *Journal of Materials Science*, 2017, **52**, 10787-10799.
212. G. Z. Kyzas, J. Fu and K. A. Matis, *Materials*, 2013, **6**, 5131-5158.
213. Y. F. Yang, Y. L. Xie, L. C. Pang, M. Li, X. H. Song, J. G. Wen and H. Y. Zhao, *Langmuir*, 2013, **29**, 10727-10736.
214. M. Rafatullah, O. Sulaiman, R. Hashim and A. Ahmad, *Journal of Hazardous Materials*, 2010, **177**, 70-80.
215. G. K. Parshetti, S. Chowdhury and R. Balasubramanian, *Bioresource Technology*, 2014, **161**, 310-319.
216. M. T. Yagub, T. K. Sen, S. Afroze and H. M. Ang, *Adv Colloid Interfac*, 2014, **209**, 172-184.
217. R. Gong, J. J. Ye, W. Dai, X. Y. Yan, J. Hu, X. Hu, S. Li and H. Huang, *Ind Eng Chem Res*, 2013, **52**, 14297-14303.
218. F. Cesano, M. M. Rahman, S. Bertarione, J. G. Vitillo, D. Scarano and A. Zecchina, *Carbon*, 2012, **50**, 2047-2051.
219. W. X. Chen, H. Jiang, Z. D. Xu and Y. Lu, *Chinese J Chem*, 1999, **17**, 125-131.
220. A. M. M. Vargas, A. L. Cazetta, M. H. Kunita, T. L. Silva and V. C. Almeida, *Chemical Engineering Journal*, 2011, **168**, 722-730.
221. H. N. Tran, S. J. You and H. P. Chao, *Korean J Chem Eng*, 2017, **34**, 1708-1720.
222. J. M. Juarez-Galan, A. Silvestre-Albero, J. Silvestre-Albero and F. Rodriguez-Reinoso, *Microporous and Mesoporous Materials*, 2009, **117**, 519-521.
223. Y. P. Guo, S. F. Yang, W. Y. Fu, J. R. Qi, R. Z. Li, Z. C. Wang and H. D. Xu, *Dyes Pigments*, 2003, **56**, 219-229.

224. F. J. Martin-Jimeno, F. Suarez-Garcia, J. I. Paredes, A. Martinez-Alonso and J. M. D. Tascon, *Carbon*, 2015, **81**, 137-147.
225. X. X. Lin, B. Tan, L. Peng, Z. F. Wu and Z. L. Xie, *Journal of Materials Chemistry A*, 2016, **4**, 4497-4505.
226. M. A. Islam, A. Benhouria, M. Asif and B. H. Hameed, *J Taiwan Inst Chem E*, 2015, **52**, 57-64.
227. Y. H. Ma, Q. H. Wang, X. N. Wang, X. H. Sun and X. Q. Wang, *J Porous Mat*, 2015, **22**, 157-169.
228. S. Lagergren, *Kungliga Svenska Vetenskapsakademiens. Handlingar*, 1898, **24**, 1-39.
229. Y. S. Ho and G. McKay, *Process Saf Environ*, 1998, **76**, 332-340.
230. Y. S. Ho, *Scientometrics*, 2004, **59**, 171-177.
231. K. Y. Foo and B. H. Hameed, *Bioresource Technology*, 2012, **112**, 143-150.
232. M. J. D. Low, *Chem Rev*, 1960, **60**, 267-312.
233. C. Aharoni and F. C. Tompkins, *Advances in Catalysis*, 1970, **21**, 1-49.
234. K. G. Sreejalekshmi, K. A. Krishnan and T. S. Anirudhan, *Journal of Hazardous Materials*, 2009, **161**, 1506-1513.
235. X. E. Shen, X. Q. Shan, D. M. Dong, X. Y. Hua and G. Owens, *J Colloid Interf Sci*, 2009, **330**, 1-8.
236. H. A. Omar and H. Moloukhia, *Journal of Hazardous Materials*, 2008, **157**, 242-246.
237. B. H. Hameed and A. A. Rahman, *Journal of Hazardous Materials*, 2008, **160**, 576-581.
238. V. O. Njoku, M. A. Islam, M. Asif and B. H. Hameed, *Chemical Engineering Journal*, 2014, **251**, 183-191.
239. ASTM, *D3174-02 Standard Test Method for Ash in the Analysis Sample of Coal and Coke from Coal*, 2002, 1-5.
240. R. F. Egerton, *Physical Principles of Electron Microscopy*, Springer, 2005.
241. N. W. Ashcroft and N. D. Mermin, in *Solid State Physics*, Harcourt, 1976, ch. 6, pp. 95-110.
242. W. H. Bragg and W. L. Bragg, *Proceedings of the Royal Society A*, 1913, **88**, 428-438.
243. J. W. Niemantsverdriet, *Spectroscopy in Catalysis*, Wiley-VCH, 3rd edn., 2007.
244. J. D. Roberts, *Nuclear Magnetic Resonance*, 1959.
245. J. K. M. Sanders and B. K. Hunter, *Modern NMR Spectroscopy*, Oxford University Press, 1987.
246. N. Baccile, J. Weber, C. Falco and M. M. Titirici, in *Sustainable Carbon Materials from Hydrothermal Processes*, ed. M. M. Titirici, John Wiley & Sons, Ltd., 2013, ch. 6, pp. 151-211.
247. F. Blanc, C. Coperet, A. Lesage and L. Emsley, *Chemical Society Reviews*, 2008, **37**, 518-526.
248. N. Baccile, G. Laurent, F. Babonneau, F. Fayon, M. M. Titirici and M. Antonietti, *J Phys Chem C*, 2009, **113**, 9644-9654.
249. B. Zeeh, in *Spektroskopische Methoden in der organischen Chemie*, eds. M. Hesse, H. Meier and B. Zeeh, Georg Thieme Verlag, Stuttgart, 7th edn., 2005, ch. 2, pp. 33-73.
250. RSC, *Infrared Spectroscopy (IR)*, 2009, 1-5.
251. PerkinElmer, *FT-IR Spectroscopy Attenuated Total Reflectance (ATR)*, 2005, 1-5.

252. J. F. Watts and J. Wolstenholme, *An Introduction to Surface Analysis by XPS and AES*, Wiley, 2003.
253. C. C. Chusuei and D. W. Goodman, *Encyclopedia of Physical Science and Technology*, Academic Press, 3rd edn., 2002.
254. F. Rouquerol, J. Rouquerol, K. S. W. Sing, G. Maurin and P. Llewellyn, in *Adsorption by Powders and Porous Solids*, Elsevier, 2nd edn., 2014, ch. 1, pp. 1-24.
255. M. Thommes, K. Kaneko, A. V. Neimark, J. P. Olivier, F. Rodriguez-Reinoso, J. Rouquerol and K. S. W. Sing, *Pure Appl Chem*, 2015, **87**, 1051-1069.
256. I. Langmuir, *J Am Chem Soc*, 1916, **38**, 2221-2295.
257. H. Freundlich, *Zeitschrift für Physikalische Chemie*, 1906, **57**, 385-470.
258. S. Brunauer, P. H. Emmett and E. Teller, *J Am Chem Soc*, 1938, **60**, 309-319.
259. P. H. Emmett and S. Brunauer, *J Am Chem Soc*, 1937, **59**, 1553-1564.
260. K. S. W. Sing, in *Adsorption by Powders and Porous Solids*
Elsevier, 2nd edn., 2014, ch. 7, pp. 237-268.
261. J. Rouquerol, P. Llewellyn and F. Rouquerol, *Studies in Surface Science and Catalysis*, 2007, **160**, 49-56.
262. DIN, *DIN ISO 9277 Determination of the specific surface area of solids by gas adsorption - BET method*, 2014, 1-30.
263. K. S. W. Sing, F. Rouquerol, P. Llewellyn and J. Rouquerol, in *Adsorption by Powders and Porous Solids*, Elsevier, 2nd edn., 2014, ch. 9, pp. 303-320.
264. N. Fechler, *Salts as Highly Diverse Porogens: Functional Ionic Liquid-Derived Carbons and Carbon-Bases Composites for Energy-Related Applications - Dissertation*, Potsdam, 2012.
265. K. K. Unger, *Handbuch der HPLC Teil 1*, GIT VERLAG, 1989.
266. RSC, *Introduction to Ultraviolet - Visible Spectroscopy (UV)*, 2009.
267. D. Licursi, C. Antonetti, J. Bernardini, P. Cinelli, M. B. Coltelli, A. Lazzeri, M. Martinelli and A. M. R. Galletti, *Ind Crop Prod*, 2015, **76**, 1008-1024.
268. J. H. Huang, K. L. Huang, S. Q. Liu, A. T. Wang and C. Yan, *Colloid Surface A*, 2008, **330**, 55-61.
269. J. D. Macedo, N. B. da Costa, L. E. Almeida, E. F. D. Vieira, A. R. Cestari, I. D. Gimenez, N. L. V. Carreno and L. S. Barreto, *J Colloid Interf Sci*, 2006, **298**, 515-522.

Appendix

Table A1 Results of elemental analysis, ash content and yield for the hydrochars from different substrates obtained in the presence of zinc chloride (chapter 4.1.1.1 & 4.1.1.3).

Sample	C [%]	H [%]	N [%]	O [%]	Ash [wt%]	Yield [wt%]
Glucose	40.25	6.71a	0.00	53.04	0.00	-
Glu_B12h180C	62.34	3.78	0.00	33.83	0.05	37.10
Glu_B12h180C60Zn	65.07	4.04	0.29	28.49	2.11	44.80
Hydroxymethylfurfural	57.14a	4.79a	0.00	38.07a	0.00	-
HMF_B12h180C	66.95	3.94	0.11	29.01	0.00	24.00
HMF_B12h180C60Zn	67.60	4.13	0.29	27.98	0.00	20.00
Cellulose	42.52	6.28	0.00	51.12	0.08	-
Cel_B12h180C	51.32	5.39	0.00	43.24	0.05	50.70
Cel_B12h180C60Zn	63.54	4.32	0.30	31.45	0.39	47.50
Lignin	47.60	4.76	0.11	29.70	17.83	-
Lig_B12h180C	52.52	4.72	0.15	21.77	20.84	58.20
Lig_B12h180C60Zn	56.42	4.48	0.27	28.18	10.65	58.40
Grasses/rushes	43.56	6.76	1.57	45.03	3.08	-
Gnr_A12h180C	56.48	5.53	2.15	34.23	1.62	45.00
Gnr_A12h180CLi(0.23)Zn	63.51	4.00	1.27	20.16	11.07	60.00
Coconut raw	49.40	6.11	0.05	43.51	0.93	-
Crw_B12h180C	60.53	5.25	0.14	34.08	0.00	62.80
Crw_B12h180C60Zn	66.00	4.28	0.21	29.46	0.05	58.70
Coconut shell powder	49.07	5.69	0.13	44.67	0.44	-
Ccn_B12h180C	59.90	5.44	0.04	34.59	0.03	60.90
Ccn_B12h180C60Zn	67.11	4.13	0.35	28.31	0.10	52.30
Rice husk	38.44	5.03	0.40	40.46	15.67	-
Rce_B12h180C	45.35	4.82	0.49	30.47	18.87	63.30
Rce_B12h180C60Zn	47.92	3.50	0.55	25.33	22.70	59.80
Dried dandelion leaves	37.47	5.50	2.06	44.31	10.66	-
Dnd_B12h180C	53.68	5.42	2.53	29.03	9.34	43.00
Dnd_B12h180C60Zn	52.52	4.32	1.80	27.81	13.55	44.50
Sawdust	46.33	6.13	0.61	46.91	0.02	-
Saw_A12h180C	49.96	5.92	0.35	43.77	0.00	63.41
Saw_A12h180CLi(0.23)Zn	60.29	3.71	0.39	35.60	0.01	55.60
Algae	46.93	0.00	11.07	34.77	7.23	-
Alg_B12h180C	61.23	7.64	8.28	13.29	9.56	14.30
Alg_B12h180C60Zn	32.88	4.62	3.93	34.31	24.26	33.70

[a] elemental % calculated from theoretical chemical formula.

Table A2 EDX results from Rce_B12h180C60Zn (chapter 4.1.1.1).

Element	**Mass%**	**Atom%**
C K	56.40	65.44
O K	35.43	30.86
Si K	6.67	3.31
S K	0.19	0.08
Cl K	0.16	0.06
Cu K	0.21	0.05
Zn K	0.94	0.20

Table A3 Results of elemental analysis, ash content and yield for the influence of temperature and time onto the hydrothermal carbonization of coconut shell powder in the presence of zinc chloride (chapter 4.1.2.1 & 4.1.2.3).

Sample	**C [%]**	**H [%]**	**N [%]**	**O [%]**	**Ash [wt%]**	**Yield [wt%]**
Coconut shell powder	49.07	5.69	0.13	44.67	0.44	-
Ccn_B04h180C	58.24	5.80	0.18	35.78	0.00	56.10
Ccn_B12h180C	59.90	5.44	0.04	34.63	0.03	60.90
Ccn_B20h180C	58.30	4.88	0.02	36.80	0.00	54.60
Ccn_B04h180C60Zn	67.02	4.37	0.35	28.25	0.01	53.90
Ccn_B12h180C60Zn	67.11	4.13	0.35	28.31	0.10	52.30
Ccn_B20h180C60Zn	67.30	4.10	0.38	28.10	0.12	55.50
Ccn_B12h200C	66.76	4.44	0.17	28.63	0.00	48.20
Ccn_B12h220C	66.73	4.43	0.15	28.63	0.06	48.60
Ccn_B12h200C60Zn	67.65	3.73	0.45	27.98	0.19	46.70
Ccn_B12h220C60Zn	68.93	3.52	0.42	27.02	0.11	46.80
Ccn_B20h220C	68.72	4.48	0.17	26.63	0.00	48.50
Ccn_B36h220C	68.64	4.73	0.20	26.43	0.00	48.00
Ccn_B20h220C60Zn	69.81	3.54	0.51	25.98	0.16	50.40
Ccn_B36h220C60Zn	70.18	3.79	0.52	25.33	0.18	49.50

Table A4 Specific surface areas (SSA) obtained by nitrogen sorption experiments and calculated by BET theorem together with the pore volumes for different hydrochars for the influence of temperature and time onto the hydrothermal carbonization of coconut shell powder in the presence of zinc chloride (chapter 4.1.2.6).

Sample	**SSA [$m^2 \cdot g^{-1}$]**	**Pore volume [$cm^3 \cdot g^{-1}$]**
Ccn_B04h180C	3.22	0.01
Ccn_B12h180C	4.19	0.00
Ccn_B20h180C	7.83	0.02
Ccn_B04h180C60Zn	97.70	0.28
Ccn_B12h180C60Zn	97.82	0.28
Ccn_B20h180C60Zn	103.24	0.29
Ccn_B12h200C	50.27	0.16
Ccn_B12h220C	51.25	0.15
Ccn_B12h200C60Zn	111.71	0.29
Ccn_B12h220C60Zn	118.23	0.30
Ccn_B20h220C	52.39	0.16
Ccn_B36h220C	43.96	0.10
Ccn_B20h220C60Zn	135.02	0.32
Ccn_B36h220C60Zn	186.11	0.29

Table A5 Results of elemental analysis, ash content and yield for the influence of water and salt content onto the hydrothermal carbonization of coconut shell powder in the presence of a salt-water mixture containing zinc chloride (chapter 4.1.3.1 & 4.1.3.2).

Sample	**C [%]**	**H [%]**	**N [%]**	**O [%]**	**Ash [wt%]**	**Yield [wt%]**
Coconut shell powder	49.07	5.69	0.13	44.67	0.44	-
Ccn_A12h180C1-0WLi(0.5)Zn[a]	62.37	3.43	0.10	33.88	0.23	41.2
Ccn_A12h180C1-2WLi(0.5)Zn	63.55	3.83	0.08	32.41	0.14	48.4
Ccn_A12h180C1-20WLi(0.5)Zn	65.13	4.38	0.13	30.07	0.29	38.6
Ccn_A12h180C1-10SLi(0.5)Zn[b]	65.21	3.55	0.13	30.37	0.73	48.9
Ccn_A12h180C1-20W1-10SLi(0.5)Zn[c]	66.16	4.22	0.12	29.05	0.45	41.8
Ccn_B12h180C1-1W	59.28	5.65	0.14	34.93	0.00	56.5
Ccn_B12h180C1-2W	59.90	5.44	0.04	34.60	0.03	60.9
Ccn_B12h180C1-4W	57.37	5.35	0.11	37.18	0.00	54.7
Ccn_B12h180C1-1W60Zn	67.73	4.20	0.31	27.75	0.02	51.1
Ccn_B12h180C1-2W60Zn	67.11	4.13	0.35	28.32	0.10	52.3
Ccn_B12h180C1-4W60Zn	68.37	4.42	0.34	26.71	0.16	51.9
Ccn_B12h180C1-2W10Zn	67.73	4.38	0.16	27.71	0.00	50.8
Ccn_B12h180C1-2W20Zn	65.67	4.44	0.18	29.71	0.00	51.3
Ccn_B12h180C1-2W40Zn	68.88	4.66	0.37	26.05	0.03	52.2
Ccn_B12h180C1-2W80Zn	65.58	3.85	0.18	27.21	3.18	52.8

[a] 1-xW - ratio substrate to water
[b] 1-xS - ratio substrate to salt
[c] 1-xW1-xS - ratio substrate to water to salt

Table A6 Specific surface areas (SSA) obtained by nitrogen sorption experiments and calculated by BET theorem together with the pore volumes for different hydrochars for the influence of water and salt content onto the hydrothermal carbonization of coconut shell powder in the presence of a salt-water mixture containing zinc chloride (chapter 4.1.3.3).

Sample	**SSA [$m^2 \cdot g^{-1}$]**	**Pore volume [$cm^3 \cdot g^{-1}$]**
Ccn_A12h180C1-0WLi(0.5)Zn[a]	0.56	0.00
Ccn_A12h180C1-2WLi(0.5)Zn	133.19	0.14
Ccn_A12h180C1-20WLi(0.5)Zn	43.69	0.15
Ccn_A12h180C1-10SLi(0.5)Zn[b]	4.30	0.01
Ccn_A12h180C1-20W1-10SLi(0.5)Zn[c]	54.55	0.16
Ccn_B12h180C1-1W	4.41	0.01
Ccn_B12h180C1-2W	4.19	0.00
Ccn_B12h180C1-4W	4.24	0.01
Ccn_B12h180C1-1W60Zn	96.63	0.26
Ccn_B12h180C1-2W60Zn	97.82	0.28
Ccn_B12h180C1-4W60Zn	92.75	0.25
Ccn_B12h180C1-2W10Zn	48.56	0.16
Ccn_B12h180C1-2W20Zn	55.24	0.17
Ccn_B12h180C1-2W40Zn	65.73	0.22
Ccn_B12h180C1-2W80Zn	21.08	0.03

[a] 1-xW - ratio substrate to water

[b] 1-xS - ratio substrate to salt

[c] 1-xW1-xS - ratio substrate to water to salt

Table A7 Results of elemental analysis, ash content and yield for the influence of lithium chloride and zinc chloride onto the hydrothermal carbonization of coconut shell powder (chapter 4.1.4.1 & 4.1.4.3).

Sample	**C [%]**	**H [%]**	**N [%]**	**O [%]**	**Ash [wt%]**	**Yield [wt%]**
Ccn_A12h180C	57.30	5.90	0.18	36.39	0.23	42.07
Ccn_A12h180CZn	64.47	4.06	0.02	29.86	1.59	41.11
Ccn_A12h180CLi(0.10)Zn	62.32	3.50	0.04	31.15	2.99	45.88
Ccn_A12h180CLi(0.30)Zn	63.16	3.80	0.22	31.42	1.40	49.30
Ccn_A12h180CLi(0.50)Zn	63.55	3.83	0.08	32.41	0.14	48.42
Ccn_A12h180CLi(0.70)Zn	61.11	4.14	0.14	32.82	1.80	52.31
Ccn_A12h180CLi(0.90)Zn	64.87	3.90	0.10	30.20	0.93	47.74
Ccn_A12h180CLi	66.61	4.26	0.08	28.92	0.14	36.08
Ccn_B12h180C	59.90	5.44	0.04	34.60	0.03	60.90
Ccn_B12h180C40Li(0.00)Zn	68.88	4.66	0.37	25.05	0.03	52.20
Ccn_B12h180C40Li(0.10)Zn	68.97	4.60	0.34	26.05	0.05	51.20
Ccn_B12h180C40Li(0.22)Zn	68.27	4.66	0.36	26.60	0.12	51.60
Ccn_B12h180C40Li(0.40)Zn	68.77	4.61	0.39	26.13	0.10	53.10
Ccn_B12h180C40Li(0.50)Zn	67.11	4.40	0.34	28.07	0.09	54.00
Ccn_B12h180C40Li(1.00)Zn	68.43	4.55	0.27	26.75	0.00	52.80

Table A8 Specific surface areas (SSA) obtained by nitrogen sorption experiments and calculated by BET theorem together with the pore volumes for different hydrochars for the influence of lithium chloride and zinc chloride onto the hydrothermal carbonization of coconut shell powder (chapter 4.1.4.4).

Sample	**SSA [m2·g-1]**	**Pore volume [cm3·g-1]**
Ccn_A12h180C	0.61	0.00
Ccn_A12h180CLi(0.00)Zn	229.64	0.29
Ccn_A12h180CLi(0.10)Zn	107.71	0.06
Ccn_A12h180CLi(0.30)Zn	124.84	0.05
Ccn_A12h180CLi(0.50)Zn	133.19	0.14
Ccn_A12h180CLi(0.70)Zn	47.01	0.07
Ccn_A12h180CLi(0.90)Zn	2.68	0.00
Ccn_A12h180CLi(1.00)Zn	3.07	0.00
Ccn_B12h180C	4.19	0.00
Ccn_B12h180C40Li(0.00)Zn	65.73	0.22
Ccn_B12h180C40Li(0.10)Zn	61.43	0.20
Ccn_B12h180C40Li(0.22)Zn	67.95	0.22
Ccn_B12h180C40Li(0.40)Zn	61.52	0.21
Ccn_B12h180C40Li(0.50)Zn	58.48	0.19
Ccn_B12h180C40Li(1.00)Zn	24.04	0.05

Table A9 Results of elemental analysis, ash content and yield for the influence of different types of salts and their mixtures onto the hydrothermal carbonization of coconut shell powder (chapter 4.1.5.1 & 4.1.5.3).

Sample	**C [%]**	**H [%]**	**N [%]**	**O [%]**	**Ash [wt%]**	**Yield [wt%]**
Ccn_B12h180C20NaCl	67.17	4.61	0.13	28.09	0.00	57.30
Ccn_B12h180C20Na(0.35)Zn	68.09	4.79	0.24	26.89	0.00	51.80
Ccn_B12h180C20KCl	66.07	4.98	0.15	28.74	0.06	55.70
Ccn_B12h180C20K(0.45)Zn	67.85	4.87	0.23	26.95	0.10	53.50
Ccn_A12h180CMgCl2	68.73	4.43	0.11	26.32	0.41	31.11
Ccn_A12h180CLiClO4	69.20	3.65	0.18	26.90	0.07	35.56
Ccn_B12h180C10Na2SO4	61.09	5.81	0.13	32.96	0.00	57.30
Ccn_B12h180C10Na2CO3	56.11	6.37	0.11	36.08	1.33	60.00
Ccn_B12h180C40ZnSO4	63.12	5.36	0.11	31.3	0.10	54.20

Table A10 Specific surface areas (SSA) obtained by nitrogen sorption experiments and calculated by BET theorem together with the pore volumes for different hydrochars for the influence of different types of salts and their mixtures onto the hydrothermal carbonization of coconut shell powder (chapter 4.1.5.4).

Sample	**SSA [$m^2 \cdot g^{-1}$]**	**Pore volume [$cm^3 \cdot g^{-1}$]**
Ccn_B12h180C20NaCl	36.98	0.11
Ccn_B12h180C20Na(0.35)Zn	49.81	0.15
Ccn_B12h180C20KCl	34.20	0.11
Ccn_B12h180C20K(0.45)Zn	49.54	0.16
Ccn_A12h180CMgCl2	64.67	0.19
Ccn_A12h180CLiClO4	155.42	0.33
Ccn_B12h180C10Na2SO4	3.64	0.01
Ccn_B12h180C10Na2CO3	2.16	0.00
Ccn_B12h180C40ZnSO4	4.09	0.01

Table A11 Results of elemental analysis, ash content and yield for the studies of possibilities for a process recycling towards a cycle loop (chapter 4.1.6.1 & 4.1.6.2).

Sample	**C [%]**	**H [%]**	**N [%]**	**O [%]**	**Ash [wt%]**	**Yield [wt%]**
Ccn_B12h180C60ZnS1[a]	67.11	4.13	0.35	28.32	0.10	52.30
Ccn_B12h180CxxZnWaste1S1	68.69	4.87	0.30	26.07	0.08	50.10
Ccn_B12h180CxxZnWaste2S1	67.47	4.50	0.16	27.80	0.07	54.30
Ccn_B12h180CxxZnWaste3S1	67.60	4.42	0.14	27.84	0.00	48.30
Ccn_B12h180C60ZnS2	68.28	4.28	0.30	27.04	0.10	54.50
Ccn_B12h180CxxZnWaste1S2	68.74	4.78	0.28	26.13	0.07	52.90
Ccn_B12h180CxxZnWaste2S2	68.25	5.15	0.17	26.36	0.08	55.00

[a] S1 - series 1, S2 - series 2

Table A12 Specific surface areas (SSA) obtained by nitrogen sorption experiments and calculated by BET theorem together with the pore volumes for different hydrochars for the studies of possibilities for a process recycling towards a cycle loop (chapter 4.1.6.3).

Sample	**SSA [$m^2 \cdot g^{-1}$]**	**Pore volume [$cm^3 \cdot g^{-1}$]**
Ccn_B12h180C60ZnS1[a]	97.83	0.28
Ccn_B12h180CxxZnWaste1S1	68.51	0.23
Ccn_B12h180CxxZnWaste2S1	54.23	0.19
Ccn_B12h180CxxZnWaste3S1	52.39	0.17
Ccn_B12h180C60ZnS2	99.46	0.26
Ccn_B12h180CxxZnWaste1S2	66.20	0.19
Ccn_B12h180CxxZnWaste2S2	47.40	0.14

Table A13 Results of elemental analysis, ash content and yield for the studies of activation of hydrochars obtained from different substrates (chapter 4.2.1.1 & 4.2.1.3).

Sample	C [%]	H [%]	N [%]	O [%]	Ash [wt%]	Yield [wt%]
Coconut shell powder	49.07	5.69	0.13	44.67	0.44	-
Ccn_A12h180C	59.50	5.35	0.13	34.99	0.03	52.25
Ccn_A12h180CLi(0.23)Zn	66.20	4.00	0.10	29.60	0.10	51.8
Ccn_A12h180CA60m500C	77.20	1.65	0.22	20.93	0.00	31.25
Ccn_A12h180CLi(0.23)ZnA60m500C	77.02	1.97	0.02	18.83	2.16	67.48
Dried dandelion leaves	37.47	5.50	2.06	44.31	10.66	-
Dnd_A12h180C	49.74	6.00	2.26	32.66	9.34	30.05
Dnd_A12h180CLi(0.23)Zn	51.88	4.07	1.44	29.06	13.55	42.69
Dnd_A12h180CA60m500C	49.81	0.51	1.87	19.82	27.99	32.59
Dnd_A12h180CLi(0.23)ZnA60m500C	53.61	1.50	1.55	17.44	25.91	65.95
Sawdust	46.33	6.13	0.61	46.91	0.02	-
Saw_A12h180C	49.96	5.92	0.35	43.77	0.00	63.41
Saw_A12h180CLi(0.23)Zn	60.29	3.71	0.39	35.61	0.00	55.60
Saw_A12h180CA60m500C	66.13	0.85	1.75	30.37	0.90	15.94
Saw_A12h180CLi(0.23)ZnA60m500C	72.97	1.68	0.58	22.00	2.78	62.96

Table A14 Specific surface areas (SSA) obtained by nitrogen sorption experiments and calculated by BET theorem together with the pore volumes for the studies of activation of hydrochars obtained from different substrates (chapter 4.2.1.5).

Sample	SSA [m2·g-1]	Pore volume [cm3·g-1]	Micropore volume [cm3·g-1]
Ccn_A12h180C	4.47	0.01	0.00
Ccn_A12h180CLi(0.23)Zn	87.60	0.11	0.02
Ccn_A12h180CA60m500C	513.30	0.20	0.18
Ccn_A12h180CLi(0.23)ZnA60m500C	517.71	0.31	0.17
Dnd_A12h180C	5.94	0.01	0.00
Dnd_A12h180CLi(0.23)Zn	8.14	0.01	0.00
Dnd_A12h180CA60m500C	386.86	0.18	0.14
Dnd_A12h180CLi(0.23)ZnA60m500C	268.42	0.12	0.12
Saw_A12h180C	2.32	0.00	0.00
Saw_A12h180CLi(0.23)Zn	32.60	0.03	0.01
Saw_A12h180CA60m500C	742.12	0.29	0.28
Saw_A12h180CLi(0.23)ZnA60m500C	395.59	0.18	0.18

Table A15 Results of elemental analysis, ash content and yield for the studies the influence of activation temperature and time onto the activation of hydrochars obtained from coconut shell powder (chapter 4.2.2.1 & 4.2.2.2).

Sample	C [%]	H [%]	N [%]	O [%]	Ash [wt%]	Yield [wt%]
Coconut shell powder	49.07	5.69	0.13	44.67	0.44	-
Ccn_A12h180C	59.50	5.35	0.13	34.99	0.03	52.25
Ccn_A12h180CLi(0.23)Zn	66.20	4.00	0.10	29.60	0.10	51.8
Ccn_A12h180CA10m500C	74.35	2.30	0.27	23.09	0.00	29.41
Ccn_A12h180CLi(0.23)Zn10m500C	75.88	2.21	0.10	19.77	2.05	69.16
Ccn_A12h180CA30m500C	76.81	1.63	0.18	21.38	0.00	31.72
Ccn_A12h180CLi(0.23)Zn30m500C	75.34	1.92	0.02	20.79	1.94	71.34
Ccn_A12h180CA60m500C	77.20	1.65	0.22	20.93	0.00	31.25
Ccn_A12h180CLi(0.23)ZnA60m500C	77.02	1.97	0.02	18.83	2.16	67.48
Ccn_A12h180CA60m200C	59.30	5.16	0.20	35.34	0.00	95.95
Ccn_A12h180CLi(0.23)Zn60m200C	65.06	3.19	0.19	31.07	0.51	95.24
Ccn_A12h180CA60m350C	69.24	3.14	0.26	27.36	0.00	63.67
Ccn_A12h180CLi(0.23)Zn60m350C	69.17	3.00	0.08	26.11	1.65	81.31
Ccn_A12h180CA60m650C	86.86	1.17	0.21	11.77	0.00	28.55
Ccn_A12h180CLi(0.23)Zn60m650C	82.89	1.14	0.06	12.84	3.07	56.30

Table A16 Specific surface areas (SSA) obtained by nitrogen sorption experiments and calculated by BET theorem together with the pore volumes for the studies of the influence of activation temperature and time onto the activation of hydrochars obtained from coconut shell powder (chapter 4.2.2.3).

Sample	SSA [m2·g-1]	Pore volume [cm3·g-1]	Micropore volume [cm3·g-1]
Ccn_A12h180C	4.47	0.01	0.00
Ccn_A12h180CLi(0.23)Zn	87.60	0.11	0.02
Ccn_A12h180CA10m500C	599.65	0.23	0.22
Ccn_A12h180CLi(0.23)Zn10m500C	509.76	0.22	0.18
Ccn_A12h180CA30m500C	495.51	0.20	0.18
Ccn_A12h180CLi(0.23)Zn30m500C	491.94	0.18	0.17
Ccn_A12h180CA60m500C	513.30	0.20	0.18
Ccn_A12h180CLi(0.23)ZnA60m500C	517.71	0.31	0.17
Ccn_A12h180CA60m200C	24.72	0.06	0.00
Ccn_A12h180CLi(0.23)Zn60m200C	169.30	0.16	0.05
Ccn_A12h180CA60m350C	9.41	0.01	0.00
Ccn_A12h180CLi(0.23)Zn60m350C	124.03	0.11	0.04
Ccn_A12h180CA60m650C	550.59	0.20	0.20
Ccn_A12h180CLi(0.23)Zn60m650C	624.85	0.32	0.21

Table A17 Dye sorption capacity q_e for different hydrochars (chapter 4.3.1 figure 123).

Sample	**q_e [mg g^{-1}]**	
	Methylene blue	**Methyl orange**
Ccn_A12h180C	35.73	9.65
Ccn_A12h180CLi(0.23)Zn	70.13	42.15
Ccn_A12h180CA30m500C	8.34	4.37
Ccn_A12h180CLi(0.23)Zn30m500C	34.78	14.47
Ccn_A12h180CA60m650C	5.91	-
Ccn_A12h180CLi(0.23)ZnA60m650C	24.36	-
Dnd_A12h180CLi(0.23)Zn	60.24	-
Dnd_A12h180CLi(0.23)Zn60m500C	10.61	-
Saw_A12h180CLi(0.23)Zn	60.33	-
Saw_A12h180CLi(0.23)Zn60m500C	13.52	-

Table A18 Dye sorption capacity q_t at different times for various hydrochars (chapter 4.3.1, figure 126).

				q_t [mg g^{-1}]			
t =	0	5	60	240	1200	1440	1680
Ccn	0.00	32.26	33.95	-	-	41.81	-
Ccn_B12h180C	0.00	28.22	40.53	53.26	65.57	71.73	70.24
Ccn_B12h180C60Zn	0.00	45.00	99.13	-	-	160.00	-
Ccn_B20h220C60Zn	0.00	58.74	126.68	177.96	218.51	222.01	221.79
Ccn_A12h180CLi(0.23) ZnA60m500C	0.00	8.57	19.43	-	-	33.42	-

Table A18 Dye sorption capacity q_t at different times (chapter 4.3.2.1, figure 127).

Time [min]	**q_e [mg g^{-1}]**
0	0.00
5	47.44
10	61.24
15	73.96
20	80.86
25	87.33
30	94.01
40	101.35
50	112.35
60	117.09
90	132.18
125	143.82
180	156.76
240	163.23
360	178.76
480	185.23
1440	206.79
1800	211.96

Table A19 Dye sorption capacity q_e at different initial concentrations (chapter 4.3.2.2, figure 129).

c_0 [mg·L^{-1}]	c_e [mg·L^{-1}]	q_e [mg g^{-1}]
25	22.73	247.65
20	18.24	321.69
15	8.52	308.42
12	6.51	253.32
10	5.13	219.56
9	4.17	223.17
8	3.48	227.49
7	1.84	181.13
6	1.22	199.44
5	0.32	195.28
3	0.00	157.82
1	0.00	47.82

List of figures

List of tables

Declaration

I hereby certify that I have written this work independently and used no resources other than those specified.

Oldenburg, February 15th, 2018
Hendrik Multhaupt